INSTITUTO POLITÉCNICO NACIONAL

ESCUELA SUPERIOR DE INGENIERÍA MECÁNICA Y ELÉCTRICA

SECCIÓN DE ESTUDIOS DE POSGRADO E INVESTIGACIÓN

"ON THE INVESTIGATION AND THE CHARACTERIZATION OF THE SOLUTIONS TO THE FORWARD AND INVERSE PROBLEMS FOR THE BI-DIMENSIONAL ELECTRICAL IMPEDANCE EQUATION WITH APPLICATION IN OBJECT IMAGE RECONSTRUCTION"

T H E S I S

TO OBTAIN THE DEGREE OF:

DOCTOR OF COMMUNICATIONS AND ELECTRONICS

PRESENTS:

M.SC. CÉSAR MARCO ANTONIO ROBLES GONZÁLEZ

THESIS DIRECTORS:

DR. VOLODYMYR PONOMARYOV

DR. MARCO PEDRO RAMÍREZ TACHIQUÍN

MEXICO CITY, JANUARY 2016.

SIP-14-BIS

INSTITUTO POLITÉCNICO NACIONAL

SECRETARÍA DE INVESTIGACIÓN Y POSGRADO

ACTA DE REVISIÓN DE TESIS

En la Ciudad de MÉXICO D. F., siendo las 12:30 horas del día 30 del mes de NOVIEMBRE del 2015 se reunieron los miembros de la Comisión Revisora de la Tesis, designada por el Colegio de Profesores de Estudios de Posgrado e Investigación de SEPI-ESIME-CULH. para examinar la tesis titulada:

ON THE INVESTIGATION AND THE CHARACTERIZATION OF THE SOLUTIONS TO THE FORWARD AND INVERSE PROBLEMS FOR THE BI-DIMENSIONAL ELECTRICAL IMPEDANCE EQUATION WITH APPLICATION IN OBJECT IMAGE RECONSTRUCTION.

Presentada por el alumno:

ROBLES	GONZÁLEZ	CÉSAR MARCO ANTONIO
Apellido paterno	Apellido materno	Nombre(s)

Con registro: A 1 2 0 3 7 6

aspirante de:

DOCTORADO EN COMUNICACIONES Y ELÉCTRONICA.

Después de intercambiar opiniones los miembros de la Comisión manifestaron ***APROBAR LA TESIS***, en virtud de que satisface los requisitos señalados por las disposiciones reglamentarias vigentes.

LA COMISIÓN REVISORA

Directores de tesis

DR. VOLODYMYR PONOMARYOV

DR. MARCO PEDRO RAMÍREZ TACHIQUÍN.

DR. HÉCTOR MANUEL PÉREZ MEANA

DR. MIGUEL CRUZ IRISSON

DR. JUAN CARLOS SÁNCHEZ GARCÍA

INSTITUTO POLITECNICO NACIONAL ESTADOS UNIDOS MEXICANOS S.E.P. SECCION DE ESTUDIOS DE POSGRADO E INVESTIGACION ESIME CULHUACAN

PRESIDENTE DEL COLEGIO DE PROFESORES

M. EN C. MIGUEL ÁNGEL RODRÍGUEZ ZUNO

INSTITUTO POLITÉCNICO NACIONAL

SECRETARÍA DE INVESTIGACIÓN Y POSGRADO

CARTA CESIÓN DE DERECHOS

En la Ciudad de México, D.F. el día 07 del mes de Diciembre del año 2015, el (la) que suscribe **CÉSAR MARCO ANTONIO ROBLES GONZÁLEZ**, alumno(a) del Programa de **DOCTORADO EN COMUNICACIONES Y ELECTRÓNICA**, con número de registro **A120376**, adscrito(a) a la **SEPI-ESIME-CULHUACAN**, manifiesto(a) que es el (la) autor(a) intelectual del presente trabajo de Tesis bajo la dirección del (de la, de los) **DR. VOLODYMYR PONOMARYOV Y DR. MARCO PEDRO RAMÍREZ TACHIQUÍN** y cede los derechos del trabajo titulado **"ON THE INVESTIGATION AND THE CHARACTERIZATION OF THE SOLUTIONS TO THE FORWARD AND INVERSE PROBLEMS FOR THE BI-DIMENSIONAL ELECTRICAL IMPEDANCE EQUATION WITH APPLICATION IN OBJECT IMAGE RECONSTRUCTION"**, al Instituto Politécnico Nacional para su difusión, con fines académicos y de investigación.

Los usuarios de la información no deben reproducir el contenido textual, gráficas o datos del trabajo sin el permiso expreso del (de la) autor(a) y/o director(es) del trabajo. Este puede ser obtenido escribiendo a las siguientes direcciones **vponomar@ipn.mx, marco.ramirez@asajiaudio.com y croblesg1101@alumno.ipn.mx ó cerobles@gmail.com**. Si el permiso se otorga, el usuario deberá dar el agradecimiento correspondiente y citar la fuente del mismo.

CÉSAR MARCO ANTONIO ROBLES GONZÁLEZ
Nombre y firma del alumno(a)

Acknowledgements

CONACyT

I would like to thank to Consejo Nacional de Ciencia y Tecnología for all the economic support to study, perform and conclude my Doctoral degree and this dissertation.

IPN

I would like to thank to Instituto Politécnico Nacional for the support to conclude my Doctoral studies.

Dedications

Quiero dedicarle este trabajo al Dr. Ponomaryov, por su sabia guía, consejos y regaños para terminar esta tesis, pero sobre todo su comprensión y amistad.

Este trabajo también quiero dedicarlo a Marco, que con mucha paciencia y tolerancia me ayudo a entender el tema y seguir trabajando, gracias a su consejo y guía es que hoy por hoy este trabajo pudo ser realizado.

Este trabajo se lo dedico con mucho cariño a una persona muy especial, que me supo guiar en las buenas y en las malas, cuando más problemas se presentaron y siempre me dio su apoyo incondicional, quien saco de mi lo mejor y siempre se esforzó para ayudarme y darme todo lo que necesite. Gracias a ella, pude terminar este sueño que con mucho trabajo se vio realizado. Gracias mamá, por todo lo que has hecho por mí.

A mi hermano y mi papá, quienes vieron como fue tomando forma este trabajo para poder ser concluido y sobre todo por el apoyo brindando.

A Paulina le dedico esta tesis por su apoyo y tolerancia, así como su consejo y paciencia, ya que en momentos críticos siempre estuvo a mi lado, soportando muchas veces mi carácter voluble y en algunas ocasiones mi desmotivación y frustración, ayudándome en muchas ocasiones a concluir este trabajo.

Este trabajo es dedicado a mis compañeros quienes tuvieron que soportar las múltiples conferencias y platicas de seminario, que en muchas ocasiones fueron aburridas. Gracias a su apoyo y preguntas es que este trabajo fue terminado.

Contents

List of Tables

List of Figures

List of Algorithms

Abstract

The Electrical Impedance Tomography (EIT) is a low-cost non-invasive technique used to monitor chronic diseases, such as tumours. This work is mainly dedicated to the study of EIT, that remains considered as an ill-posed and high-complexity problem.

The main of this dissertation is the designing of numerical solutions for EIT, and for the forward problem of the electrical impedance equation.

In order to better understand the EIT problem, different State-of-the-Art techniques are reviewed, with the purpose to select a convenient reference method. Among all studied techniques, the Finite-Element Method (FEM) has been chosen because it has proven its efficiency and permits an easy adaptation for the electrical impedance equation. One drawback of this technique is the difficulty if reconstruction for conductivity distribution in form of geometrical figures, with edges or non-smooth shapes.

In the current work, the Taylor's series in formal powers' method (NPSM) was performed and was justified as an adequate approach for forward problem. This novel method was compared with FEM employing imposed conductivity functions as initial data.

The Lebesgue measure is used as accuracy metric for comparison of the designed method with the FEM one. Even though the results were acceptable, the stability obtained by NPSM demonstrated the necessity to employ a regularization process. The Tikhonov's regularization method has been introduced to stabilize the NPSM's approximation, modifying designed method. The stabilized approximation was obtained resulting in novel hybrid method in two variants that use together NPSM and FEM approaches.

Novel proposal approximates the inverse problem of the electrical impedance equation proving its computational efficiency and reconstruction accuracy. The accuracy of the method was investigated using the quality image assessments, in particularly employing commonly used criteria: PSNR,

MSE, SSIM, and via subjective perception analysis, exposing error images of conductivity reconstructed.

The designed hybrid approach can easily be adapted depending upon the initial conditions given for the problem. This new technique has been tested in real-physics measurements demonstrating the possibility to utilize this novel approach under practical conditions. The comparison of the designed hybrid approach and FEM in inverse EIT problem clearly shows the advantage of novel method, performing better quality results in form as objective criteria PSNR and SSIM values as well in subjective perception analysing reconstructed images.

Meanwhile, the analysis of the obtained results showed that the stability and speed of designed proposals are better than the approximation obtained by FEM.

Resumen

La técnica de Tomografá por Impedanca Eléctrica es una herramienta de imagenología médica no invasiva y de bajo costo, si se compara con las técnicas de más frecuente uso en hospitalización. La disertación está principalmente dedicada al estudio de este tipo de tomografía, que hasta la fecha de edición del presente documento, se considera aún un problema incorrectamente planteado y con un muy alto grado de complejidad matemática para resolverse.

Una de las principales aportaciones de este tratado es la aproximación de soluciones numéricas para el problema de Tomografía por Impedancia Eléctrica, comenzando por aproximar soluciones para el problema directo de la ecuación de impedancia eléctrica, mediante el uso del método de series de Taylor en potencias formales, para ser usadas posteriormente como punto de partida en nuevos algoritmos basados en el Método del Elemento Finito, reforzado con un proceso de regularización, que aproximan soluciones numéricas del problema inverso.

Más aun, esta tesis contiene una extensa revisión crítica del Estado del Arte de los métodos basados en elemento finito, que ha probado su eficacia en la resolución de este tipo de problemas, pero que aún presenta serias desventajas, como el alto costo computacional que exige el estudio de distribuciones de conductividad con figuras geométricas que contienen esquinas, o cuyos dominios incluyen puntos no suaves.

La medida de Lebesgue se emplea como referencia de exactitud y precisión para comparar el desempeño entre las diversas variaciones mejoradas del elemento finito, que emplea como método de regularización adicional una variación optimizada del método de Tikhonov.

De hecho, como consecuencia de la combinación del cálculo de soluciones para el problema directo empleando series de Taylor en potencias formales, y el uso de dichas soluciones como condiciones de frontera para la resolu-

ción del problema inverso empleando el Método del elemento Finito antes referido, esta disertación presenta un método híbrido novedoso para estudiar el problema de Tomografía por Impedancia Eléctrica, que desde las perspectivas descritas en las páginas consecuentes, arroja resultados superiores a los obtenidos con el resto de los métodos analizados en el Estado del Arte.

Debe resaltarse que en no pocas ocasiones, los datos empleados en el análisis numérico provinieron de mediciones físicas reportadas en otros trabajos, y que la calidad de las imágenes obtenidas da fe de la contribución científica de esta disertación.

Chapter 1

Introduction

The Electrical Impedance Tomography (EIT) is a non-invasive imaging procedure that can be used in Medicine. EIT uses electrodes that are set in the surface of any object, in this case the human body, in order to introduce low-voltages to the inner body. These voltages are used to show the inner parts of an object or body (see e.g. [60]).

There exists an assortment of techniques that are employed for monitoring and constructing the inner body into images. All these works use the different approximation techniques to perform real applications in order to estimate the solution to this difficult problem. Following to [65], the neural networks and fuzzy sets are employed to calculate the forward problem of (1.1). These researches are developed in order to approximate faster solutions to both problems, but emphasizing the results obtained in the artificial intelligence field.

In [53], the authors use electrodes in a human thorax. The approximation was made by a conductivity estimation using the fast inversion of the eigenvalue and eigenvector in the electrical impedance equation (see e.g. [52]). On the other hand, [61] proposed a multi-phase flowing monitoring using a phantom for EIT problem. Furthermore, [51] uses a multi-phase level framework to obtain the bio-luminescence inside the human body. Nevertheless, the wide variety of the algorithms and methods has the same goal that it is necessary to obtain a solution for EIT.

EIT was mathematically posed in 1980 by A. P. Calderon (see e.g. [23]), in which the equation that represents the problem is as follows:

$$\operatorname{div}(\sigma \operatorname{grad} u) = 0, \tag{1.1}$$

where σ is the conductivity, and u is the electric potential in the boundary Γ for a domain Ω within.

The equation (1.1) is very important to understand the main problem, that shall be divided in two different sub-problems:

- Forward problem.
- Inverse problem.

The forward problem of (1.1) is easier to solve than the inverse problem. For the forward problem of the electrical impedance equation, the initial conditions are the conductivity σ for a unit disk domain Ω, in which the electric potential $u|_\Gamma$ should be calculated.

However, the inverse problem of the electrical impedance equation of (1.1) is more difficult to solve because the initial conditions given are the electric potential u at the boundary Γ for a unit disk domain Ω and the calculation of the conductivity σ should be performed.

For more than twenty years since the formulation of the problem was published, the mathematical complexity of (1.1) was considered for many experts in the field as an ill-posed problem and *impossible* to obtain an analytic general solution (see e.g. [98]), even for the simple cases for the conductivity σ. In this case the correct understanding of the Maxwell's equations in a differential form should be used for a better analysis (see e.g. [68]).

Some works are dedicated to medical applications such as the study of the human thorax. In this study the comparisons between all the soft tissues within the thorax were developed to determine the lung function (see e.g. [15]). In addition, [14] describes the lung airing in mechanically ventilated patients, showing the physiological measurements between the inspiration and expiration.

Other works dedicated to the study of EIT are: According to [49], in which the detection/location of cancer in skin, breast or cervix were developed. In addition, following to [26], in which the obtained localization of the epileptic foci imaging brain activity is the main contribution.

Nevertheless, FEM is not closed only to the Medical Imaging field, it is also used in geophysics and industrial process monitoring, where the technique is known as *electrical resistivity tomography* (see e.g. [12]). Similar to EIT, surface electrodes are placed on the earth, within bore holes, or inside a vessel or pipe in order to locate resistivity anomalies or monitoring mixtures of conductivity fluids.

1.1 Aims

1.1.1 General aims

- Design a method that calculates the electric potential u when the conductivity σ is known within the domain (Forward Dirichlet boundary value problem).

- Design a method that reconstructs the conductivity σ function for given electric potential u to the boundary domain (Inverse Dirichlet boundary value problem, or EIT).

1.1.2 Goals

1.1.2.1 Forward Dirichlet boundary value problem

- Study and justify the relationship between the electric potential u at boundary and the inner conductivity function σ into the domain.

- Propose and develop a novel method that estimates the electric potential u through conductivity σ inside the domain.

- Optimize the numerical algorithm proposed that calculates the electric potential u at boundary domain.

- Compare the proposal technique with State-of-the-Art methods.

1.1.2.2 Inverse Dirichlet boundary value problem, or EIT

- Investigate and synthesize the relationship between the conductivity function σ and the electric potential u for a chosen domain.

- Design a method that uses the electric potential u to reconstruct the estimated conductivity function σ within the domain.

- Optimize the numerical algorithm that calculates the conductivity function σ.

- Compare the proposed method with state-of-the-art techniques.

1.2 Problem statement

The concept of ill-posed was changed in 2005 when V. Kravchenko (see e.g. [55]) noticed that the two-dimensional case of (1.1) was completely equivalent to the special case of the Vekua equation (see e.g. [95]). One year later, K. Astala and L. Päivärinta (see e.g. [3]) discovered independently this relation, giving a positive answer to the Calderon's problem in the plain (see e.g. [23]).

Many important works were developed later, such as [57] published in 2007. It can be considered as the first general analytic solution of (1.1). Furthermore, this solution was proposed at least for certain σ conductivity distributions and using the Taylor's series in formal powers (see e.g. [56], [27], [25] and [24]). All these works began their analysis with the Pseudoanalytic Function Theory posed by L. Bers in 1963 (see e.g. [13]) and analyzed again by V. Kravchenko in 2005 (see e.g. [56]).

Current study tries to focus on a relevant and recently discovery, in which a completeness proof using the set of Taylor's series in formal powers (NPSM) in a delimited domain could be used to approximate solutions to Dirichlet boundary problems in the plane for the electrical impedance equation (see e.g. [25] and [78]). This proposition is valid when the conductivity σ distribution can be expressed by a piece-wise separable variable function (see e.g. [47] and [81]).

1.3 Proposed solution

Current dissertation is fully dedicated to analysis and study the forward and inverse Dirichlet boundary value problems. Such problems were considered as an ill-posed problem in the Hadamard sense (see e.g. [43]). It is known that a problem can be considered well-posed if a mathematical and physics phenomenon should have the following properties:

1. The solution exists.
2. The solution is unique.
3. The solution's behavior does not strongly change with the small alterations of the initial conditions.

Summarizing, even when the solution exists and could be considered as unique, the behavior of (1.1) is changed depending on the conditions given (see e.g. [98]).

In this sense the forward problem could be solved by NPSM (see e.g. [70]). Furthermore, this technique could be used for given initial conditions to the inverse problem of (1.1). A discussion takes place when the conductivity σ is extended in cases for non-separable variables in the plane (see e.g. [90] and [100]). This research will emphasize the numerical approximations obtained by NPSM.

This study relies in the form to employ the elements of the Pseudoanalytic Function Theory in more specific problems, such as in the engineering and other scientific fields. One of the most important fields is Medical Imaging, where its main objective is to obtain a more accurate and fast method to diagnose and monitoring diseases. For this reason, this work is dedicated to study NPSM that could obtain better approximations, and could be considered as a possible solution in this field (see e.g. [73]).

Furthermore, in this work, the possibility to employ the forward problem of (1.1) is analyzed to compute an approximation of the electric potential u. Once it has been computed, the solution is utilized in the inverse problem to calculate the conductivity function σ. It means that the solution to the forward problem is employed as the initial condition to the inverse problem.

Basically, the proposed method is used in presence of non-separable and piece-wise separable conductivity variable functions to perform these approximations (see e.g. [100]). Moreover, the possibility to use this method in non-smooth domains is introduced, but it is studied widely in these works (see e.g. [72] and [79]).

1.4 Thesis organization

The structure of current dissertation contains the following chapters, that they will be organized as follows:

- **Chapter 1 (Introduction)** explains the problem to be analysed, it is EIT problem. This chapter contains the subsections: Aims, problem statement, in which the problem is explained and the reasons to use this theory; the proposed solution that is used and explained for the EIT problem and its possible approximations. Finally, the organization of the present work is exposed.

- **Chapter 2 (State of Art)** the State-of-the-Art techniques are introduced where several important techniques that could be used to

approach the solution to the forward and inverse problem of (1.1). This chapter contains a brief demonstration of the approximation of the classical methods such as Finite-Element Method (FEM) and the problem statement as well as the deduction of the electrical impedance equation.

- **Chapter 3 (Forward Dirichlet boundary value problem)** NPSM and its origin are exposed in this chapter. At last but not the least, the Pseudoanalytic Function Theory is used to develop a base method upon this theory. Lastly, a comparison of this method with FEM closes this chapter, including a discussion and conclusion for this chapter.

- **Chapter 4 (Inverse Dirichlet boundary value problem)**, the novel proposals are introduced in this chapter. Two-hybrid methods are utilized to approximate the solution to the inverse problem. In the end of this chapter, the discussion and conclusion are exposed.

- **Chapter 5 (Conclusions)**, the general conclusions are exposed explaining the possibility to obtain and to study these methods in a different field of the engineering. Lastly, a possible future works are discussed.

- **Appendices A, B and C**, presents the scientific papers published during the elaboration of this dissertation, (book chapters, conference papers proceedings, JCR articles) published during the post-grade period and the awards granted obtained.

a

Chapter 2

State of the Art

2.1 Problem statement

The contemporary form of the problem finds its origin upon the classical electrodynamics field theory. More precisely, the Maxwell's equations are a set of partial differential equations and, together with the Lorentz force law, represent the main of the Electrical Impedance Tomography (EIT) problem (see e.g. [68]). In addition, [63] conforms the background of the main problem by means of the Maxwell's equation, presented in differential form, and it shall be analysed in the forward paragraphs.

Ampere's Law

This law states that the electric field emanated from within a closed three-dimensional body, is proportional to the charge confined inside it. Furthermore, the equation governing this phenomena is usually posed as follows (see e.g. [64] and [63]).

$$\mathrm{rot}\overrightarrow{H} = \overrightarrow{j} + \partial_t \overrightarrow{D}, \tag{2.1}$$

where $\overrightarrow{H}$ is the magnetizing field, $\overrightarrow{j}$ is the vectorial current density, and $\overrightarrow{D}$ is the electrical current induction vector for the static case. Thus, for this particular case $\partial_t \overrightarrow{D} = 0$.

Ohm's Law

This law establishes that the current flowing within a conductor from one transversal section till another, is directly proportional to the voltage across those sections (see e.g. [64] and [63]). A simple example in Physics is expressed as follows:

$$\overrightarrow{j} = \sigma \overrightarrow{E}, \tag{2.2}$$

where σ is the conductivity function, $\overrightarrow{j}$ is denoting the current density vector and $\overrightarrow{E}$ represents the electric field.

Faraday's Law

This law describes how a time varying magnetic field induces an electric field. The subsequent statement expresses this law (see e.g. [64] and [63]):

$$\mathrm{rot}\,\overrightarrow{E} = -\partial_t \overrightarrow{B}, \tag{2.3}$$

where $\overrightarrow{E}$ is the electric field and $\overrightarrow{E} = -\mathrm{grad}u$, $\overrightarrow{B}$ denotes the induction magnetic field. The (rot) operator can also be expressed as $(\nabla\times)$ operator and it is known as curl.

Gauss' Law

This law studies the relationship existing among a static electric field and the electric charges that cause it (see e.g. [64] and [63]). The static electric field points away from positive towards negative charges.

$$\mathrm{div}\,\overrightarrow{B} = 0, \qquad \mathrm{div}\,\overrightarrow{D} = \rho, \tag{2.4}$$

where ρ is the total charge density and $\overrightarrow{D}$ is the displacement field or the electric induction.

Constitutive relations

For the Maxwell's macroscopic equations, it is necessary to specify the relations between the displacement field D, the magnetizing field H, the magnetic field B and the electric field E (see e.g. [64] and [63]). In Real-world materials, it is equivalent to constitute these rarely equations that are fully equivalent

to specify the dependence of the polarization P or the bound charge and the magnetisation M, or the bound current on the applied magnetic field.

These equations can be observed in the following statement:

$$\overrightarrow{D} = \xi \cdot \overrightarrow{E}, \qquad \overrightarrow{B} = \mu \cdot \overrightarrow{H}, \tag{2.5}$$

where ξ denotes the electric permittivity, μ represents the magnetic permeability and $\overrightarrow{H}$ is the magnetic field.

Deduction of the Electrical Impedance Equation

Once the Maxwell's basic theory has been exposed, the deduction of the electrical impedance equation follows immediately (see e.g. [64] and [63]). Thus, let us employ the Ampere's law in a differential form:

$$\mathrm{rot}\overrightarrow{H} = \overrightarrow{j} + \partial_t \overrightarrow{D}.$$

The divergence (div) operator is applied in both sides of the equation, and taking into consideration that $\mathrm{div}(\mathrm{rot}\overrightarrow{H}) = 0$, the resultant statement is given as:

$$0 = \mathrm{div}(\overrightarrow{j} + \partial_t \overrightarrow{D}).$$

By using the commutative property, this last equation turns into

$$0 = \mathrm{div}\overrightarrow{j} + \partial_t \mathrm{div}\overrightarrow{D}. \tag{2.6}$$

By considering the static case, this is $\partial_t \mathrm{div}\overrightarrow{D} = 0$, we obtain $div\overrightarrow{j} = 0$. Furthermore, utilizing (2.2), the equation can be expressed as follows:

$$\mathrm{div}\,(\sigma\ \mathrm{grad}u) = 0. \tag{1.1}$$

This equation is also known as the *electrical impedance equation* or *electrical conductivity equation*, and the inverse problem is usually referred as *Electrical Impedance Tomography* (EIT) (see e.g. [23] and [98]).

2.2 Main problem

As a matter of fact, we are interested in two particular classes of boundary value problem: the forward problem and the inverse problem. From another

point of view, the mathematical expression (1.1) can be employed to represent two different sub-problems, depending on the complexity and the imposed initial conditions. Both problems are highly difficult to solve. For this work, on behalf of simplification for numerical calculations, the proposed domain is the unit disk (see e.g. [20]).

The first problem of (1.1), also known as the forward problem of the electrical impedance equation, attempts to obtain the electric potential u when the inner conductivity σ is given. The awkwardness is to approximate the electric potential $u|_\Gamma$ at the boundary. Meanwhile, the second problem of (1.1), also known as the inverse problem of the electrical impedance equation, requires to calculate the inner conductivity distribution when the electric potential u is given for (1.1) at the boundary.

For the forward problem of (1.1), there are many different techniques that approximate the electric potential $u|_\Gamma$. The Finite-Element Method (FEM) proves to be one of the best choices for this difficult toil.

The FEM attempts to convert a complex mathematical expression into a linear equation to solve (see e.g. [31]). These classes of problems are commonly studied in the Engineering fields (see e.g. [38] and [41]).

This chapter is dedicated to study different techniques that are used to approximate the solution for both forward and inverse problems of (1.1) (see e.g. [70]). The following methods are used because of its importance when solving such problems of (1.1).

- Variation of sparse matrix method.
- Trust region sub-problem method.
- Neural networks and fuzzy sets approaches.
- Finite-Element Method:
  - Gauss-Newton model.
  - Back-projection model.
  - Tikhonov regularization method.

All these techniques are used in the Calderon's problem (see e.g. [23]), another for to refer EIT problem, to approximate the solution. In the following sections, these techniques will be studied to understand better the behaviour of EIT problem.

2.3 Variations of the sparse matrix method

Let us establish a finite set of points $\{z_k\}_{k=1}^N$ belonging to the boundary Γ of the domain Ω, and let $\{u_k\}_{k=1}^N$ be the values of the electric potential u at such points. Let the unitary vector $\overrightarrow{n}_k$ be tangent to some point $z_k \in \{z_k\}_{k=1}^N$. Then, the Neumann condition for (1.1) at the z_k point can be posed as:

$$j_k = \langle \sigma \text{ grad } u, \overrightarrow{n}_k \rangle \,, \tag{2.7}$$

where $\langle , \rangle$ represents the two-dimensional Cartesian inner product, and j_k is the superficial current density at such point; whereas the Dirichlet condition will be given by (1.1)

$$\text{div}\,(\sigma \text{ grad } u)\,|_\Gamma = 0, \tag{2.8}$$

evaluated in such z_k.

Furthermore, let us suppose that the conductivity σ within the domain Ω can be represented as the junction of identical geometric figures σ_M, in which all of them posses a constant conductivity value. Let the vector $\overrightarrow{\sigma} = (\sigma_1, \sigma_2, \ldots, \sigma_M)$ be conformed by such values.

Thence, introducing a vector

$$\overrightarrow{u} = (u_1, u_2, \ldots, u_N) \,, \tag{2.9}$$

where $u_k, k = 1, 2, \ldots, N$ are the elements that belongs to $\{u_k\}_{k=1}^N$, then it can be established a relationship between $\overrightarrow{u}$ and $\overrightarrow{\sigma}$ as it follows:

$$A_\sigma \overrightarrow{\sigma} = \overrightarrow{u}. \tag{2.10}$$

Hence, the main is to approximate the A_σ matrix such that the last equality is true. Therefore, when $N = M$, it is possible to use the *incomplete Cholesky factorization method*, in which it is considered a sparse matrix method, to approach A_σ (see e.g. [40]). This is a classic method used to approximate the solution of the inverse problem of (1.1), and properly analysed in many works (see e.g. [98]).

In the following paragraphs, an important example can be found in [11], where it is used the incomplete Cholesky factorization method together the *conjugated gradient method* (see e.g. [4]), in which it is suggested a first-class technique for the lung function medical monitoring of the neonate.

Principally, the conjugated gradient method supplies a convenient computational velocity taking into a consideration its importance for the medical

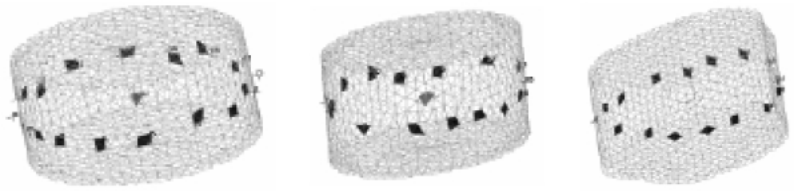

Figure 2.1: Variation of the sparse matrix method.[98]

imaging. It is remarkable, that the authors in [45] considered a complementary technique that allows to estimate the shape of the surface where EIT is taking place, in order to improve the accuracy and the image resolution.

However, a natural limitation of this technique resides within the maximum number N of points belonging to the boundary Γ, that will be taken into account when making the calculus. It becomes evident in the necessity of establishing a convenient relationship between the computing time and the desired accuracy of the image.

It is possible to infer that when the number N increases the resolution (without over passing the physical restrictions), and the accuracy of the reached image do it too. However, for this case, the time needed for the mathematical calculation could be consequently very large, and the techniques could be useless for the clinical applications described before. Furthermore, the convergence problems that are presented when the number of equations increase depends upon the size of the matrix A_σ.

Another challenge is posed due to the geometrical shapes selected for the components σ_M, in which the domain Ω will be divided. Hence, such behaviour could be irregular, sometimes is considered chaotic, then, the selection of a geometrical shape for the components σ_M in the domain Ω will be decomposed and play an important role when solving the inverse problem of (1.1).

2.4 Trust region sub-problem method

This method was posed to set a regularization criterion that can be used for the measurements, in which an analogical noise was presented in the boundary electrodes around the domain. However, this application can be extended to the adjustment of the conductivity σ distribution, once an error

$\mathcal{E}$ function is given.

In general, the procedure rises from a basic property of EIT problem. The relation between the perturbations in the inner conductivity σ and the perturbations at the boundary data, is non-linear. Nevertheless, under some certain circumstances, it is possible to represent this non-linear condition via convenient arrangement of a finite set of linear relations.

A brief description of this idea can be formulated following to [69], let $\Delta\Omega$ be a continuous region inside the domain Ω, and let j be the Fréchet derivative of the electric potential u with respect of its conductivity σ in $\Delta\Omega$. Therefore, it is possible to verify that the following linear relations holds:

$$J \cdot x = \delta u, \tag{2.11}$$

where $x \in \mathbb{R}^n$ represents the perturbations on the conductivity σ; $\delta u \in \mathbb{R}^m$, and J is indeed the Jacobian matrix $J \in \mathbb{R}^{m \times n}$.

Obtaining x of (2.11) is not a trivial task due to its non-linear relation mention before. In [4], it is applied the Conjugate Gradient Method in (2.11) to overcome it. Therefore, a least square conjugate gradient can be constructed to approximate the solution to the inverse problem of (1.1):

$$\min_x ||J \cdot x - \delta u||, \tag{2.12}$$

where $\|\cdot\|$ represents the classical Cartesian norm for the Banach space $\mathbb{R}^n$.

In this sense, the least square conjugate gradient is used to construct finite elements in the direction of the vector related to large values at the very first iterations. Since the components associated with singular values become effective when more iterations occur. It can say that the number of iterations η can be considered as a regularization parameter. Then, the stop condition must be estimated before unwanted elements appear.

Following to [39], an approximation method is used to obtain the solution of the trust region sub-problem. In [42], a modification of the trust region sub-problem method is developed for EIT, in which the regularization problem can be posed as the following quadratically constrained least squared problem:

$$R_\varepsilon = \min_x ||J \cdot x - \delta u||, \tag{2.13}$$

where $\|x\| < \varepsilon$ and $\varepsilon > 0$.

Furthermore, following to [92], it is possible to prove that the last formulation is equivalent to the Tikhonov Regularization Method (often used

when dealing with special class of ill-posed inverse problems). This implies that (2.13) can be rewritten as:

$$\left(J^T J + \alpha^2 I\right) x_\alpha = J^T \delta U, \tag{2.14}$$

where J^T represents the transpose matrix J, I is the identity matrix and α is the Tyhonov's parameter. Thus, eqn. (2.13) rises as an optimization problem of finding the minimum η such that

$$\eta = x^T J^T j x - J^T \delta u x, \tag{2.15}$$

where $\|x\|^2 < \varepsilon^2$.

Moreover, the optimization problem of (2.13) is also known as Trust Region Sub-problem (TRSP), and its resolution can be approached by sequentially solving (2.15). Thus, it is possible to perform a curve where the minimum reaches the regularization parameter ε and, in consequence, the optimal number of iterations η, in which the vector x will be the solution of (2.11) fulfils the desire accuracy.

According to [39], the main contribution of this method is the possibility to use the mathematical tools developed by Tikhonov to approach the solutions of EIT problem. However, two critical matters rise immediately when this method is used:

- The selection of the geometrical shape $\Delta\Omega$ of the sub-region is strongly related with the preferred variation of the FEM used for solving the forward problem of (1.1).

- The optimum number of iterations η, in which the calculus might be stopped.

It is possible to notice that the first problem has a great influence into the second due to its non-liner relation. Indeed, it can be considered chaotic (see e.g. [66]), considering the low stability in the solutions for EIT problem. However, the geometry $\Delta\Omega$ and the number of iterations η are still considered as an open problem, that it could contribute to TRSP, and it could increase their viability. Furthermore, it could represent a disadvantage when applying this method to EIT, but the lack of this study also enhances the relevance of [39], in which it is posed an interesting application.

2.5 Finite-Element Method

The main objective to employ the Finite-Element Method (FEM) is to approach solution for equation the (1.1). This equation can be represented in two-dimensions as a complex partial derivative expression, that it is very difficult to solve, but it can still be approximated. Further subsections are fully dedicated to study FEM that it is used to approximate the forward and inverse problems, achieving good solutions for them.

The first one introduces a commonly used technique to approach the solution of the forward problem of (1.1). The problem resolution depends upon the problem to be studied, when the forward problem is approximated, the known condition is the conductivity σ function and the unknown condition is the electric potential u (see e.g. [98]).

Meanwhile, the inverse problem possesses higher complexity to solve, because in this case, the known condition is the electric potential u and the unknown condition is the conductivity function σ. Many experts in the field considered this problem as an ill-posed (see e.g. [23] and [98]).

This mathematical tool has an implementation known as PDE toolbox (Partial Differential Equation toolbox), that employs FEM to obtain the forward problem approximation. On the other hand, there exists another implementation also called EIDORS (Electrical Impedance Tomography and Diffuse Optical Tomography Resonance Software). This software is implemented in some mathematical frameworks. The advantage to use it is the possibility to compute the approximation to the inverse problem, as well as to the forward problem.

Some disadvantages are presented when FEM is used, for example, calculating a complex and accurate problem requires high computational resources and the time-computing increases considerably. In this case, the mesh generation is a complex task because it requires to divide the domain into small finite-elements, making the resolution fully dependent upon the mesh conditions, and due to the mesh robustness, this technique is considered slow.

2.5.1 Mesh generation

The mesh generation is the most important task to be developed before using FEM (see e.g. [46]). Dividing the domain Ω into a definite number of finite-elements is the first effort. For this case, it is commonly used geometrical figures such as: triangles or quadrangles (a quadrangle can be divided into

two triangles, so is more often employed the triangle).

In EIT problem, it is assumed that the resistivity in each element is homogeneous and isotropic. Thus, this technique turns a continuous problem with a finite-number of unknown expressions into an interpolation between its elements. This technique is also known as discretization.

The elements constitute a determined number of variables taken from the nodes. Then each value is interpolated in order to give a solution for the generated functions. This process will be done depending upon the problem to be solved. For example: the forward problem performs the process from the centre to the boundary and vice versa for the inverse problem for (1.1).

2.5.2 Electrodes number, independent measurements and resolution.

The number of electrodes are closely related to the image resolution, since the electrodes represent the independent measurements that shall be introduced into the system (see e.g. [44], [30]). Moreover, these electrodes represent the number of mathematical expression to be solved by FEM (see e.g. [98]). For the mesh calculation, it should consider the $\mathbf{E}$ number of electrodes at the boundary as a maximum number of equations to be calculated, following the expression:

$$f(t) = \frac{\mathbf{E}\,(\mathbf{E}-1)}{2}. \tag{2.16}$$

However, even if the solution can be posed theoretically for a wide amount of equations, it is possible to suggest a lower number of electrodes at the boundary and changing the behaviour of the method [98]. Once the mesh is computed the solution approximation takes place.

2.5.3 Finite-Element mesh warping

The forward problem can be solved by different methods, in which FEM is the most important technique. Nonetheless, an interesting alternative for redistributing and changing the initial values given can be gotten when a proper observation on the electric distribution is applied. This property has remarked in some works dedicated to EIT for the brain monitoring (see e.g. [5] and [11]).

Following to [93], a quickly modification of the finite-element distribution algorithm is described and proposed for human-head modelling, in which

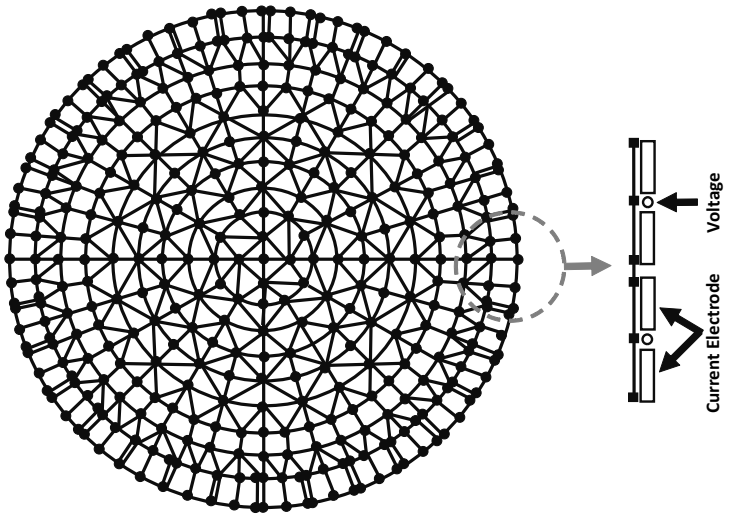

Figure 2.2: Finite-Element Method (see [98]).

an *elastic deformation* took place. In addition, the departure point for this method takes place on the principle of the minimum potential energy, as it is suggested in [94]. This deformation is a common technique used to search an equilibrium when FEM is employed to configure the mesh.

Hence, one of the main contributions of this reconstruction method relies, at least from the theoretical point of view, into the possibility to dash as smooth as desired from one finite-element distribution to another, in some sense, it reduces the posed instability for the inverse problem of (1.1).

However, a disadvantage of this method could be the increment in the complexity needed for the mathematical calculations, since the variation in the shape for FEM took place every iteration. Implying the increment on the computational resources used when FEM approximates the solution for the forward problem. Some strategies are studied in the following subsections to understand the functionality of FEM.

2.5.4 Gauss-Newton Model

This model is a recursive method to solve non-linear equations, and it is useful to obtain images by applying the following equation:

$$\theta_{k+1} = \theta_k + \alpha \left(J_k^t J_k + \lambda W\right)^{-1} \left(J_k^t W \left(z - h(\theta_k)\right)\right) - \lambda W(\theta_k), \qquad (2.17)$$

where θ is the unknown physics vector (it could be the conductivity or the resistance); λ is the regularization parameter, and J_k is the Jacobian matrix such as:

$$J_{k,i,j} = \frac{\partial(z_i - h_i(\theta))}{\partial\theta_j}, \tag{2.18}$$

in which z is the physic vector measurement of the electric potential, W denotes the regularization matrix, and $h(\theta_k)$ refers to the observation model obtained by FEM (see e.g. [98]).

This model is based on the Newton-Raphson method, in which, all the modifications and variations on the method are taken into account. This method is exposed in further sections, which main goal is to obtain better results for the forward and inverse problems (see e.g. [93]).

2.5.5 Backprojection Model

Considering the electrical conductivity equation (1.1), it follows:

$$\text{div}\,(\sigma \text{grad} u) = 0, \tag{1.1}$$

where σ is the conductivity and u is the electric potential. Then

$$\sigma\frac{\partial U}{\partial n} = j \in \partial\Omega, \tag{2.19}$$

where u is the electric potential, j is the current density in the boundary and Ω is the main domain.

Thus, when the variations in the equations (1.1) and (2.19) are considering, the variation in the conductivity σ is referred as $\delta\sigma$, and the variation of the electric potential U is also denoted as δU, such that:

$$\text{div}\,(\sigma \text{grad}\delta u) + \text{ div}\,(\delta\sigma \text{ grad } u) = 0 \in \Omega. \tag{2.20}$$

Moreover, the equation can be exposed as:

$$\sigma\frac{\partial(\delta u)}{\partial n} + \delta\sigma\frac{\partial u}{\partial n} = 0 \in \partial\Omega. \tag{2.21}$$

So, the linearising of the main problem is presented as follows:

$$\nabla^2\delta u = -\text{div}(\delta\sigma)\text{grad}u \in \Omega, \tag{2.22}$$

$$\frac{\partial(\delta u)}{\partial n} = 0 \in \partial\Omega. \tag{2.23}$$

The linearising of the inverse problem is related to the equations (2.22) and (2.23) becomes $\delta u|_{\partial\Omega}$ due to the variation in the electric potential presented in the boundary. A constant increasing $\delta\sigma$ determines by the different dipoles setting at the boundary.

The equations (2.22) and (2.23) are simplified using the coordinates (u, v), where $V > \frac{1}{2}$ and P is defined for a rectangular region:

$$\nabla^2 \delta u = -\frac{\partial(\delta\sigma)}{\partial u} \in P, \tag{2.24}$$

$$\frac{\partial(\delta u)}{\partial v} = 0 \in \partial P = v > \frac{1}{2}. \tag{2.25}$$

Following to [9], the next statement can be represented as the average of the functions:

$$\delta\sigma = \frac{1}{m}\sum_{j=1}^{m} \mathbf{W}(s, \omega_j)|_{s=u(s,\omega_j)}(2V(x, \omega_j - 1)), \tag{2.26}$$

where m is the number of electrodes, $\mathbf{W}$ is denoted as the boundary measure voltage, ω is represented by the position of the electrode, and v is the current intensity function (see e.g. [101]).

2.5.6 Tikhonov's Regularization Method

Following to [35], this method is frequently used to express non-linear solutions into a finite set of linear solutions. Furthermore, supposing that for a continuous region $\Delta\Omega$ within the domain Ω, the following equation:

$$J \cdot x = \delta u, \tag{2.27}$$

where J is the Jacobian matrix related to the conductivity σ; $x \in \mathbb{R}^m$ represents a perturbation in the conductivity distribution σ and $\delta u \in \mathbb{R}^{m\times n}$ denotes the derivative matrix for u.

Then, following to [48] and by using the *least squares conjugate gradient* method, the inverse problem of (1.1) can be approached through the following equation:

$$R_{\mathcal{E}} = \min_x \|J \cdot x - \delta u\|, \tag{2.28}$$

where $\|\cdot\|$ is the Cartesian norm for the Banach Space, $\|x\| < \mathcal{E}$ and $\mathcal{E} > 0$, being eqn. (2.28) equivalent to the *Tikhonov regularization method*, implying that it can be rewritten as follows:

$$\left(J^T J + \alpha^2 I\right) x_\alpha = J^T \delta u, \tag{2.29}$$

where α is the Tikhonov's parameter [92].

Moreover, the eqn. (2.27), it can be solved as an optimization problem, in which the minimum η needs to be found, as follows:

$$\eta = x^T J^T J \cdot x - J^T \delta u x, \tag{2.30}$$

in this equation $\|x\|^2 \leq \mathcal{E}^2$ is also known as the TRSP for the equation (2.28), and its approximation is given for the equation (2.30) (see e. g. [6] and [34]).

The problem relies in searching a continuous region $\triangle\Omega$ inside the domain Ω that depends on FEM rules. The computational complexity is still a problem that increases the calculus of η due to the number of iterations needed to reach a possible solution (see e.g. [98]).

In addition, TRSP is noise sensible and incorporates the Tikhonov's regularization method, which let us approximate better the conductivity σ within the domain Ω. This method is exposed in detail in further sections.

2.6 Simulations

The simulations performed using FEM, in which the forward problem was the backbone for this state of-the-art. Then, just before doing the simulations, it is proposed a methodology section that explains how to use this numerical method. This methodology is explained in the following subsection describing the numerical method.

2.6.1 Methodology

The methodology used in FEM is shown below:

1. The problem needs to be formulated as a variational method.

2. The independent variables' domain should be divided into subdomains and fully filled with finite-elements.

3. Once the subdomains are located and filled, the variational problem is obtained as a system of equations.

4. Finally, the numerical calculation takes place with this system of equations.

The variational method is obtained by dividing the domain into a fixed number of finite-elements. In this case, each finite-element represents an unknown value, and the resolution depends upon the created mesh. As it was mentioned before, an arbitrary domain could be approximated by polygons, and each polygon is divided into a fix number of elements, that it could be a triangle or a quadrangle.

Thus, the complete polynomial order would be expressed as:

$$\Pi_m (x, y) = \sum_{k,l=0}^{m} \alpha_{kl} x^k y^l, \tag{2.31}$$

where α is a constant and (x, y) represents a coordinate in the plane; in such case, the function obtained is $U(x, y)$ in symmetrical nodes, $\frac{1}{2}(m + 1)(m + 2)$ set in a triangle.

Three special cases exist with triangle representation $\overline{P_1 P_2 P_3}$ with the coordinates of the edges beginning at (x_1, y_1), (x_2, y_2) and (x_3, y_3).

Following to [98], the finite-element generation is represented by a triangle shape, the mathematical equations express roughly FEM employment.

So, the following equation represents the lineal case when $m = 1$.

$$\Pi_1(x, y) = \alpha_1 + \alpha_2 x + \alpha_3 y = \sum_{j=1}^{3} U_j p_j^{(1)}(x, y),$$

where $\{U_j\}_{j=1}^{3}$ are values of the function $U(x, y)$ on the vertices p_j that are represented in the following statement:

$$p_j^1(x, y) = \frac{1}{C_{jkl}} (\tau_{kl} + \eta_{kl} x - \xi_{kl} y) = \frac{D_{kl}}{C_{jkl}}. \tag{2.32}$$

Moreover,

$$\tau_{kl} = x_k y_l - x_l y_k, \quad \xi_{kl} = x_k - x_l, \quad \eta_{kl} = y_k - y_l.$$

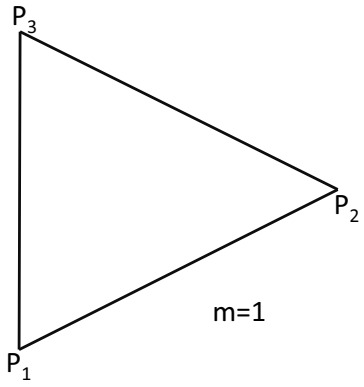

Figure 2.3: Triangle shape for the FEM, lineal model.

This lineal method is fully represented as:

$$D_{kl} = \det \begin{bmatrix} 1 & x & y \\ 1 & x_k & y_k \\ 1 & x_l & y_l \end{bmatrix}. \tag{2.33}$$

Furthermore, with any (j,k,l) permutation of $(1,2,3)$, it provokes that the modulus will be twice times the area of the triangle $\overline{P_1P_2P_3}$:

$$C_{jkl} = \det \begin{bmatrix} 1 & x_j & y_j \\ 1 & x_k & y_k \\ 1 & x_l & y_l \end{bmatrix}. \tag{2.34}$$

It is more easy to appreciate that the vertices can be calculated as:

$$p_j^{(1)}(x_k, y_k) = \begin{cases} 1 & (j=k) \\ 0 & (j \neq k) \end{cases} \quad (1 \leq j,k \leq 3).$$

The meshing process could be more accurate if the main triangle is divided into small triangles, such as the image presented in figure 2.4.

This is an important case to be considered, because it helps to obtain a more accurate solution for the polynomial. For this case, the polynomial representation is:

$$\Pi_2(x_k, y_k) = \sum_{j=1}^{6} U_j p_j^{(2)}(x,y),$$

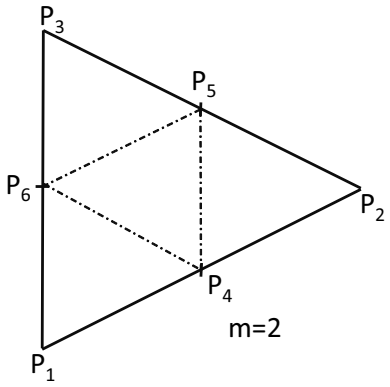

Figure 2.4: Finite-Element Method, refined triangle.

where $\{U_j\}_{j=1}^{6}$ represent the values of $U(x,y)$ at the vertices $P_j(1,2,3)$ and the intermediate values $P_j(4,5,6)$ for the sides P_1P_2, P_2P_3 and P_3P_1 respectively.

Then, the equation $p_j^{(2)}(x,y);(j=1,2,\ldots,6)$ is given according to:

$$p_j^{(2)}(x,y) = p_1^{(1)}(2p_1^{(1)} - 1),$$

with similar data for $p_2^{(2)}(x,y)$ and $p_3^{(2)}(x,y)$:

$$p_2^{(4)}(x,y) = 4p_1^{(1)}p_2^{(1)}.$$

Additionally, in the same manner, the vertices $p_5^{(2)}(x,y)$ and $p_6^{(2)}(x,y)$ are obtained by using the following statement:

$$p_j^{(2)}(x_k,y_k) = \begin{cases} 1 & (j=k) \\ 0 & (j\neq k) \end{cases} \quad (1\leq j,k\leq 6)$$

As well as in the previous cases, this triangle frame can be better adapted more by dividing into smaller triangles, such as in the figure 2.5.

For the last case, in which the triangle shape grants more accuracy, the polynomial equation is presented as in the following equation with order $m=3$:

$$\Pi_3(x,y) = \sum_{j=1}^{10} U_j p_j^{(3)}(x,y),$$

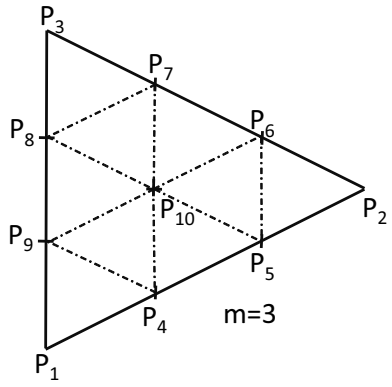

Figure 2.5: Finite-Element Method, triangle shape with polynomial order three.

in the last statement, $\{U_j\}_{j=1}^{3}$ represent the values for $U(x,y)$, in which the vertices P_1, P_2, P_3 and $\{U_j\}_{j=4}^{9}$ are the values for the intermediate intersections of the sides, for this case U_{10} is the value at the center on the figure.

Thus, the basic expressions are given for:

$$p_1^{(3)}(x,y) = \frac{1}{2}p_1(3p_1-1)(3p_1-2),$$

such as the last statement, $p_2^{(3)}(x,y)$ and $p_3^{(3)}(x,y)$ are obtained in similar manner.

Moreover, the other statements for the triangle shape are:

$$p_4^{(3)}(x,y) = \frac{9}{2}p_1p_2(3p_1-1),$$

$$p_5^{(3)}(x,y) = \frac{9}{2}p_1p_2(3p_2-1),$$

like in the previous calculus, the other vertices $p_6^{(3)}(x,y), \ldots, p_9^{(3)}(x,y)$ are computed similar.

Finally, the last vertex is computed as follows:

$$p_{10}^{(3)}(x,y) = 27p_1p_2p_3.$$

The tenth parameter could be eliminated by using the lineal relation:

$$U_{10} = \frac{1}{4}\sum_{j=4}^{9} U_j - \frac{1}{6}\sum_{j=1}^{3} U_j.$$

The last statements presented in previous cases for polynomial functions illustrated the finite-element's mesh generation. This process can be done for any number of finite-elements needed. Meanwhile the subdivision processes were done inside the domain. This procedure is not exclusively for the triangle shape. It can be used other geometrical figures, but the most used for this mesh, is the triangle shape.

The following figure 2.6 illustrates the common mesh generation for a circle domain, in which the accuracy and resolution depend upon the number of finite-elements subdivision.

In the subsequently section, PDE toolbox is used in order to obtain an approximation for analytical expressions.

2.6.2 Exact analytic expressions

In this subsection, FEM is used to check the accuracy and the behaviour presented by solving the forward problem of (1.1). Consequently, FEM is used on four mathematical expressions to confirm and achieve the approximations. The mathematical expression used are:

- Exponential.
- Polynomial.
- Lorentzian.
- Sinusoidal.

These mathematical equations are very different, so, this selection helps to analyse the behaviour of FEM, when different expressions are used to approximate the solution to the forward problem of eqn. (1.1). In order to confirm the approximation of FEM, the domain to be used is the unit disk domain, because it is more convenient to work with it.

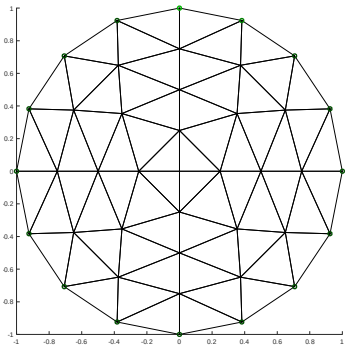

(a) 64 finite elements mesh.

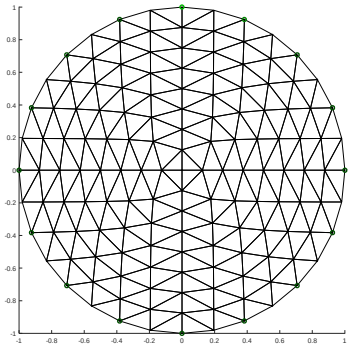

(b) 256 finite elements mesh.

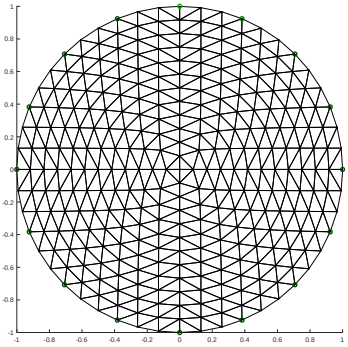

(c) 512 finite elements mesh.

Figure 2.6: Finite-Element Method mesh.

2.6.2.1 Exponential conductivity function

Let us suppose the following exponential conductivity σ equation:

$$\sigma = e^{x+y}. \tag{2.35}$$

Using the exact function solution for (2.35), the electric potential u is imposed in the boundary of the unit disk domain.

$$u|_{\Gamma} = e^{-x-y}. \tag{2.36}$$

Both equations (2.35) and (2.36) consider the solution to the forward problem of equation (1.1). For this reason FEM is used to confirm that both equations are solution. In this case, FEM uses the conductivity function σ

and approximate the electric potential u that it is the solution for the forward problem and it is illustrated in figure 2.7.

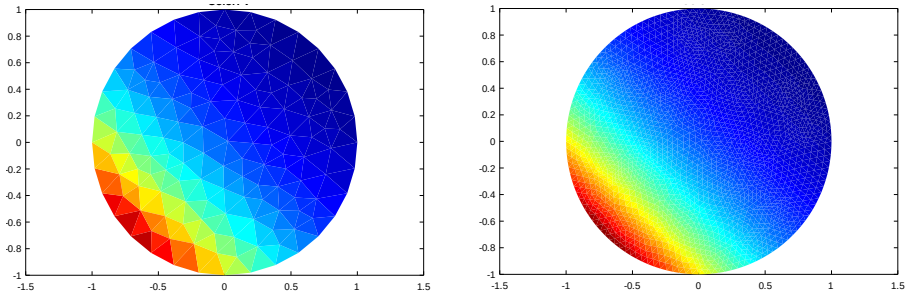

(a) Simple mesh **(b)** Complex mesh

Figure 2.7: a) Exponential function $\sigma = e^{x+y}$, b) FEM approximation.

2.6.2.2 Polynomial conductivity function

Other important case to understand the behaviour of FEM is the polynomial case, where conductivity function σ is represented as follows:

$$\sigma = a + cx + cy, \tag{2.37}$$

where a and c are coefficients that are used in the expression to change its behaviour.

The comparison between the exact solution and the approximation is needed, and the imposed boundary condition is the electric potential u. That it is considered as a solution for equation (1.1). It is presented below:

$$u|_\Gamma = \ln(a + cx + cy). \tag{2.38}$$

The polynomial case is approximated to obtain a solution by using FEM for the equations (2.37) and (2.38). This approximation is illustrated in the figure 2.8.

2.6.2.3 Lorentzian conductivity function

Likewise, in the last cases, this mathematical expression is used to understand the behaviour of FEM. This case is presented when the conductivity function

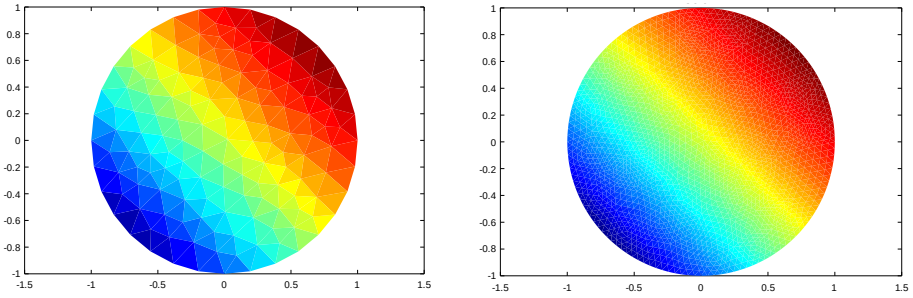

(a) simple mesh. **(b)** complex mesh

Figure 2.8: a) Polynomial function $\sigma = a + cx + cy$, b) FEM approximation.

σ possesses the following form:

$$\sigma = \left(\frac{1}{x^2 + L_c}\right) \cdot \left(\frac{1}{y^2 + L_c}\right), \tag{2.39}$$

where L_c is a parameter that cause a change in the expression given. Using the approximation of the exact solution, in which this electric potential u is presented as:

$$u|_\Gamma = \frac{1}{3}(x + L_c)^3 + \frac{1}{3}(y + L_c)^3 + L_c(x + y). \tag{2.40}$$

Following last cases, the solution is compared with the exact function. Thence, the equation (2.39) and (2.40) is used by FEM to approximate the solution. The approximation obtained is considered as the solution to the forward problem of equation (1.1). This approximation is illustrated in figure 2.9.

2.6.2.4 Sinusoidal conductivity function

This case is the most difficult among all analytical cases, it helps to understand better the behaviour of FEM and the relationship between the conductivity σ function and the electric potential u. For this special case, the mathematical expression that represents this function is:

$$\sigma = (2 + \cos(\omega\pi x)) \cdot (2 + \sin(\omega\pi y)), \tag{2.41}$$

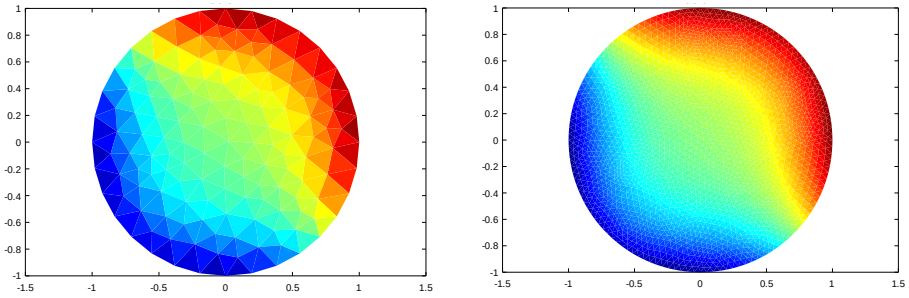

(a) mallado simple **(b)** mallado complejo

Figure 2.9: a) Lorentzian function $\sigma = \left(\frac{1}{x^2+L_c}\right) \cdot \left(\frac{1}{y^2+L_c}\right)$, b) FEM approximation.

where ω is the parameter to be used in order to modify the behaviour of the mathematical expression.

Then, the exact function is used to compare the result obtained by FEM. This function is the electric potential u, and it is represented as:

$$u|_\Gamma = \left(\frac{\tan(xy)}{2} + 1\right)^{-1}. \tag{2.42}$$

Such approximation is compared to confirm the solution to the forward problem of (1.1). For this comparison, the equations (2.41) and (2.42) are used to approach the forward problem, and the result is illustrated in the figure 2.10.

2.6.3 Geometrical conductivity functions

The analysis of FEM can not be completed without the analysis of geometrical conductivity functions σ. These geometrical conductivity functions are representative and are employed to determine the behaviour of FEM when non-smooth shapes within its domain are used.

The geometric shapes used here are:

- Circle at center.
- Five disk structure.

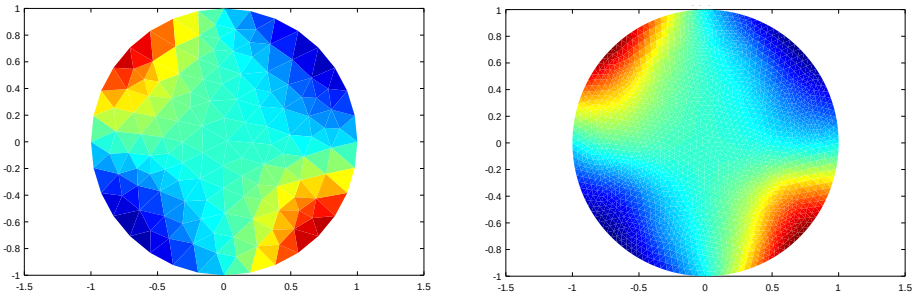

(a) Simple mesh **(b)** Complex mesh

Figure 2.10: a) Sinusoidal function $(2 + \cos(\omega\pi x)) \cdot (2 + \sin(\omega\pi y))$, b) FEM approximation.

- Triangles.

To perform this analysis, the mathematical tool known as EIDORS is used, confirming the possibility to use FEM to approximate the inverse problem, in which the conductivity σ function is unknown and the electric potential u is given at the boundary.

In this case, the mesh will be computed for 16 electrodes equidistantly set at the boundary of the domain. Figure 2.11 illustrates the mesh to be employed by the FEM, including the electrodes used that will be utilized in the following subsections.

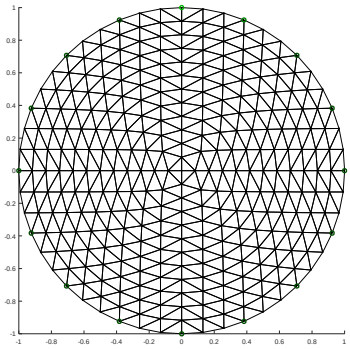

Figure 2.11: FEM domain with 16 electrodes mesh.

2.6.3.1 Circle at center conductivity function

For this case, in which a geometric case is employed within a unit disk domain, the conductivity function σ is represented by a small disk at the center of the domain, for this conductivity its value is fixed at $\sigma = 40$. The figure 2.12 illustrates the description given.

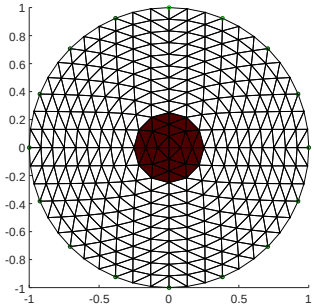

Figure 2.12: Circle at center within a unit disk domain.

In this case, several approximations were calculated by the lack of a regularization process. Despite the absence of a regularization process, the approximation of the inverse problem of equation (1.1) has been achieved by FEM.

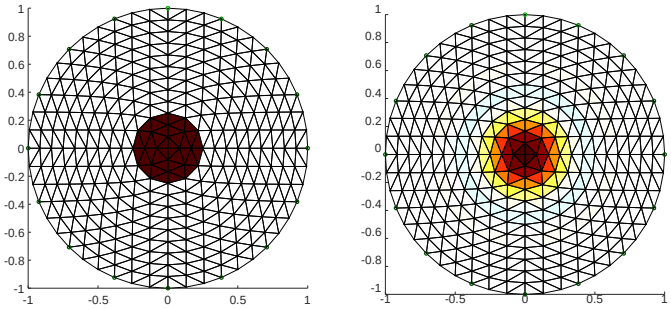

(a) Original conductivity function.

(b) Approximation done.

Figure 2.13: FEM approximation.

The figure 2.13 illustrates the approximation obtained, even when the

approximation is acceptable, it is far to be the optimal approximation that the method can reach.

2.6.3.2 Five-disk structure conductivity function

The proposal conductivity function σ is a structure composed of five-disk at the center of the domain, in which all the disks inside posses different conductivity values. The smallest circle possesses a conductivity function $\sigma_1 = 100$, the second disk has $\sigma_2 = 50$, the third one has $\sigma_3 = 30$, the fourth possesses $\sigma_4 = 20$ and the last one $\sigma_5 = 10$. The figure 2.14 illustrates the distribution for this conductivity function.

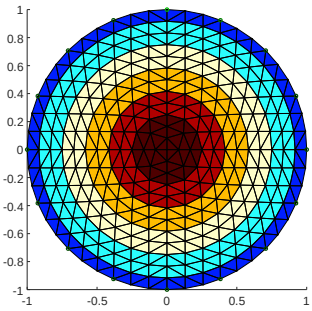

Figure 2.14: Five-disk structure conductivity function within a unit disk domain.

The comparison is performed in order to analyse the behaviour of FEM, when a different conductivity function is presented. The figure 2.15 shows this comparison.

This sample was performed to confirm the possibility to approximate the solution by means of FEM, even though the distributions inside the unit disk domain are non-smooth.

In the figure 2.15, the approximation could be considered acceptable. Nevertheless, the approximation was made without a regularization process. The complexity of this conductivity structure demonstrates the necessity of the use of a regularization process.

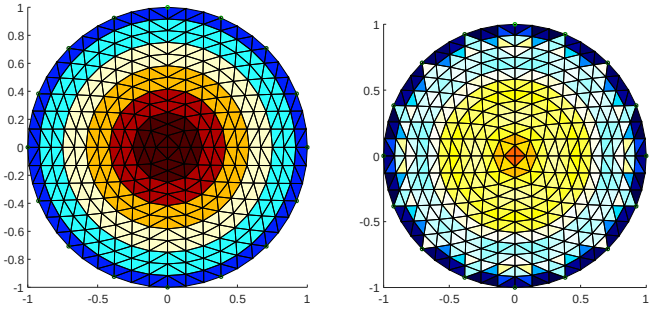

(a) Original conductivity fucntion. **(b)** Finite-Element Method

Figure 2.15: Comparison using FEM.

2.6.3.3 Triangles conductivity function

FEM stand with difficulty to make an approximation when the conductivity σ inside the domain possesses edges. This difficulty is due to the mesh generation procedure. For this special case, it will be important to determine the behaviour and the possibility to obtain an approximation. The comparison for this conductivity structure is illustrated in the figure 2.16.

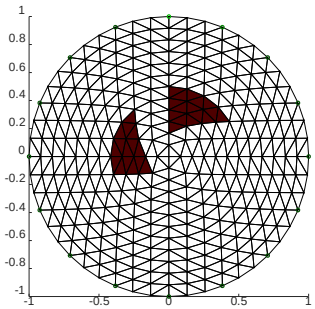

Figure 2.16: Triangle shape conductivity function within a unit disk domain.

Based upon the result presented in figure 2.16, it is necessary to use a regularization process to better approach solutions for the inverse problem. Furthermore, FEM has the possibility to work with the inverse problem regardless the conductivity σ function inside the domain. The approximation is exposed in the figure 2.17.

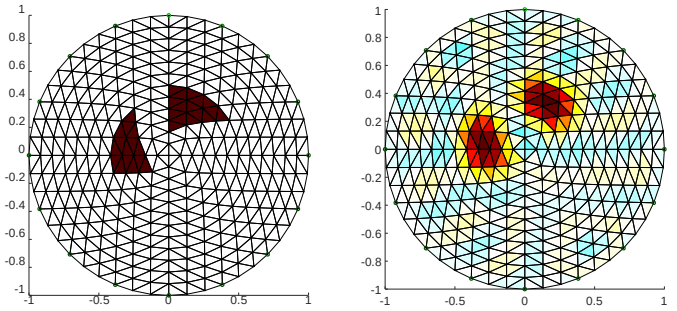

(a) Original conductivity. **(b)** Finite-Element Method.

Figure 2.17: FEM approximation.

The approximation shown in the figure 2.17 is not acceptable, where the main obstacle is the mesh generation procedure and the absence of a regularization process. This regularization process shall help to improve the results of the approximation for non-smooth shapes.

2.6.4 Discussion

The employment of the Ampere's law in differential form is actually the very foundation of the Electrical Impedance Tomography, since when considering the static case (this is no displacement electrical currents are taken into account), it rises up the so-called electrical impedance equation for which we analysed within these paragraphs two kinds of Dirichlet boundary value problems: the forward problem and the inverse problem.

About the forward problem for the electrical impedance equation the conductivity function is known, as well the boundary condition. This is the electric potential or voltage is known long around the boundary of a certain domain, and the task consists into the approaching of a solution fulfilling such boundary condition. In the second case, only the boundary condition (voltage) is known, and given the correct statement of the problem provided by A. P. Calderon, one and only one conductivity function corresponds to such boundary condition. Thus, the inverse problem relies in the approximation of such conductivity function. This is a brief description of the electrical impedance equation.

Since, the forward problem is to be deeply analysed in further chapters,

the classical variations of the Finite-Element Method, to approach solutions for the inverse problem, find their place into our dissertation as a critical reviewed of the State-of-the-art. Therefore, we state the discussion on certain the variations of the sparse matrix method, that posses among their advantages the possibility introducing regularization methods. Illustrating these paragraphs a general background of experimental results, exploiting such properties, come along with the general theoretical description.

Immediately, we briefly study the trust region sub-problem method which provides a fast convergence for the inverse problem by reposing the question as a minimization problem bias the employment of Jacobian matrices.

Only then, we completely enter the formal study of the Finite-Element Method employed for solving partial differential equations in the plane. Of course, we pay full attention to the electrical impedance equation, therefore, the location of electrodes along the boundary is briefly studied and from this point we consider the question of how to trace the related mesh. The basis stated we go straight forward to reviewed two different variations of the Finite-Element Method to solve the inverse problem. The first one is the Gauss-Newton model, and it is shown that it represents one of the simplest and lowest computational costed methods, with the corresponding consequence of a low convergence.

The second variation is the Backprojection model whose main strength is the simple correlation among the electrodes distributed on the perimeter of the domain.

Independently of the Finite-Element Method selection it is highly advised the employment of a regularization method. Many of these techniques are available in the literature, but specifically in this work, the Tikhonov's regularization method was selected because methodologically is very often recommended, yet, several previous work could not exploit it in full scale because of the high computational accuracy that the method requires. Nonetheless, the experimental results will demonstrated that such limitation was indeed overpassed allowing a considerable better development of this regularization method.

More precisely, the simulations that extend stilled the previous statements are methodological founded in the programming and execution of the Finite-Element Method for two different kinds of conductivity distributions: those that posses an exact mathematical representation and those defined by geometrical figures contained within the domain. On behalf of briefness only the Gauss-Newton variation is reported, and about it was shown that

the convergence was considerably better for the analytical cases, as it was somehow expected since for such cases no discontinuities are present.

The most important method is FEM that demonstrates its capability to approximate the solution of (1.1). This method can perform a faster and accurate approximation to the forward and inverse problems, but it depends upon the mesh generation procedure. Nevertheless, the mesh generation represents a problem in terms of the time-computing and the computational-resources used.

Meanwhile, a robust mesh possesses great resolution, this calculus is very difficult to perform and in some cases impossible to achieve. However, the employment of a simple mesh represents a non-accurate approximation, but it can be computed very fast. In some cases, the size of the mesh is not enough to calculate a precise solution. In those cases, the conductivity σ function needs to be studied in order to understand its behaviour and its complexity to determine if the method could achieve a positive solution.

FEM method can achieve approximations for the analytical and geometric conductivity σ functions. Nevertheless, a correct approximation is depended on the inclusion of a regularization process. In addition, the lack of this regularization procedure does not represent a problem when simple conductivity functions are approximated. Furthermore, when non-smooth conductivity σ functions are employed, the regularization process determines the possibility to reach a solution. Moreover, if smooth conductivity σ functions are utilized, the regularization process can perform a more accurate approximation.

2.6.5 Conclusions

The goal of this state-of-the-art chapter is to analyse, study and illustrate the most important techniques used in EIT problem. In this particular case, EIT problem can be calculated depending on the initial conditions. This problem is divided into two sub-problems, in which the more easy to solve is the forward problem, the second one is very complicate to approximate.

In this brief analysis, FEM approximates both problems, emphasizing its results into the forward problem, performing with an optimal accuracy. FEM method gives this opportunity to resolve both problems with minimal changes in its structure.

For this reason, FEM is considered in this study as a principal in comparison with proposed novel methods, but it requires an exhaustive analysis to determine if the function to be used can be solved with this method. For

example, the usage of geometrical figures that posses corners or non-smooth shapes represents a hard task for FEM.

Furthermore, the possibility to employ a regularization method that helps to improve the approximation makes it a powerful tool to solve the eqn. (1.1). Nevertheless, the method is considered unstable because the mesh computations changes the approximation.

The maximum resolution does the method can achieve is determined by the size of the mesh. Concerning the computational resources needed to perform an approximation, the mesh size is taken into consideration. For this reason, EIT is not considered as standard Medical Imaging technique.

Chapter 3

Forward Dirichlet boundary value problem

In this chapter, the forward problem of EIT is analysed in order to develop a novel technique that can approach the solution of the problem of the equation (1.1). In this case, following to [56], the Pseudoanalytic Function Theory is applied to design an algorithm based upon the Taylor's series in formal power (see e.g. [72]). The designed algorithm is used to approximate the solution to cited problem. Furthermore, Finite-Element Method (FEM) is utilized to compare the results of both algorithms.

According to [98], most of the algorithms that approximate the solution to the inverse problem are based on iterative methods, which examine solutions to the forward problem and introduce certain variations in the conductivity σ, attempting to minimize the difference between the approximated solution u_{app} and the boundary condition $u_c|_\Gamma$. It is convenient to emphasize that the majority of these methods are based on variations of FEM (see e.g. [98] and [97]).

Furthermore, the usage of techniques upcoming from completely different branches of the applied mathematics (see e.g. [58] and [85]), could well show off new information about the behaviour of the solutions for the forward problem for equation (1.1) in the plane, which eventually could allow to propose new techniques for analysing the inverse problem. Moreover, its common classification of ill-posed problem could be reconsidered (see e.g. [43]).

Additionally, the discovering of the relationship between two-dimensional case of (1.1) and the Vekua equation (see e.g. [95]), possesses a special rel-

evance, since it opens a new path for analysing the solutions of (1.1) in the plane by using the so-called Taylor's series in formal powers (see e.g. [13]).

As a matter of fact, the Vekua equation has been deeply studied in a variety of interesting works published along the last five decades, before the relationship has been first noticed. Indeed, two of the most important works published concerning the Vekua equation were [13] and [95].

It is not clear how to adapt the elements of the Pseudoanalytic Function Theory to experimental physical requirements [54], so this chapter is dedicated to this study and shall give a possible contribution for the Electric Impedance Tomography problem by providing the elements to employ this theory and its adaptation in various cases that can easily be identified with physical experimental models.

3.1 Taylor's series in formal powers method

Following to [54], the elements of the Pseudoanalytic Function Theory have permitted to establish a relation between the bi-dimensional electrical impedance equation (1.1) and a special class of the Vekua equation (see e.g. [95]).

Thanks to this, the general solution can be rewritten as follows:

$$\operatorname{div}(\sigma \operatorname{grad} u) = 0, \tag{1.1}$$

where σ is the conductivity function, u represents the electric potential in terms of the so-called Taylor's series in formal powers (see e.g. [13]). This relation was noticed independently first in [56] and [2]. Furthermore, in a wide variety of works dedicated to the mathematical and numerical analysis contributed to this field (see e.g. [56], [74] and [71]).

This new approximation is very important in order to obtain a solution to the forward problem of (1.1), which is extremely useful to understand better the inverse problem. The inverse problem can also be known in the literature as EIT problem (see e.g. [98]).

This section is dedicated to the numerical analysis in the forward problem of equation (1.1), using the simplified and improved method presented for first time in [86] and based on the conjecture proposed (see e.g. [76] and [75]).

In this chapter, a wide variety of analytic and geometric cases is studied to represent a different type of conductivity functions that could be used to represent the behaviour of the method. Indeed, every illustrated sample is

based on the total parameters used to emphasize a possible characterization of the developed method presented in published papers (see e.g. [80] and [86]).

The results will be shown further, and it could be classified as:

1. Samples that correspond to exact analytic expressions and geometric shape distributions, both inside a unit disk domain in the plane.

2. Functions that do not require a regularization process to be approximated.

The importance of this case is to show that the improved method could approach solutions for (1.1). In this sense, the main contribution of this chapter is: the possibility to use this method to obtain a solution for the forward problem, regardless the shape of the domain and the conductivity presented inside. The boundary Γ of the domain Ω and the conductivity σ could be a smooth or non-smooth shape, and the method should approximate the solution well (see e.g. [84]).

Nevertheless, a disadvantage of this method is the limit number of approximated solutions. This situation is due to the technique employed to obtain the coefficients. Considering the technique, the boundary condition is approached by using a fixed number of base functions. In this chapter, a characterization takes place to prove the efficiency of the proposed method.

3.1.1 Preliminaries

In this section, the mathematical preliminaries will be exposed in order to focus this work in the Pseudoanalytic Funtion Theory (see e.g. [13]).

Thence, following this theory, it considers a pair of function complex-valued (F, G) which fulfils the condition:

$$\mathrm{Im}\left(\overline{F}G\right) > 0, \tag{3.1}$$

where $\overline{F}$ denotes the complex conjugate of $F : \overline{F} = \mathrm{Re}F - i\mathrm{Im}F$, and $i^2 = -1$ is the standard imaginary unit.

Thus, any complex-valued function W can be expressed by the linear combination of F and G, such as:

$$W = \phi F + \psi G,$$

where ϕ and ψ are real-valued functions. So, any two complex functions that fulfil(3.1) should be called (F,G)-*generating pair*. Professor L. Bers also introduced the (F,G)-*derivative* of the function W according to the expression:

$$\partial_{(F,G)}W = (\partial_z\phi)\,F + (\partial_z\psi)\,G, \tag{3.2}$$

this derivative exists if and only if

$$(\partial_{\bar{z}}\phi)\,F + (\partial_{\bar{z}}\psi)\,G = 0, \tag{3.3}$$

where

$$\partial_z = \partial_x - i\partial_y,\ \ \partial_{\bar{z}} = \partial_x + i\partial_y.$$

We can notice that these operators are classically introduced with the factor $\frac{1}{2}$ but it is more convenient to work without it at least for this work.

Then, introducing the following functions:

$$\begin{array}{ll} A_{(F,G)} = \frac{\overline{F}\partial_z G - \overline{G}\partial_z F}{F\overline{G}-G\overline{F}}, & a_{(F,G)} = -\frac{\overline{F}\partial_{\bar{z}} G - \overline{G}\partial_{\bar{z}} F}{F\overline{G}-G\overline{F}} \\ B_{(F,G)} = \frac{F\partial_z G - G\partial_z F}{F\overline{G}-G\overline{F}}, & b_{(F,G)} = -\frac{G\partial_{\bar{z}} F - F\partial_{\bar{z}} G}{F\overline{G}-G\overline{F}}; \end{array} \tag{3.4}$$

the expression (F,G)-derivative shown in (3.2) turns into

$$\partial_{(F,G)}W = \partial_z W - A_{(F,G)}W - B_{(F,G)}\overline{W}, \tag{3.5}$$

and the condition (3.3) will be rewritten as:

$$\partial_{\bar{z}}W - a_{(F,G)}W - b_{(F,G)}\overline{W} = 0. \tag{3.6}$$

The mathematical expression exposed in (3.4) are called *characteristics coefficients* of the generating pair (F,G), whereas the functions W that are solutions of the equation (3.6) are called (F,G)-*pseudoanalytic* functions. As a matter of fact, the equation (3.6) are also known as the Vekua equation (see e.g. [95]), and it is the basis of this work.

Furthermore, the following statements were exposed for first time in [13], and they are adapted for the purposes of the current work (see e.g. [56]).

Theorem 1. *The elements of the generating pair (F,G) are (F,G)-pseudoanalytic:*

$$\partial_{(F,G)}F = \partial_{(F,G)}G = 0.$$

Remark 1. *Let p be a non-vanishing function within a bounded domain $\Omega(\mathbb{R}^2)$. The function*

$$F_0 = p,\ G_0 = \frac{i}{p}, \tag{3.7}$$

establish a generating pair, whose characteristic coefficients (3.4) are:

$$\begin{array}{c} A_{(F_0,G_0)} = a_{(F_0,G_0)} = 0, \\ B_{(F_0,G_0)} = \frac{\partial_z p}{p}, \\ b_{(F_0,G_0)} = \frac{\partial_{\overline{z}} p}{p}. \end{array} \tag{3.8}$$

Definition 1. *Let (F_0, G_0) and (F_1, G_1) be two generating pair of the form (3.6) and let their characteristics coefficient fulfils the following relation*

$$B_{(F_1,G_1)} = -b_{(F_0,G_0)}. \tag{3.9}$$

Thus, the pair (F_1, G_1) are called the successor of the pair (F_0, G_0). Meanwhile (F_0, G_0) are called the predecessor of (F_1, G_1).

Definition 2. *Considering:*

$$\{(F_m, G_m)\},\ m = 0, \pm 1, \pm 2, ...$$

as a set of generating pair, where each (F_{m+1}, G_{m+1}) is a successor of (F_m, G_m).

Therefore, the $\{(F_m, G_m)\}$ set is going to be known as a generating sequence. Moreover, if it exists a number c such that $(F_m, G_m) = (F_{m+c}, G_{m+c})$ the generating sequence will be periodic, with period c.

Lastly, if $(F, G) = (F_0, G_0)$, it will say that the generating pair (F, G) is embedded into the generating sequence $\{(F_m, G_m)\}$.

Theorem 2. *Let (F_0, G_0) be a generating pair of the form (3.7), and let p be a separable-variable function:*

$$p = p_1(x) \cdot p_2(y),$$

where $x, y \in \mathbb{R}$. Then, (F_0, G_0) will be embedded into a generating sequence with $c = 2$ period, such that:

$$F_m = \frac{p_2(y)}{p_1(x)},\ G_m = i\frac{p_1(x)}{p_2(y)};$$

when the subindex m is an even number, and

$$F_m = p_1(x) \cdot p_2(y),\ G_m = \frac{i}{p_1(x) \cdot p_2(y)};$$

when m is an odd number.

Furthermore, if $p_1(x) \equiv 1,\ x \in \Omega\,(\mathbb{R}^2)$, it is easy to verify that the generating sequence in which (F, G) is embedded will be periodic, but with periodic $c = 1$.

The concept of the (F, G)-integral was also introduced by L. Bers such as a complex-valued function. In order to know more about this concept, you should go over the specialized literature (see e.g. [13] and [56]), in which the concept and the existence of this integral are described. In the following paragraphs, each complex-valued function contained into an (F_0, G_0)-integral will be by definition integrable.

Definition 3. *Let (F_m, G_m) be a generating pair of the form (3.7). Its adjoin generating pair (F_m^*, G_m^*) is defined according to the formulas:*

$$F_m^* = -iF_m, \quad G_m^* = -iG_m.$$

Definition 4. *The (F_m, G_m)-integral of a complex-valued function W (when it exists (see e.g. [13])) is defined as:*

$$\begin{gathered}\int_\tau W d_{(F_m,G_m)}z = \\ = F_m Re \int_\tau G_m^* W dz + G_m Re \int_\tau F_m^* W dz,\end{gathered}$$

where τ is a rectifiable curve within the domain in the complex plane.

Precisely, if it is considered the (F_m, G_m)-integral of the (F_m, G_m)-derivative of W, the equation obtained is:

$$\begin{gathered}\int_{z_0}^{z} \partial_{(F_m,G_m)} W(z) d_{(F_m,G_m)}z = \\ = -\phi(z_0)F_m(z) - \psi(z_0)G_m(z) + W(z).\end{gathered} \tag{3.10}$$

where $z = x + iy$, and z_0 is a fixed point in the complex plane.

According to the theorem 1, the (F_m, G_m)-derivative of F_m and G_m vanish identically, thus the expression (3.10) can be considered as the $\partial_{(F_m,G_m)}W$.

3.1.2 Formal powers

Definition 5. *The formal power* $Z_m^{(0)}(a_0, z_0; z)$ *belonging to the generating pair* (F_m, G_m)*, with the formal degree* 0*, complex constant coefficient* a_0*, center at* z_0*, and depending upon* $z = x + iy$*, is defined according the following expression:*

$$Z_m^{(0)}(a_0, z_0; z) = \lambda F_m(z) + \mu G_m(z), \tag{3.11}$$

where λ *and* μ *are complex-valued constants fulfilling the condition:*

$$\lambda F_m(z_0) + \mu G_m(z_0) = a_0.$$

The formal powers with higher n *degrees are approached by the recursive formulas shown subsequently:*

$$Z_m^{(n)}(a_n, z_0; z) = \\ = n \int_{z_0}^{z} Z_{(m-1)}^{(n-1)}(a_n, z_0; z)\, d_{(F_m, G_m)} z,$$

where $n = 1, 2, 3, ...$

Notice the integral operators in the right-hand side of the last equation are (F_m, G_m)*-antiderivatives.*

Theorem 3. *The formal powers posses the coming properties:*

1. *Every* $Z_m^{(n)}(a_n, z_0; z)$*,* $n = 0, 1, 2, 3, ...$ *is a* (F_m, G_m)*-pseudoanalytic function.*

2. *Let* $a_n = a_n' + i a_n''$*, where* $a_n', a_n'' \in \mathbb{R}$*. The following relation holds that:*

$$Z_m^{(n)}(a_n, z_0; z) = \\ = a_n' Z_m^{(n)}(1, z_0; z) + a_n'' Z_m^{(n)}(i, z_0; z).$$

3. *Finally,*

$$\lim_{z \to z_0} Z_m^{(n)}(a_n, z_0; z) = a_n (z - z_0)^n.$$

Theorem 4. *Let* W *be an* (F_m, G_m)*-pseudoanalytic function. Then it can be expressed in terms of the so-called Taylor's series in formal powers, such as:*

$$W = \sum_{n=0}^{\infty} Z_m^{(n)}(a_n, z_0; z). \tag{3.12}$$

Furthermore, since any (F_m, G_m)*-pseudoanalytic function* W *accepts this expansion, (3.12) is an analytical representation of the general solution for the Vekua equation (3.8).*

3.1.3 Bi-dimensional electrical impedance equation

Considering the electrical impedance equation (1.1) in the plane:

$$\operatorname{div}(\sigma \operatorname{grad} u) = 0. \tag{1.1}$$

As it has been shown in several works (see e.g. [56] and [73]), if σ can be expressed by means of separable-variables function:

$$\sigma(x, y) = \sigma_1(x)\sigma_2(y), \tag{3.13}$$

by introducing the notations:

$$\begin{aligned} W &= \sqrt{\sigma}\left(\partial_x u - i\partial_y u\right), \\ p &= \left(\sigma_1^{-1} \cdot \sigma_2\right)^{\frac{1}{2}}; \end{aligned} \tag{3.14}$$

the equation (1.1) turns into the Vekua equation:

$$\partial_{\bar{z}} W - \frac{\partial_{\bar{z}} p}{p}\overline{W} = 0, \tag{3.15}$$

for which the functions:

$$F_0 = p,\, G_0 = \frac{i}{p}, \tag{3.16}$$

conform a generaiting pair.

From (3.14), and according to theorem 2, it is possible to verify that this pair is embedded into a generating sequence, with period $c = 2$, being p a separable-variable function.

3.2 Numerical approximation of the formal powers

In [80], it was studied an improved numerical method for approximating the elements in the finite subset of formal powers:

$$\left\{Z_0^{(n)}(1, 0; z), Z_1^{(n)}(i, 0; z)\right\}_{n=0}^{N}, \tag{3.17}$$

whose linear combination will allows to approximate any pseudoanalytic function W, solution of (3.15). Moreover, in [25], it was proven that the real parts

of the elements of (3.17), valued at the boundary Γ of the domain Ω, constitute a complete set to approach solutions for the forward problem of (1.1) in the plane.

Since the results of the integral expressions (3.10) are path independent (see e.g. [13]), the numerical calculations can be performed on a set of radial trajectories, whose origin coincides with the zero in the plane. Then, the following procedure is employed in each Radius R within the domain Ω, going from the coordinates origin until the boundary Γ.

Considering τ as a radius R within, the unit disk domain with center at $z_0 = 0$. For the interpolation process, it is used $P + 1$ equidistant points distributed on R, being the first $r[0] = 0$ and the last one $r[P] = 1$:

$$\left\{ r[p] = \frac{p}{P} \right\}_{p=0}^{P}. \tag{3.18}$$

It can immediately construct a set of coordinates according to the formulas:

$$\begin{aligned} x[p] &= r[p] \cos \theta_q, \\ y[p] &= r[p] \sin \theta_q; \end{aligned} \tag{3.19}$$

where θ_q is the angle which corresponds to R.

Following (3.7), the coordinates (3.19) can be employed to obtain the set of values:

$$\{F_0(z[p]), G_0(z[p])\},\ \{F_1(z[p]), G_1(z[p])\}; \tag{3.20}$$

where the complex-valued numbers $z[p]$ have the form:

$$z[p] = x[p] + iy[p].$$

The set of values of the adjoin pairs

$$\{F_0^*(z[p]), G_0^*(z[p])\},\ \{F_1^*(z[p]), G_1^*(z[p])\}, \tag{3.21}$$

will have the form shown in the Definition 3.

Using the expression (5), it follows that:

$$\begin{aligned} Z_0^{(0)}(1, 0; z[p]) &= F_0(z[p]), \\ Z_1^{(0)}(1, 0; z[p]) &= F_1(z[p]). \end{aligned}$$

Hereafter, each formal power with $n > 0$ will be always approximated considering $P + 1$ equidistant points within the closed interval $[0, 1]$. Taking

into account that not any methodological difference takes place when approximating the formal powers with the coefficients $a_n = i$, it will focus in the explanation for the cases when $a_n = 1$.

A numeric property was first noticed in [76], for approximating the formal powers, can significantly reduce the computer resources invested in the complete procedure, at the time it allows to employ a posed numerical method for analysing non-separable conductivity functions.

The statements presented before and proved in [76], together with representative samples are shown before.

Conjecture 1. *Let σ be an arbitrary conductivity function defined within a bounded domain $\Omega(\mathbb{R}^2)$. Then, it can be approximated by means of a piece-wise separable-variables function, as it is shown below:*

$$\sigma_{pw} = \begin{cases} \frac{x+g}{\chi_1-\chi_0+g} \cdot f_1(y) : x \in [\chi_0, \chi_1)\,; \\ \frac{x+g}{\chi_2-\chi_1+g} \cdot f_2(y) : x \in [\chi_1, \chi_2)\,; \\ \vdots \\ \frac{x+g}{\chi_K-\chi_{K-1}+g} \cdot f_K(y) : x \in [\chi_{K-1}, \chi_K]\,; \end{cases}$$

where g is a real constant that $x + g \neq 0 : x \in \Omega(\mathbb{R}^2)$; and $\{f_k\}_{k=1}^{K}$ are interpolating functions constructed with a finite number of samples $\mathcal{M}$ of the σ function. It is valued along an y-axis parallel lines within the subdomain of Ω, created when tracing the set of y-axis parallel lines $\{\chi_k\}_{k=0}^{K}$.

This piece-wise separable-variable conductivity function can be employed for numerically approximating the set of formal powers (3.21).

Remark 2. *Following to [76], let σ be an arbitrary conductivity function defined within a bounded domain $\Omega(\mathbb{R}^2)$. It can be considered as the limit case of a piece-wise separable-variables conductivity function, in which its form is presented as in the Conjecture 1, when the number of the subdomains K and the number of samples $\mathcal{M}$ at every sub-domain tend to infinity:*

$$\lim_{K,\mathcal{M}\to\infty} \sigma_{pw} = \sigma.$$

Furthermore, since:

$$\lim_{K,\mathcal{M}\to\infty} \frac{x+g}{\chi_k - \chi_{k-1} + g} = 1,\ k = 0, 1, ..., K;$$

according to the Theorem 2, the corresponding generating sequence will be periodic and its period is $c = 1$.

This immediately implies that:

$$F_0(z[p]) = F_1(z[p]) = F(z[p]),$$

it simplifies the reconstruction of the sets (3.20) and (3.21).

Using this property, the numerical formal powers $Z_0^{(n)}(z[p])$ at the points $z[p] = x[p] + iy[p]$, located along the radius R, can be approximated using a variation of the trapezoidal integration method over the complex plane:

$$\begin{gathered} Z^{(n)}(z[p]) = \delta F(z[p])\cdot \\ \cdot \mathrm{Re} \sum_{s=0}^{p-1} \left(Z^{(n-1)}(z[s+1]) \cdot G^*\left(z[s+1]\right)\right) dz[s] + \\ + \delta F(z[p]) \mathrm{Re} \sum_{s=0}^{p} \left(Z_1^{(n-1)}(z[s]) \cdot G^*\left(z[s]\right)\right) dz[s] + \\ + \delta G(z[p])\cdot \\ \cdot \mathrm{Re} \sum_{s=0}^{p-1} \left(Z_1^{(n-1)}(z[s+1]) \cdot F^*\left(z[s+1]\right)\right) dz[s] + \\ + \delta G(z[p]) \mathrm{Re} \sum_{s=0}^{p} \left(Z_1^{(n-1)}(z[s]) \cdot F^*\left(z[s]\right)\right) dz[s]; \end{gathered} \tag{3.22}$$

where

$$dz[s] = \left(z[s+1] - z[s]\right),$$

and δ is a real constant factor, empirically selected, that contributes to the numerical stability of the method.

It should remark that the usage of this expression (3.22), for approaching the formal powers, such as it was appointed in [76], implicitly performs a piece-wise polynomial interpolating function of degree 1, to relate every value $Z^{(n)}(z[p])$, for $p = 0, 1, ..., P$; and $n = 0, 1, ..., N$; taking into consideration the third property of the Theorem 3 that implies $\forall n > 0$:

$$Z_0^{(n)}(1, 0; z[0]) \equiv 0.$$

Thus, performing the full process for a wide enough quantity of Q of radii R, each one corresponding to some angle θ_q:

$$\left\{ \theta_q = q \cdot \frac{2\pi}{Q} \right\}_{q=0}^{Q-1}, \tag{3.23}$$

due to this, it will be able to approximate the finite set

$$\left\{\mathrm{Re}Z^{(n)}\left(1,0;z\right),\ \mathrm{Re}Z^{(n)}\left(i,0;z\right)\right\}_{n=0}^{N}, \tag{3.24}$$

that once is valued for the boundary Γ of the domain $\Omega\left(\mathbb{R}^2\right)$, it will provide a set of $2N+1$ base functions for approximating solutions of the forward problem of (1.1), when a boundary condition $u_{\mathbf{c}}|_{\Gamma}$ is imposed.

Indeed, the set (3.24) can be orthonormalized, conforming a new base:

$$\{\upsilon_0^{(n)}(l)\}_{n=0}^{2N},\ l\in\Gamma, \tag{3.25}$$

that can be interpolated by standard methods in order to obtain continuous functions at Γ.

Summarizing, if the number of radii R, points per radius P, and the base functions $2N+1$, are adequate (as it will be explained further), a boundary condition $u_{\mathbf{c}}|_{\Gamma}$ can be approximated by the linear combination:

$$u_{\mathbf{c}}|_{\Gamma}\sim\sum_{k=0}^{2N+1}\beta_k\upsilon_k,$$

where the real constant coefficients β_k are approximated by the standard inner product

$$\beta_k=\langle\upsilon_k,u_{\mathbf{c}}|_{\Gamma}\rangle=\int_{\Gamma}\upsilon_k(l)\cdot u_{\mathbf{c}}|_{\Gamma}(l)dl. \tag{3.26}$$

This section is synthesized well by means of the algorithm used to approximate the Taylor's series in formal power method (NPSM), that it is shown in the algorithm 1.

3.3 Comparison with the Finite-Element Method

Following to [10], FEM is used to compute a solution to the forward problem of equation (1.1). Nonetheless, in [17] NPSM is exposed. Meanwhile, in [89], a comparison between both methods are presented.

In this section, the elements used to compare FEM with NPSM are shown. For this comparison, a smooth domain should be used for example the unit disk domain, in which both methods could perform a good approximation.

Algorithm 1: Sequential algorithm for solving the forward problem of the 2D impedance equation. (see e.g. [19])

S; (Number of radii)
N; (Maximum number of formal powers)
$K+1$; (Number of points per radius)
while $s = 1 \rightarrow S$
  while $n = 1 \rightarrow N$
    while $q = 0 \rightarrow K$
      Function *Coordinates_ Operations*
      Function *Conductivity_ Calculations*
      Function *Generating_ Pairs*
Function *Orthonormalization*
  Classsical Gram-Schmidt Orthonormalization Process
Function *Approached_ Boundary_ Condition*
  $\sum_{n=0}^{N} \left(\alpha_n u^{(n)}(1,0;z) + \beta_n u^{(n)}(1,0;z)\right)$
Function *Lebesgue_ Measure*
  $\mathcal{E} = \left(\int_\Gamma \left(u_c|_\Gamma - u_{app}\right)^2 dl\right)^{\frac{1}{2}}$

In order to make this comparison, a metric in form of the Lebesgue measure is used to perform this analysis (see e.g. [77]):

$$\mathcal{E} = \left(\int_\Gamma \left(u_{\mathbf{c}}|_\Gamma - u_{app}\right)^2 dl\right)^{\frac{1}{2}}, \tag{3.27}$$

where $u_{\mathbf{c}}$ is the imposed electric potential, and u_{app} is the approximated electric potential (see e.g. [80]).

The electric potential u_{app} used in the last equation (3.27), will be different depending on the method that is utilized to perform the approximation. Meanwhile, the u_c is the electric potential imposed as a result of the analytical solution of equation (1.1) (see e.g. [77]).

A characterization using the NPSM and a comparison with FEM is presented in the following paragraphs. The main idea is to expose a new technique that could be employed to approximate the solution for the forward problem of equation (1.1).

3.4 Simulation results

The simulations presented in this section are, firstly, obtained by NPSM, and then a comparison by using FEM will take place. The domain used will

be the unit disk for both methods. Meanwhile, the conductivity function is changed depending upon the sample to be used.

For both methods, the exact mathematical expression is used as it is employed in several works (see e.g. [80], [77] and [17]). The analytic cases employed were: the Lorentzian, exponential, sinusoidal and polynomial. Although, the geometric cases performed were: the circle at center, circle out of center, five disk structure and a square at the center.

3.4.1 Smooth domain

According to [80], the number of formal powers N are fixed, the number of radii S and the number of points per radius K do not introduce any kind of significant error $\mathcal{E}$, at least for the equation employed in (3.27). For this reason, the number of values are fixed at $S = K = 200$.

Then, once the criteria are given to the algorithm 1 exposed before, it is used to compute the solution for all the conductivity cases. For this brief characterization, all the conductivity functions are studied at the unit disk domain, and the conductivity σ functions used are: exponential, sinusoidal, polynomial and Lorentzian, for the analytic case. Meanwhile, for the geometric case, the circle at the center, circles out of center, five-disk structure and square are used.

Finally, the exact solution $u_c|_\Gamma$ is compared with the electric potential u_{app} approximation obtained by NPSM method by means of use the Lebesgue measure. The approached solution depends on the method that it is employed to calculate the approximation to (1.1).

3.4.1.1 Exponential conductivity case

Considering a piece-wise exponential conductivity σ function with the following form:

$$\sigma = e^{\alpha xy}, \tag{3.28}$$

where α represents a coefficient used to change the behaviour of the function.

In this case, the boundary condition, which is exact solution for (1.1), to be imposed:

$$u|_\Gamma = e^{-\alpha xy}. \tag{3.29}$$

Remembering that K represents the number of radii employed. In this case, the approximation obtained by NPSM is illustrated in the table 3.1.

Table 3.1: Exponential conductivity function approximation.

N	S	K	α	$\mathcal{E}$
121	200	200	2	6.88×10^{-15}
81	200	200	2	7.31×10^{-15}
41	200	200	2	1.11×10^{-6}
121	200	200	6	3.41×10^{-14}
81	200	200	6	3.42×10^{-14}
41	200	200	6	1.17×10^{-7}
121	200	200	10	4.22×10^{-14}
81	200	200	10	4.30×10^{-14}
41	200	200	10	2.35×10^{-6}

Table 3.1 shows the maximum number of formal powers to be used to grant a good convergence. As a matter of fact, when the number of formal powers is increasing the convergence does it too. In addition, the stability of the method does not show significant variation.

3.4.1.2 Lorentzian conductivity case

For this case, the conductivity σ function to be used is:

$$\sigma = \left((x + d_x)^2 + L_c\right)^{-1} \cdot \left((y + d_y)^2 + L_c\right)^{-1}, \tag{3.30}$$

where d_x and d_y denotes a displacement over the plane in the x and y axes and L_c denotes a real-value constant.

For this particular case, the imposed boundary condition that represent the solution for (1.1) is:

$$u|_\Gamma = \frac{1}{3}(x + d_x)^3 + \frac{1}{3}(y + d_y)^3 + L_c(x + d_x + y + d_y). \tag{3.31}$$

Then, the table 3.2 shows the results when NPSM is used to approximate the solution. This method is exposed in algorithm 1.

In this simulation, the fixed values $L_c = \{0.2, 0.4, 0.6, 0.8\}$ and the displacement $d_x = d_y = 0$ are the best initial conditions to approximate the solution.

Table 3.2: Lorentzian conductivity distribution approximation.

N	S	K	L_c	$\mathcal{E}$
121	200	200	0.2	2.41×10^{-13}
81	200	200	0.2	2.17×10^{-9}
41	200	200	0.2	2.59×10^{-5}
121	200	200	0.4	1.52×10^{-15}
81	200	200	0.4	3.85×10^{-12}
41	200	200	0.4	1.25×10^{-6}
121	200	200	0.6	2.14×10^{-15}
81	200	200	0.6	4.34×10^{-14}
41	200	200	0.6	1.47×10^{-7}
121	200	200	0.8	2.19×10^{-15}
81	200	200	0.8	2.53×10^{-15}
41	200	200	0.8	2.75×10^{-8}

The table 3.2 shows that the convergence on the solution increases every time the number of formal powers is increased. Although, when the L_c constant is a very low valued, the error increases significantly. The behaviour of the Lorentzian case should be considered and studied to understand the behaviour of NPSM. In this particular case, the stability of the method is still constant, but an exhaustive studied should be performed to analyse the behaviour of the NPSM.

3.4.1.3 Polynomial conductivity case

In this case, the polynomial conductivity *sigma* function is used. Its representative equation is shown below:

$$\sigma = \alpha + Cx + Cy. \tag{3.32}$$

The imposed boundary condition, that is the solution for (1.1), is the following:

$$u|_\Gamma = \ln\left(\alpha + Cx + Cy\right), \tag{3.33}$$

where α and c are real-value constant, such that: $\alpha + Cx + Cy > 0$, $\forall x, y \in \Omega$.

The table 3.3 demonstrates the behaviour when a polynomial conductivity function is used to approximate the solution to the forward problem of the electrical impedance equation (1.1).

Table 3.3: Polynomial conductivity distribution approximation.

N	S	K	α	C	$\mathcal{E}$
121	200	200	10	2	5.43×10^{-15}
81	200	200	10	2	5.43×10^{-15}
41	200	200	10	2	5.43×10^{-15}
121	200	200	10	4	4.23×10^{-15}
81	200	200	10	4	4.23×10^{-15}
41	200	200	10	4	5.24×10^{-12}
121	200	200	10	6	5.52×10^{-15}
81	200	200	10	6	5.97×10^{-12}
41	200	200	10	6	1.37×10^{-6}

The table 3.3 shows the same behaviour, when the number of formal powers increases, the error decreases, performing a good convergence in the method. This case is particularly important, because it helps to understand better the forward problem. The benefits of using this conductivity function, implies that NPSM could approach any polynomial conductivity function with high accuracy. Nevertheless, the stability of the method is being irregular, because the computed error changes between the number of formal power used. This behaviour should be studied in detail to perform a more stable approximation.

3.4.1.4 Sinusoidal conductivity case

Using a sinusoidal conductivity σ function that is shown in the following statement:

$$\sigma = (\alpha + \cos \omega\pi x)\,(\alpha + \sin \omega\pi y)\,, \tag{3.34}$$

where α is a real-value constant, ω is the phase or constant of change uses in the equation, and (x, y) are spatial coordinates.

The following statement represents the imposed solution:

$$u|_{\Gamma} = \left(\frac{\tan xy}{2} + 1\right)^{-1}. \tag{3.35}$$

It is necessary to remark that this function is not an exact solution of (1.1). Indeed, this is a true solution for the case when $\sigma = 1 + \sin xy$. This

simulation becomes interesting when the exact solution of (1.1), and the conductivity σ has the form of (3.34) and it is unknown.

This sample illustrates the effectiveness of the method when arbitrary parameters are introduced into the analysis.

Table 3.4: Sinusoidal conductivity distribution approximation.

N	S	K	α	ω	$\mathcal{E}$
121	200	200	5	2	7.81×10^{-12}
41	200	200	5	2	8.53×10^{-5}
121	200	200	5	6	4.59×10^{-5}
41	200	200	5	6	2.76×10^{-2}
121	200	200	5	10	3.54×10^{-3}
41	200	200	5	10	1.94×10^{-1}
121	200	200	10	2	1.25×10^{-14}
41	200	200	10	2	9.23×10^{-6}
121	200	200	10	6	4.08×10^{-6}
41	200	200	10	6	1.19×10^{-2}
121	200	200	10	10	8.56×10^{-4}
41	200	200	10	10	9.70×10^{-2}

The table 3.4 shows that the increment on N approaches better the solution. Despite the results are worst when the α or ω parameters are increased. In this sense, the table 3.4 offers the possibility to establish a limit case simulation, in which the method is still valid.

Nevertheless, the stability of the method presents an irregular behaviour, this analysis should be studied in detail to propose a possible technique that can increase the convergence rate of the approximation.

3.4.1.5 First geometric case: Circle at center

Considering a geometric conductivity distribution σ within a unit disk domain Ω, as it can be observed in the figure 3.1.

This conductivity σ distribution consists of two disks located at the center of the domain. The small disk plotted in red possesses a conductivity $\sigma_1 = 100$, meanwhile the rest of the conductivity $\sigma_2 = 10$. For the little disk, the radius is denoted by r.

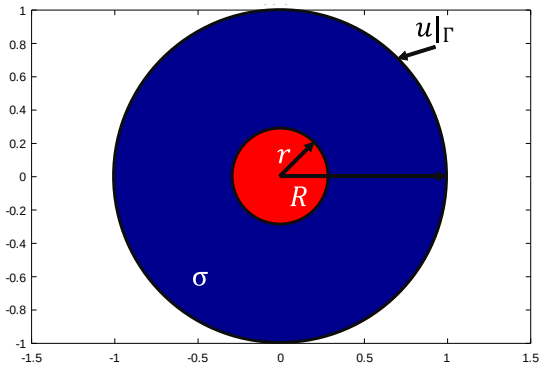

Figure 3.1: First geometric conductivity case: Two disks located at center within the domain Ω.

Following to [80], the boundary condition to be imposed is quite difficult to obtain without physical measurements. Furthermore, calculating the imposed boundary condition for geometrical shape problems will depend upon the shape within the domain. Despite this problem, one easy manner to approximate the solution to the forward problem will be imposing a boundary condition that could be representative for the geometric shapes. The chosen condition is the Lorentzian, because it represents better a smooth domain.

Then, the Lorentzian boundary condition to be imposed is the following:

$$u|_\Gamma = \frac{1}{3}(x + d_x)^3 + \frac{1}{3}(y + d_y)^3 + L_c(x + d_x + y + d_y). \tag{3.31}$$

The table 3.5 shows the numerical approximation for the forward problem to (1.1). As it was mentioned before, the Lebesgue measure is employed to compute the error.

The table 3.5 proves that the convergence of the method increases when the number of formal powers increment. This behaviour is well-known, and it is the same like in the previous samples. An identical behaviour on the converge still preserves when the radius r magnitude increases. Nevertheless, when the radius $r \sim \mathbf{R}$ reaches the boundary, the error increases considerably. In addition, the stability of the method does not present a significant variation. Demonstrating the importance of the initial conditions introduced in the algorithm.

Table 3.5: First geometric conductivity distribution approximation. RD is the value imposed for the red disk and BD is the value for the blue one.

N	S	K	r	RD	BD	$\mathcal{E}$
121	200	200	0.2	10	100	5.32×10^{-15}
41	200	200	0.2	10	100	7.19×10^{-15}
121	200	200	0.4	10	100	6.06×10^{-15}
41	200	200	0.4	10	100	8.13×10^{-15}
121	200	200	0.6	10	100	4.32×10^{-15}
41	200	200	0.6	10	100	5.21×10^{-15}
121	200	200	0.8	10	100	3.47×10^{-15}
41	200	200	0.8	10	100	4.43×10^{-15}

3.4.1.6 Second geometric case: Circle out of center

This case is similar to previous case, and in this special analysis the conductivity distribution σ shows a small disk displaced from the center of the domain Ω. The displacement presented in the small disk corresponds to $x = 0.25$ and $y = 0$. This geometric conductivity case distribution is illustrated on the figure 3.2.

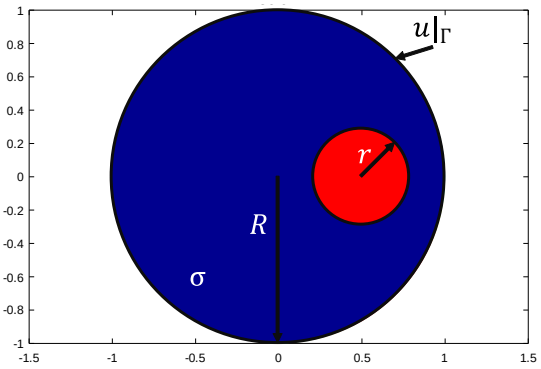

Figure 3.2: Second geometric case: Circle out of the center.

As it was mention before in the subsection 3.4.1.5, the imposed boundary condition $u|_\Gamma$ used is the Lorentzian equation that is represented in (3.31). For this special case, $L_c = 0.5$ can change the behaviour of the approximation.

Thus, for the imposed boundary condition $u|_\Gamma$ the following statement is used:

$$u|_\Gamma = \frac{1}{3}(x+0.25)^3 + \frac{1}{3}y^3 + 0.5(x+0.25+y),$$

The table 3.6 expresses the results for this conductivity σ distribution.

As in the previous case, the small red disk possesses a conductivity $\sigma_1 = 100$, but it has a displacement in the x-axis of 0.25, meanwhile, the biggest disk represented by a conductivity $\sigma_2 = 10$. This case is utilized because inside the domain a small displacement on the tiny disk could be considered as a geometric rotation of the entire domain.

Table 3.6: Second geometric case: Small disk out of the center domain. Variation of the first geometric case.

N	S	K	r	RD	BD	$\mathcal{E}$
121	200	200	0.2	10	100	3.81×10^{-2}
41	200	200	0.2	10	100	8.45×10^{-2}
121	200	200	0.4	10	100	4.61×10^{-3}
41	200	200	0.4	10	100	7.27×10^{-3}
121	200	200	0.6	10	100	3.27×10^{-3}
41	200	200	0.6	10	100	4.46×10^{-3}
121	200	200	0.8	10	100	9.87×10^{-2}
41	200	200	0.8	10	100	2.06×10^{-1}

The table 3.6 proves the same behaviour, meanwhile the formal powers increments its value, the error decreases. Moreover, it is not necessary to make another displacement inside the domain, because the results will be the same, due to the geometric rotation presented in this case.

Nevertheless, the convergence shown in the table 3.6 is not the best, and significant variation is presented in this case. In comparison with the previous case, this sample requires an extra procedure that can stabilize the approximation in order to improve the convergence. This technique could help this special conductivity distribution to obtain more accurate solution.

3.4.1.7 Third geometric case: five-disk structure.

In this case, a five-disk structure σ conductivity distribution located at the center within a unit disk domain Ω is considered. Then, the smallest disk

consists of a conductivity $\sigma_1 = 100$ and radius $r_1 = 0.2$, the second disk possesses a conductivity $\sigma_2 = 30$ and radius $r_2 = 0.4$, the third disk has a conductivity $\sigma_3 = 20$ and radius $r_3 = 0.6$, the fourth disk is a conductivity $\sigma = 15$ and radius $r_4 = 0.8$. Finally, the last disk is represented by a conductivity $\sigma = 10$ and a radius $r_5 \sim \mathbf{R} = 1$. This conductivity is shown in the figure 3.3.

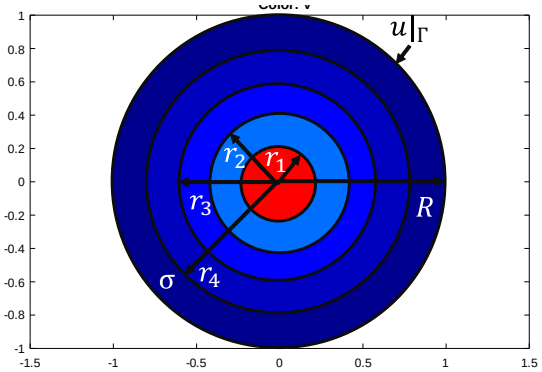

Figure 3.3: Third geometric case: Five disk structure.

As it was mentioned before, the imposed boundary condition $u|_\Gamma$ is the Lorentzian function shown in equation (3.31). For this case, the Lorentzian equation is not presented any modification like in the previous case.

The table 3.7 shows the same behaviour, when the formal powers increase the convergence do it too. Although, an interesting case could be a sample that does not increment due to the decrement in the base functions generated by the formal powers.

Table 3.7: Third geometric conductivity distribution: Five-disk structure approximation.

N	S	K	$\mathcal{E}$
121	200	200	3.04×10^{-15}
101	200	200	3.02×10^{-15}
61	200	200	2.93×10^{-15}
21	200	200	2.81×10^{-15}

The table 3.8 shows an interesting case performed, in which the number of radii and points per radii increments considerably.

Table 3.8: Complementary case approximation. Five-disk structure

N	S	K	$\mathcal{E}$
61	1000	200	5.03×10^{-15}
61	600	200	5.49×10^{-15}
61	200	200	2.93×10^{-15}
41	1000	200	4.81×10^{-15}
41	600	200	5.30×10^{-15}
41	200	200	2.88×10^{-15}
21	1000	200	4.39×10^{-15}
21	600	200	4.93×10^{-15}
21	200	200	2.81×10^{-15}

The behaviour in both tables 3.7 and 3.8 is still the same. Furthermore, this sample is exposed the possibility to increment the number of radii and points per radii without any significant change in the accuracy of the method.

In this case, the stability does not present any significant variation such as in other cases. The structure of the conductivity function is quite similar to a Lorentzian distribution and for this reason, the approximation can be performed very stable and accurate.

3.4.1.8 Fourth geometric case: non-smooth shape within

This case is representative and has been chosen because it cannot be approximated by using classical techniques such as the Gauss-Newton model in FEM. For this case, it should require a special technique that helps the proposed method approximates better the solution to (1.1).

In this case, the conductivity σ distribution is a square at the center of the unit disk domain. For this special case, the square has an apothem $a = 0.65$ and $\sigma_1 = 100$ and $\sigma_2 = 10$ for the rest of the domain. All the corners belonging to the square have the same distance to the center of the domain.

This shape can be appreciated in figure 3.4.

As a matter of fact, the method is modified in order to get the approximation using the corners in the square, and the imposed condition is the

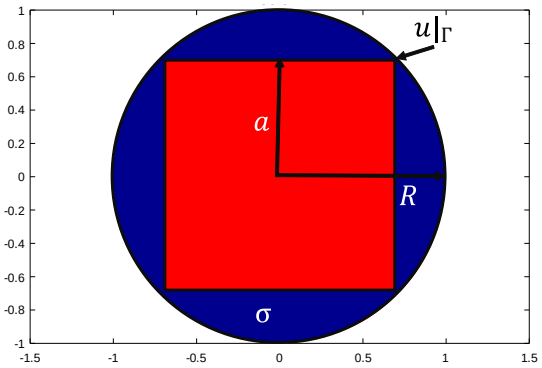

Figure 3.4: Square conductivity distribution.

same condition using for the geometric cases. It means that the Lorentzian condition is imposed at the boundary.

$$u|_\Gamma = \frac{1}{3}(x^3 + y^3) + 0.5(x + y).$$

The results are exposed in the table 3.9, for this special case, in which the conductivity distribution is a non-smooth shape, the convergence is very low. The error $\mathcal{E}$ computed for this case is very high. This simulation was performed in order to understand the behaviour of the Taylor's series in formal power method.

Table 3.9: Square conductivity distribution.

N	S	K	$\mathcal{E}$
121	200	200	1.32×10^{-2}
101	200	200	1.63×10^{-2}
81	200	200	2.23×10^{-2}
61	200	200	3.02×10^{-2}
41	200	200	5.45×10^{-2}
21	200	200	1.16×10^{-1}

Comparing with the previous cases, the table 3.9 indicates that the number of formal powers to be used, does not represent an improvement. Instead of it, the relevance is the fact that this method could be used to approximate

non-smooth and difficult conductivity distributions at least for a unit disk domain.

In addition to this simulation, another experiment was performed to understand better the behaviour of the method. In this case, the number of radii and points per radii were increased to get accuracy results. The table 3.10, which exposes the results of this simulation, presents the same condition, even when the number of radii and points per radii increment, do not affect in the accuracy of the method.

Table 3.10: Complementary simulation for square conductivity distribution.

N	S	K	$\mathcal{E}$
121	500	500	2.90×10^{-2}
101	500	500	3.24×10^{-2}
81	500	500	3.84×10^{-2}
61	500	500	4.67×10^{-2}
41	500	500	6.79×10^{-2}
21	500	500	1.22×10^{-1}

Both tables 3.9 and 3.10 present an important advanced in this field, the convergence is not the best, but it can achieve an approximation. For this reason, a possibility to obtain a more stable method is required.

In addition, a possible method to be used it could be a regularization process that is the classic technique and this novel proposal can obtain more stable solutions. Further studies shall be performed in this direction to confirm that the regularization procedure can help this method to achieve an accurate and stable approximation.

3.4.2 Comparison with the Finite-Element Method

NPSM proves to be an accurate technique to approximate the solution for (1.1), but this method presents an instability sometimes. Furthermore, it seems that it could compete with FEM. For this reason, following to [89], the comparison should be performed to demonstrate that NPSM could be used to get solutions for (1.1).

In order to perform this comparison, it is necessary to refer the reader to the previous chapter 2, specifically to the subsection 2.5 that exposed briefly

FEM (see e.g. [43] and [4]).

Regarding FEM, the employment of non-smooth conductivities makes the task be quite difficult to approximate. Despite this fact, in [98], it said that FEM could also approach the solution to (1.1). Moreover, the comparison is done by using analytical and smooth simulations that are within a unit disk domain.

Then, In [80], the Lebesgue measure is used to test the simulation perform by the proposed methods. This measure is presented as follows:

$$\mathcal{E} = \left(\int_{\Gamma} \left(u_{\mathbf{c}}|_{\Gamma} - u_{app} \right)^2 dl \right)^{\frac{1}{2}}. \tag{3.27}$$

where $u_{\mathbf{c}}|_{\Gamma}$ is the imposed boundary condition, and u_{app} is the approximated electric potential.

So, the simulations represent the solution obtained by FEM and NPSM, in which the initial conditions are fixed depending upon the applied technique. The analysis is exposed in the following section.

3.4.2.1 Exponential conductivity function case

Let it to be an exponential conductivity distribution σ represented as follows:

$$\begin{aligned} \sigma &= e^{\alpha \cdot x \cdot y}, \\ \alpha &= \{2, 4, 6, 8\}, \end{aligned} \tag{3.36}$$

where α is the coefficient that is used to change the behaviour of the equation.

Particularly, the imposed boundary condition is expressed as follows:

$$\begin{aligned} u_{\mathbf{c}}|_{\Gamma} &= e^{-\alpha \cdot x \cdot y}, \\ \alpha &= \{2, 4, 6, 8\}. \end{aligned} \tag{3.37}$$

Hence, the table 3.11 shows the comparison by using the equation (3.36)and (3.37). For this case the NPSM has its conditions fixed; Number of formal powers $N = 30$, $S = 100$ and $K = 1000$.

In addition, the table 3.11 exposes the increment on the error due to the increasing α parameter. This pattern has been analysed and known (see e.g. [89] and [80]), but it has been used to characterize and proof the stability and convergence of both methods.

The figure 3.5 illustrates the approximation obtained by these methods, when the coefficient $\alpha = 8$.

Table 3.11: Exponential conductivity σ function approximation. A comparison between the FEM and NPSM.

N	S	K	α	$\mathcal{E}$-FEM	$\mathcal{E}$-NPSM
30	100	1000	2	0.0013	6.87×10^{-15}
30	100	1000	4	0.0113	2.12×10^{-14}
30	100	1000	6	0.0617	1.15×10^{-11}
30	100	1000	8	0.2752	1.24×10^{-9}

At last but not the least, both methods showed that the error in their approximation is increasing. This error increases due to the coefficient α introduced in the equation. On the other hand, the approximation performed by FEM is more stable than NPSM. Although NPSM is more accurate than FEM, as it was plotted in the figure 3.5. This simulation proves that NPSM would require a regularization process to perform a more stable method.

3.4.2.2 Sinusoidal conductivity function case

Considering the sinusoidal conductivity σ distribution as follows:

$$\begin{gathered} \sigma = (a + \cos(\omega\pi x)) \cdot (a + \sin(\omega\pi x)) \,, \\ a = \{2\} \,; \;\; \omega = \{2, 4, 6, 8, 10\} \,, \end{gathered} \tag{3.38}$$

where a is a coefficient that changes the behaviour of the expression (3.38), ω represents the variation on the phase, this variation will change dramatically the approximation that it will be plotted.

Then, for the last statement (3.38), the imposed boundary condition will be the following:

$$\begin{gathered} u_{\mathbf{c}}|_{\Gamma} = \left(\tan\left(\tfrac{x \cdot y}{2}\right) + 1\right)^{-1} \\ \alpha = \{2\} \,; \;\; \omega = \{2, 4, 6, 8, 10\} \,. \end{gathered} \tag{3.39}$$

Coming from the mathematical analysis of (1.1), the imposed condition (3.39) is considered as the general solution for this particular case.

The table 3.12 shows a brief comparison between NPSM and FEM method. Such as previous cases, the initial conditions for NPSM are fixed and the ω coefficient present variations, but the α coefficient remains constant.

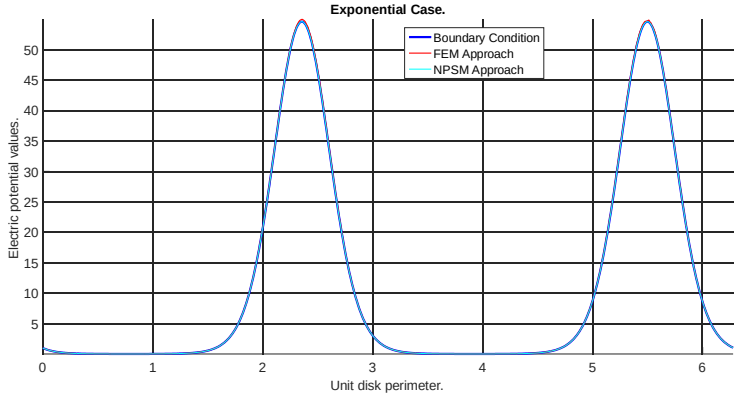

(a) Exponential.

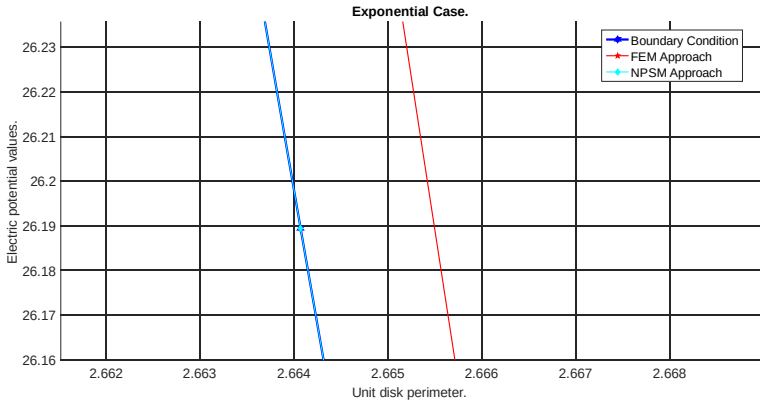

(b) Exponential zoom.

Figure 3.5: Comparison between NPSM and FEM methods. Comparison for an exponential conductivity function within a unit disk domain.

Table 3.12 shows that FEM is the best method to get the solution for (1.1), in this case it shows a better accuracy and stability than NPSM. It is important to remark that NPSM could approach the solution, and the optimal approximation is presented when $\alpha = 2$ and $\omega = 2$. Furthermore, these simulations prove that the method could be improved to obtain a better solution and convergence.

Then, in the figure 3.6, one can appreciate that the behaviour changes depending on the parameters used.

At last but not the least, the graphic illustrated in figure 3.6, which is

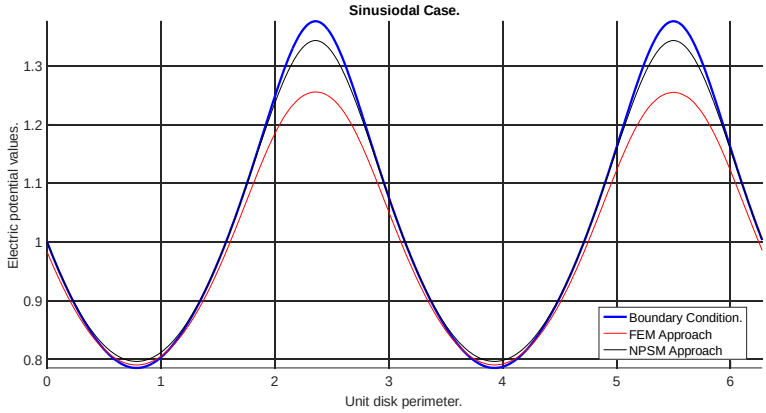

(a) Sinusoidal conductivity distribution.

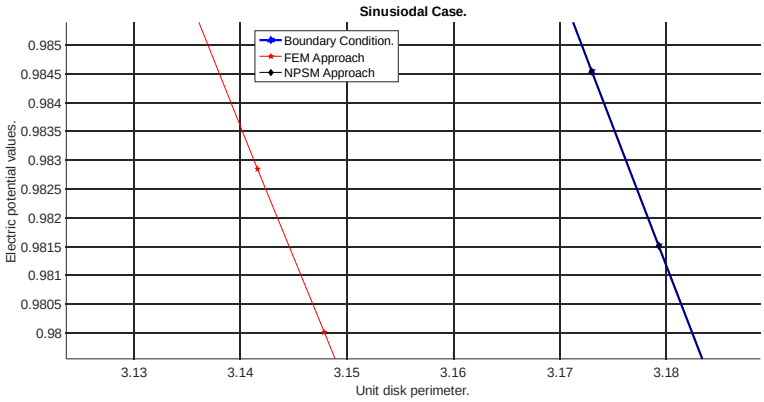

(b) Sinusoidal conductivity zoom.

Figure 3.6: Sinusoidal conductivity distribution. Comparison between NPSM and FEM methods.

Table 3.12: Sinusoidal conductivity function: Comparison between NPSM and FEM methods.

N	S	K	α	ω	$\mathcal{E}$-FEM	$\mathcal{E}$-NPSM
30	100	1000	2	2	0.0561	2.05×10^{-4}
30	100	1000	2	4	0.0549	0.07
30	100	1000	2	6	0.0537	0.06
30	100	1000	2	8	0.0522	0.10
30	100	1000	2	10	0.0515	0.25

based on the table 3.12, presents an interesting behaviour when the conditions change. This approximation proves that it is required a regularization process in the NPSM method.

This regularization process helps the method to approach a better the solution for (1.1), presenting an improvement in the accuracy and stability. Although, the approximation got by NPSM is not the best, this simulation helps to begin an analysis to determine, which conditions are important for the forward problem of (1.1).

In addition, the possibility to increase the number of formal powers should help the method to obtain a better approximation, but the problem is still the computer resources used to approximate the solution and the instability do the method presented.

3.4.2.3 Lorentzian conductivity function case

The Lorentzian conductivity σ distribution is denoted as follows:

$$\begin{aligned} \sigma &= \left(\tfrac{1}{x^2+L_c}\right) \cdot \left(\tfrac{1}{y^2+L_c}\right), \\ L_c &= \{0.2, 0.4, 0.6, 0.8\}, \end{aligned} \tag{3.40}$$

where L_c represents the coefficient used to modify the behaviour of the last statement.

As in previous cases, the imposed boundary condition is:

$$\begin{aligned} u_c|_\Gamma &= \tfrac{x^3+y^3}{3} + L_c\,(x+y)\,, \\ L_c &= \{0.2, 0.4, 0.6, 0.8\}\,. \end{aligned} \tag{3.41}$$

The table 3.13 shows the comparison between FEM and NPSM methods, in which the values are fixed for the last one.

Table 3.13: Lorentzian conductivity distribution. A comparison between NPSM and FEM method.

N	S	K	L_c	$\mathcal{E}$-FEM	$\mathcal{E}$-NPSM
30	100	1000	0.2	2.2946×10^{-4}	1.51×10^{-7}
30	100	1000	0.4	2.3460×10^{-4}	1.24×10^{-9}
30	100	1000	0.6	2.3703×10^{-4}	4.17×10^{-11}
30	100	1000	0.8	2.3839×10^{-4}	2.87×10^{-12}

As in previous cases, the behaviour exposed in the figure 3.13 is stable for FEM. Meanwhile, NPSM exposes a better convergence. As a matter of fact, when the conditions change, they introduce an instability in FEM. However, this method can reach a good approximation.

Furthermore, the figure 3.7 shows the behaviour and the comparison between both methods. The best approximation is obtained by NPSM, but it is required more computational resources to perform the simulation and the instability indicates that the method could need a regularization process. This study should be performed in further works.

Figure 3.7 exposes the best approximation for both methods. By the analysis of the table 3.13 and figure 3.7, a regularization procedure should be used to improve the stability of the proposed method.

3.5 Discussion

The possibility of applying the numerical analysis originated in the Pseudoanalytic Function Theory, to conductivity distributions that are arbitrary, and not only of separable variables form, opened a complete branch of analysis to be applied into the Electrical Impedance Tomography theory, since most of the interesting cases precisely consist in geometrical conductivity functions, whose separable-variables representation is unknown.

Therefore, we fully covered the elements of the Pseudoanalytic Function Theory in order to construct solutions for the direct problem utilizing Taylor's series in formal powers, illustrating the acceptable convergence of this method that can be even superior to the results provided by the Finite-Element Method, as a brief comparison provided within the previous pages states.

The importance of approaching several terms of the so-called Taylor's

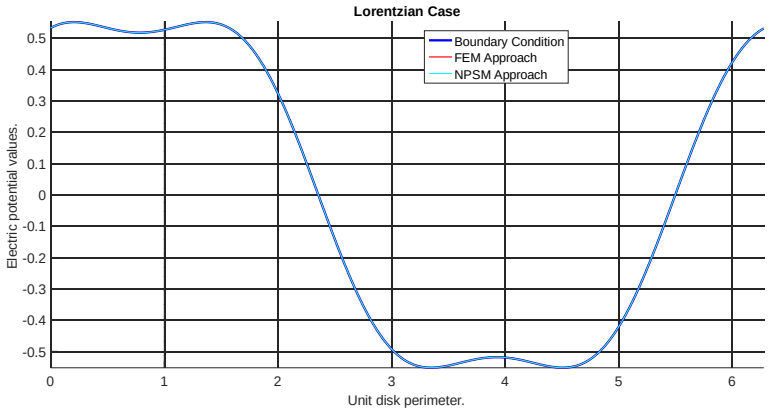

(a) Lorentzian conductivity distribution.

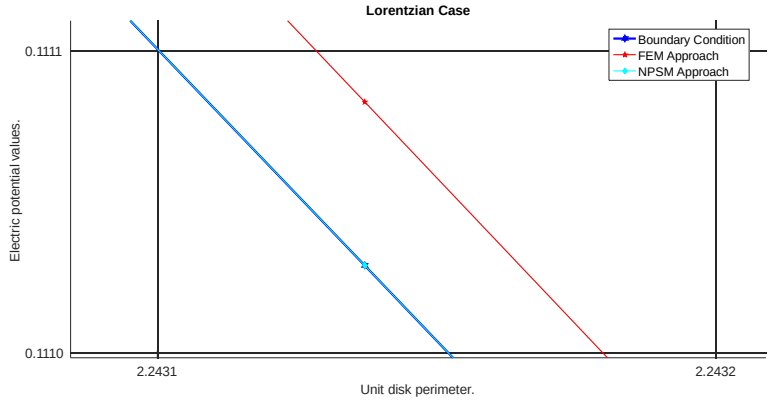

(b) Lorentziana conductivity approximation zoom.

Figure 3.7: Comparison between NPSM and FEM approximation for a Lorentzian conductivity distribution.

series at the boundary of the selected domains, realised into the possibility of employing them precisely as boundary conditions, when identical conductivity distributions are the expected results of the algorithms dedicated to the inverse problem. No any previous thesis is known to contain this specific analysis, thus, its very existence is an important contribution. Beside, since the numerical stability of the presented results is also warranted by the programming framework and the highly specialized development tools, these results can be used as a reference for future works.

Specifically, four different conductivity distributions with analytical rep-

resentation are analysed by means of the Taylor's series in formal powers, and on behalf of briefness only three are reused when comparing the convergence with the results provided by the Finite-Element Method. Another four cases were considered all of them containing geometrical figures, yet, for these cases the comparison with the Finite-Element Method was not included exclusively because the very high-complexity for tracing their corresponding mesh. Nonetheless, we can expect also a better convergence upcoming from the analysis with Taylor's series, since the presence of discontinuities has already been proved as a strong challenge for FEM.

Both methods can achieve an approximation to the forward problem of (1.1), but the solution is quite different. For some cases, the approximation obtained by FEM is better that NPSM, and vice-versa for other cases. However, the stability that FEM reach is better that NPSM. For this reason, a useful technique that it can be used is a regularization process.

Furthermore, FEM can achieve good approximation of the solution to (1.1), even though the lack of a regularization process. The basic scheme of FEM performs the approximation to prove the effectiveness and accuracy of the method. The difficulty rises when a non-smooth conductivity σ function is used. Nonetheless, this technique approximates the solution, but it depends upon the robustness of the mesh. Implying that an increment on its robustness can perform a better approximation. In addition, any modification made on the mesh implies the increment or decrement of the computer resources and the computing-time.

On the other hand, NSPM is an effective method that it can achieve good approximations despite the conductivity σ distribution used inside the domain. Its effectiveness relies on the initial conditions set. Nevertheless, the stability of the solution is not the best, and it depends on the conductivity employed. Even though the approximation achieved is better than FEM, the computational resources could be improved. Considering this method such as an alternative to FEM.

In addition, NPSM method could be partially parallelized to reach faster approximation and preserving the obtained accuracy. However, this method depends completely on the number of obtained solutions.

3.6 Conclusions

Summarising all the simulations performed by FEM and NPSM prove their effectiveness to solve the forward problem of (1.1). Even though NSPM demonstrates to be better than FEM, its stability is not the best. In comparison with FEM, NPSM should include an extra technique that proves to be effective, and it is used to solve and stabilize inverse problems. This technique is known as regularization and some studies should be done in order to understand its behaviour and to determine if this technique could help to get more accurate and stable solutions.

Both techniques depend on the initial conditions given to approximate the forward problem of (1.1). Furthermore, the comparison done demonstrates that both method could obtain better approximations when different conditions are employed.

As a matter of fact, both methods use dramatic computer resources to perform its approximation. However, NPSM method can be parallelized in order to obtain faster solutions, even though the possibility to be parallelized, it cannot be achieved in the whole algorithm. For this reason, further works should be done to understand better this novel proposal and determine, which process can be optimized.

On the other hand, FEM cannot be parallelized due to its recursive design. However, the approximations that the method can perform, make it very competitive. In addition, this method can be optimized to obtain better accuracy and faster solutions, but the computer resources will increase considerably. For this reason, the possibility to employ an alternative technique to perform the same analysis is considered by many experts on the field.

Chapter 4

Inverse Dirichlet boundary value problem

The inverse Dirichlet boundary value problem is posed from (1.1). In this case, as it is for the direct problem, the boundary condition is given (see e.g. [23]). Whereas, in the forward problem the conductivity σ distribution is given, and the task is to approach the electric potential u (see e.g. [33]), in the inverse problem, the task is to approach the conductivity σ within the domain (see e.g. [3]).

For the inverse problem, any variation in the input data shall reach a significant different solution. Therefore, if any measurement is taken with variations, as the environmental noise could be, the solution can not be calculated into an acceptable range of accuracy (see e.g. [98], [4] and [43]). Therefore, to warrant some minimum accuracy in the approximation of the solution, regularization methods should be applied (see e.g. [6]). Some advantages and disadvantages are presented by the inclusion of this regularization processes (see e.g. [29]).

Following to [91], [22] and [62], the Tikhonov's regularization procedure permits the influence diminution of the noise in real-measurements. In addition, EIT problem cannot be considered as practical medical imaging procedure due to the continuous advances in the trefoil field and the presence of these perturbations (see e.g. [32]).

Several works are dedicated to approximate the solution for both problems. And more specifically, following to [28], the existence of a technique to obtain solution in term of linear operators, is shown to analyse and study the inverse problem.

Furthermore, the connection between pseudoholomorfic functions and the Beltrami equations can be used to deduce the well-possessedness on smooth domains for these class of problems (see e.g. [7]). In addition, utilizing the theory of conjugate functions to solve the Dirichlet and the Neumann's problems for conductivity and electric potential equations, in which the density properties are considered to trace a possible solution, it could be employed to approximate the inverse problem (see e.g. [8]).

The possibility to use any classical method to approximate the solution, supports the idea to combine the Taylor's series in formal power method (NPSM) with the Finite-Element Method (FEM) in order to obtain more accurate solutions. This chapter is dedicated to proposed a hybrid method, that shall be employed to get a precise solution for the inverse problem of (1.1).

4.1 Preliminaries

The inverse problem of the electrical impedance equation (1.1) possesses a high complexity (see e.g. [98]). Furthermore, due to such complexity a methodology is proposed to develop an hybrid method that can be used to obtain a more direct approximation (see e.g. [3], [18] and [67]).

In this section, NPSM is used to approximate the forward problem of (1.1). The obtained solution is employed as initial condition for the inverse problem. Nevertheless, this technique requires a regularization process in order to compute and to estimate more stable solutions. Beside, FEM is analysed to understand better their advantages and disadvantages by performing a comparison between these methods.

Continuing the dissertation, the following subsection is dedicated to a regularization process, that it can be adapted in order to work with NPSM method, such as FEM.

4.1.1 Regularization process

The regularization methods are employed in many fields, introducing additional information with the purpose to solve ill-posed problems (see e.g. [62]). Ancillary, this method shall also be used to prevent overfitting and it is usually presented in form of a penalty for the complexity, such as restrictions for smoothness or bounds in the space norm of a vector. In a particular case,

including these methods in the designed algorithm presents an advantage to compute a solution for inverse problems to fit the data in order to reduce a norm of the solution (see e.g. [36]).

For the current problem, the imposed electric potential $u|_\Gamma$ represents a finite number of current densities $j_k|_{k=0}^m$ for a domain Ω with a boundary Γ and the knowledge of the Neumann-Dirichlet map (see e.g. [62]) where:

$$\operatorname{div}(\sigma \operatorname{grad} u) = 0, \quad \sigma \partial_\Gamma u = j. \tag{1.1}$$

Evoking the notations for the last equation we have σ representing the conductivity distribution in a domain Ω for the boundary Γ, whereas the u represents the electric potential, being $\partial_\Gamma u = \partial u / \partial_\Gamma$, and j is the current density.

Hence, the Tikhonov's regularization procedure is presented as follows:

$$\min_x \left(\|Ax - b\|^2 + \gamma^2 \|x\|^2 \right), \tag{4.1}$$

where $\|\cdot\|$ denotes the Lebesgue norm, usually denoted as L_2 norm, A can be a square matrix or a matrix of $r \times s$ dimensions, b denotes a vector with r rows, γ is the regularization parameter, turning the problem into a minimization of the x parameter.

Thus, (4.1) has an explicit solution expressed as follows:

$$x = \left(A^T A + \gamma^2 I \right)^{-1} \cdot A^T b, \tag{4.2}$$

where I is the identity matrix with the same dimension of A in this case $A = Z^{(n+1)[K]}$ that represents the orthonormalized system which is the result of the formal powers employing the conductivity σ and the imposed boundary condition, b is the electric potential $u|_\Gamma$, and the regularization parameter $\gamma > 0$.

The main problem is to choose the correct parameter γ, which approximates the solution of (4.2). In order to choose such γ, the next expression shall be used:

$$\gamma = \sum_{k=1}^{m} \frac{A_{kk}^T \cdot A_{kk}}{u_k^T \cdot u_k}, \tag{4.3}$$

where A is the orthonormalized solution of NPSM and u denotes the electric potential.

However, following to [21], NPSM requires modifications to obtain a more stable approximations for (1.1). This consists in the insertion of a regularization process to the main algorithm (see e.g. [83] and [6]).

Following to [92] and [1], this regularization process was posed by A. Tikhonov and it is very useful when studying inverse problems. This modification can be observed in the algorithm 2 (see e.g. [83]).

Algorithm 2: Modified Taylor's series in formal power method.

$S \leftarrow 500$; $N \leftarrow 20$; $K+1 \leftarrow 501$;
while $s = 1 \rightarrow S$
  while $n = 1 \rightarrow N$
    while $k = 0 \rightarrow K$
      $Z^{(n+1)}[k] = \mathcal{B}\left[Z^{(n)}[k]\right]$;
while $\gamma > \gamma_e$
  Function *Orthonormalization*
    Classical Gram-Schmidt Orthonormalization Process
  Function *Regularization*
    Tikhonov Regularization Process
  Function *Approach_Boundary_Condition*
    $u_{app} = \sum_{n=0}^{N} \left(\alpha_n u^{(n)}(1,0,z) + \beta_n u^{(n)}(i,0,z)\right)$;
  $\gamma_e = \sum_{k=1}^{m} \frac{A_{kk}^T A_{kk}}{u_{app}^T u_{app}}$;
Function *Save Orthonormal_Sytem;*
Function *Save Coefficients;*

NPSM can be observed graphically in the flowchart shown in figure 4.1a. In the figure 4.1b is shown the particular variation of FEM that will be used. As it was mention, FEM can achieve and perform an approximation to the inverse problem of (1.1) by itself (see e.g. [98], [9] and [8]). Nevertheless, due to its maximum resolution obtained, it is not considered as standard technique in the Medical Imaging.

The aim is to achieve a possible approximation that can be considered useful to understand the inverse problem of (1.1). This development is the first tried to fusion NPSM and FEM. In addition, the methodology used for both methods is the following:

- Forward Dirichlet boundary value problem:
  1. Select the main domain.
  2. Choose a conductivity distribution σ within the domain.

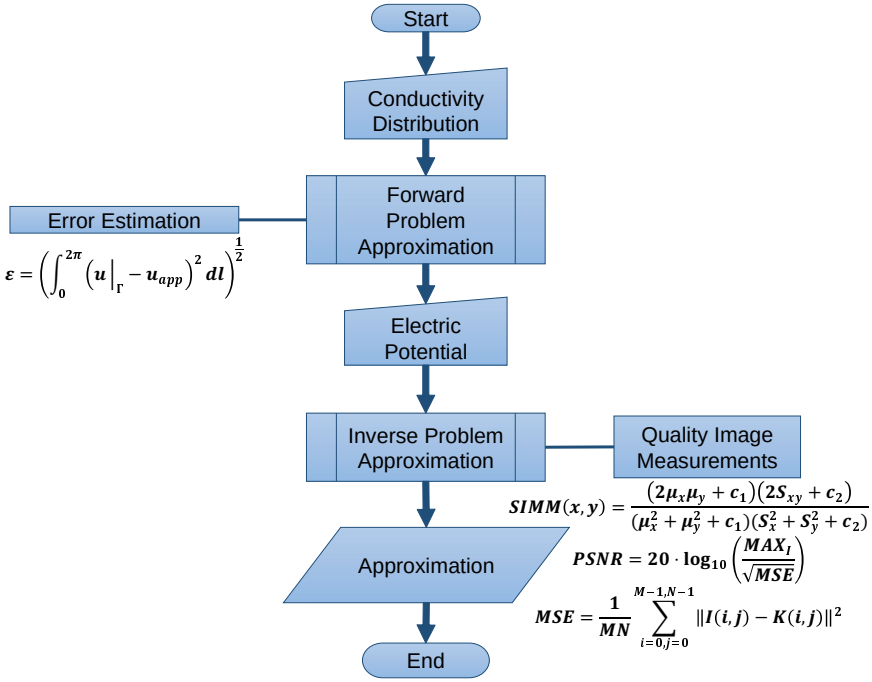

(a) Forward Dirichlet boundary value problem.

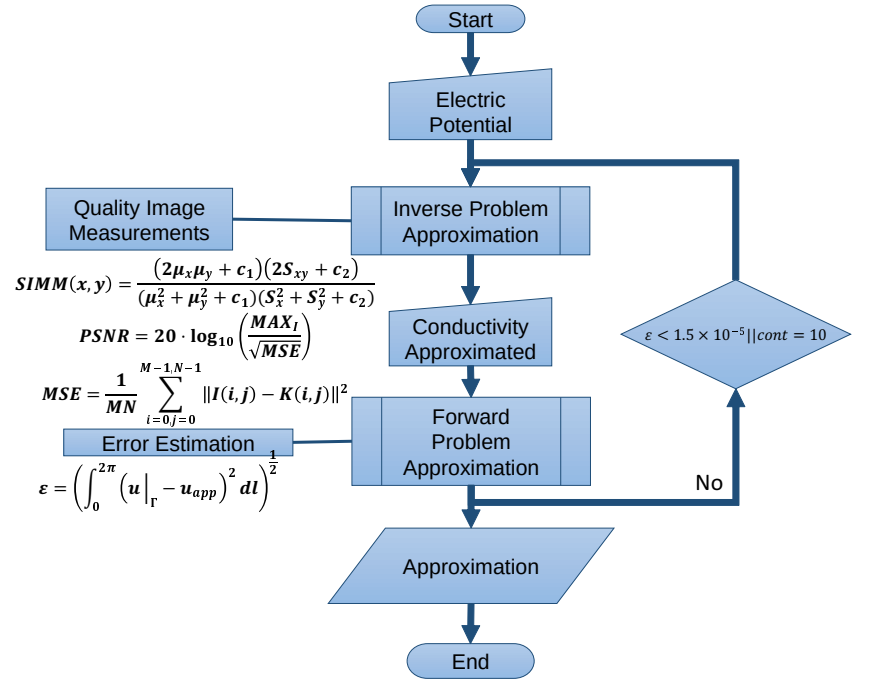

(b) Inverse Dirichlet boundary value problem.

Figure 4.1: Flowcharts use for the Electrical Impedance Tomography problem.

3. Approximate the solution by means of NPSM.
4. Applying Tikhonov's regularization procedure to the approximation computed.
5. Perform the computation of the electric potential $u|_\Gamma$ at the boundary.

- Inverse Dirichlet boundary value problem:

1. Select the main domain.
2. Choose the electric potential $u|_\Gamma$ at the boundary
3. Approximate the solution by means of FEM.
4. Perform the computation of the conductivity σ distribution within the domain.

As it was mentioned in the last paragraphs, the approximation obtained depends upon the initial condition given. This regularization process is employed to understand the behaviour of the problem leaving for the next section the methodology of the main process for approximation of the solution (see e.g. [102]).

In this section, two hybrid methods are proposed, in which the main idea for these methods is to fusion the forward problem and the inverse problem. The forward problem is approximated by NPSM and the inverse problem is solved by FEM (see e.g. [99]).

This is not a novel idea (see e.g. [50] and [87]), and yet the usage of NPSM into the basic scheme of FEM represents a possibility to approximate the solution with high precision and faster. Both methods are exposed in the following subsections, presenting the algorithm and the flowcharts to understand better these proposals.

4.1.2 Proposed hybrid method 1

This novel proposal tries to analyse the behaviour of (1.1). The analysis permits to design a method that could be used to obtain faster and more accurate solutions. In addition, the designed method proposes a form to use the classical methods instead of avoiding them. In this case, this method can be considered hybrid, because it involves NPSM (chapter 3) in its computational scheme. Yet, the inherent instability of NPSM is diminished by the inclusion of a regularization technique.

Hence, the methodology used is the following:

1. Select a domain, and choose a conductivity σ distribution.
2. Compute the forward problem to obtain the electric potential $u|_\Gamma$ at the boundary.
3. Using the calculated electric potential $u|_\Gamma$, the solution to the inverse problem is approximated.
4. Using the quality image assessments the comparison between the approximation and the original distribution takes place.

The methodology can be observed in the flowchart exposed in the figure 4.2.

On the other hand, the developed method is shown in the algorithm 3.

It is important to mention that the conductivity distribution σ used in the proposed method is only known for the forward problem. It means that the approximation obtained by NPSM is used as the initial condition for the inverse problem and approximated by FEM.

For the purposes of this work, the approximation of this hybrid method is compared with the conductivity σ distribution selected by the SIMM (4.6), PSNR (4.4) and MSE (4.5) criteria, which it exposes the error between the approximation computed and the original conductivity (see e.g. [67] and [82]).

4.1.3 Proposed hybrid method 2

This second method shares the main the first one. However, this method is a variation of the first method exposed. As it was mentioned before, it uses the forward and inverse approximation to propose a hybrid method that can be used to study the EIT problem.

Hence, the methodology for this method is the following:

1. A domain is selected and the electric potential u is employed as initial condition.
2. The inverse problem is computed to obtain the conductivity σ distribution inside the domain.
3. Once the conductivity σ distribution is computed, the forward problem computation takes place.

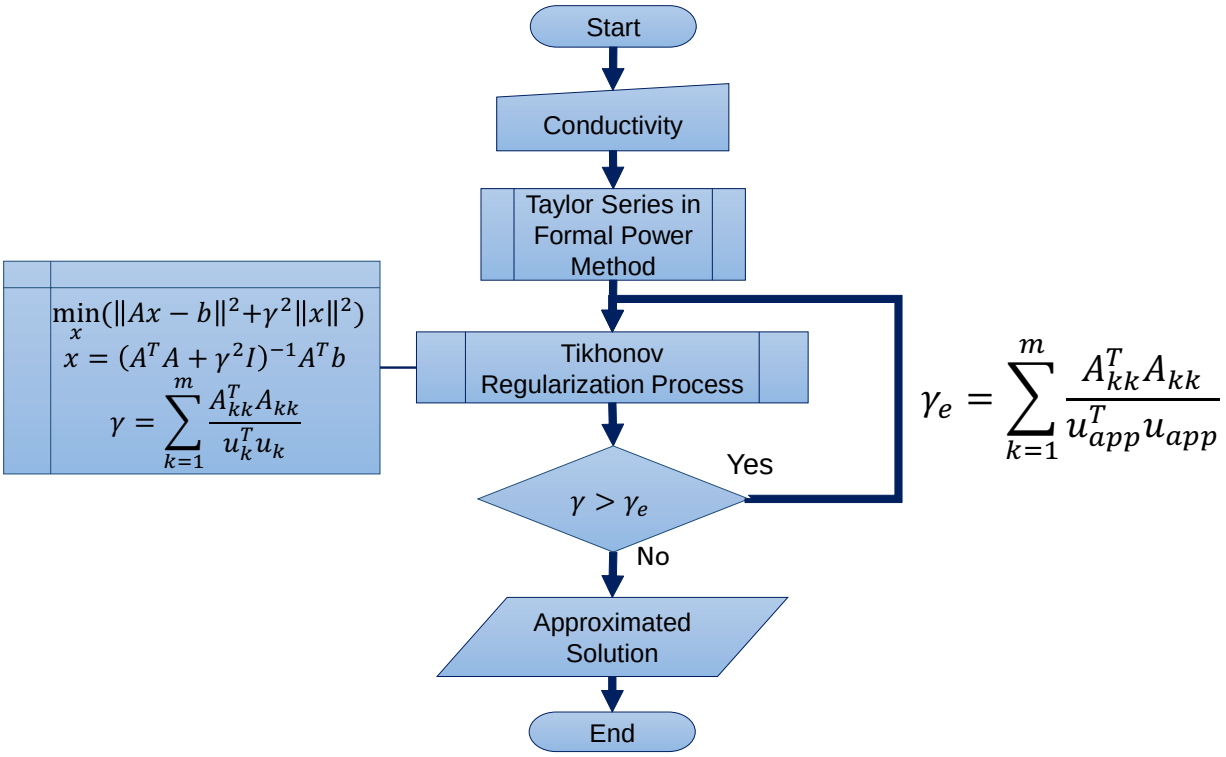

Figure 4.2: Hybrid method 1, first approximation by the NPSM and the final approaching by the FEM.

Algorithm 3: Hybrid method 1: Forward then inverse approximation.

$S \leftarrow 500$; $N \leftarrow 20$; $K+1 \leftarrow 501$;
while $s = 1 \rightarrow S$
  while $n = 1 \rightarrow N$
    while $k = 0 \rightarrow K$
      $Z^{(n+1)}[k] = \mathcal{B}\left[Z^{(n)}[k]\right]$;
while $\gamma > \gamma_e$
  Function *Orthonormalization*
    Classical Gram-Schmidt Orthonormalization Process
  Function *Regularization*
    Tikhonov Regularization Process
  Function *Approach_Boundary_Condition*
    $u_{app} = \sum_{n=0}^{N} \left(\alpha_n u^{(n)}(1,0,z) + \beta_n u^{(n)}(i,0,z)\right)$;
  $\gamma_e = \sum_{k=1}^{m} \frac{A_{kk}^T A_{kk}}{u_{app}^T u_{app}}$;
Function *Save Orthonormal_Sytem;*
Function *Save Coefficients;*
$U \leftarrow Coefficients(u_{app})$;
Function *Finite Element Method*
  Mesh definition;
  Mesh Approximation;
  ϱ conductivity
Function *Save Conductivity;*
Function *Quality Image Measurements*
  $\text{MSE} \leftarrow \frac{1}{m \cdot n} \sum_{k=0,l=0}^{m-1,n-1} (I(k,l) - R(k,l))^2$;
  $PSNR \leftarrow 20 \cdot \log_{10}\left(\frac{MAX_I}{\sqrt{MSE}}\right)$;
  $\text{SSIM} \leftarrow \left(\frac{(2\mu_x\mu_y + c_1)(2\varsigma_{xy} + c_2)}{(\mu_x^2 + \mu_y^2 + c_1)(\varsigma_x^2 + \varsigma_y^2 + c_2)}\right)$;

4. The Lebesgue measure compares the approximation with the original function.

5. If the Lebesgue measurement does not fulfil the desire error, the electric potential u pass once again to the inverse problem to recompute all the process (see e.g. [59]).

This method can be observed on the flowchart exposed in the figure 4.3.

In comparison with the algorithm 4.2, the difference is the initial condition given. In this case, the electric potential u is used as initial condition in order to obtain the conductivity distribution σ. The main goal of this method is to obtain an accurate approximation by iterating constantly the forward problem using it as initial condition for this method (see e.g. [59]).

The flowchart illustrated in figure 4.3 can be represented as a process as it is shown in the algorithm 4. This algorithm shows the full method developed in order to approximate the solution with better acuracy.

Algorithms 3 and 4 are used in the simulation section to approximate the solution to the inverse problem, both methods exposed its advantages and disadvantages. Comparing its approximation with classical methods exposed before (see e.g. [98]).

4.2 Simulations results

The methodology depends upon the initial condition given. Both algorithms approximate the solution to the forward and inverse problem, but the solution obtained will be different.

In order to make a comparison and to understand the behaviour of the method, the Lebesgue measure (3.27) is included for the forward problem, in which the approximation of the electric potential u_{app} is compared with the original electric potential $u_{\mathbf{c}}|_{\gamma}$ imposed at the boundary.

The Lebesgue measure is the following:

$$\mathcal{E} = \left(\int_{\Gamma} \left(u_{\mathbf{c}}|_{\Gamma} - u_{app} \right)^2 dl \right)^{\frac{1}{2}}. \tag{3.27}$$

On the other hand, for the inverse problem the quality assessments are utilized. These statements are expressed as following:

$$PSNR = 20 \cdot \log_{10} \left(\frac{MAX_{Im}}{\sqrt{MSE}} \right), \tag{4.4}$$

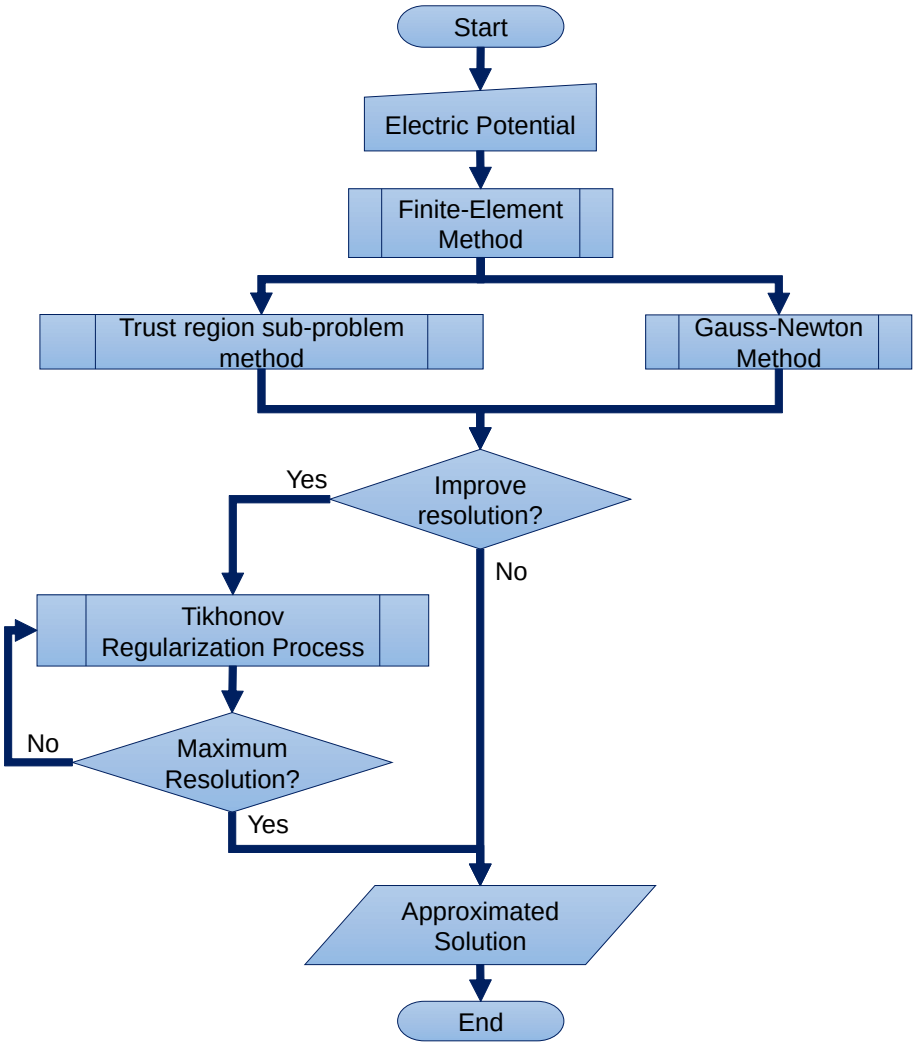

Figure 4.3: Hybrid method 2, first approximation by FEM and the final approaching by NPSM.

Algorithm 4: Hybrid method 2: Inverse then forward approximation.

$U \leftarrow 1$; $cont \leftarrow 0$;
while $(\mathcal{E} < 1.5 \times 10^{-5}) \| (cont = 10)$
  if $cont > 0$
    $U \leftarrow u_{app}$;
  Function *Finite Element Method*
    Mesh definition;
    Mesh Approximation;
    ϱ conductivity
  Function *Save Conductivity;*
  Function *Quality Image Measurements*
    $\text{MSE} \leftarrow \frac{1}{m \cdot n} \sum_{k=0,l=0}^{m-1,n-1} (I(k,l) - R(k,l))^2$;
    $PSNR \leftarrow 20 \cdot \log_{10} \left(\frac{MAX_I}{\sqrt{MSE}} \right)$;
    $\text{SSIM} \leftarrow \left(\frac{(2\mu_x\mu_y + c_1)(2\varsigma_{xy} + c_2)}{(\mu_x^2 + \mu_y^2 + c_1)(\varsigma_x^2 + \varsigma_y^2 + c_2)} \right)$;
  $S \leftarrow 500$; $N \leftarrow 20$; $K + 1 \leftarrow 501$;
  while $s = 1 \rightarrow S$
    while $n = 1 \rightarrow N$
      while $k = 0 \rightarrow K$
        $Z^{(n+1)}[k] = \mathcal{B}\left[Z^{(n)}[k]\right]$;
  while $\gamma > \gamma_e$
    Function *Orthonormalization*
      Classical Gram-Schmidt Orthonormalization Process
    Function *Regularization*
      Tikhonov Regularization Process
    Function *Approach_ Boundary_ Condition*
      $u_{app} = \sum_{n=0}^{N} \left(\alpha_n u^{(n)}(1,0,z) + \beta_n u^{(n)}(i,0,z) \right)$;
    $\gamma_e = \sum_{k=1}^{m} \frac{A_{kk}^T A_{kk}}{u_{app}^T u_{app}}$;
  Function *Save Orthonormal_ Sytem;*
  Function *Save Coefficients;*
  Function *Lebesgue measure;*
    $\mathcal{E} = \int_0^{2\pi} \left((u|_\Gamma - u_{app})^2 \, dl \right)^{\frac{1}{2}}$;
  if $\mathcal{E} > 1.5 \times 10^{-5}$
    $cont \leftarrow cont + 1$;

where $MAX_{Im} = 255$ is the maximum pixel value of the image (8 bits), and the MSE is the mean square error which expression is the following:

$$MSE = \frac{1}{m \cdot n} \sum_{k=0,l=0}^{m-1,n-1} \left(Im\left(k,l\right) - R\left(k,l\right) \right)^2, \tag{4.5}$$

where $Im\left(k,l\right)$ is the $k \times l$ conductivity image for σ_{or} and R is the $k \times l$ for the approximated conductivity σ_{app}.

Then, the structural similarity index measure is represented as follow:

$$SSIM = \left(\frac{(2\mu_x\mu_y + c_1)(2\varsigma_{xy} + c_2)}{(\mu_x^2 + \mu_y^2 + c_1)(\varsigma_x^2 + \varsigma_y^2 + c_2)} \right), \tag{4.6}$$

where μ_x is the average of x, μ_y is the average of y, ς_x^2 is the variance of x, ς_y^2 is the variance of y, ς_{xy} is the covariance of x and y, $c_1 = (k_1 L)^2$ and $c_2 = (k_2 L)^2$ are variables to stabilize the division with weak denominator, where $k_1 = 0.01$, $k_2 = 0.03$ by default, and L is the dynamic range of the pixel values, commonly $2^{(\#bits\_per\_pixel)} - 1$, and x and y denote two windows of common size $N \times N$.

These quality image assessments permit to estimate the error in the image to be computed by FEM.

4.2.1 Theoretical proposed cases

This section is dedicated to study the behaviour of both hybrid methods designed to compute the solution to the inverse problem of EIT. Moreover, to determine the similarity with the initial data the image quality assessments are employed in which the PSNR (4.4), MSE (4.5) and SSIM (4.6) are used in the inverse problem approximation step.

The Lebesgue measure (3.27) is used to determine the error when the forward problem takes place in the problem approximation. Depending on the algorithm used, the inverse and the forward problem would determine the order of the approximation. The following section exposes briefly the methodology to obtain the solution of the artificial cases, in which geometric conductivity σ distributions are employed.

4.2.1.1 Methodology

In order to compute the approximation to the forward and inverse problems, the algorithms 3 and 4 are used. In this case, the problem approximation

depends upon the initial conditions given by the problem.

For example, when the initial condition is the conductivity σ, the algorithm 3 is used. Furthermore, as it can be appreciate in the flowchart 4.2, NPSM method is used first, for this algorithm the number of formal powers increase depending on the number of solution to be obtained, but the total number of points per radius and the number of radii are fixed to compute the solution faster.

In this case, the approximation obtained is the electric potential u_{app} at the boundary and it is compared with the imposed condition $u|_\Gamma$ by the Lebesgue measure. This approximation is used later as initial condition for the inverse problem, in which, the solution is the conductivity σ and it is compared by means of the image quality assessments (4.5), (4.4) and (4.6).

On the other hand, when the initial condition is the electric potential u, the algorithm 4 is used. In this case, the approximation is the solution to the inverse problem of (1.1). The comparison by means of the image quality assessments (4.5), (4.4) and (4.6) is used, comparing the approximation obtained with the initial condition.

Once the solution is obtained, in this case the conductivity σ, the second part of the method is employed. For this step, the electric potential u is calculated by means of NPSM. This approximation is compared with the original by using the Lebesgue measure (3.27). If the approximation does not fulfil the conditions given, the solution is introduced again at the beginning of the algorithm to recompute it again.

The following section is dedicated to the study of artificial conductivity cases proposed to analyse the behaviour of both hybrid methods, and determine which method is the best. Furthermore, a comparison with FEM is performed to determine is the solution is well-done.

4.2.1.2 First geometric case: Circle at centre

Considering a geometric conductivity σ distribution with the form exposed in the figure 4.4. This case is represented by a small disk located at the centre of the domain, which conductivity $\sigma_1 = 100$ and in the rest of the domain $\sigma_2 = 10$.

For the correct approximation of the forward problem, the imposed boundary condition to be used is the Lorentzian (3.31). This equation is

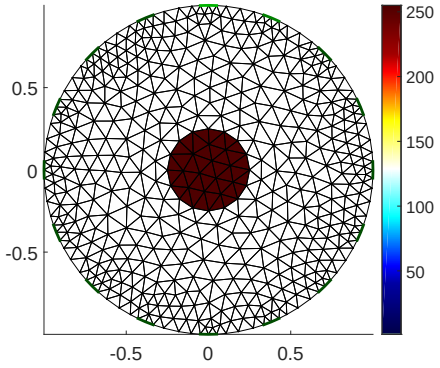

Figure 4.4: First geometric case: Circle at centre conductivity distribution.

Table 4.1: Centred circle error assessment and computing time.

Formal powers	Approximation HM1		Approximation HM2		Approximation FEM	
N	$\mathcal{E}$	t	$\mathcal{E}$	t	$\mathcal{E}$	t
10	9.84×10^{-15}	165.79	9.45×10^{-7}	200.20	5.45×10^{-6}	205.50
20	8.10×10^{-15}	252.76	8.90×10^{-7}	295.90	4.23×10^{-6}	315.15
30	7.24×10^{-15}	317.41	7.54×10^{-7}	360.08	3.12×10^{-6}	405.5
40	6.21×10^{-15}	453.56	6.39×10^{-7}	595.51	2.41×10^{-6}	650.99

the following one:

$$u|_{\Gamma} = \frac{1}{3}(x + d_x)^3 + \frac{1}{3}(y + d_y)^3 + L_c(x + d_x + y + d_y). \tag{3.31}$$

Hence, the table 4.1 exposed the solutions obtained by both methods and FEM. Remember that the employing of both problems of (1.1) is autonomous and the usage of both hybrid methods is doing independently, but the table shows the solution of its approximation using the forward problem.

The table 4.1 shows that the best result is achieved by the first hybrid method proposed. Nevertheless, FEM does not be discarded, because its approximation solution is considered accurate. Even thou the approximations for the forward problem are computed with high accuracy, it needs to be checked with the inverse problem.

Table 4.2: Centred circle conductivity distribution.

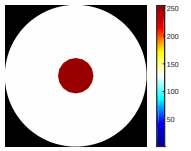 a)	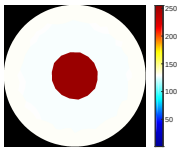 b)	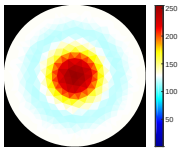 c)	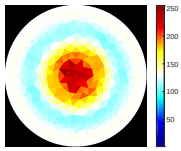 d)
	 e)	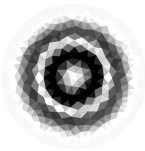 f)	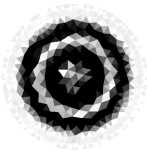 g)
	$PSNR = 20.1476$ $SSIM = 0.9282$ $MSE = 0.0097$	$PSNR = 19.8442$ $SSIM = 0.9041$ $MSE = 0.0104$	$PSNR = 16.1862$ $SSIM = 0.8543$ $MSE = 0.0241$

a) Original conductivity, b) HM1
c) HM2, d) FEM
e) Error HM1, f) Error HM2, g) Error FEM.

Thus, the table 4.2 shows the approximation obtained by the inverse problem, which it is approached by FEM and both hybrid proposed methods. In this case, for the employment of the second hybrid method, the number of iterations to be done is fixed at 10 times. Furthermore, in order to illustrate better the error, it is amplified 10 times.

Considering the table 4.2, the best approximation is obtained by the first hybrid method proposed. The reason is that the forward problem is very accurate, and it helps to obtain a better approximation in comparison with the other two methods. The result exposed by FEM method should not be discarded, because it is employing the basic scheme and the approximation could be best when other models are included.

In this case, the forward problem can achieve faster, accurate and stable solution due to the inclusion of the regularization process in its scheme. The results exposed in terms of the image quality assessments demonstrates that the best approximation is gotten by the first hybrid method. The image

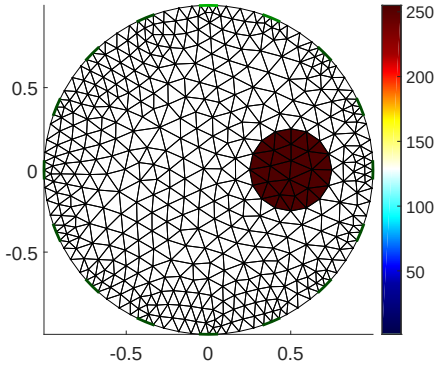

Figure 4.5: Displaced circle conductivity distribution.

quality assessments illustrates similarity between the methods. In this case, the results depends completely upon the image obtained by these methods.

4.2.1.3 Second geometric case: Circle out of centre

This case represents a conductivity σ distribution in which a small disk displaces from the center. This case is particularly important because it shows the behaviour of the method when a tiny disk is located in any part of the domain, and any displacement of the small disk can be considered as a geometric rotation.

The figure 4.5 shows the geometric distribution described before, in which the small displaced disk possesses a conductivity $\sigma_1 = 100$ and the rest of the domain $\sigma_2 = 10$. Actually, the imposed boundary condition to be used in this case is the equivalent like in the previous case that is (3.27).

The table 4.3 shows the error in the approximation obtained by NPSM and FEM. The table also exposed the computing-time for the three methods.

At the light of the results exposed in the table 4.3, in which the best result is the approximation using the first hybrid method, whereas the worst is the second hybrid method proposed. FEM can approximate with more accuracy than the second hybrid method proposed. More experiments should be done to check this behaviour.

Hence, in table 4.4 exposes the approximation and a comparison between the three methods.

Table 4.3: Displaced circle conductivity distribution error and computing time.

Formal powers N	Approximation HM1		Approximation HM2		Approximation FEM	
	$\mathcal{E}$	t	$\mathcal{E}$	t	$\mathcal{E}$	t
10	9.97×10^{-5}	157.75	8.89×10^{-3}	201.11	9.54×10^{-4}	225.54
20	9.10×10^{-5}	201.31	8.01×10^{-3}	290.81	8.15×10^{-4}	305.56
30	8.53×10^{-5}	300.91	7.51×10^{-3}	395.05	7.25×10^{-4}	482.25
40	7.07×10^{-5}	450.50	6.26×10^{-3}	534.23	6.63×10^{-4}	599.09

Table 4.4: Displaced circle conductivity distribution.

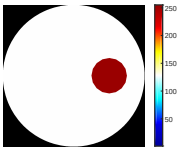 a)	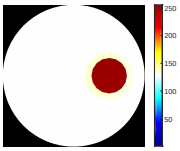 b)	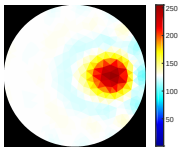 c)	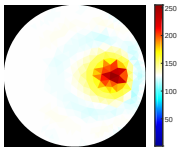 d)
	e)	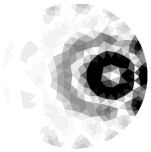 f)	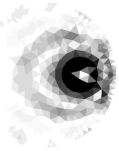 g)
	$PSNR = 49.2329$ $SSIM = 0.9990$ $MSE = 1.1932 \times 10^{-5}$	$PSNR = 24.5484$ $SSIM = 0.9385$ $MSE = 0.0035$	$PSNR = 19.9407$ $SSIM = 0.8358$ $MSE = 0.0101$

a) Original conductivity, b) HM1
c) HM2, d) FEM
e) Error HM1, f) Error HM2, g) Error FEM.

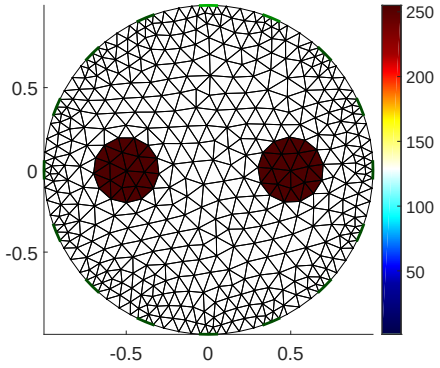

Figure 4.6: Two circles conductivity distribution.

Considering the table 4.4, the best approximation is obtained by the first hybrid method, but FEM method should not be discarded, because it uses the Gauss-Newton model in its basic scheme, and the approximation should be improved when a more effective model is used.

All in all, the second hybrid method performs a good approximation even when the maximum iterations are fixed at 10 times. Nevertheless, the approximation could be improved by iterating more times the algorithm. The results of the approximation obtained by the exposed methods show in table 4.4 the similarity between the original data and the approximation. In this case, the best method is the first one, due to its capacity to employed more accurate algorithms to approximate solutions. However, the FEM could achieve better approximations, if the employed model is changed.

4.2.1.4 Third geometric case: Two circles within

This special case show two tiny disk located within a unit disk domain. This conductivity distribution σ is used only for the forward problem. Then, the two small disk posses a conductivity $\sigma_1 = \sigma_2 = 100$, and the rest of the domain has a conductivity $\sigma_3 = 10$.

Hence, the figure 4.6 illustrates the geometric distribution employ to check the behaviour of both hybrid propose methods and FEM method in its basic scheme.

The imposed boundary condition is represented in equation (3.27). The table 4.5 exposed the relation of the three employed methods.

Table 4.5: Two circles conductivity distribution errors and computing times.

Formal powers	Approximation HM1		Approximation HM2		Approximation FEM	
N	$\mathcal{E}$	t	$\mathcal{E}$	t	$\mathcal{E}$	t
10	8.28×10^{-3}	199.99	6.12×10^{-1}	240.70	9.29×10^{-2}	265.91
20	7.71×10^{-3}	261.43	5.81×10^{-1}	345.29	8.88×10^{-2}	395.93
30	6.99×10^{-3}	375.51	4.44×10^{-1}	495.75	7.18×10^{-2}	505.01
40	5.81×10^{-3}	499.09	3.82×10^{-1}	630.91	6.29×10^{-2}	721.61

On the light of the results exposed on the table 4.5, the approximation error decreases considerably in comparison to the previous cases. This decrement is explained by the presence of the small disks, inserted inside the domain. In case of FEM, the mesh is the responsible to locate the tiny disks within and for the forward problem, in which the method employed is NPSM, the mapping within the domain provokes that the approximation cannot be obtained correctly. Even thou the best approximation is obtained by the first hybrid method.

Then, the table 4.6 exposes the approximation got by the three methods. In the case of the second hybrid method, the approximation is limited to 10 iterations and the errors obtained by these methods are amplified 10 times to appreciate better the error.

Considering the results contained in table 4.6, the best approximation is obtained by the first hybrid method. Nevertheless, as it was mention before, FEM uses basic scheme, in which the Gauss-Newton model. Furthermore, if the essential model is changed the approximation obtained by the FEM should be better.

Taking into consideration the image quality assessments, the first hybrid method achieves the best similarity with the original data. This statements helps to recognize the best approximation exposing the image reconstruction. Even though the obtained approximation, FEM should be taken into consideration because a simple modification in its scheme can perform better approximations.

Table 4.6: Two circles conductivity distribution.

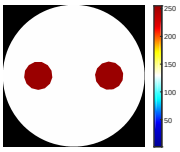 a)	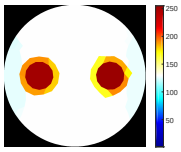 b)	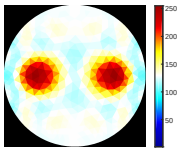 c)	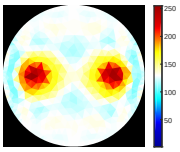 d)
	 e)	 f)	 g)
	$PSNR = 23.21$ $SSIM = 0.9462$ $MSE = 0.0048$	$PSNR = 21.4687$ $SSIM = 0.8750$ $MSE = 0.0071$	$PSNR = 20.0309$ $SSIM = 0.8666$ $MSE = 0.0099$

a) Original conductivity, b) HM1
c) HM2, d) Approximation FEM
e) Error HM1, f) Error HM2, g) Error FEM.

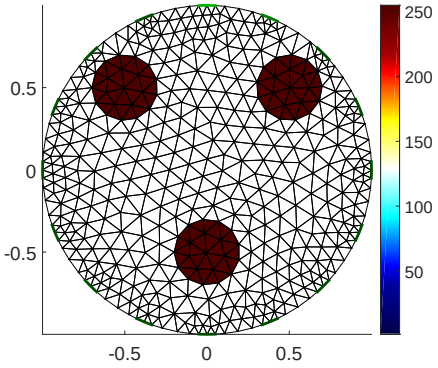

Figure 4.7: Three disk located within the unit disk domain.

Table 4.7: Three disk within domain error assessment and computing time.

Formal powers	Approximation HM1		Approximation HM2		Approximation FEM	
N	$\mathcal{E}$	t	$\mathcal{E}$	t	$\mathcal{E}$	t
10	3.45×10^{-1}	160.99	4.45×10^{1}	200.20	5.90×10^{-2}	205.50
20	3.10×10^{-1}	250.86	3.90×10^{1}	295.90	4.81×10^{-2}	315.15
30	2.98×10^{-1}	310.51	2.54×10^{1}	360.08	3.72×10^{-2}	405.5
40	2.78×10^{-1}	450.66	1.39×10^{1}	595.51	2.63×10^{-2}	650.99

4.2.1.5 Fourth geometric case: Three circles within

In this case, there are set three small circles inside a unit domain. Furthermore, the conductivity $\sigma_1 = \sigma_2 = \sigma_3 = 100$ is the same for the three objects. Respectively, for the rest of the domain the conductivity is fixed at $\sigma_4 = 10$. The figure 4.7 illustrates the geometric distribution of the conductivity.

Therefore, table 4.7 exposes the error in the approximation obtained by the three method. In addition, the imposed boundary condition to be imposed is the same like in the equation (3.27), that it is the Lorentzian boundary condition.

In this particular case, table 4.7 shows that the best method to approach the solution in FEM, meanwhile the results obtained by the hybrid proposal should not be discarded. There are many reasons that can explain the result obtained by these methods, but it simply determines that the accuracy in

Table 4.8: Three circle located within the domain.

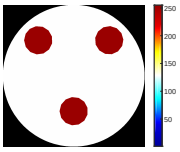 a)	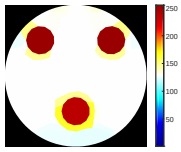 b)	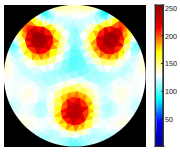 c)	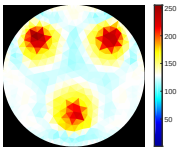 d)
	 e)	 f)	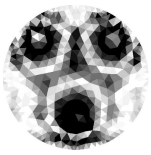 g)
	$PSNR = 34.2474$ $SSIM = 0.9855$ $MSE = 3.7606 \times 10^{-4}$	$PSNR = 19.4981$ $SSIM = 0.8269$ $MSE = 0.0112$	$PSNR = 17.9035$ $SSIM = 0.8458$ $MSE = 0.0162$

a) Original conductivity, b) HM1
c) HM2, d) FEM
e) Error HM1, f) Error HM2, g) Error FEM.

the method cannot be reach at least for this case. Nevertheless, the mesh configuration is better than the mapping by a piece-wise separable variable method.

Hence, table 4.8 exposes and illustrates the result for the inverse problem approximation. In this case, the hybrid proposals depend upon the approximation of the forward problem, and if these approximations are not accurate, the result could not be obtained precisely.

Nevertheless, the table 4.7 shows the approximation to the forward problem at least for the proposal methods are not the best, the results obtained in the inverse problem outweigh the expectations. Even though FEM obtains the best approach due to its mesh, when the inverse problem is approximated, the result is not the best one. This behaviour is due to model employed with FEM. In spite of this situation, the behaviour and the approximation accuracy should be improved when another model is used.

The image quality shows the inverse problem approximation, in which

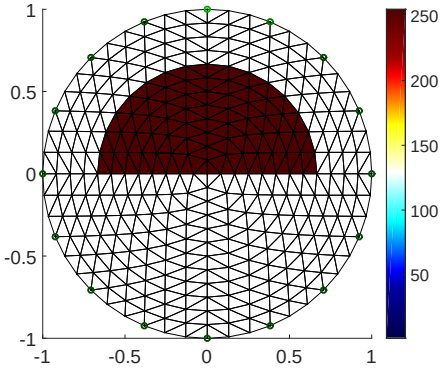

Figure 4.8: Half centred circle inside a unit disk domain.

the best solution is obtained by the first hybrid method. Furthermore, in this case, the approximation performed should be analysed and studied in detail to determine the behaviour. One point in favour is the unit disk domain that it is more convenient for the sample approached.

4.2.1.6 Fifth geometric case: Half circle within

The following conductivity σ distribution is a half circle at the centre of the unit disk domain. For this distribution the conductivity is $\sigma_1 = 100$. Concurrently for the shape inside the conductivity is $\sigma_2 = 10$ for the rest of the domain. The following figure 4.8 illustrates the unit disk domain with the conductivity function to be used.

Hereafter, such as in the previous cases, the imposed boundary condition to be used only for the forward problems is the Lorentzian condition presented in equation (3.27). The table 4.9 exposes the numerical error and the time computing for the approximation done by the forward problem using NPSM and FEM.

In order to make a comparison in the approximation, the image quality assessment is employed to determine if the approximation is similar to the original conductivity. This comparison can be observed in table 4.10, in which the approximation is done by FEM.

Considering the results exposed in table 4.10, in this particular case, the best approximation is gotten by the first hybrid method, and the worst is obtained by FEM. The approximation should improve if the model used with

Table 4.9: Half circle centred error assessment and computing time.

Formal powers N	Approximation HM1		Approximation HM2		Approximation FEM	
	$\mathcal{E}$	t	$\mathcal{E}$	t	$\mathcal{E}$	t
10	1.81×10^{-7}	165.79	9.14×10^{-4}	200.20	5.90×10^{-3}	205.50
20	1.59×10^{-7}	252.76	8.16×10^{-4}	295.90	5.10×10^{-3}	315.15
30	1.34×10^{-7}	317.41	7.15×10^{-4}	360.08	3.86×10^{-3}	405.5
40	1.21×10^{-7}	453.56	6.92×10^{-4}	595.51	3.52×10^{-3}	650.99

Table 4.10: Half circle centred conductivity distribution.

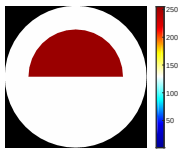 a)	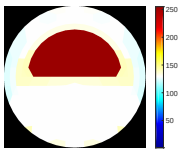 b)	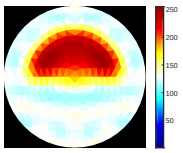 c)	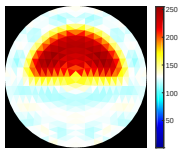 d)
	 e)	 f)	 g)
	$PSNR = 27.4690$ $SSIM = 0.9866$ $MSE = 0.0018$	$PSNR = 19.3014$ $SSIM = 0.8475$ $MSE = 0.0117$	$PSNR = 19.4205$ $SSIM = 0.8297$ $MSE = 0.0114$

a) Original conductivity, b) HM1
c) HM2, d) FEM
e) Error HM1, f) Error HM2, g) Error FEM.

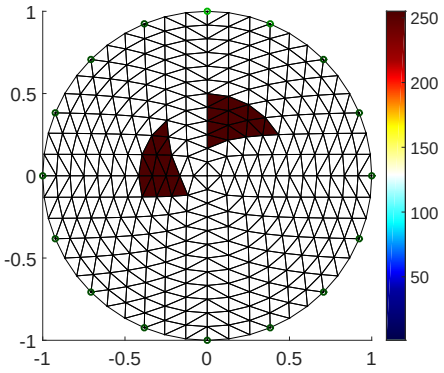

Figure 4.9: Triangles within the domain.

Table 4.11: Two triangles error assessment and computing time.

Formal powers N	Approximation HM1		Approximation HM2		Approximation FEM	
	$\mathcal{E}$	t	$\mathcal{E}$	t	$\mathcal{E}$	t
10	8.45×10^3	165.79	9.90×10^4	200.20	5.48×10^1	205.50
20	8.10×10^3	252.76	8.88×10^4	295.90	4.43×10^1	315.15
30	7.99×10^3	317.41	7.57×10^4	360.08	3.52×10^1	405.5
40	7.65×10^3	453.56	6.30×10^4	595.51	2.59×10^1	650.99

FEM is different.

In terms of the image similarity, the best result is achieved by the first hybrid method. As it was mentioned before, the image quality assessments illustrates the error between the original data and the approximation that the methods can get.

4.2.1.7 Sixth geometric case: Triangles

In this case, two triangles are used inside the domain, these triangles posses a conductivity $\sigma_1 = \sigma_2 = 100$ distribution and for the rest of the domain $\sigma_3 = 10$. This conductivity distribution is illustrated in figure 4.9.

The table 4.11 exposes the result of the three methods.

Hence, the table 4.12 shows the comparison that is made using the quality image assessments, in which the approximation is compared with the original

Table 4.12: Two triangles within a unit disk conductivity distribution.

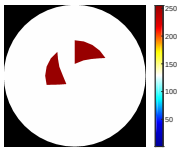 a)	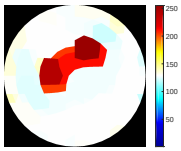 b)	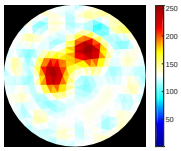 c)	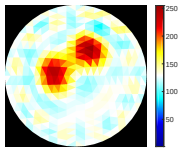 d)
	 e)	 f)	 g)
	$PSNR = 15.5200$ $SSIM = 0.9028$ $MSE = 0.0281$	$PSNR = 19.9845$ $SSIM = 0.8497$ $MSE = 0.0100$	$PSNR = 19.4051$ $SSIM = 0.8200$ $MSE = 0.0115$

a) Original conductivity, b) HM1
c) HM2, d) FEM
e) Error HM1, f) Error HM2, g) Error FEM.

conductivity to determinate the accuracy of the method.

Summing up the results in the table 4.12, the best approximation is obtained by means of the first hybrid method. This sample is used to understand the behaviour of the three methods when non-smooth conductivity distribution is selected. However, FEM should not be discarded. Instead of it, the basic model should be changed in order to get better results.

The image quality assessments were used to determined the similarity with the original data employed for the main problem. In this case, the best approximation was achieved by the second hybrid method. but the solution obtained could be improved for the other two methods, if more accurate and robust mesh are employed. The image quality helps to understand the behaviour of the problem.

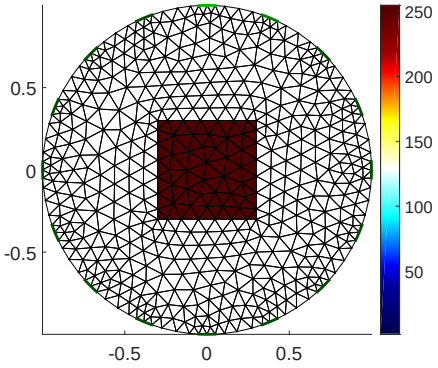

Figure 4.10: Centred square conductivity distribution.

4.2.1.8 Seventh geometric case: Square at center

In this particular case, the square at center conductivity distribution σ is representative of a non-smooth distribution inside. For this case the conductivity distribution possesses $\sigma_1 = 100$ and the rest of the domain has $\sigma_2 = 10$.

This shape distribution is illustrated in the figure 4.10.

Furthermore, the imposed boundary condition is the Lorentzian conductivity function represented in the equation (3.27). The table 4.13 shows the results for the approximation for the forward problem. This approximation presents the error in the approximation comparing with the imposed boundary condition.

Table 4.13: Centred square conductivity distribution errors and computing time.

Formal powers	Approximation HM1		Approximation HM2		Approximation FEM	
N	$\mathcal{E}$	t	$\mathcal{E}$	t	$\mathcal{E}$	t
10	2.34×10^{-1}	169.19	6.35	210.10	8.28×10^{1}	225.10
20	2.04×10^{-1}	255.81	5.10	298.41	9.81×10^{1}	225.10
30	1.90×10^{-1}	300.00	4.56	370.15	10.16×10^{1}	405.51
40	1.61×10^{-1}	451.95	3.33	590.62	12.41×10^{1}	645.06

In this case, the best approximation is obtained by the first hybrid

method, in which the forward problem is computed first and then the inverse problem. Furthermore, the three methods proof to be stable and all can be employed to approximate the solution to the inverse problem.

Like in the previous cases, a comparison is taken into consideration, where the image quality assessments are used to compare the approximation to the inverse problem and comparing with the original conductivity distribution.

The table 4.14 shows the simulations and the results for the approximation obtained by these three methods.

Table 4.14: Approximation for square at center conductivity distribution.

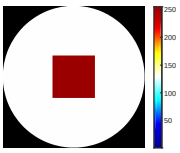 a)	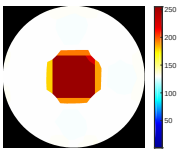 b)	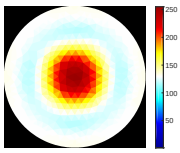 c)	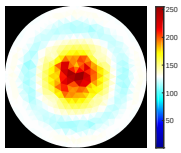 d)
		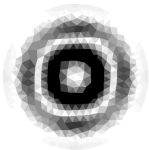	
	e)	f)	g)
	$PSNR = 23.1058$ $SSIM = 0.9570$ $MSE = 0.0049$	$PSNR = 21.0459$ $SSIM = 0.8995$ $MSE = 0.0079$	$PSNR = 17.61$ $SSIM = 0.8631$ $MSE = 0.0173$

a) Original conductivity function, b) Approximation hybrid method 1
c) Approximation hybrid method 2, d) Approximation FEM
e) Error hybrid method 1, f) Error hybrid method 2, g) Error FEM.

Summarizing up the results gotten in both tables 4.14 and 4.13, the best approximation method is the first one. Nevertheless, the other two methods should not be discarded, especially FEM, but the approximation should be improved when other model is in use instead of the basic.

The image quality assessments determines that the method, which approximates the solution best, is the first hybrid method. In this case, the image should be analysed to determine if the shape of the domain does not

affect directly to the image quality. More simulations need to be performed to analyse and to understand the behaviour of the three methods. Furthermore, these methods try to obtain the solution to the inverse problem, but all the samples are created artificially.

4.2.1.9 Discussion

On the light of the presented results and without jumping into conclusions, the hybrid method posed in this dissertation shall well be one of the most advance propositions for the theoretical foundations of the Electrical Impedance Tomography, since it incorporates the advantages provided by the use of the extended Pseudoanalytic Function Theory, also a research result reported in these pages and the application of refined variations of the Finite-Element Method.

In this sense, we shall aboard the gamma of examples from two different classification those experiments based upon theoretical conductivity distributions and those incoming from laboratory models together with their corresponding physical measurements. Here we discuss the theoretical cases.

The simulations are all around purely geometrical conductivity distributions as it should be for a proper comparison with real cases. Seven different examples are included and at each one them, the hybrid method is applied: a certain number of formal powers are approached employing the extended principles of the Pseudoanalytic Function Theory. Intermediately after such formal powers are employed as boundary conditions for the novel variation of the Finite-Element Method is to solve the inverse problem.

In general, we can enhance that the examples corresponding to first four cases presented the best convergence according to the numerical evaluation. Nonetheless, the qualitative convergence is discourage because it strongly depends of the criteria of the observer, we shall also emphasized that the remaining examples might also be qualified as acceptable if we appoint that the geometrical figures within the domains possessed non-smooth points. Once more, the last sentence shall be only be considered from an engineering point of view, since the appreciation remains qualitative.

The proposed hybrid methods have proven its effectiveness to approximate the solution of the inverse problem of EIT. In this case, the approximation by the hybrid methods depends upon the given initial conditions. In addition, the Tikhonov's regularization process helps to stabilize the approximation. Moreover, the procedure helps to improve the accuracy in the

method, as it was exposed in the tables.

A disadvantage of the first hybrid method is that it requires necessarily the conductivity σ distribution to begin the calculation. An advantage is that the computing-time decreases considerably when the estimate solution of the forward problem is used in the inverse problem.

The second hybrid method needs the electric potential $u|_\Gamma$ to begin the calculation. Nevertheless, this method is slower than the first hybrid method, because it needs to perform the analysis of the whole method to determine if the solution is right and fulfil the conditions. For this reason a stop criterion and a threshold is used to stop the algorithm.

A disadvantage of this method is the large computing-time due to the high number of iterations. However, the advantages of this method is that in some cases it performs better approximation.

The comparison with FEM is considered, because this method is used in many works dedicated in this field. However, FEM is a slower process that requires many computational resources, and this method can not be parallelized such as NPSM (see e.g. [67], [88]).

A disadvantage of this method is the mesh construction, it means that if the solutions need to be more accurate the mesh should be bigger.

For this reason, the maximum resolution relies on the mesh size. However, an advantage of this method is the possibility to adapt by changing some parameters in its scheme, this change can produce a better and accurate approximation to the analysed problem.

4.2.1.10 Conclusion

The inverse problem of EIT is considered very difficult to solve, for this reason, the designed hybrid methods are proposed to analysed the behaviour of (1.1). In this case, the complexity relies on the initial conditions.

All the exposed methods can perform and achieve solutions to the inverse problem, but the requirement of more techniques to achieve a possible solution depends on the method to be used. In case of the hybrids methods, NPSM needs obligatory a regularization procedure to obtain stable solutions. However, the computational resources increase by the addition of these techniques.

The goal is to design a technique that it could compete with FEM and used in the Medical Imaging. For this reason, the study of the geometrical cases, let us to perform this analysis to create a possible method that

can be used with physical real-measures in the practice. Furthermore, this measurements should be obtained by a data acquisition system.

Further works should be included the analysis of these real-measurements and the design of a data acquisition system to used in the practice.

4.2.2 Real measurements simulation case

In this section, the study of the electrical impedance equation (1.1) takes place, in which real measurements are used instead of artificial conductivity distributions. Furthermore, both hybrid methods are used to approximate the solution to the inverse problem. In addition, in [37], the methods are analysed and studied to understand the real physics measurements.

Following to [37], [9] and [98], the approximation model is the backprojection and it is used because of its simplicity and the possibility to employ this method to generate more accurate approximations. In this case, the procedure is used to generate a 2D and 3D models. Sometimes this method is combined with a Tikhonov regularization process to stabilize and correct non-smoothness (see e. g. [92] and [42]).

In [37], the first step in this section is to get the results exposed. Nevertheless, in the second step, a comparison between the proposed algorithm and the method is presented. In order to understand better the methodology that it is exposed later, the general backprojection model is explained in the following section.

4.2.2.1 Generallized backprojection model

Following to [37], the backprojection model is used to approximate the solution to the inverse problem. Furthermore, the electric potential $u|_\Gamma$ is obtained from real physics measurements and they are gotten from a Phantom-EIT. This device is known as *Applied Potential Tomography System Mark I* (IBEES, Sheffield, UK) (see e.g. [16]).

Considering the measurements given, the backprojection model needs to be analysed in order to compute the solution for the inverse problem. For this reason, the generalized backprojection model is studied in detail to compute the approximation of the solutions (see e.g. [37]). Furthermore, once the approximation are done, a comparison using both hybrid methods is used to confirm the functionality of both methods.

Following to [96], the electrical impedance equation (1.1) is employed and presented as follows:

$$\operatorname{div}(\sigma \operatorname{grad} u) = 0. \tag{1.1}$$

In this case, the imposed boundary conditions to (1.1) is:

$$\begin{cases} u = u_0 & \in \Gamma_1 \\ \sigma \frac{\partial_u}{\partial_n} = -j_n & \in \Gamma_2, \end{cases} \tag{4.7}$$

where σ is the conductivity and u is the electric potential for a domain Ω with boundary Γ, in this case j_n is the current density addition and n is the outgoing vector.

Considering the Gauss divergence theorem for boundaries (see e.g. [63]), it is assume that G is a continuous vectorial function, then:

$$\int_{\Gamma} G \cdot dS = \int_{\Gamma} \text{ grad } G dV. \tag{4.8}$$

Hereafter, when two scalar functions ψ and ϕ are considered, and supposing that σ is an scalar vector, the following statement is obtained by the substitution of G for $\psi\,(\sigma \text{ grad } \phi)$:

$$\int_{\Gamma} \psi\sigma \text{ grad } \phi \cdot dS = \int_{\Gamma} \psi \text{ grad } \left(\sigma \text{ grad } \phi\right) dV + \int_{\Omega} \sigma \text{ grad } \psi \text{ grad } \phi dV. \tag{4.9}$$

Then, let us suppose ϕ as a solution of (1.1), in which the left-hand term in the equation (4.9) is vanished as follows:

$$\int_{\Gamma} \psi\sigma \text{ grad } \phi \cdot dS = \int_{\Gamma} \sigma \text{ grad } \psi \cdot \text{ grad } \phi dV. \tag{4.10}$$

Supposing that a current I is introduced into the region Ω by using the electrodes in the boundary, then a potential field ϕ is set over the region and the surface Γ. By means of the Ohm's law the current density is:

$$\int_{\Gamma} \psi\sigma \text{ grad } \phi \cdot dS = I_{\psi}. \tag{4.11}$$

Similarly, considering ψ as a solution to (1.1) when the current I is conducted trough the electrodes in the boundary, then the integral surface turns into:

$$u = \psi = \phi = \int_{\Gamma} \sigma \text{ grad } \psi \text{ grad } \psi dV. \tag{4.12}$$

Then, the general conductivity distribution and its association with the voltage measurements in terms of the perturbation and the uniform conductivity distribution can be expressed as:

$$\begin{cases} \sigma = \sigma_u + \sigma_p \\ u = u_u + u_p \\ \text{grad } \psi = \text{ grad } \psi_u + \text{ grad } \psi_p \\ \text{grad } \phi = \text{ grad } \phi_u + \text{ grad } \phi_p \end{cases} \tag{4.13}$$

where u and p are uniform and equivalent respectively.

Then, (4.12) can be expanded as:

$$u = \int_{\Omega} \sigma \left(\text{ grad } \psi_u + \text{ grad } \psi_p \right) \cdot \left(\text{ grad } \phi_u + \text{ grad } \phi_p \right). \tag{4.14}$$

Supposing that the current is constant and it is applied into the region Γ for the equation (4.14), such as it follows:

$$u_p = - \int_{\Omega} \sigma_p \text{ grad } \psi_u \cdot \text{ grad } \phi dV. \tag{4.15}$$

So, if the conductivity σ_p is minor than grad $\phi_p \ll$ grad ϕ_u and the relation on the integral grad ϕ_p in (4.15), the result is the following statement:

$$u_p = - \int_{\Omega} \sigma_p \text{ grad } \psi_u \text{ grad } \phi_u dV. \tag{4.16}$$

In terms of the uniform conductivity distribution and the voltage is monotonic. In those case, the potential of an element corresponds to a unique value. Then, the electric potential for any electrode v^i could be computed by FEM with the following equation:

$$u^i = f_{u^i}(x), \tag{4.17}$$

where x is the boundary current into the coordinate to the axis, i corresponds to i^{th} conductor pair.

Then, each electric potential element can be calculated by ϕ:

$$\tilde{v}_u^i = \phi^{-1}\left(v_u^i\right) = \phi^{-1}\left(f_{v_u^i}(x_K), f_{v_u^i}(x_M), f_{v_u^i}(x_N)\right). \tag{4.18}$$

Moreover, if the voltage is normalized such as the following form:

$$u_n^i = \frac{u_p^i}{u_u^i}, \tag{4.19}$$

where u_u^i is the i^{th} voltage measurement in terms of the conductivity uniform distribution such as:

$$u_u^i = \sigma_u \int_{\Omega} \text{ grad } \phi_u^i \text{ grad } \psi_u^i dV, \tag{4.20}$$

the by substituting 4.20 into 4.19 it turns into:

$$u_u^i = \frac{-\int_\Omega \tilde{\sigma}_p \text{ grad } \psi_u \text{ grad } \phi_u dV}{\sigma_u \int_\Omega \text{ grad } \phi_u^i \text{ grad } \psi_u^i dV}, \tag{4.21}$$

in this case the electric potential corresponds to a measurement in at the boundary, being:

$$\tilde{v}_u^i = u_u^i. \tag{4.22}$$

Actually,

$$\phi^{-1}\left(f_{v_u^i}(x_K), f_{v_u^i}(x_M), f_{v_u^i}(x_N)\right) = \frac{-\int_\Omega \tilde{\sigma}_p \nabla\psi_u \cdot \nabla\phi_u dV}{\sigma_u \int_\Omega \text{ grad } \phi_u^i \text{ grad } \psi_u^i dV} \tag{4.23}$$

where σ_u is constant in terms of the distribution, so its normalized form is:

$$\tilde{\sigma}_n = \frac{\tilde{\sigma}_p}{\tilde{\sigma}_u}. \tag{4.24}$$

Rewriting the last equation:

$$\phi^{-1}\left(f_{v_u^i}(x_K), f_{v_u^i}(x_M), f_{v_u^i}(x_N)\right) = \frac{-\int_\Omega \tilde{\sigma}_n \nabla\psi_u \cdot \nabla\phi_u dV}{\int_\Omega \text{ grad } \phi_u^i \text{ grad } \psi_u^i dV}. \tag{4.25}$$

Using the (4.25) should be rewritten in a matrix form such as:

$$\Phi^{-1} u_n = G S^{-1} \tilde{\sigma} \tag{4.26}$$

where Φ is the element projection and S is the sensitivity matrix whose coefficients are given for;

$$S_{ij} = -\int_{\Omega^j} \text{ grad } \phi_u^i \text{ grad } \psi_u^i dV, \tag{4.27}$$

indeed, the diagonal matrix G is different to zero, such as:

$$G_{ii} = \int_\Omega \text{ grad } \phi_u^i \text{ grad } \psi_u^i dV. \tag{4.28}$$

Summarising up, when the equation (4.26) is solved, the distribution could be constructed into a normalize conductivity.

4.2.2.2 Methodology

In case, in which the conductivity σ distribution is unknown, and the electric potential u is given at the boundary. The methodology is the following one:

1. Using the electric potential $u|_\Gamma$.
2. Calculating the inverse problem by using FEM with the backprojection model.
3. Employing the conductivity σ approximated. The NPSM takes places to approximate the solution.
4. The solution is compared with the Lebesgue measure and the image quality assessments.

The designed hybrid method employs the approximation to the forward and inverse problem, but this solution depends on the initial conditions. In this case, the conductivity σ distribution is unknown and the goal is to compute this one. Then, the first hybrid method is useless. However, the second hybrid method is used instead to compute this solution.

In this case, an EIT phantom that is data acquisition system use small electrodes equidistantly located at the boundary of any body. Then, small voltages are introduced by means of these electrodes. Furthermore, this phantom registered the electric potential $u|_\Gamma$ at the boundary.

Hence, this electric potential u is employed in the hybrid method to compute an approximation. The real-measurements are given by the University of Götingen in Germany, and the phantom that they used to obtain this electric potential is the *"Applied Potential Tomography System Mark I"*. This device employs 16 electrodes located at the boundary of a body (see e.g. [37]).

4.2.2.3 Simulations

According to [96] and [37], using the generalize backprojection model, the approximations of real measurements for five-controlled hogs are improved.

In this case, the main domain considered is the perimeter of the hog-thorax. Moreover, the measurements in the boundary are known, and the exact position of the electrodes at the boundary. However, the conductivity inside the domain is unknown. In addition, these five controlled porcine laboratory subjects are injured with acid, it was introduced in the lungs of the subjects and monitored to obtain the approximation.

Table 4.15: Five controlled porcine laboratory subjects with left lung injured by acid [37].

	1	2	3	4	5
Control	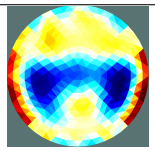	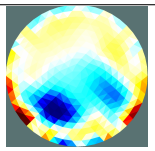	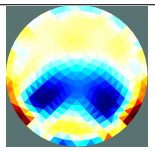	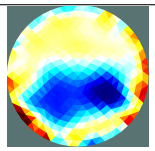	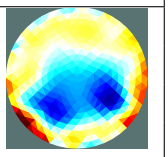
Left Lung Injury	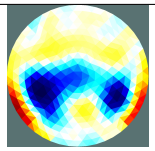	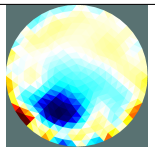	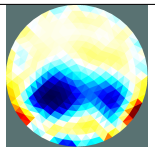	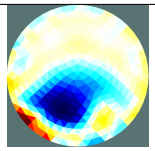	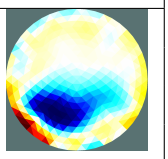

The approximations are illustrated in the table 4.15. These approximations are performed using FEM together with a backprojection model. In this table, the first image is an example of a thorax, and the approximations that are shown in a unitary disk domain are the approximation for the five-controlled animals. The other approximation that is exposed into the table are the injured subjects.

Summarizing up the table 4.15, these approximations are shown without the image quality assessments, because the conductivity image distribution σ is not given to make this comparison. All these ten approximations are similar to the images that the tested work exposes (see e.g. [37]).

Hence, for the further simulation data to be approached, these images are going to be considered as the original conductivity distribution. Furthermore, the employing of the hybrid methods are restricted to the knowledge of the forward problem. For this reason, the first hybrid method can be employed but the solution could not be possible achieved.

Table 4.16: Real approximation for the first controlled hog image.

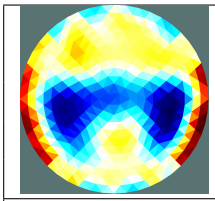	Second Hybrid Method	
	Gauss-Newton	Gauss-Newton Tikhonov
Approx.	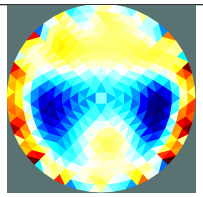	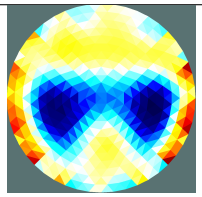
Error		

4.2.2.4 First controlled-hog simulation

On the other hand, the approximation doing is performed by the second hybrid method. These approximations are exposed in the table 4.16.

The table 4.17 illustrates the approximation to the forward problem by using the Taylor's series in formal powers method.

The table 4.17 exposes the results for the second hybrid method, obtaining and performing a good approximation. Nevertheless, FEM approximates better the solution of (1.1). In addition, FEM employed for this approximation is combined with the backprojection model to obtain more accurate solutions to the inverse problem of (1.1).

In order to proof the robustness of the algorithm 4, the mesh generation is improved ten times. This improvement could be observed in the table 4.18. Moreover, for this approximation case, the error is ten times increased.

The table 4.19 illustrates the approximation to the forward problem by using NPSM.

The table 4.19 exposed the results for the second hybrid method, per-

Table 4.17: Real approximation for the first-controlled hog error assessment and computing time.

Formal powers N	Approximation HM2		Approximation FEM	
	$\mathcal{E}$	t	$\mathcal{E}$	t
10	3.15×10^{1}	200.20	5.48×10^{-1}	205.50
20	5.43×10^{1}	295.90	4.43×10^{-1}	315.15
30	4.71×10^{1}	360.08	3.52×10^{-1}	405.5
40	3.21×10^{1}	595.51	2.59×10^{-1}	650.99

Table 4.18: Real approximation for the first controlled hog image improved resolution.

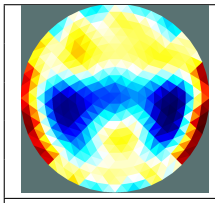	Second Hybrid Method	
	Gauss-Newton	Gauss-Newton Tikhonov
Approx.	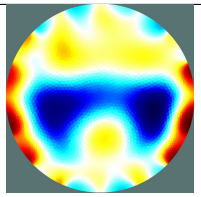	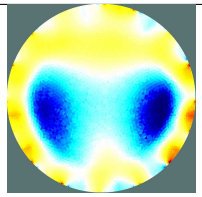
Error		

Table 4.19: Real approximation for the first-controlled hog with improved resolution error assessment and computing time.

Formal powers N	Approximation HM2		Approximation FEM	
	$\mathcal{E}$	t	$\mathcal{E}$	t
10	5.51×10^{-2}	400.20	5.48×10^{-2}	405.50
20	5.63×10^{-2}	695.90	4.43×10^{-2}	615.15
30	5.94×10^{-2}	860.08	3.52×10^{-2}	805.5
40	5.28×10^{-2}	1095.51	2.59×10^{-2}	1050.99

forming and obtaining a good approximation. However, FEM approximates better the solution of (1.1). In addition, FEM is combined with the back-projection model to obtain more accurate solutions to the inverse problem of (1.1).

4.2.2.5 Second controlled-hog simulation

Similarly to the previous simulation case, the results that table 4.20 exposes, show the behaviour of the algorithm 4. Furthermore, in this case, another image is employed to proof that the behaviour is the same. This table shows the comparison between the hybrid method and the approximation obtained by the proposed method (see e.g. [37]).

The table 4.21 illustrates the approximation to the forward problem by using NPSM with an improved mesh.

A modification in the mesh takes place for FEM, in which the resolution increases considerably. In addition, the table 4.22 shows the approximation when the mesh is increased 10 times.

The table 4.23 illustrates the approximation to the forward problem by using NPSM with an improved mesh.

The table 4.23 exposes the results for the second hybrid method, performing a good approximation. Nevertheless, FEM approximates better the solution of (1.1). Moreover, FEM is combined with the backprojection model to obtain more accurate solutions to the inverse problem of (1.1).

The behaviour of the method proofs that it can be used, but due to the initial condition give, the method to be chosen could not be suitable to perform the task. For all the approximations done in the tables 4.16, 4.18,

Table 4.20: Real approximation for the second controlled hog.

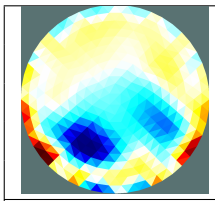	Second Hybrid Method	
	Gauss-Newton	Gauss-Newton Tikhonov
Approx.	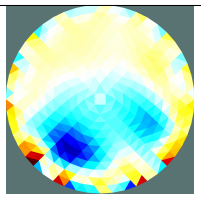	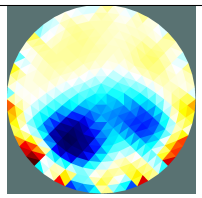
Error	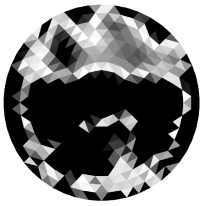	

Table 4.21: Real approximation for the second-controlled hog resolution error assessment and computing time.

Formal powers	Approximation HM2		Approximation FEM	
N	$\mathcal{E}$	t	$\mathcal{E}$	t
10	5.43×10^{1}	200.10	9.80×10^{-1}	202.50
20	5.19×10^{1}	395.45	9.61×10^{-1}	315.51
30	4.96×10^{1}	465.22	9.23×10^{-1}	440.76
40	4.60×10^{1}	595.51	9.01×10^{-1}	525.99

Table 4.22: Real approximation for the second controlled hog image improved resolution.

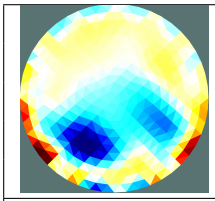	Second Hybrid Method	
	Gauss-Newton	Gauss-Newton Tikhonov
Approx.	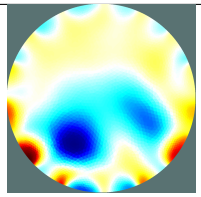	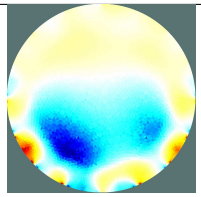
Error	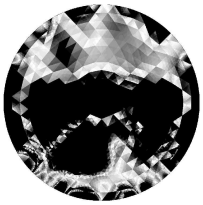	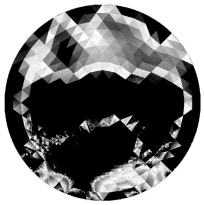

Table 4.23: Real approximation for the second-controlled hog with improved resolution error assessment and computing time.

Formal powers N	Approximation HM2		Approximation FEM	
	$\mathcal{E}$	t	$\mathcal{E}$	t
10	3.12×10^{-2}	400.20	5.81×10^{-2}	405.50
20	3.39×10^{-2}	695.90	4.32×10^{-2}	615.15
30	3.46×10^{-2}	860.08	3.23×10^{-2}	805.5
40	3.80×10^{-2}	1095.51	2.94×10^{-2}	1050.99

4.20 and 4.22 illustrate the behaviour of the hybrid method.

4.2.2.6 Discussion

As a continuation of the discussion stated for the theoretical cases, when applying the novel methodology to the pair of examples corresponding to real measurements. The hybrid method showed up a better convergence than such reported in the previously published literature employing the same data. This shall be the strongest argument to sustain the originality and pertinence of this dissertation.

The hybrid methods that have been developed to approximate the inverse problem of EIT, demonstrates it effectiveness. However, these methods depend upon the initial conditions given. In this special case, the first hybrid method needs the conductivity distribution as initial condition, for this reason, this method is useless when real-measurements are given.

Nonetheless, the second hybrid method has proven its effectiveness, because it needs the electric potential $u|_\Gamma$ as initial condition to begin the computation of the inverse problem. However, both methods require FEM to compute the solution, in comparison with the standard FEM, these hybrid proposals prove its effectiveness to compute the solution.

The importance of this section relies on the possibility to employ real-measurements to begin and to prove the correct functionality of the method. The second hybrid method can work with real measurements and compared with FEM. In this case, the second hybrid method can achieve results by using the electric potential u given. Moreover, the mesh size is very important to compute more accurate solutions to this problem.

The comparison made between the second hybrid method and FEM is not correctly compared due to the lack of a conductivity model. In this case, the controlled-pig image is used as the original conductivity distribution at it is compared with the approximation. For this reason, the image quality assessments and the Lebesgue measure cannot achieve a good comparison.

4.2.2.7 Conclusions

The second hybrid method has proven it effectiveness when the mesh is amplified achieving a better approximation than the solutions obtained by FEM with backprojection model. In this case, it is supposed that the best approximation performed demonstrates that FEM and second hybrid method could

be used to obtain solutions to the inverse problem.

The second hybrid method and FEM depend completely on the mesh size and for this reason the resolution obtained by both methods could be considered good. Furthermore, the increment on the mesh provokes that the computational resources increase considerably. Taking into consideration the computational resources, the computing-time to calculate the approximation increases too.

One possibility to decrease the computing-time is the parallel computing, but due to the high recursivity in the methods employed makes this possibility impossible. Furthermore, NPSM can be parallelized in some functions making the process faster and preserving its accuracy.

For this reason, it is important to begin a study and to design a method that uses NPSM to solve the inverse problem by itself. The hybrid method helps to understand the behaviour of this difficult problem to develop a method to use real-measurements and NPSM to achieve an better approximation.

Chapter 5

General conclusions

The main of this work is to study of State-of-The-Art techniques of the Electrical Impedance Tomography, to found and design a novel and effective approach in this are, where the solutions to the forward and inverse problems can be constructed with a higher degree of accuracy.

The Finite-Element Method (FEM) is a technique able to obtain accurate and effective solutions to the forward and inverse problems. Nonetheless, the maximum resolution and precision that FEM can achieve depends strongly upon the mesh size.

The reconfiguration of the mesh consumes considerable resources, thus the computational time becomes too long, without mentioning that the very nature of the FEM does not allow the application of parallel computing algorithms. Furthermore, the use of geometrical figures possessing edges or non-smooth boundaries, represents a very hard task for FEM. Therefore, in many cases the EIT technique cannot be considered a standard Medical Imaging method, and cannot be applied in more general practical applications.

On the other hand, the Taylor's series in formal powers' method (NPSM), which is performed in this work with the purpose of approximating the forward problem of the electrical impedance equation, turns out to be more efficient and accurate than FEM. One drawback of mentioned method is that the stability possesses by NPSM is low. In this dissertation, we resolved this disadvantage incorporating the Tikhonov's regularisation into the basic scheme of NPSM approach, finally obtaining a stable solution.

Both methods FEM and, NPSM use dramatic computer resources to perform good approximation. However, NPSM method can be parallelized in order to obtain faster solutions. Modified regularised NPSM method has

been used as a principal component in designing a novel hybrid approach for EIT problem, resulting in better approximation for the inverse problem.

We proposed two hybrid structures where the NPSM and FEM are used together and can be adapted according to the given initial conditions for the inverse problem. The drawback of the first proposed hybrid method is that it requires necessarily the conductivity distribution to begin the calculation; in opposite, the advantage is in low computing charges when the estimated solution of the forward problem is used in the inverse problem.

The second proposed hybrid method employs the electric potential at beginning and it runs slowly where a stop criterion is used to finish the calculations. The drawback of this method is the high computing charges but in change it has ability to perform better approximation in comparison with FEM.

Also, the FEM is a slower process and it principally cannot be parallelized in opposite to our NPSM technique. The disadvantage of the FEM method is the mesh performing, because if the solutions need to be more accurate the mesh should be bigger.

Two variants of the proposal designed in this dissertation appear to demonstrate better approximations in the inverse problem for the electrical impedance equation proving their computational efficiency and reconstruction accuracy. The accuracy of the proposed approach was investigated using the quality image assessments, in particularly employing commonly used criteria: PSNR, MSE, SSIM, and via subjective perception analysis, exposing error images of conductivity reconstructed.

Let also note that FEM should not be discarded, because this method can perform better when the discretization model is changed. An additional advantage of novel hybrid approach, presented in this dissertation, is that it can be adapted in order to use real-physic measurements in conductivity reconstructions, proving it higher accuracy in practical application in comparison with the State-of-the-Art methods.

It has been demonstrated that the second hybrid method performs better quality reconstruction results using real medical measurements in comparison with FEM method, justifying this in form of objective criteria (PSNR and SSIM) as well as in subjective perception.

Finally, the principal contributions of this dissertation are:

1. We have designed a novel method in resolving forward problem in Electrical Impedance Tomography that uses a Taylor's series in formal pow-

ers approach with Tikhonov's regularization modification.

2. A novel approach to solve the inverse problem is introduced in this work. This approach is developed in form of two hybrid frameworks employing together the NPSM and FEM methods and optimizing them via a regularization procedure. Novel procedures confirmed their efficiency in comparison with State-of-the Art methods.

3. Novel techniques have been used to reconstruct the conductivity in EIT using real medical data, demonstrating better stability, accuracy and speed that basic FEM method.

5.1 Future work

Future work can be devoted to:

1. Design of a method for the EIT problem based strictly on the Pseudo-analytic Function Theory.

2. A new characterization that can be done regardless the domain shape.

3. Possibility to generalize the proposed hybrid method in the 3D EIT model.

4. Designing of a data-acquisition system to prove the developed methods.

5. Using parallel-computing to optimize computation charges in the designed techniques.

Bibliography

[1] A. Abbasi and B. Vosoughi Vahdat. A non-iterative linear inverse solution for the block approach in eit. *Journal of Computational Science*, 1(4):190–196, December 2010.

[2] K. Astala and L. Päivarintä. Calderon's inverse conductivity problem in the plane. *Annals of Mathematics*, 163:265–299, 2006.

[3] K. Astala, L. Päivarintä, J. M. Reyes, and S. Siltanen. Nonlinear fourier analysis for discontinuous conductivities: Computational results. *Journal of Computational Physics*, 276:74–91, November 2014.

[4] M. Avriel. *Nonlinear Programming: Analysis and Methods*. Dover Books on Computer Science. Dover Publications, dover edition edition, September 2003. Originally Plublished: Englewood Cliffs, N.J.: Prentice Hall, cl976.

[5] A. Bagshaw, A. Liston, R. Bayford, A. Tizzard, A. Gibson, A. Tidswell, M. Sparkes, H. Dehghani, C. Binnie, and D. Holder. Electrical impedance tomography of human brain function using reconstruction algorithms based on the finite element method. *NeuroImage*, 20(2):752 – 764, October 2003.

[6] J. Bangati and P. Maass. An analysis of electrical impedance tomography with applications to tikhonov regularization. *ESAIM: Control, Optimisation and Calculus of Variations*, 18(4):1027 –1048, October 2012.

[7] L. Baratchart, A. Borichev, and S. Chaabi. Pseudo-holomorphic functions at the critical exponent. *Journal of the European Mathematical Society*, page 43, September 2013.

[8] L. Baratchart, Y. Fischer, and J. Leblond. Dirichlet/neumann problems and hardy classes for the planar conductivity equation. *Journal of the European Mathematical Society*, page 41, December 2011.

[9] D. Barber and B. Brown. Errors in reconstruction of resistivity images using a linear reconstruction technique. *IOP: Clinical Physics and Physiological Measurement*, 9(101):5, November 1988.

[10] R. Bayford, A. Gibson, A. Tizzard, and D. Holder. Solving the forward problem in electrical impedance tomography for the human head using ideas (integrated design engineering analysis software), a finite element modelling tool. *IOP:Physiologial Measurment*, 22(1):55 – 64, February 2001.

[11] R. Bayford, P. Kantartzis, A. Tizzard, R. Yerworth, P. Liatsis, and A. Demosthenous. *Reconstruction Algorithms to Monitor Neonate Lung Function*, volume 17 of *IFMBE Proceedings*. Springer Berlin Heidelberg, 2007.

[12] M. Beck and R. Williams. *Process Tomography: Principles, Techniques and Applications*. Butterworth-Heinemann, 1st edition edition, August 1995.

[13] L. Bers. *Theory of pseudo-analytic functions*. New York University, 1953.

[14] M. Bodenstein, M. David, and K. Markstaller. Principles of electrical impedance tomography and its clinical application. *Critical care medicine*, 37(2):713 – 724, January 2010.

[15] B. Brown. Electrical impedance tomography (eit): a review. *Journal of Medical Engineering & Technology*, 27(3):97 – 108, 2003.

[16] B. Brown and A. Seagar. The sheffield data collection system. *IOP Clinical Physics and Physiological Measurement*, 8(91):91 – 97, 1987.

[17] A. Bucio R., R. Castillo-Perez, and M. P. Ramirez T. On the numerical construction of formal powers and their application to the electrical impedance equation. In *8th International Conference on Electrical Engineering, Computing Science and Automatic Control (CCE2011)*, pages 769–774, October 2011.

[18] A. Bucio R., R. Castillo-Perez, M. P. Ramirez T., and C. M. A. Robles G. A simplified method for numerically solving the impedance equation in the plane. In *th International Conference on Electrical Engineering, Computing Science and Automatic Control (CCE2012)*, pages 225–230, October 2012.

[19] A. G. Bucio Ramirez, R. A. Hernandez-Becerril, C. M. A. Robles Gonzalez, and M. P. Ramirez Tachiquin. On the performance of sequential and parallel algorithm for solving the forward problem of the two-dimensional impedance equation. In S.-I. Ao, C. Douglas, W. Grundfest, and J. Burgstone, editors, *Proceedings of the World Congress on Engineering and Computer Science 2014*, IAENG-WCECS2014, pages 221 – 226, October 2014.

[20] A. G. Bucio Ramirez and C. M. A. Robles Gonzalez. Sobre los métodos numéricos empleados en la ecuación de conductividad eléctrica bidimensional: Aproximación pseudoanalática. In IEEE-CEPPIC, editor, *Congreso Estudiantil de Proyectos y Prototipos de Ingeniería en Computación*, 9no Congreso Estudiantil de Proyectos y Prototipos de Ingeniería en Computación, pages 1 – 6. IEEE-CEPPIC, IEEE-CEPPIC, May 2012.

[21] A. G. Bucio Ramirez, C. M. A. Robles Gonzalez, M. P. Ramirez Tachiquin, and V. Ponomaryov. An optimized numerical method for solving the two-dimensional impedance equation employing pseudoanalytic approach. In IPN, editor, *Quantum Fest 2013*, Quantum Fest 2013, page 1, October 2013.

[22] M. Buhmann. *Radial Basis Functions: Theory and Implementations*, volume 1 of *Cambridge Monographs on Applied and Computational Mathematics*. Cambridge University Press, first edition edition, February 2003.

[23] A. P. Calderon. On an inverse boundary value problem. *Computational & Applied Mathematics*, 25:133–138, 1980.

[24] H. Campos, R. Castillo Perez, and V. Kravchenko. Construction and use of reproducing kernels for boundary and eigenvalue problems in the

plane using pseudoanalytic function theory. In *International Conference on Mathematical Methods in Electromagnetic Theory (MMET), 2010*, pages 1 – 5, September 2010.

[25] H. Campos, R. Castillo Perez, and V. Kravchenko. Construction and application of bergman-type reproducing kernels for boundary and eigenvalue problems in the plane construction and application of bergman-type reproducing kernels for boundary and eigenvalue problems in the plane. *Complex Variables and Elliptic Equations*, 57(7 - 8):787 – 824, January 2012.

[26] J. Carpenter. Images capture moment brain goes unconscious. BBC News: Science & Environment (UK: BBC), June 2011.

[27] R. Castillo Perez, V. Kravchenko, and R. Resendiz Vazquez. Solution of boundary and eigenvalue problems for second-order elliptic operators in the plane using pseudoanalytic formal powers. *Mathematical Methods in the Applied Sciences*, 34(4):455 – 468, March 2011.

[28] I. Chalendar, J. Leblond, and J. R. Partington. *Approximation problems in some holomorphic spaces, with applications*, volume 129 of *Systems, Approximation, Singular Integral Operators, and Related Topics*. Birkhäuser Basel, 2001.

[29] E. Chung, T. Chan, and X.-C. Tai. Electrical impedance tomography using level set representation and total variational regularization. *Journal of Computational Physics*, 205(1):357–372, May 2005.

[30] J. Cuan Lee, R. Martinez Alonso, R. G. Moreno Alvarado, J. J. Gutierrez Cortes, and M. P. Ramirez Tachiquin. On a new electronic design for data acquisition and conditioning for electrical impedance tomography measurements. In M. Soleimani and E.-J. Woo, editors, *Proceeding of the 12th International Conference in Electrical Impedance Tomography, Bath 2011*, volume 1, pages 1 – 4, May 2011.

[31] R. Duraiswami, K. Sarkar, and G. Chahine. Efficient 2d and 3d electrical impedance tomography using dual reciprocity boundary element techniques. *Engineering Analysis with Boundary Elements*, 22(1):13–31, July 1998.

[32] J. Flemming. Theory and examples of variational regularization with non-metric fitting functionals. *Journal of Inverse and Ill-posed Problems*, 18(6):677–699, December 2010.

[33] J. Flemming. Solution smoothness of ill-posed equations in hilbert spaces: four concepts and their cross connections. *Applicable Analysis: An International Journal*, 91(5):1029–1044, August 2012.

[34] J. Flemming and B. Hofmann. A new approach to source conditions in regularization with general residual term. *Numerical Functional Analysis and Optimization*, 31(3):254–284, June 2010.

[35] J. Flemming and B. Hofmann. Convergence rates in constrained tikhonov regularization: equivalence of projected source conditions and variational inequalities. *IOP: Inverse Problems*, 27(8), August 2011.

[36] J. Flemming, B. Hofmann, and P. Mathé. Sharp converse results for the regularization error using distance functions. *IOP:Inverse Problems*, 27(2), February 2011.

[37] I. Frerichs, G. Hahn, T. Schröder, and G. Hellige. Electrical impedance tomography in monitoring experimental lung injury. *Intensive Care Medicine*, 24(8):829 –836, August 1998.

[38] M. Gehrea and B. Jinb. Expectation propagation for nonlinear inverse problems with an application to electrical impedance tomography. *Journal of Computational Physics*, 259:513–535, February 2014.

[39] M. Goharian, M. Soleimani, and A. Jegatheesan. Regularization of eit problem using trust region subproblem method. In H. Scharfetter and R. Merwa, editors, *13th International Conference on Electrical Bioimpedance and the 8th Conference on Electrical Impedance Tomography*, volume 17 of *IFMBE Proceedings*, pages 400 – 403. Springer Berlin Heidelberg, September 2007.

[40] G. Golub and C. Van Loan. *Matrix Computations*. Johns Hopkins Studies in the Mathematical Sciences. Johns Hopkins University Press, fourth edition edition, December 2012.

[41] P. Grasland-Mongrain, J. Martial Mari, J.-Y. Chapelon, and C. Lafon. Lorentz force electrical impedance tomography. *IRBM*, 34(4-5):357–360, November 2013.

[42] O. Grodzevich and H. Wolkowicz. Regularization using a parameterized trust region subproblem. *Mathematical Programming*, 116(1 - 2):193 – 220, January 2009.

[43] J. Hadamard. *Lectures on Cauchy's problem in linear partial differential equations*. Nabu Press, 2nd edition, August 2010.

[44] M. Hadinia and R. Jafari. Flow measurement and instrumentation. *Flow Measurement and Instrumentation*, 45:68–74, October 2015.

[45] A. Hampshire, R. Smallwood, B. Brown, and R. Primhak. Multifrequency and parametric eit images of neonatal lungs. *Physiological Measurement*, 16(3A):175 – 189, August 1995.

[46] D. Han and A. Prosperetti. A shape decomposition technique in electrical impedance tomography. *Journal of Computational Physics*, 155(1):75–95, October 1999.

[47] R. A. Hernandez-Becerril. Estudio de un método de interpolación para obtener funciones de conductividad en variables separables. Master's thesis, Universidad La Salle, May 2011.

[48] B. Hofmann and T. Hohage. *Generalized Tikhonov regularization: Basic theory and comprehensive results on convergence rates*. PhD thesis, Technische Universität Chemnitz, October 2011.

[49] D. Holder. *Electrical Impedance Tomography: Methods, History and Applications*. IOP: Series in Medical Physics and Biomedical Engineering. CRC Press, December 2004.

[50] C.-T. Hsiao, G. Chahine, and N. Gumerov. Application of a hybrid genetic/powell algorithm and a boundary element method to electrical impedance tomography. *Journal of Computational Physics*, 173(1):433–454, November 2001.

[51] H. Huang, X. Qu, J. Liang, X. He, X. Chen, D. Yang, and J. Tian. A multi-phase level set framework for source reconstruction in bioluminescence tomography. *Journal of Computational Physics*, 229(13):5246–5256, July 2010.

[52] B. S. Kim and K. Y. Kim. Estimation of conductivity distribution based on fast inversion using eigenvalue and eigenvector in electrical impedance tomography. *Flow Measurement and Instrumentation*, June 2015. In Press, Accepted Manuscript.

[53] K. Y. Kim, J. Webster, and W. Tompkins. Electrical impedance imaging of the thorax. *Journal of Microwave Power*, 18(3):245 – 257, 1983.

[54] V. Kravchenko. On a relation of pseudoanalytic function theory to the two-dimensional stationary schrödinger equation and taylor series in formal powers for its solutions. *Journal of Physics A: Mathematical and General*, 38(18):3947 – 3964, May 2005.

[55] V. Kravchenko. A representation for solutions of the sturm-liouville equation. *Complex Variables and Elliptic Equations: An International Journal*, 53(8):775–789, February 2008.

[56] V. Kravchenko. *Applied Pseudoanalytic Function Theory.* Frontiers in Mathematics. Birkhäuser Basel, 1 edition, 2011.

[57] V. Kravchenko and H. Oviedo. On explicitly solvable vekua equations and explicit solution of the stationary schrödinger equation and of the equation $div(\sigma\nabla u) = 0$. *Complex Variables and Elliptic Equations: An International Journal*, 52(5):353 – 366, May 2007.

[58] V. Kravchenko and M. P. Ramirez Tachiquin. New exact solutions of the massive dirac equation with electric or scalar potential. *Mathematical Methods in the Applied Sciences*, 23(9):769 –776, June 2000.

[59] J. Lalis, B. Gerardo, and Y.-C. Byun. An adaptive stopping criterion for backpropagation learning in feedforward neural network. *International Journal of Multimedia and Ubiquitous Engineering*, 9(8):149–156, 2014.

[60] M. Leinonen, H. Hakula, and N. Hyvönen. Application of stochastic galerkin fem to the complete electrode model of electrical impedance tomography. *Journal of Computational Physics*, 269:181–200, July 2014.

[61] D. Liu, A. K. Khambampati, S. Kim, and K. Y. Kim. Multi-phase flow monitoring with electrical impedance tomography using level set based method. *Nuclear Engineering and Design*, 289:108–116, August 2015.

[62] M. Lukaschewitsch, P. Maass, and M. Pidcock. Tikhonov regularization for electrical impedance tomography on unbounded domains. *Institue of Physics: Inverse Problems*, 19(3):585–610, 2003.

[63] J. C. Maxwell. A dynamical theory of the electromagnetic field. In T. R. S. of London, editor, *Philosofical Transactions.*, volume 155, pages 459 –512, January 1865.

[64] R. A. Millikan and E. Sherwood Bishop. *Elements of Electricity: A Practical Discussion of the Fundamental Laws and Phenomena of Electricity and Their Practical Applications in the Business and Industrial World.* The University of Michigan. American Technical Society, June 1917.

[65] A. Nejatali. *Electrical impedance tomography with neural networks and fuzzy sets.* PhD thesis, University of Manitoba, 1997.

[66] H. Peitgen, H. Jürgens, and D. Saupe. *Chaos and Fractals.* Springer New York, 2004.

[67] V. Ponomaryov, M. Robles-Gonzalez, A. Bucio-Ramirez, M. Ramirez-Tachiquin, and E. Ramos-Diaz. Parallel hybrid algorithm for solution in electrical impedance equation. In N. Kehtarnavaz and M. Carlsohn, editors, *SPIE Proceedings: Real-Time Image and Video Processing 2015*, volume 9400 of *Proc. SPIE*, page 14. SPEI, February 2015.

[68] D. Powers. *Boundary Value Problems and Partial Differential Equations.* Academic Press, 6 edition, August 2009.

[69] E. Previato. *Dictionary of Applied Math for Engineers and Scientists.* Comprehensive Dictionary of Mathematics. CRC Press, 1st edition edition, October 2002.

[70] M. P. Ramirez T., C. M. A. Robles G., and R. A. Hernandez-Becerril. On the computational methods employed in two-dimensional electical impedance tomography. In *Proceedings of the 7th International Conference on Electrical Engineering, Computing Science and Automatic Control (CCE2010)*, pages 274–279. IEEE, September 2010.

[71] M. P. Ramirez T., C. M. A. Robles G., and R. A. Hernandez-Becerril. On the construction of separable-variables conductivity functions, and their application for approaching numerical solutions of the two-dimensional electrical impedance equation. In I. Publication, editor, *Proceedings of the World Congress on Engineering 2011*, volume III, pages 2699–2704, July 2011.

[72] M. P. Ramirez T., C. M. A. Robles G., R. A. Hernandez-Becerril, and A. Bucio R. First characterization of a new method for numerically solving the dirichlet problem of the two-dimensional electrical impedance equation. *Journal of Applied Mathematics*, 2013:14, 2013.

[73] M. P. Ramirez Tachiquin. On the electrical current distributions for the generalized ohm's law. *Mathematical Physics*, 1(1):24, Novembre 2010.

[74] M. P. Ramirez Tachiquin, R. A. Hernandez-Becerril, and C. M. A. Robles Gonzalez. On a numerical interpolation technique for abtaining picewise separable-variables conductivity functions. In M. Soleimani and E.-J. Woo, editors, *Proceeding of the 12th International Conference in Electrical Impedance Tomography, Bath 2011*, volume 1, pages 1–4, May 2011.

[75] M. P. Ramirez Tachiquin, C. M. A. Robles Gonzalez, A. G. Bucio Ramirez, and V. Ponomaryov. On a conjecture for analyzing arbitrary inhomogeneous media employing pseudoanalytic function theory. In IPN-CINVESTAV, editor, *Waves in Science and Engineering 2013*, WiSE 2013, page 1, November 2013.

[76] M. P. Ramirez Tachiquin, C. M. A. Robles Gonzalez, and R. A. Hernandez-Becerril. Study of the numerical solutions for the electrical impedance equation in the plane: A pseudoanalytic approach of the forward dirichlet boundary value problem. *Mathematical Physics*, 1(1):1 – 39, October 2012.

[77] M. P. Ramirez Tachiquin, C. M. A. Robles Gonzalez, R. A. Hernandez-Becerril, and A. G. Bucio Ramirez. First characterization of a new method for numerically solving the dirichlet problem of the two-dimensional electrical impedance equation. *Journal of Applied Mathematics*, 2013(Article ID 493483):1 – 14, May 2013.

[78] M. P. Ramirez Tachiquin, V. D. Sanchez Nava, and A. Fleiz Jaso. On the solutions of the electrical impedance equation, applying quaternionic analysis and pseudoanalytic function theory. In *12th International Conference on Mathematical Methods in Electromagnetic Theory, 2008.*, pages 190 – 192. IEEE, June 2008.

[79] M. P. Ramirez Tachiquin, V. D. Sanchez Nava, O. Rodriguez Torres, and A. Gutierrez Solares. On the general solution for the two-dimensional electrical impedance equation in terms of taylor series in formal powers. *IAENG International Journal of Applied Mathematics*, 39(4):1 – 6, November 2009.

[80] C. M. A. Robles G., A. Bucio R., and M. P. Ramirez T. An optimized numerical method for solving the two-dimensional impedance equation. In I. Publication, editor, *Proceedings of the World Congress on Engineering and Computer Science 2012 (WCECS 2012)*, volume 1 of *Lecture Notes in Engineering and Computer Science*, pages 116–121. IAENG, October 2012.

[81] C. M. A. Robles Gonzalez. Caracterización de un método de interpolación para funciones en variables separables y su aplicación a la ecuación de conductividad eléctrica bidimensional: Estudio sobre funciones exactas. Master's thesis, Universidad La Salle, October 2011.

[82] C. M. A. Robles Gonzalez, A. G. Bucio Ramirez, and V. Ponomaryov. Sobre la ecuación de conductividad eléctrica, problema directo e inverso: Métodos empleados. In *Foro BEIFI 2014*, FORO BEIFI 2014, page 1, July 2014.

[83] C. M. A. Robles Gonzalez, A. G. Bucio Ramirez, V. Ponomaryov, and M. P. Ramirez Tachiquin. A regularization process for electrical impedance equation employing pseudoanalytic function theory. *Mathematical Problems in Engineering*, 2014:13, 2014.

[84] C. M. A. Robles Gonzalez, A. G. Bucio Ramirez, and M. P. Ramirez Tachiquin. New characterization of an improved numerical method for solving the electrical impedance equation in the plane: An approach from the modern pseudoanalytic function theory. *IAENG International Journal of Applied Mathematics*, 43(1):17–29, 2012.

[85] C. M. A. Robles Gonzalez, A. G. Bucio Ramirez, M. P. Ramirez Tachiquin, and V. Ponomaryov. Métodos numéricos para aproximación de ecuaciones en diferencias. In U. L. Salle, editor, *XVI Coloquio para la Enseñanza de las Matemáticas "Alfonso Nápoles Góndara"*, XVI Coloquio para la Enseñanza de las Matemáticas "Alfonso Nápoles Góndara", October 2013.

[86] C. M. A. Robles Gonzalez, A. G. Bucio Ramirez, M. P. Ramirez Tachiquin, and V. D. Sanchez Nava. *On the Numerical Solutions of Boundary Value Problems in the plane for the Electrical Impedance Equation: A Pseudoanalytic Approach for Non-Smooth Domains*, volume 247 of *Special Issue of the World Congress on Engineering and Computer Science 2012*, chapter 31, pages 447–453. Springer Netherlands, September 2013.

[87] C. M. A. Robles Gonzalez and V. Ponomaryov. Método híbrido para el problema de tomografía por impedancia eléctrica. In IPN, editor, *Expociencias Metropolitana 2015*, ExpoCiencias Metropolitana 2015, page 1, February 2015.

[88] C. M. A. Robles Gonzalez, V. Ponomaryov, and M. P. Ramirez Tachiquin. A hybrid method to find the solution for electrical impedance tomography. *Computational Physics*, 2015. Submitted to publication.

[89] C. M. A. Robles Gonzalez, V. Ponomaryov, M. P. Ramirez Tachiquin, and A. Bucio R. Numerical algorithm for electrical impedance tomography problem using pseudoanalytic approach. In IEEE, editor, *International Kharkov Symposium on Physics and Engineering of Microwaves, Millimeter and Submillimeter Waves (MSMW), 2013*, pages 629 – 631. IEEE, June 2013.

[90] M. Sadd. *Elasticity Theory, Applications, and Numerics*, volume 1. Academic Press, 3rd edition, February.

[91] S. Savchev and J. Ottesen. *Tikhonov Regularization in Kronecker Product Approximation for Image Restoration with Mean Boundary Conditions*. PhD thesis, Roskilde University, January 2012.

[92] A. Tikhonov. On the stability of inverse problem. *Doklady Akademii Nauk SSSR*, 39(5):195–198, 1943.

[93] A. Tizzard and R. Bayford. Improving the finite element forward mode of human head by warping using elastic deformation. *Institute of Physics: Physiological Measurement*, 28(13):163–182, July 2007.

[94] A. Tizzard, L. Horesh, R. Yerworth, D. Holder, and R. Bayford. Generating accurate finite element meshes for the forward model of the human head in eit. *IOP: Physiological Measurement*, 26(1):251–261, April 2005.

[95] I. Vekua. *Generalized Analytic Functions*. International Seriesof Monographs in Pure and Applied Mathematics. Pergamon Press Ltd., 1st edition edition, 1962.

[96] H. Wang, G. Xu, S. Zhang, N. Yin, and W. Yan. Implementation of generalized back projection algorithm in 3-d eit. *IEEE Transactions on Magnetics*, 47(5):1466–1469, May 2011.

[97] P. Wang, H.-l. Li, L.-l. Xie, and Y.-c. Sun. The implementation of fem and rbf neural network in eit. In *Intelligent Networks and Intelligent Systems, 2009. ICINIS '09. Second International Conference on*, pages 66–69. IEEE, November 2009.

[98] J. Webster. *Electrical Impedance Tomography*. Biomedical Engineering. The Adam Hilger Series on Biomedical Engineering, 1st edition edition, 1990.

[99] F. Yang, L. Ling, and T. Wei. An adaptive greedy technique for inverse boundary determination problem. *Journal of Computational Physics*, 229(23):8484–8496, An adaptive greedy technique for inverse boundary determination problem 2010.

[100] T. Yorkey. Electrical impedance tomography with piecewise polynomial conductivities. *Journal of Computational Physics*, 91(2):344–360, December 1990.

[101] B. Zhao, H. Wang, L. Hu, L. Xu, and Y. Yan. An adaptive multigrid method for eit. In *Instrumentation and Measurement Technology Conference Proceedings, 2007. IMTC 2007. IEEE*, pages 1–4, May 2007.

[102] X.-L. Zhao, T.-Z. Huang, X.-G. Lv, Z.-B. Xu, and J. Huang. Kronecker product approximations for image restoration with new mean boundary conditions. *Applied Mathematical Modeling*, 36(1):225–237, January 2012.

Index

Appendix A: List of publications

Scopus

2015	C. Marco A. Robles G., V. Ponomaryov and M. P. Ramirez T., "***On the Artificial Neural Networks used for the Forward Problem for the Electrical Impedance Equation***", Proceedings of the World Congress on Engineering and Computer Science 2015 Vol I, USA.
	Volodymyr Ponomaryov, Marco Robles-Gonzalez, Ariana Bucio-Ramirez, Marco Ramirez-Tachiquin and Eduardo Ramos-Diaz., "***Parallel Hybrid Algorithm for Solution in Electrical Impedance Equation***", Real-Time Image and Video Processing 2015, edited by Nasser Kehtarnavaz, Matthias F. Carlsohn, Proc. of SPIE-IS&T Electronic Imaging, SPIE Vol. 9400, 94000I.
2014	A. Bucio R., A. Hernandez-Becerril, C. M. A. Robles G. and M. P. Ramirez T., "***On the Performance of Sequential and Parallel Algorithm for Solving the Forward Problem of the Two-Dimensional Impedance Equation***", Proceedings of the World Congress on Engineering and Computer Science 2014 Vol I, USA
	Cesar Marco Antonio Robles Gonzalez, Ariana Guadalupe Bucio Ramirez, Volodymyr Ponomaryov and Marco Pedro Ramirez Tachiquin, "***A Regularization Process for Electrical Impedance Equation Employing Pseudoanalytic Function Theory***", Hindawi Publishing Corporation, Mathematical Problems in Engineering, Volume 2014, Article ID 964081, 13 pages.
2013	A. Bucio R., A. Hernandez-Becerril, C. M. A. Robles G., M. P. Ramirez T. and A. Arista-Jalife, "***Construction of a New Cryptographic Method, Employing Pseudoanalytic Function Theory***", Proceedings of the World Congress on Engineering and Computer Science 2013 Vol I, USA.
	M. Robles-Gonzalez, V. Ponomaryov, M. Ramirez-Tachiquin and A. Bucio-Ramirez, "***NUMERICAL ALGORITHM FOR ELECTRICAL IMPEDANCE TOMOGRAPHY PROBLEM USING PSEUDOANALYTIC APPROACH",*** *MSMW'13, Kharkov, Ukraine, June 23-28.*
	C. M. A. Robles G., A. Bucio R. and M. P. Ramirez T., "***New Characterization of an Improved Numerical Method for Solving the Electrical Impedance Equation in the Plane: An Approach from the Modern Pseudoanalytic Function Theory***", IAENG International Journal of Applied Mathematics, 43:1, IJAM_43_1_03.
	Marco Pedro Ramirez Tachiquin, Cesar Marco Antonio Robles Gonzalez, Rogelio Adrian Hernandez Becerril and Ariana Guadalupe Bucio Ramirez., "***First Characterization of a New Method for Numerically Solving the Dirichlet Problem of the Two-Dimensional Electrical Impedance Equation***", Hindawi Publishing Corporation, Journal of Applied Mathematics, Volume 2013, Article ID 493483, 14 pages.
	Cesar Marco Antonio Robles Gonzalez, Ariana Guadalupe Bucio Ramirez, Marco Pedro Ramirez Tachiquin and Victor Daniel Sanchez Nava, "***On the Numerical Solutions of Boundary Value Problems in the plane for the Electrical Impedance Equation: A Pseudoanalytic Approach for Non-Smooth Domains***", IAENG Transactions on Engineering Technologies, Volume 247 of the series Lecture Notes in Electrical Engineering pp 447-453.
2012	A. Bucio R., R. Castillo-Perez, M. P. Ramirez T. and C. M. A. Robles G., "***A Simplified Method for Numerically Solving the Impedance Equation in the Plane***", 2012 9th International Conference on Electrical Engineering, Computing Science and Automatic Control, Mexico City, Mexico. September 26-28, 2012.
2011	M. P. Ramirez T., M. C. Robles G. and R. A. Hernandez-Becerril, "***On the Construction of Separable-Variables Conductivity Functions, and Their Application for Approaching Numerical Solutions of the Two-Dimensional Electrical Impedance Equation***", Proceedings of the World Congress on Engineering 2011 Vol III, UK.
2010	M. P. Ramirez T., M. C. Robles G. and R. A. Hernandez-Becerril, "***On the Computational Methods Employed in Two-Dimensional Electrical Impedance Tomography***", 7th International Conference on Electrical Engineering, Computing Science and Automatic Control (CCE2010), Mexico.

Other publications

2014	C. M. A. Robles G. and V. Ponomaryov, "***Sobre la Ecuación de Conductividad Eléctrica, Problema Directo e Inverso: Métodos Empleados***", FORO BEIFI.
	Ariana Guadalupe Bucio Ramirez, Cesar Marco Antonio Robles Gonzalez, Marco Pedro Ramirez Tachiquin and Rogelio Adrian Hernandez Becerril, "***Algorithmic Analysis of the Pseudoanalytic Cryptographic Algorithm***", Transactions on Engineering Technologies, pp 207-212.
2013	M. P. Ramirez T., C. M. A. Robles G., A. Bucio R. and V. Ponomaryov, "***On a Conjecture for Analyzing Arbitrary Inhomogeneous Media Employing Pseudoanalytic Function Theory***", International Conference Waves in Science & Engineering (WISE 2013).
	A. Bucio-Ramirez, M. Robles-Gonzalez, M. Ramirez-Tachiquin and V. Ponomaryov, "***AN OPTIMIZED NUMERICAL METHOD FOR SOLVING THE TWO-DIMENSIONAL IMPEDANCE EQUATION EMPLOYING PSEUDOANALYTIC APPROACH***", Quantum Fest 2013.
	C. M. A. Robles G., A. Bucio R., M. P. Ramirez T. and V. Ponomaryov, ***"Métodos Numéricos para Aproximación de Ecuaciones en Diferencias***", XVI Coloquio para la Enseñanza de las Matemáticas "Alfonso Nápoles Gándara"
2012	C. M. A. Robles G., A. Bucio R., M. P. Ramirez T., "***An Optimized Numerical Method for Solving the Two-Dimensional Impedance Equation***", Proceedings of the World Congress on Engineering and Computer Science 2012 Vol I, USA.
	C. M. A. Robles G. and R. A. Hernandez-Becerril, "***Seismic Alert System based on Artificial Neural Networks***", World Academy of Science, Engineering and Technology 66, Paris.
	C. M. A. Robles G. and R. A. Hernandez-Becerril, "***Seismic Alert System based on Artificial Neural Networks: A Novel Approach***", Microsoft Research Faculty Summit 2012.
	A. Bucio R. and C. M. A. Robles G., "***Sobre los Métodos Numéricos Empleados en la Ecuación de Conductividad Eléctrica Bidimensional: Aproximación Pseudoanalítica***", Congreso Estudiantil de Proyectos y Protocolos de Ingeniería (CEPPIC 2012).
2011	M. P. Ramirez T., R. A. Hernandez-Becerril and M. C. Robles G., "***On a numerical interpolation technique for obtaining piecewise separable-variables conductivity functions***", EIT 2011, Dept. Electronic & Electrical Engineering, University of Bath, UK.

Appendix B: Published papers

Scopus citation references

Journals

Hindawi Publishing Corporation
Mathematical Problems in Engineering
Volume 2014, Article ID 964081, 13 pages
http://dx.doi.org/10.1155/2014/964081

Research Article

A Regularization Process for Electrical Impedance Equation Employing Pseudoanalytic Function Theory

Cesar Marco Antonio Robles Gonzalez,[1] Ariana Guadalupe Bucio Ramirez,[2] Volodymyr Ponomaryov,[1] and Marco Pedro Ramirez Tachiquin[1]

[1]*Instituto Politecnico Nacional, SEPI ESIME Culhuacan, Avenida Santa Ana No. 1000, 04430 Ciudad de México, DF, Mexico*
[2]*Instituto Politecnico Nacional, SEPI UPIITA, Avenida IPN 2580, 07340 Ciudad de México, DF, Mexico*

Correspondence should be addressed to Cesar Marco Antonio Robles Gonzalez; croblesg1101@alumno.ipn.mx

Received 11 June 2014; Revised 13 November 2014; Accepted 17 November 2014; Published 8 December 2014

Academic Editor: Peter Liu

The electrical impedance equation is considered an ill-posed problem where the solution to the forward problem is more easy to achieve than the inverse problem. This work tries to improve convergence in the forward problem method, where the Pseudoanalytic Function Theory by means of the Taylor series in formal powers is used, incorporating a regularization method to make a solution more stable and to obtain better convergence. In addition, we include a comparison between the designed algorithms that perform proposed method with and without a regularization process and the autoadjustment parameter for this regularization process.

1. Introduction

The electrical impedance tomography (EIT) problem, which is set by employing the electrical impedance equation, was mathematically posed by Calderon [1] in 1980 proving that the solution of this problem exists as being unique and steady. This problem is exemplified by the following equation:

$$\operatorname{div}(\sigma \operatorname{grad} u) = 0, \tag{1}$$

where σ represents the conductivity and u denotes the electric potential for a domain Ω within a boundary Γ.

This equation is considered ill-posed problem, due to its high complexity to find a solution in terms of the initial data; it means that every variation in the input data can approximate in different way the solution to this problem. Therefore, if a measurement presents any variation or noise, this variation presents difficulty to obtain good approximation; for example, when the finite element method is employed in noise presence in the electrodes, we need to introduce an extra process to correct this fault or the approximation could not be reached.

Some methods should be employed to correct these perturbations present advantages and disadvantages, such as a regularization method that permits to suppress the noise in the measurements. Due to this problem and the continuous advances in the field, the EIT is not considered a practical medical imaging procedure.

Employing (1), we can approach two types of problems; in the first one, the conductivity σ value is known and the task is to approximate the electric potential in the boundary $u|_\Gamma$. This problem is known as forward Dirichlet boundary value problem; it is also known as nonhomogeneous Laplace equation. For the second problem, the value of the electric potential in the boundary $u|_\Gamma$ is known, but the conductivity σ within the domain Ω is unknown; this problem is formulated as inverse Dirichlet boundary value problem or electrical impedance tomography problem [2].

The EIT was considered very unsteady, as well as ill-posed problem [2], but, in 2009, Kravchenko [3] and, independently in 2006, Astala and Päivärinta [4] noticed for first time that the two-dimensional case was completely equivalent to special case of Vekua equation [5].

There exist several assortment methods that try to solve forward and inverse problem for (1), where the best mathematical tool to approximate the solution for both problems by now is the finite element method (FEM). It proves to be

stable and easy to employ, but it presents a difficulty when it computes the approximation; this difficulty is presented in the initial data and the variations on it [2].

The existence of different techniques and methods to reach a solution of inverse problems, in which the solutions are interpreted in terms of linear operators [6], permits analysing and studying inverse problems in order to find a solution. Other works employ the connection between pseudoholomorphic functions and conjugate Beltrami equations to deduce the well-posedness on smooth domains of the Dirichlet problem for 2D isotropic conductivity equations [7]. There exists a theory of conjugate functions to solve Dirichlet and Neumann problems for conductivity equations, in which they consider some density properties to trace solutions with a boundary approximation issues [8].

All these works contribute to analysing and reaching a solution to the forward problem and continuing working on the solution to the inverse problem of the electrical conductivity equation. Employing all these techniques and analysis the study of the forward problem could help to find a solution to the inverse problem, but the study to be done should be extensive and incorporate different techniques and methods proposed by the different authors.

For the correct understanding of the inverse problem, first, we need to analyse and study the forward problem, to determinate how the energy propagates within the domain; with the collected data we can determine that the convergence and the performance will be very important to design a method that can be employed in the medical imaging in a future.

In this study, the main purpose is to analyse the behaviour of the algorithm based on the Pseudoanalytic Function Theory, which applies the Taylor series in formal powers as the support, proposing additionally to employ a regularization process to improve the stability. The results obtained are compared with the results presented in previous paper [9, 10], in order to analyse the improvement or decrement in the convergence due to the method designed.

The remainder of this paper is organized as follows. Section 2 shows the mathematical tools for the electrical impedance equation; in Section 3, the methodology that contains the main idea of the algorithm is presented; following, a brief review of regularization procedure employed to design this algorithm is explained; Sections 4 and 5 show several experiments to compare the results and a discussion about this comparison; finally Section 6 expresses the conclusions about the behaviour of the novel method and discusses a future work.

2. Electrical Impedance Equation

2.1. Preliminaries. Employing the Pseudoanalytic Function Theory [11], let us consider a pair of complex valued functions (F, G) that fulfills the condition

$$\operatorname{Im}\left(\overline{F}G\right) > 0. \tag{2}$$

For (2), we have $\overline{F} = \operatorname{Re}(F) - i \operatorname{Im} F$ complex conjugation of F, and $i^2 = -1$ is the imaginary standard unit.

Then, any complex function W can be represented by the linear conjugation of F and G:

$$W = \phi F + \psi G, \tag{3}$$

where ϕ and ψ are indeed real valued functions. Therefore, the pair (F, G) is called *generating pair*. Following the Pseudoanalytic Function Theory posed by Bers [11], it is possible to introduce the derivative and antiderivative form of a complex valued function w, which can be reviewed in the mentioned work.

Let us suppose (F, G) *generating pair* with the form

$$F = p, \qquad G = \frac{i}{p}, \tag{4}$$

where p is a nonvanishing function within a domain $\Omega(\mathbb{R}^2)$. Then considering this (F, G) generating pair with a p separable variable function within the domain,

$$p(x, y) = p_1(x) \cdot p_2(y); \quad x, y \in \mathbb{R}. \tag{5}$$

Thereby (F, G) is embedded into a periodic sequence, in which for an m even the generating pair are

$$F_m = \frac{p_2(y)}{p_1(x)}, \qquad G_m = i\frac{p_1(x)}{p_2(y)}; \tag{6}$$

and for the odd generating pair the forms are

$$F_m = p_1(x) \cdot p_2(y), \qquad G_m = i\left(p_1(x) \cdot p_2(y)\right)^{-1}. \tag{7}$$

Consider the formal powers $Z_m^0(a_0, z_0; Z)$, associated with a (F_m, G_m) generating pair, with the formal degree 0, complex constant coefficient a_0, and center z_0, and depending upon $Z = x + iy$, are defined in agreement with the expression

$$Z_m^{(0)}(a_0, z_0; z) = \lambda F_m(z) + \mu G_m(z), \tag{8}$$

where λ and mu are complex constants which fulfills the condition

$$\lambda F_m(z_0) + \mu G_m(z_0) = a_0. \tag{9}$$

Now, let us suppose W to be a (F_m, G_m)-pseudoanalytic function. Thus, we can express it in terms of the so-called Taylor series in formal powers:

$$W = \sum_{n=0}^{\infty} Z_m^{(n)}(a_0, z_0; z). \tag{10}$$

Since every (F, G)-pseudoanalytic function W accepts this expansion, the last equation is an analytic representation of the general solution for the Vekua equation.

Consider the two-dimensional case of the electric impedance equation (1), and suppose that the conductivity σ function can be expressed in terms of a separable variable function; it follows that

$$\sigma(x, y) = \sigma_1(x) \cdot \sigma_2(y). \tag{11}$$

Introducing the notations

$$W = \sqrt{\sigma} \cdot \left(\partial_x u - \partial_y u\right), \qquad p = \sqrt{\sigma_1 (x)^{-1} \sigma_2 (y)}, \tag{12}$$

where $\partial_x = \partial/\partial_x$ and $\partial_y = \partial/\partial_y$, then (1) turns into special case of Vekua equation with the form

$$\partial_{\overline{z}} W - \frac{\partial_{\overline{z}} p}{p} \overline{W} = 0, \tag{13}$$

where $\partial_{\overline{z}} = \partial_x - i\partial_y$ and $i^2 = -1$ for the standard imaginary unit.

Employing the last statement presented in (13), we have to introduce some expressions that were presented in the Pseudoanalytic Function Theory [3] and in assortment works [9, 10, 12], explaining the mathematical basis of the Taylor series in formal powers:

$$W = \sum_{n=0}^{\infty} Z_m^{(n)} (a_n, z_0; z); \qquad a_n = \frac{1}{n!} \partial_{(F_m, G_m)}^{(n)} W (z_0). \tag{14}$$

Equation (14) was proved in [11], showing that any (F_m, G_m)-pseudoanalytic function can be represented in Taylor series in formal powers. So, from this point of view, (14) is an analytical representation of the general solution of the Vekua equation (13).

In (14), we used the Pseudoanalytic Function Theory to approximate the special case of Vekua equation in Taylor series in formal powers, where we can read in the last statement that it has a center in z_n, depending upon z and approximating the coefficient a_n, like a Taylor series.

For this case, we also remember that Taylor series in formal powers are performed by introducing a generating pair (F_m, G_m) and the real constants λ_m and μ_m that fulfill the condition presented before in (9) for the expression (8).

The admittance of the integral was also introduced in [11], taking place when the next notation is written according the recursive formula:

$$Z_{m+1}^{(n+1)} (a_{n+1}, z_0; z) = (n+1) \int_{z_0}^{z} Z_m^{(n)} (a_0, z_0; z)\, d_{(F_m, G_m)} z, \tag{15}$$

where (15) is employed to approximate higher exponents of the formal powers.

Employing the structure of (8), (9), and (15), the special case of Vekua equation presented in (13) can be approached by the next statement introducing the factors from (14) to (16), obtaining the next equation:

$$\int_{z_0}^{z} W\, d_{(F_m, G_m)} z = F_m \operatorname{Re} \int_{z_0}^{z} G_m^* W\, dz + G_m \operatorname{Re} \int_{z_0}^{z} F_m^* W\, dz.$$

$$F_m = p; \quad G_m = \frac{i}{p}; \quad p = p_1 (x) \cdot p_2 (y); \quad p = \sqrt{\sigma}. \tag{16}$$

Equation (16) is the definition of a (F, G)-integral of a complex valued function W. Specifically, since (F_m, G_m)-integral of the (F_m, G_m)-derivative of W reaches

$$\int_{z_0}^{z} \partial_{(F_0, G_0)} W\, d_{(F_0, G_0)} z = W - \phi (z_0) F_0 - \psi (z_0) G_0, \tag{17}$$

taking into account that

$$\partial_{(F_0, G_0)} F_0 = \partial_{(F_0, G_0)} G_0 = 0, \tag{18}$$

the integral expression (17) can be considered the (F_0, G_0)-antiderivative of the function $\partial_{(F_0, G_0)} W$.

For the correct approximation of the electric potential $u|_\Gamma$ for (1), using the Taylor series in formal powers, let us note that this electric potential can be found by the next statements:

$$u^n (1, 0; z) = \operatorname{Re} Z_m^{(n)} (1, 0; z)\Big|_\Gamma; \qquad u^n (i, 0; z) = \operatorname{Re} Z_m^{(n)} (i, 0; z)\Big|_\Gamma. \tag{19}$$

In this case, if the boundary condition $u|_\Gamma$ is provided by (19), we can always approximate asymptotically the experimental electric potential $u|_{\text{app}}$ by the next expression:

$$u_{\text{app}} = \lim_{N \to \infty} \sum_{n=0}^{N} \left(\alpha_n u^n (1, 0; z) + \beta_n u^n (i, 0; z)\right), \tag{20}$$

where α_n and β_n are real numbers. This procedure has proven its effectiveness in assortment works [9, 10, 12], where the numerical approximation achieved highly accurate results.

The analysis of the problem can include samples in piecewise and nonpiecewise separable variable functions for the conductivity σ; to understand this situation we have to employ the conjecture exposed in [10].

Conjecture 1. *Suppose a σ arbitrary conductivity function defined within a bounded domain $\Omega(\mathbb{R}^2)$. This function can be approximated by means of a piecewise separable variables function in the form*

$$\sigma_{pw} = \begin{cases} \dfrac{x+g}{(\rho_1 - \rho_0) + g} \cdot f_1 (y), & x \in [\rho_0, \rho_1); \\ \dfrac{x+g}{(\rho_2 - \rho_1) + g} \cdot f_2 (y), & x \in [\rho_1, \rho_2); \\ \vdots & \vdots \\ \dfrac{x+g}{(\rho_K - \rho_{K-1}) + g} \cdot f_K (y), & x \in [\rho_{K-1}, \rho_K); \end{cases} \tag{21}$$

here g is a real constant such that $x + g \neq 0 : x \in \Omega(\mathbb{R}^2)$ and $\{f_k\}_{k=1}^K$ are the constructed interpolation functions with a finite number of samples $\mathscr{M}$ of the conductivity function σ, valued in the y-axis that is parallel line within the subdomain Ω, created by tracing $\{\rho\}_{k=0}^K$ parallel lines.

These piecewise separable variable functions can be employed for numerically approximating the set of formal powers.

Proposition 2. *Consider an arbitrary conductivity function σ defined within a domain $\Omega(\mathbb{R}^2)$. It can be considered the limiting case of a piecewise separable variables function, expressed in the form of the Conjecture (21), when K subdomains and $\mathscr{M}$ number of samples are every subdomain tending to infinity:*

$$\lim_{K,\mathscr{M}\to\infty} \sigma_{pw} = \sigma. \tag{22}$$

A regularization process is needed to increase the precision of the algorithm and obtain a better solution to be analysed for further research in the inverse problem; in the next section we introduce a simple idea to employ a regularization process in the Taylor series in formal powers and iterative method using this idea to improve the results, or at least to obtain a better convergence.

2.2. Regularization Process. Regularization methods are employed in many fields, introducing additional information with the purpose to solve ill-posed problems. Also, they are employed to prevent overfitting and are usually presented in form of penalty for complexity, such as restrictions for smoothness or bounds in the space norm for a vector. In particular case, the including of these methods to the algorithm designed to compute a solution for inverse problems is essential to fitting the data in order to reduce a norm of the solution.

For current problem, the imposed electric potential $u|_\Gamma$ represents a finite number of current densities $j_k|_{k=0}^m$ for a domain Ω with a boundary Γ and the knowledge of the Neumann-Dirichlet map [13] where

$$\operatorname{div}(\sigma \operatorname{grad} u) = 0, \qquad \sigma\partial_\Gamma u = j. \tag{23}$$

Remember the notations introduced before in (1); we know that σ represents the conductivity and u denotes the electric potential in the electric conductivity equation, where $\partial_\Gamma u = \partial u/\partial_\Gamma$, being all the values of the electric potential u in the boundary domain Γ, and j is the current density.

For the forward Dirichlet boundary problem, we know the value of the conductivity σ but the electric potential $u|_\Gamma$ is unknown. In this work, the electric potential $u|_\Gamma$ is imposed, and, for the purpose of this paper, the approximation of an experimental value u is computed comparing the results by means of the Lebesgue measure and determining if the method employed is being corrected [14].

The Tikhonov regularization process can be presented in such form

$$\min_x \left(\|Ax - b\|^2 + \gamma^2 \|x\|^2 \right), \tag{24}$$

where $\|\cdot\|$ denotes the L_2 norm, A can be a square matrix or a matrix of $r \times s$ dimension, b denotes a vector with r rows, γ is the regularization parameter, and the problem turns into a minimization of the parameter x.

Algorithm 1, which we propose in this study, is based on the Pseudoanalytic Function Theory, employing the Taylor series in formal powers, and it approximates the forward Dirichlet boundary value problem for (1), by means of S total number of radii, N maximum number of formal powers, and K total number of points.

(1) $S \leftarrow 500$; $N \leftarrow 20$; $K+1 \leftarrow 501$;
(2) **while** $s = 1 \rightarrow S$
(3) **while** $n = 1 \rightarrow N$
(4) **while** $k = 0 \rightarrow K$
(5) $Z^{(n+1)}[k] = \mathscr{B}\left[Z^{(n)}[k]\right]$;
(6) **Function** *Orthonormalization*
(7) Classical Gram-Schmidt Orthonormalization Process
(8) **Function** *Regularization*
(9) Tikhonov Regularization Process
(10) **Function** *Approach_Boundary_Condition*
(11) $u_{\text{app}} = \sum_{n=0}^{N} \left(\alpha_n u^{(n)}(1,0,z) + \beta_n u^{(n)}(i,0,z) \right)$;
(12) **Function** *Save Orthonormal_Sytem*;
(13) **Function** *Save Coefficients*;

Algorithm 1: Boundary value with regularization approximation.

Thus, (24) has an explicit solution expressed as follows:

$$x = \left(A^T A + \gamma^2 I \right)^{-1} A^T b, \tag{25}$$

where I is the identity matrix with the same dimension of matrix A, the regularization parameter $\gamma > 0$, in this case $A = Z^{(n+1)}[k]$ represents the orthonormalized system, which is the result of the formal powers employing the conductivity σ and the imposed boundary condition, and b is the electric potential $u|_\Gamma$. The main problem is to choose the correct parameter γ, which approximates the solution for (25).

To choose a parameter γ, the next expression should be used:

$$\gamma = \sum_{k=1}^{m} \frac{A_{kk}^T A_{kk}}{u_k^T \cdot u_k}, \tag{26}$$

where A, as it was mentioned before, is the orthonormalized Taylor series in formal powers and u represents the electric potential [15]. We employ this regularization process to understand the behaviour of the problem leaving for the next section the methodology of the main process for approximation of the solution.

3. Procedure

The main goal is to develop an effective stable method, which let us to obtain better approximations for the forward problem by the employment of a regularization procedure for better convergence. The results obtained will be analysed in order to understand the problem presented in (1).

For this analysis, to find the forward Dirichlet boundary value problem using the methodology shown before, we use the algorithm from [9, 10]; as a result we obtain an accurate solution with a lower computer cost.

The principal difficulty, when the algorithm is being employed, lies in the instability of the method when the approximations are taking place. So, in order to improve the convergence of the result, a regularization process is included in the approximation process.

(1) $S \leftarrow 500$; $N \leftarrow 20$; $K+1 \leftarrow 501$;
(2) **while** $s = 1 \rightarrow S$
(3) **while** $n = 1 \rightarrow N$
(4) **while** $k = 0 \rightarrow K$
(5) $Z^{(n+1)}[k] = \mathscr{B}\left[Z^{(n)}[k]\right]$;
(6) **while** $\gamma > \gamma_e$
(7) **Function** *Orthonormalization*
(8) Classical Gram-Schmidt Orthonormalization Process
(9) **Function** *Regularization*
(10) Tikhonov Regularization Process
(11) **Function** *Approach_Boundary_Condition*
(12) $u_{\text{app}} = \sum_{n=0}^{N} \left(\alpha_n u^{(n)}(1,0,z) + \beta_n u^{(n)}(i,0,z)\right)$;
(13) $\gamma_e = \sum_{k=1}^{m} \frac{A_{kk}^T A_{kk}}{u_{\text{app}}^T u_{\text{app}}}$;
(14) **Function** *Save Orthonormal_Sytem*;
(15) **Function** *Save Coefficients*;

Algorithm 2: Boundary value with autoadjustment regularization approximation.

A procedure for the approximation consists of the following.

(1) Choose a domain.

(2) Select a conductivity.

(3) Apply Taylor series in formal powers approximation.

(4) Apply regularization process.

(5) Perform the computation of the electric potential.

First, a domain should be chosen, employing Algorithm 1. According to [9], there can be used smooth and nonsmooth domains, below; to analyse the results a unitary disk domain is chosen. Then, a conductivity function has to be chosen, and, in this study, the conductivity function is taken from the mathematical analysis and geometrical distribution; both cases are within the domain Ω.

Once the domain Ω and the conductivity function sigma are selected, the process continues by selecting the N maximum number of formal powers, S number of radii. and K number of points per radius, the approximation of the Taylor series in formal powers is performed, and the result obtained from this process should pass through the algorithm to the Gram-Schmidt orthonormalization method.

In this part of the procedure, the boundary solution can be computed, but we propose to modernize the procedure using a regularization method, in order to obtain better convergence of the method. Figure 1(a) shows graphically the procedure explained before.

The main idea is to confirm that novel regularized algorithm is able to compute more stable solution for the electric potential in the boundary and to express numerically the convergence of the method.

Additionally, we propose a modification of the explained algorithm where an autoadjustment should be performed before the error estimation process. Here, we use iterative scheme that can estimate the regularization parameter improving the convergence property of the algorithm.

Figure 2 illustrates the diagram of the algorithm proposed. The procedure analyses the convergence and the stability when an automatic adjustment takes place.

The modification made to Algorithm 1 presents a condition that should be satisfied, presenting an iterative method to approximate the solution of (1). In this algorithm, the condition is the same as presented before in (26), where the u_k in the iterative algorithm is the approximation of the electric potential u_{app}, as it is exposed in Algorithm 2. This autoadjustment introduced in the algorithm computes the solution of the forward problem increasing the computational cost but permits obtaining a better solution that is more stable and convergent.

Applying Algorithms 1 and 2 shown above, we perform the numerical experiments using mathematical expressions, such as exponential and sinusoidal function, and geometrical distributions such as disk center, and five disks' structure at the center.

This set of examples gives us a full perspective of the behaviour of the method, because we employed some samples to analyse the convergence of the method and then make experiments with the geometric distributions to analyse the results that are reviewed in the next section.

The examples investigated in the next section are designed to compare the results when a regularization method is used in the process versus the actual method, which does not employ a regularization procedure.

4. Results

As it is exposed in the works [9, 10], the possibility to employ geometrical distributions functions and mathematical expression in the algorithm, which use the Taylor series in formal powers, let us analyse the electrical impedance equation (1), emphasizing the possibility to approximate the forward problem to this equation.

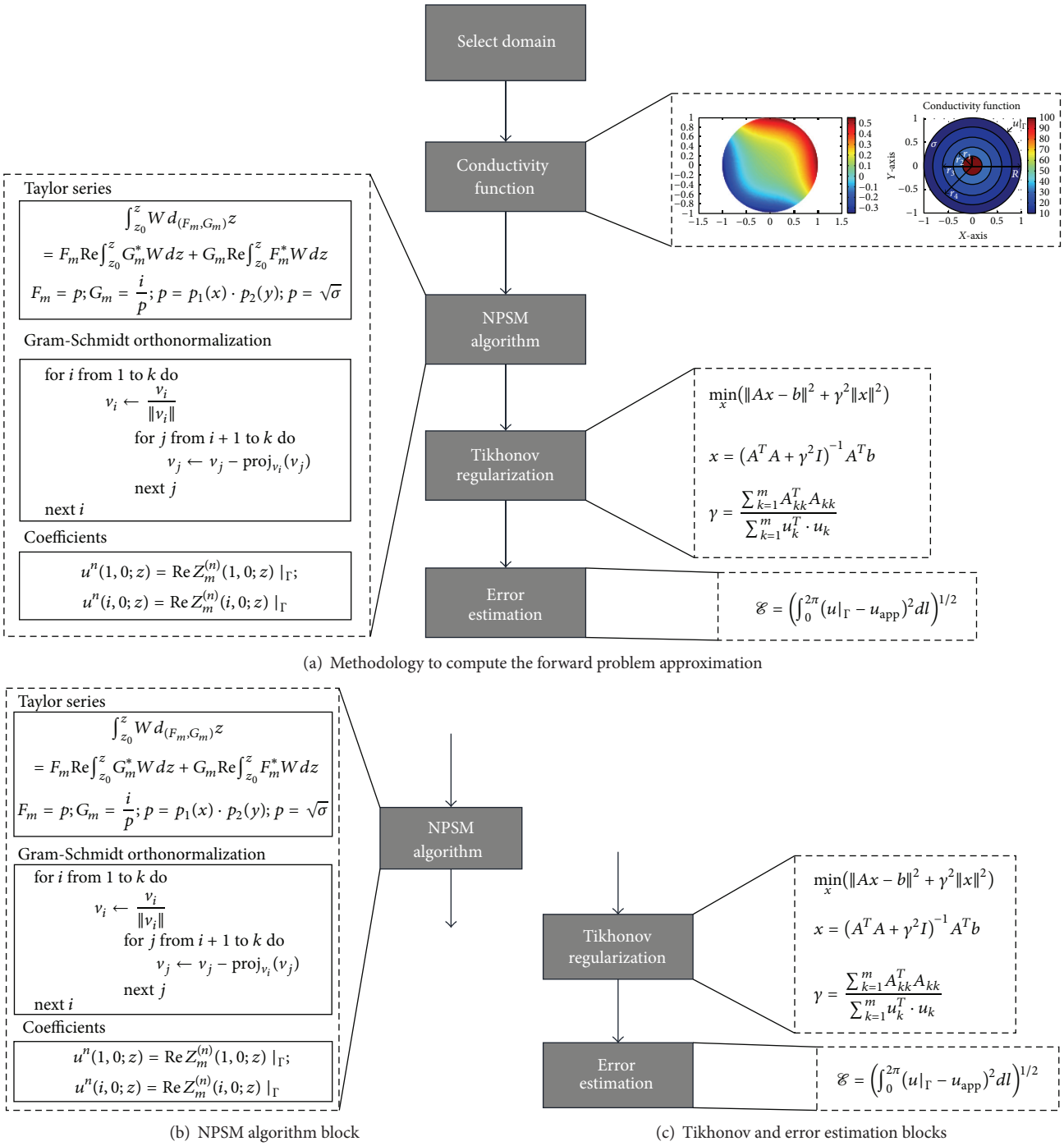

(a) Methodology to compute the forward problem approximation

(b) NPSM algorithm block

(c) Tikhonov and error estimation blocks

Figure 1: Methodology to compute the forward problem approximation.

Applying this analysis, we used an exponential and sinusoidal function coming from the mathematical analysis, circle at center, and the five disks' structure at center geometrical distributions. These cases are computed within the domain, and the results of the approximation are passed to regularization process in order to analyse the approximation and stability of the method, obtaining the electric potential in the boundary.

The solution for error, in order to analyse behaviour of the solution, is used in form of the Lebesgue measure

$$\mathscr{E} = \left(\int_0^{2\pi} \left(u|_\Gamma - u_{\mathrm{app}} \right)^2 dl \right)^{1/2}, \tag{27}$$

where $u|_\Gamma$ is the imposed boundary condition and u_{app} denotes the approximation by using the original algorithm

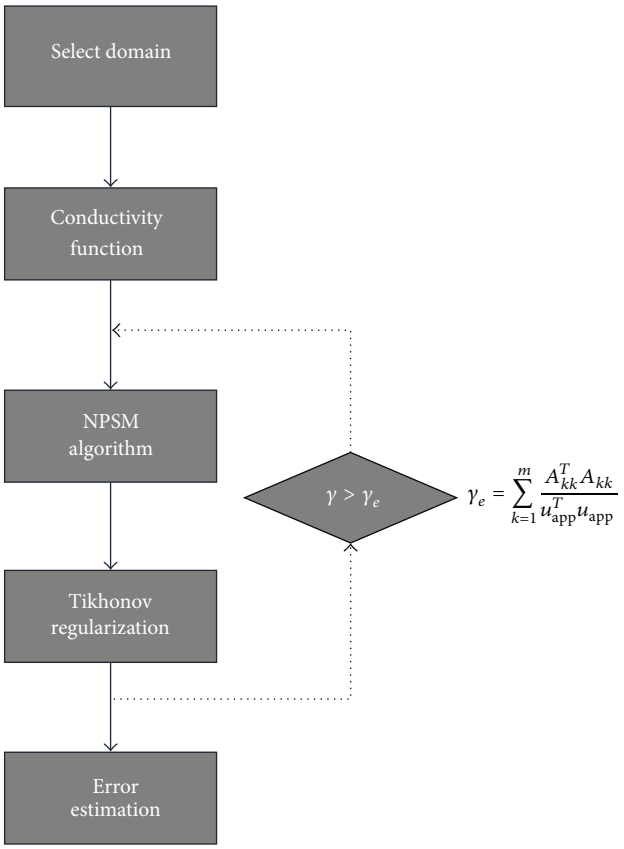

Figure 2: Methodology to compute the forward problem approximation employing autoadjustment regularization.

and the new modification employing the regularization process of everything within the unitary disk. We show the results in tables to compare and analyse the results obtained by these methods.

The next sections show the results for analytical and geometrical cases, in which the analytical cases are representatives due to the consideration of nonseparable conductivity functions in which the results can be achieved; for the geometrical case, the conductivity employed does not possess a boundary condition, imposing an artificial condition to compare the results and determine the accuracy of the method.

4.1. Exponential Conductivity Function. Let us use conductivity function, which fulfills (12) and possesses the form

$$\sigma = e^{-\mu xy}, \tag{28}$$

and this expression is shown in Figure 3(a), and for the boundary condition the expression to be imposed is

$$u = e^{\mu xy}, \tag{29}$$

where μ denotes the coefficient employed to change the behaviour of the function employed.

Table 1 expresses the behaviour when the μ coefficient increases and demonstrates the stability property of the method in two cases when the regularization method is employed and when this regularization process is not used.

The results in Table 1 show the known behaviour; meanwhile the number of formal powers increases and the error decreases, demonstrating a better convergence when the regularization method is employed.

The comparison between two algorithms that use the regularization procedure with and without the autoadjustment algorithms has been proved, the convergence and stability in the autoadjustment procedure being better than for comparison methods, but the computational cost considerably increases due to the iterative procedure performed.

This comparison is presented in Figure 3(b); in this graphic the three methods show the behaviour of the expression and in this case all methods reached a good approximation; since the three methods possess a low error, the difference can not be appreciated in the graphic matter, but Table 1 resumes correctly the full error analysis between all the methods.

4.2. Sinusoidal Conductivity Function. Let us employ a conductivity function, with the form

$$\sigma = 1 + \sin(\mu xy). \tag{30}$$

Figure 4(a) shows the expression within the unit disk, and, imposing a boundary condition,

$$u = \frac{1}{\tan(\mu xy/2) + 1}, \tag{31}$$

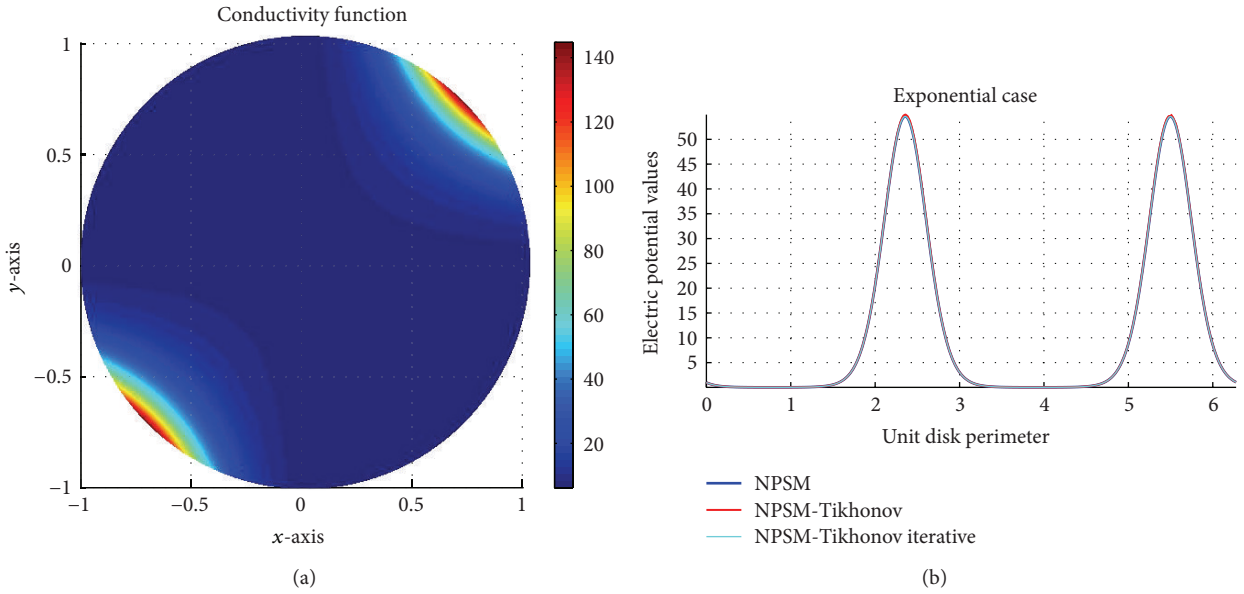

Figure 3: (a) Exponential conductivity function. (b) Comparison.

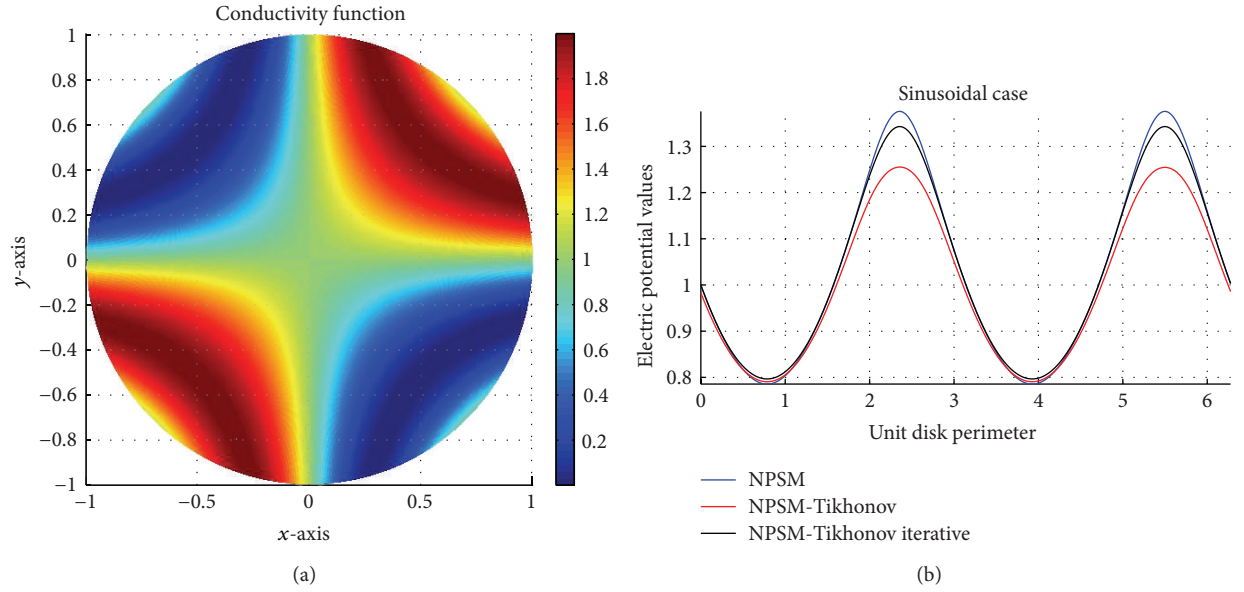

Figure 4: (a) Sinusoidal conductivity function. (b) Comparison.

where μ denotes the coefficient used to change the behaviour of the function employed.

Table 2 shows the behaviour of the method when the μ coefficient increases its value, including the simulation with and without the regularization process.

The results in this case are better with a regularization procedure; due to the conductivity that presents so many vibrations in the domain, the algorithm tries to reach a solution but its behaviour is bad; differently, when the regularization process is introduced, the results expose better performance because the perturbations or vibrations within the domain are smoothed and it is more easy to compute an approximation to (1).

In comparison with the other methods, the behaviour of the proposed algorithms is similar: using more formal powers the error is decreased and by the employing a regularization method the stability and convergence are improved considerably, but due to the iterative method used the computational cost is increased.

In Figure 3(b), the behaviour of all methods is shown; in this case the approximation can be appreciated because of the values of its error; for this case, the error can be analysed in

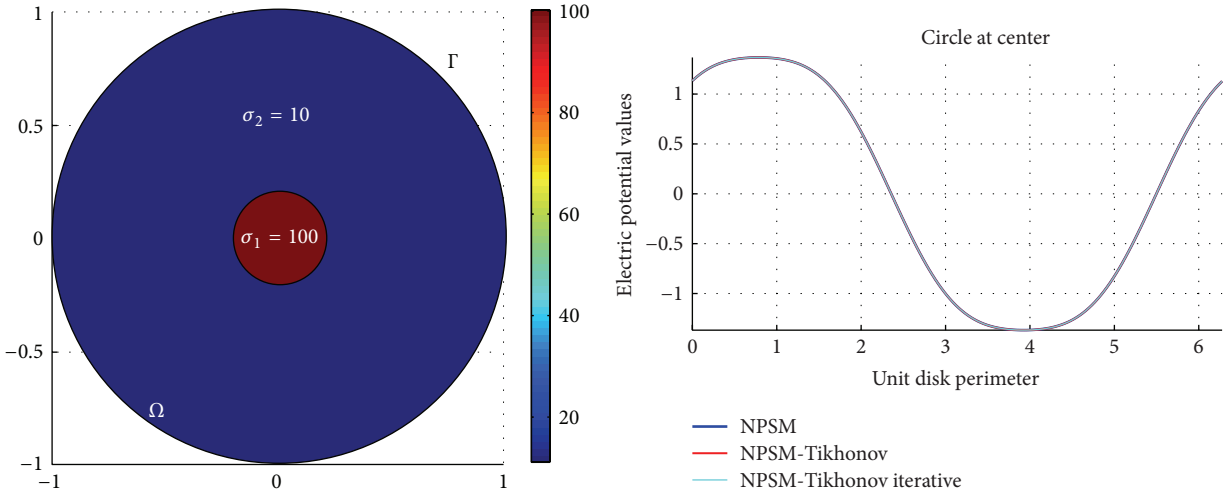

(a) (b)

FIGURE 5: (a) Disk at center conductivity function, $\sigma_1 = 100$; $\sigma_2 = 10$. (b) Comparison.

TABLE 1: Exponential conductivity function $\sigma = e^{-\mu xy}$.

N	S	K	μ	$\mathscr{E}$ NPSM	$\mathscr{E}$ NPSM-Tikhonov	$\mathscr{E}$ NPSM-Tikhonov autoadjustment
20	500	500	10	7.9269×10^{-4}	4.3572×10^{-7}	9.5152×10^{-9}
40	500	500	10	1.2168×10^{-12}	3.2525×10^{-7}	9.4462×10^{-9}
60	500	500	10	9.9732×10^{-13}	3.0521×10^{-7}	9.4187×10^{-9}
80	500	500	10	9.9623×10^{-13}	3.0021×10^{-7}	9.3702×10^{-9}
100	500	500	10	9.9450×10^{-13}	3.0015×10^{-7}	9.3651×10^{-9}
120	500	500	10	9.9230×10^{-13}	3.0005×10^{-7}	9.3551×10^{-9}
20	500	500	20	4.8450	12.5271×10^{-7}	3.5451×10^{-9}
40	500	500	20	2.6416×10^{-6}	11.1423×10^{-7}	3.4570×10^{-9}
60	500	500	20	7.5986×10^{-10}	11.0912×10^{-7}	3.3721×10^{-9}
80	500	500	20	7.5983×10^{-10}	11.0510×10^{-7}	3.2987×10^{-9}
100	500	500	20	7.5985×10^{-10}	11.0031×10^{-7}	3.1067×10^{-9}
120	500	500	20	7.5979×10^{-10}	10.9998×10^{-7}	3.0923×10^{-9}

terms of the method employed, proving that a regularization method is needed to approximate and reach a better solution.

4.3. Circle at Center. For the next case, we employed a disk at the center with conductivity $\sigma_1 = 100$ and the conductivity in the rest of the domain Ω is $\sigma_2 = 10$, as is shown in Figure 5(a).

For this case, we imposed the following boundary condition:

$$u = \frac{1}{3}\left(x^3 + y^3\right) + 0.5\left(x + y\right). \tag{32}$$

The results are shown in Table 3, where the behaviour of the method with and without the regularization process is presented.

In this case, the figure inside the domain is a circle with a variable radius (in concrete case, radius is 0.5); we know that if the disk within the domain is bigger, the approximation will be good, but if the inner conductivity is smaller, the algorithm could not detect the conductivity good; differently, when a regularization process is introduced, it warrants that the conductivity will be employed to compute the solution and the regularization process permits smoothing the conductivity to reach results.

This example provides unexpected results, because the convergence of the NPSM-Tikhonov and NPSM-Tikhonov with autoadjustment process does not obtain the convergence that the NPSM method can obtain. This case presents the best convergence and stability obtained by the NPSM algorithm, and the method with regularization process appears to obtain worse convergence but is still acceptable due to the error estimated.

This example gives us different ideas to improve and to analyse the problem for the optimized method. The first idea about the bad convergence in the solution is that the imposed

Table 2: Sinusoidal conductivity function $\sigma = 1 + \sin(\mu xy)$.

N	S	K	μ	$\mathscr{E}$ NPSM	$\mathscr{E}$ NPSM-Tikhonov	$\mathscr{E}$ NPSM-Tikhonov autoadjustment
20	500	500	6	47.8026	1.2558×10^{-3}	4.9995×10^{-5}
40	500	500	6	49.9321	1.2143×10^{-3}	4.9301×10^{-5}
60	500	500	6	54.7917	1.2013×10^{-3}	4.9015×10^{-5}
80	500	500	6	61.9715	1.1970×10^{-3}	3.8084×10^{-5}
100	500	500	6	70.3529	1.1905×10^{-3}	3.7970×10^{-5}
120	500	500	6	80.2248	1.2013×10^{-3}	3.6523×10^{-5}
20	500	500	12	42.5009	1.0078×10^{-3}	7.2012×10^{-5}
40	500	500	12	42.3868	1.0009×10^{-3}	7.1562×10^{-5}
60	500	500	12	42.5782	2.2561×10^{-4}	7.1132×10^{-5}
80	500	500	12	42.9195	1.2013×10^{-3}	7.0999×10^{-5}
100	500	500	12	43.1998	1.1817×10^{-3}	7.0741×10^{-5}
120	500	500	12	43.6383	1.1098×10^{-3}	7.0594×10^{-5}
20	500	500	18	54.2971	5.2045×10^{-4}	9.5051×10^{-5}
40	500	500	18	54.6205	5.1270×10^{-4}	9.5005×10^{-5}
60	500	500	18	56.3661	5.0976×10^{-4}	9.4980×10^{-5}
80	500	500	18	59.4942	5.0081×10^{-3}	9.4953×10^{-5}
100	500	500	18	64.2429	4.9954×10^{-3}	9.4032×10^{-5}
120	500	500	18	69.9109	4.8013×10^{-3}	9.3511×10^{-5}

Table 3: Disk at center with $\sigma_1 = 10$ and $\sigma_2 = 100$.

N	S	K	$\mathscr{E}$ NPSM	$\mathscr{E}$ NPSM-Tikhonov	$\mathscr{E}$ NPSM-Tikhonov autoadjustment
20	500	500	5.3404×10^{-15}	5.8084×10^{-7}	3.1415×10^{-9}
40	500	500	6.8485×10^{-15}	5.8590×10^{-7}	3.1010×10^{-9}
60	500	500	7.7718×10^{-15}	5.9150×10^{-7}	3.0578×10^{-9}
80	500	500	8.5317×10^{-15}	6.1232×10^{-7}	3.0020×10^{-9}
100	500	500	9.3593×10^{-15}	6.2140×10^{-7}	3.0001×10^{-9}
120	500	500	9.8723×10^{-15}	6.2491×10^{-7}	2.9982×10^{-9}

boundary condition is not the correct condition for this case; another idea is to employ a different approximation process based on mesh and finally to determine if the regularization process can improve; a better solution can be imposed in the boundary when it comes from the approximation in the same method, which comes from the Taylor series.

Figure 5(b) shows the behaviour of the solution in terms of the error computed; in this case, due to the low error, the difference in the graphic cannot be observed, but the difference exists and can be appreciated in the analysis of Table 3. For this case, the error increases a little, but it possesses a steady behaviour.

4.4. Concentric Disk at Center. In this experiment, we used a disk with four rings at the center with different radius and conductivities: $\sigma_1 = 10$ for the disk, $\sigma_2 = 15$ for the first ring, $\sigma_3 = 20$ for the second ring, $\sigma_4 = 30$ for the third ring, and $\sigma = 100$ for the last ring, as is shown in Figure 6(a).

For this case, we imposed the boundary condition (32).

The simulation results are shown in Table 4, presenting the behaviour of the method with and without the regularization process.

This case is difficult due to the disk structure inside the domain; both methods proved to be good when they approximate the electric potentials, in which the algorithm without regularization presents better convergence, compared to the one which used a regularization process presenting smoothing within the domain to find an approximation with more stability.

The best approximation is obtained for the NPSM algorithm, and the NPSM-Tikhonov with and without autoadjustment presents worse approximation but is useful for the problem to be solved. The behaviours of the methods are similar: a high number of formal powers give a better convergence, the number of radii and points per radius do not affect the convergence, and the regularization process

Table 4: Disk at center conductivity function, $\sigma_1 = 10$, $\sigma_2 = 15$, $\sigma_3 = 20$, $\sigma_4 = 30$, and $\sigma_5 = 100$.

N	S	K	$\mathscr{E}$ NPSM	$\mathscr{E}$ NPSM-Tikhonov	$\mathscr{E}$ NPSM-Tikhonov autoadjustment
20	500	500	5.7828×10^{-15}	3.1309×10^{-7}	1.8012×10^{-8}
40	500	500	5.9170×10^{-15}	3.2404×10^{-7}	1.7925×10^{-8}
60	500	500	6.0634×10^{-15}	3.2602×10^{-7}	1.6841×10^{-8}
80	500	500	6.2671×10^{-15}	3.2702×10^{-7}	1.5165×10^{-8}
100	500	500	6.3172×10^{-15}	4.0112×10^{-7}	1.4409×10^{-8}
120	500	500	6.3476×10^{-15}	4.0201×10^{-7}	1.3001×10^{-8}

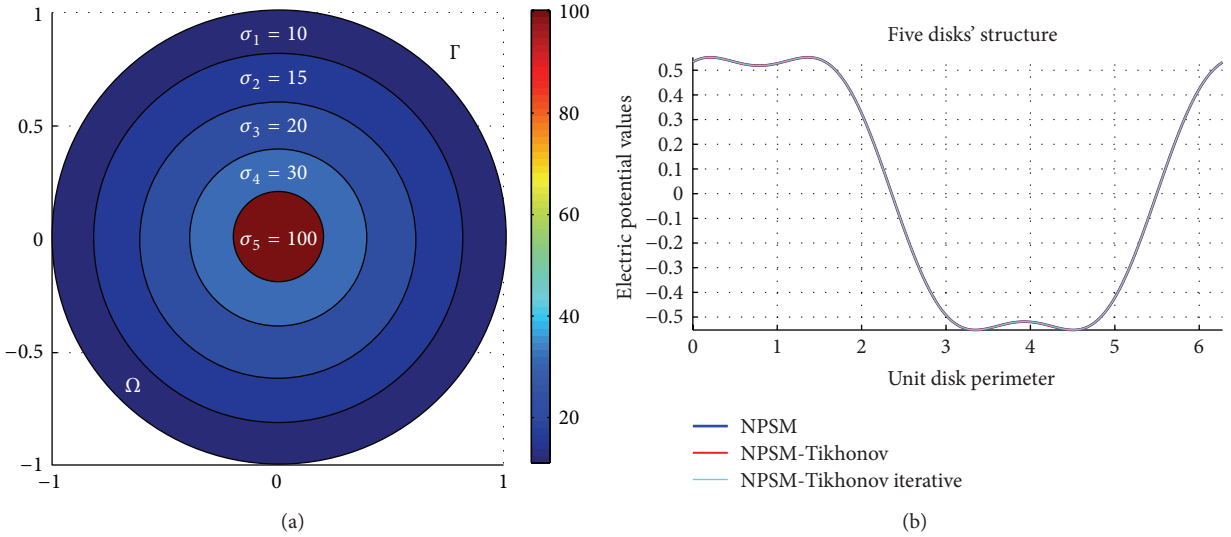

(a) (b)

Figure 6: (a) Five disks' structure at center conductivity function, $\sigma_1 = 10$, $\sigma_2 = 15$, $\sigma_3 = 20$, $\sigma_4 = 30$, and $\sigma_5 = 100$. (b) Comparison.

with and without an autoadjustment method only affects the convergence and stability in the solution. In this case, the approximation that is obtained by these methods is considered good, proving that the regularization method can be used for this problem.

This example is useful to understand the behaviour and, thanks to this analysis, the main idea is preserved; a complex study needs to be performed paying more attention to the boundary condition and employing the results obtained in the Taylor series instead of employing the imposed boundary condition in order to determine if the boundary condition which is employed is the best condition to fulfill the domain and the conductivity within; this analysis could be demonstrated if the inverse problem can be approached by means of the Taylor series in formal powers with and without a different interpolation procedure including the regularization process.

Figure 6(b) shows the error analysis of the example employed, in which the behaviour is the same; the method proves to be steady and to reach the solution in terms of the error computed. For this case, the solution shown in the graphic does not express a considerable difference and fits correctly, but in terms Table 4 shows that the error increases and decreases depending upon the data introduced in the problem.

5. Discussion

The examples exposed in Tables 1, 2, 3, and 4 illustrate the behaviour of the algorithms with and without the regularization process. In the tables, the columns with the title E NPSM, proved this behavior; meanwhile the formal powers increase, the convergence of the approximation is better, and the number of points and radii do not affect considerably the approximation in this method.

Then, the regularization process, which is employed in all cases, showed better stability and in some examples a better convergence; this is the proof that a regularization process could be employed in order to approximate forward problems when the conductivity function presents a nonsmooth conductivity function, giving the possibility to approximate the forward Dirichlet boundary value problem for (1) when the regularization is employed.

All the cases analyzed and discussed in the last section show better convergence and stability. The reasons for these approximations are due to the conductivity employed in

every case, where the exponential conductivity case does not present problem to approximate employing any of the methods; the case when the conductivity function is a disk at center presents a better convergence without the regularization method, but the results are more stable when regularization is employed.

In cases such as sinusoidal function, where the conductivity function presents vibrations and the possibility to obtain an approximation is more difficult, the regularization process presents better convergence and stability here; the reason for it is the smoothing phase for the conductivity function within the domain, because the regularization process is added to the algorithm.

The last case that is analysed exposes the structure of the five disks at center; a Gibbs phenomenon is presented, provoking disaster in the computing process and presenting a better convergence in the method without the regularization process, but, oppositely, the proposed method exposes more stability with regularization process.

All these examples have shown that a regularization process can be involved to stabilise the process and to obtain better approximation. Such performance of the proposed method is crucial in developing a novel numerical tool for a solution to inverse problem for (1).

The proposed autoadjustment algorithm with a regularization process shows better stability due to the regularization parameter chosen experimentally. This advantage is presented when employing mentioned autoadjustment parameter, which permits the stability and convergence to reach their maximum value generating a reliable approximation. Drawback of the method is a considerable increment in the computational cost. So, we can obtain the solution more slowly comparing with the basic algorithm without regularization procedure.

These examples let us analyze the behaviour in analytical and geometrical cases near to finding a new idea to improve the algorithm and optimize the process. This study arouses several questions that need to be analysed in future work. In the interpolation procedure where the method employed is a radial basis interpolation, the approximation by means of a regularization procedure is a good idea but thanks to this analysis it should be analysed; what happens if the imposed boundary condition does not fulfill the conductivity within the domain and its boundary? Some ideas for future work in order to solve this query come, beginning with the employment of a mesh grid instead of a radial base function of interpolation and the use of a Taylor series approximation instead of the full boundary condition imposed in the domain with boundary.

6. Conclusions

The regularization method employed in the approximation for the forward Dirichlet boundary value problem for (1) gives a stability to the process permitting better convergence by smoothing the conductivity functions employed within the domain.

The conductivity is employed in the analytical cases, in which the conductivity function is presented in nonseparable variables; the convergence of the method permits employing also separable variables conductivity function presenting the same convergence. As it is shown, independently of the conductivity function, both algorithms reached a good accuracy, and let us analyse their behaviour to reach a possible solution for the inverse problem.

The results obtained in this study have proven that a regularization method is important to solve these problems, when considered as an ill-posed task. The incorporating of this regularization process presents smoothing in the conductivity functions within the domain to approximate the solution, independently of the domain that we employ.

For the nonsmooth domain, the regularization method can approximate the solution independently of domain; it means that if the boundary of the domain is not smooth, the regularization method smoothing it approaches the solution, but the convergence it is not the best.

Both methods have proven good approximation of the solution for the forward Dirichlet boundary value problem, where the autoadjustment regularization algorithm shows that it is possible to obtain a better convergence and stability than other proposed and analysed algorithms.

More experiments should be performed to determine if the novel algorithm can approximate different class of conductivity functions also. In future investigations, it should be checked if the algorithm can approximate real medical images obtaining the estimation of the conductivity employing image processing techniques.

At the light of the results and the discussion generated by means of both proposed algorithms, based on regularization process, it seems that novel proposal can be useful for ill-posed problems as it presents (1).

We leave for a future work the analysis of the data and the proposition of the method, which can be used for the approximation of the forward problem to obtain a solution for the inverse problem. This is a hard task and still open problem, due to the complexity of the electrical impedance tomography problem. Analysing the computer complexity of the algorithm employed, we ensure that it can be parallelized in order to compute the solution faster, and a characterization of the formal power should be performed to determine if the imposed boundary condition is correct or not for all cases used before.

Conflict of Interests

All the authors declare that there is no conflict of interests regarding the publication of this article, due to the numerical methods used along this work were fully developed in GNUC/C++ Compiler.

Acknowledgments

The authors would like to thank Consejo Nacional de Ciencias y Tecnologia (CONACyT) and Instituto Politecnico Nacional (IPN) for the economic support to develop this research.

References

[1] A. P. Calderon, "On an inverse boundary value problem," in *Proceedings of the Seminar on Numerical Analysis and Its Applications to Continuum Physics*, pp. 65–73, Sociedade Brasileira de Matematica, 1980.

[2] J. G. Webster, *Electrical Impedance Tomography*, Adam Hilger Series on Biomedical Engineering, 1990.

[3] V. V. Kravchenko, *Applied Pseudoanalytic Function Theory*, Frontiers in Mathematics, 2009.

[4] K. Astala and L. Päivärinta, "Calderón's inverse conductivity problem in the plane," *Annals of Mathematics: Second Series*, vol. 163, no. 1, pp. 265–299, 2006.

[5] I. N. Vekua, *Generalized Analytic Functions*, International Series of Monographs on Pure and Applied Mathematics, Pergamon Press, 1962.

[6] I. Chalendar, J. Leblond, and J. R. Partington, "Approximation problems in some holomorphic spaces, with applications," in *Systems, Approximation, Singular Integral Operators, and Related Topics (Bordeaux, 2000)*, vol. 129 of *Operator Theory: Advances and Applications*, pp. 143–168, Birkhäauser, Basel, Switzerland, 2001.

[7] L. Baratchart, A. Borichev, and S. Chaabi, "Pseudo-holomorphic functions at the critical exponent," http://arxiv.org/abs/1309.3079.

[8] L. Baratchart, Y. Fischer, and J. Leblond, "Dirichlet/Neumann problems and Hardy classes for the planar conductivity equation," http://arxiv.org/abs/1111.6776.

[9] C. M. A. Robles Gonzalez, A. G. Bucio Ramirez, M. P. Ramirez Tachiquin, and V. D. Sanchez Nava, "On the numerical solutions of boundary value problems in the plane for the electrical impedance equation: a pseudoanalytic approach for non-smooth domains," in *IAENG Transactions on Engineering Technologies*, Lecture Notes in Electrical Engineering, Springer, 2012.

[10] C. M. A. Robles, R. A. Bucio, and T. M. P. Ramirez, "New characterization of an improved numerical method for solving the electrical impedance equation in the plane: an approach from the modern pseudoanalytic function theory," *IAENG International Journal of Applied Mathematics*, vol. 43, no. 1, 2013.

[11] L. Bers, *Theory of Pseudoanalytic Functions*, IMM, New York University, New York, NY, USA, 1953.

[12] M. P. Ramirez-Tachiquin, C. M. A. R. Gonzalez, R. A. Hernandez-Becerril, and A. G. B. Ramirez, "First characterization of a new method for numerically solving the Dirichlet problem of the two-dimensional electrical impedance equation," *Journal of Applied Mathematics*, vol. 2013, Article ID 493483, 14 pages, 2013.

[13] M. Lukaschewitsch, P. Maass, and M. Pidcock, "Tikhonov regularization for electrical impedance tomography on unbounded domains," *Journal of Inverse Problems*, vol. 19, no. 3, pp. 585–610, 2003.

[14] S. Savchev and J. Ottesen, "Tikhonov regularization in Kronecker product approximation for image restoration with mean boundary conditions," *Applied Mathematical Modelling*, vol. 36, pp. 225–237, 2011.

[15] B. Hofmann and T. Hohage, *Generalized Tikhonov Regularization: Basic Theory and Comprehensive Results on Convergence Rates*, Technische Universität Chemnitz, Fakultät fur Mathematik, 2011.

Hindawi Publishing Corporation
Journal of Applied Mathematics
Volume 2013, Article ID 493483, 14 pages
http://dx.doi.org/10.1155/2013/493483

Research Article

First Characterization of a New Method for Numerically Solving the Dirichlet Problem of the Two-Dimensional Electrical Impedance Equation

Marco Pedro Ramirez-Tachiquin,[1] Cesar Marco Antonio Robles Gonzalez,[2] Rogelio Adrian Hernandez-Becerril,[2] and Ariana Guadalupe Bucio Ramirez[3]

[1] *Communications and Digital Signal Processing Group, Faculty of Engineering, La Salle University, B. Franklin 47, Mexico City 06140, Mexico*
[2] *SEPI, ESIME Culhuacan, National Polytechnic Institute, Avenue Santa Ana No. 1000, Mexico City 04430, Mexico*
[3] *SEPI, UPIITA, National Polytechnic Institute, Avenue IPN 2580, Mexico City 07340, Mexico*

Correspondence should be addressed to Marco Pedro Ramirez-Tachiquin; marco.ramirez@lasallistas.org.mx

Received 13 March 2013; Accepted 31 May 2013

Academic Editor: Yansheng Liu

Based upon the elements of the modern pseudoanalytic function theory, we analyze a new method for numerically solving the forward Dirichlet boundary value problem corresponding to the two-dimensional electrical impedance equation. The analysis is performed by introducing interpolating piecewise separable-variables conductivity functions in the unit circle. To warrant the effectiveness of the posed method, we consider several examples of conductivity functions, whose boundary conditions are exact solutions of the electrical impedance equation, performing a brief comparison with the finite element method. Finally, we discuss the possible contributions of these results to the field of the electrical impedance tomography.

1. Introduction

The study of the forward Dirichlet boundary value problem for the electrical impedance equation in the plane,

$$\operatorname{div}(\sigma \operatorname{grad} u) = 0, \tag{1}$$

is fundamental for understanding its inverse problem, commonly known as electrical impedance tomography, first correctly posed in mathematical form by Calderon [1] in 1980. It is remarkable that, for more than twenty years after the problem was stated, the mathematical complexity of (1) could provoke that many experts considered impossible to obtain its general solution in analytic form [2], even for the simplest cases of σ, excluding the constant case.

This perception changed when, independently, Kravchenko in 2005 [3] and Astala and Päivärinta [4] in 2006 noticed that the two-dimensional case of (1) was completely equivalent to a special class of Vekua equation [5].

Many other important results were obtained soon after. Indeed, Kravchenko et al. published in 2007 what can be considered the first general solution of (1) in analytic form [6], when σ possesses a certain form, employing Taylor series in formal powers [7]. Moreover, when the conductivity is separable variables, the real parts of the formal powers conform a complete set for approaching solutions of the forward Dirichlet boundary value problem of (1) in the plane [8].

The main objective of this work is to start a discussion about the application of the Pseudoanalytic function theory when σ is not, in general, a separable-variables function, which would allow the study of conductivity cases more interesting in physics and engineering. As a matter of fact, even it is not clear yet how to extend the proof provided in [8], about the completeness of the set of formal powers for the cases when σ is piecewise separable variables, the numerical calculations will show that a variation of the technique,

originally posed for purely mathematical problems, could well serve for analyzing more general cases, providing quite acceptable results with compared when classical methods.

In other words, this work states that if the values of the electrical conductivity are known at every point within a bounded domain Ω in the plane, it will be always possible to introduce a piecewise separable-variables function, such that we can use it to obtain a set of base functions for approaching solutions of the forward Dirichlet boundary value problem of (1), employing pseudoanalytic functions. This would be true for a certain class of bounded domains, but this class will be wide enough to include many interesting cases for the applied sciences. Nonetheless, on behalf of briefness, we will only study the unit circle. The reader will appreciate that most of the results will be valid for more domains.

In order to prove the veracity of the last assessments, we will consider a set of conductivity examples, separable variables, and nonseparable variables, for which we can obtain exact solutions, to be imposed as boundary conditions. The effectiveness of the approaches will be estimated by comparing them with the boundary conditions, employing a standard Lebesgue measure.

Finally, we will discuss how this numerical technique could contribute to the study of the inverse Dirichlet boundary value problem of (1) in the plane, also known as the Electrical Impedance Tomography problem.

2. Preliminaries

According to the Pseudoanalytic function theory posed by Bers [7], let the pair of complex-valued functions F and G fulfill the condition:

$$\operatorname{Im}\left(\overline{F}G\right) > 0, \tag{2}$$

where $\overline{F}$ represents the complex conjugation of F: $\overline{F} = \operatorname{Re} F - i \operatorname{Im} F$ and i denotes the standard imaginary unit $i^2 = -1$. This condition implies that the functions F and G are linearly independent, therefore any complex-valued function W can be expressed by their linear combination:

$$W = \phi F + \psi G, \tag{3}$$

where ϕ and ψ are purely real-valued functions. On the light of this idea, L. Bers introduced the concept of the (F, G)-derivative of W in the form

$$\partial_{(F,G)} W = \left(\partial_z \phi\right) F + \left(\partial_z \psi\right) G. \tag{4}$$

This derivative will exist if and only if the following equality is true:

$$\left(\partial_{\overline{z}} \phi\right) F + \left(\partial_{\overline{z}} \psi\right) G = 0. \tag{5}$$

Hereafter, we will use the notations $\partial_z = \partial_x - i\partial_y$ and $\partial_{\overline{z}} = \partial_x + i\partial_y$. These pairs of partial differential operators are usually introduced with the factor $1/2$, but in this work it will be somehow more convenient to work without it.

Introducing the notations:

$$\begin{aligned} A_{(F,G)} &= \frac{\overline{F}\partial_z G - \overline{G}\partial_z F}{F\overline{G} - G\overline{F}}, \qquad a_{(F,G)} = -\frac{\overline{F}\partial_{\overline{z}} G - \overline{G}\partial_{\overline{z}} F}{F\overline{G} - G\overline{F}}, \\ B_{(F,G)} &= \frac{F\partial_z G - G\partial_z F}{F\overline{G} - G\overline{F}}, \qquad b_{(F,G)} = -\frac{G\partial_{\overline{z}} F - F\partial_{\overline{z}} G}{F\overline{G} - G\overline{F}}, \end{aligned} \tag{6}$$

the derivative presented in (4), that we will refer to as the (F, G)-derivative of W, can be rewritten as

$$\partial_{(F,G)} W = \partial_z W - A_{(F,G)} W - B_{(F,G)} \overline{W}, \tag{7}$$

whereas condition (5) will become

$$\partial_{\overline{z}} W - a_{(F,G)} W - b_{(F,G)} \overline{W} = 0. \tag{8}$$

A pair of complex functions (F, G) satisfying condition (2) will be called a *generating pair*, and the functions introduced in (6) will be referred to as the *characteristic coefficients* of the generating pair (F, G). As a matter of fact, the expression (8) is known as the *Vekua equation* [5], and every function W, solution of (8), will be called (F, G)-*pseudoanalytic*.

The following statements were originally posed in [7]. We present them with certain modifications, in order to better analyze the special class of Vekua equation corresponding to the electrical impedance equation (1) in the plane.

Theorem 1. *The functions F and G, constituting the generating pair of the form* (2)*, are (F, G)-pseudoanalytic, and their (F, G)-derivatives vanish identically:*

$$\partial_{(F,G)} F \equiv \partial_{(F,G)} G \equiv 0. \tag{9}$$

Theorem 2 (see [7, 9])**.** *Let p be a nonvanishing function, defined within some domain $\Omega(\mathbb{R}^2)$, and let*

$$F = p, \qquad G = \frac{i}{p}. \tag{10}$$

It is easy to verify that F and G conform a generating pair (2)*, whose characteristic coefficients, according to* (6)*, are*

$$\begin{aligned} A_{(F,G)} &= a_{(F,G)} = 0, \\ B_{(F,G)} &= \frac{\partial_z p}{p}, \\ b_{(F,G)} &= \frac{\partial_{\overline{z}} p}{p}. \end{aligned} \tag{11}$$

Therefore, for this special class of generating pairs, the corresponding Vekua equations will have the form

$$\partial_{\overline{z}} W - \frac{\partial_{\overline{z}} p}{p} \overline{W} = 0. \tag{12}$$

Definition 3. Let (F_0, G_0) and (F_1, G_1) be two generating pairs of the form (10), and let their characteristic coefficients fulfill the condition

$$B_{(F_0,G_0)} = -b_{(F_1,G_1)}. \tag{13}$$

Thus the generating pair (F_1, G_1) will be called a *successor* pair of (F_0, G_0), as well (F_0, G_0) will be called a *predecessor* of (F_1, G_1).

Definition 4. Let the elements of the set

$$\{(F_m, G_m)\}, \quad m = 0, \pm 1, \pm 2, \ldots, \tag{14}$$

be all generating pairs, and let every (F_{m+1}, G_{m+1}) be a successor of (F_m, G_m). Hence, the set (14) will be called a *generating sequence*. If $(F, G) = (F_0, G_0)$, we will say that (F, G) is embedded into (14). Moreover, if there exists a number k such that $(F_{m+k}, G_{m+k}) = (F_m, G_m)$, we will say that the generating sequence (14) is periodic, with period k.

L. Bers also introduced the concept of the (F, G)-integral of a complex function W. The reader can find the conditions for warranting its existence and a detailed description of its properties in [7, 9]. Since the functions employed in this work are, by definition, (F, G)-integrable, we will only present a certain set of those properties.

Definition 5. Let (F_0, G_0) be a generating pair with the form (10). Its adjoin pair (F_0^*, G_0^*) is defined as

$$F_0^* = -iF_0, \qquad G_0^* = -iG_0. \tag{15}$$

Definition 6. The (F_0, G_0)-integral of a complex function W (when it exists) is defined according to the expression

$$\int_\Lambda W d_{(F_0,G_0)} z = F_0 \operatorname{Re} \int_\Lambda G_0^* W dz + G_0 \operatorname{Re} \int_\Lambda F_0^* W dz, \tag{16}$$

where Λ is a rectifiable curve going from z_0 up to z_1, in the complex plain. In particular, the (F_0, G_0)-integral of $\partial_{(F_0,G_0)} W$ reaches

$$\int_{z_0}^{z} \partial_{(F_0,G_0)} W d_{F_0,G_0} z = W - \phi(z_0) F_0 - \psi(z_0) G_0. \tag{17}$$

But according to Theorem 1, the (F_0, G_0)-derivatives of F_0 and G_0 vanish identically, hence (17) can be considered the (F_0, G_0)-*antiderivative* of $\partial_{(F_0,G_0)} W$.

2.1. Formal Powers

Definition 7. The formal power $Z_m^{(0)}(a_0, z_0; z)$ belonging to the generating pair (F_m, G_m), with formal exponent 0, complex coefficient a_0, center at z_0, and depending upon the complex variable $z = x + iy$, is defined by the expression

$$Z_m^{(0)}(a_0, z_0; z) = \lambda F_m + \mu G_m, \tag{18}$$

where λ and μ are constants that fulfill the condition

$$\lambda F_m(z_0) + \mu G_m(z_0) = a_0. \tag{19}$$

The formal powers with higher formal exponents are defined according to the recursive formulas

$$Z_m^{(n)}(a_n, z_0; z) = n \int_{z_0}^{z} Z_{m-1}^{(n-1)}(a_n, z_0; z)\, d_{(F_m,G_m)} z. \tag{20}$$

Notice the integral operators at the right hand side of the last equality are all (F_m, G_m)-antiderivatives.

Remark 8. The formal powers possess the following properties:

(1) $Z_m^{(n)}(a_n, z_0; z) \to a_n (z - z_0)^n$ when $z \to z_0$.

(2) Every $Z_m^{(n)}(a_n, z_0; z)$ is (F_m, G_m)-pseudoanalytic.

(3) If $a_n = a_n' + i a_n''$, where a_n' and a_n'' are real constants, we will have

$$Z_m^{(n)}(a_n, z_0; z) = a_n' Z_m^{(n)}(1, z_0; z) + a_n'' Z_m^{(n)}(i, z_0; z). \tag{21}$$

Theorem 9. *Every complex-valued function W, solution of the Vekua equation* (8)*, can be expanded in terms of the so-called Taylor series in formal powers:*

$$W = \sum_{n=0}^{\infty} Z^{(n)}(a_n, z_0; z), \tag{22}$$

where the absence of the subindex "m" indicates that all formal powers belong to the same generating pair.

Remark 10. Since every complex-valued function W, solution of (8), can be expressed in the form (22), it is possible to assert that (22) is an analytic representation of the general solution for the Vekua equation (8).

2.2. The Electrical Impedance Equation in the Plane.

As it has been previously posed in several works (see, e.g., [3, 9, 10]), when the conductivity function σ can be expressed in terms of a separable-variables function

$$\sigma = \sigma_1(x)\, \sigma_2(y), \tag{23}$$

by introducing the notations

$$W = \sqrt{\sigma} \partial_x u - i \sqrt{\sigma} \partial_y u, \qquad p = \frac{\sqrt{\sigma_2}}{\sqrt{\sigma_1}}, \tag{24}$$

the two-dimensional electrical impedance equation (1) can be rewritten precisely as a Vekua equation of the form (12). Moreover, its corresponding generating pair

$$F_0 = p, \qquad G_0 = \frac{i}{p} \tag{25}$$

is embedded into a periodic generating sequence, with period $k = 2$, such that

$$F_m = \frac{\sqrt{\sigma_2}}{\sqrt{\sigma_1}}, \qquad G_m = i \frac{\sqrt{\sigma_1}}{\sqrt{\sigma_2}}, \tag{26}$$

when m is an even number, and

$$F_m = \sqrt{\sigma_1 \sigma_2}, \qquad G_m = \frac{i}{\sqrt{\sigma_1 \sigma_2}}, \tag{27}$$

when m is odd.

Therefore, based upon the statements posed in Definition 7, possessing a generating sequence will allow us to approach a set of formal powers:

$$\left\{Z_0^{(n)}(1,0;z), Z_0^{(n)}(i,0;z)\right\}_{n=0}^{N}, \tag{28}$$

within a bounded domain Ω, and, subsequently by virtue of Remark 8, we will be able to approach any formal power $Z_0^{(n)}(a_n,0;z)$, at any point $z \in \Omega$.

Because the present work intends to contribute to the construction of a novel theory for the electrical impedance tomography problem, we will focus our attention into a classic domain Ω, the unit disk with center at $z_0 = 0$.

2.3. A Complete Orthonormal System. In [8] Campos et al. posed a very important property of the formal powers.

Theorem 11 (see [8]). *The set of real parts of the formal powers, with coefficients* 1 *and i, valued at the boundary* Γ *of a bounded domain* Ω

$$\left\{\operatorname{Re} Z^{(n)}(1,0;z)|_\Gamma, \operatorname{Re} Z^{(n)}(i,0;z)|_\Gamma\right\}_{n=0}^{\infty}, \tag{29}$$

constitutes a complete system for approaching solutions of the forward Dirichlet boundary value problem for the electrical impedance equation (1) *in the plane.*

That is, any boundary condition $u|_\Gamma$ can be approached asymptotically by the linear combination of the elements belonging to (29):

$$\lim_{N\to\infty} u|_\Gamma - \left(\sum_{n=0}^{N} c_n^{(1)} \operatorname{Re} Z^{(n)}(1,0;z)|_\Gamma + c_n^{(i)} \operatorname{Re} Z^{(n)}(i,0;z)|_\Gamma\right) = 0, \tag{30}$$

where the coefficients $c_n^{(1)}$ and $c_n^{(i)}$ are all real constants.

Since the elements of the set (29) are, by definition, linearly independent [7], it is possible to perform a standard Gram-Schmidt orthonormalization process in order to obtain the set of functions

$$\{u_n\}_{n=0}^{2N-1}, \tag{31}$$

defined on the boundary Γ, such that when imposing a boundary condition $u|_\Gamma$, we will have

$$u|_\Gamma \sim \sum_{n=0}^{2N-1} \alpha_n u_n. \tag{32}$$

Because the set $\{u_k\}_{k=0}^{2N-1}$ is orthonormal, the calculation of the coefficients α_n can be performed by several classical methods. Particularly, we will employ the scalar product

$$\alpha_n = \left\langle u_n, u|_\Gamma \right\rangle. \tag{33}$$

2.4. A Basic Numerical Approach. Remembering that Γ coincides with the perimeter of the unit circle, we can employ the numerical methods detailed in [11] for obtaining a system of $2N+1$ formal powers (notice that, according to (25), $\operatorname{Re} Z_0^{(0)}(i,z_0;z) = 0$), defined at the boundary Γ:

$$\left\{\operatorname{Re} Z_0^{(n)}(1,0;z)|_\Gamma, \operatorname{Re} Z_0^{(n)}(i,0;z)|_\Gamma\right\}_{n=0}^{N}. \tag{34}$$

More precisely, let us consider the formal powers $Z_0^{(n)}(1,0;z)$. Taking into account that the integral expressions introduced in (17) are path independent [7], we can choose the rectifiable curve Λ to be a straight line segment, going from $z_0 = 0$ until some point of the unit circle. Thus, we can allocate P points equidistantly distributed on such line, obtaining the set of complex numbers

$$\left\{z[p] = \frac{p}{P}\cos\theta[r] + i\frac{p}{P}\sin\theta[r]\right\}_{p=0}^{P-1}, \tag{35}$$

where $\theta[r]$ is some angle associated to the radius. Given this set of points, and considering that the generating sequence corresponding to the pair (25) is periodic with period $k = 2$, we can numerically approach the formal powers employing, for example, a variation of the trapezoidal integration method according to the expressions

$$\begin{aligned}
&Z_0^{(n)}(z[p]) \\
&\quad = (n-1)F_0(z[p]) \\
&\qquad \times \operatorname{Re}\sum_{q=0}^{p-1}\left(Z_1^{(n-1)}(z[q+1])\,G_0^*(z[q+1])\right)dz[q] \\
&\qquad + (n-1)F_0(z[p]) \\
&\qquad \times \operatorname{Re}\sum_{q=0}^{p}\left(Z_1^{(n-1)}(z[q])\,G_0^*(z[q])\right)dz[q] \\
&\qquad + (n-1)G_0(z[p]) \\
&\qquad \times \operatorname{Re}\sum_{q=0}^{p-1}\left(Z_1^{(n-1)}(z[q+1])\,F_0^*(z[q+1])\right)dz[q] \\
&\qquad + (n-1)G_0(z[p]) \\
&\qquad \times \operatorname{Re}\sum_{q=0}^{p}\left(Z_1^{(n-1)}(z[q])\,F_0^*(z[q])\right)dz[q],
\end{aligned} \tag{36}$$

where $p, q = 0, 1, \ldots, P-1$, and

$$dz[p] = z[p+1] - z[p]. \tag{37}$$

Besides, we can introduce a set of R angles $\theta[r]$, to be employed in (35), according to the formula

$$\left\{\theta[r] = \frac{2\pi r}{R}\right\}_{r=0}^{R-1} \tag{38}$$

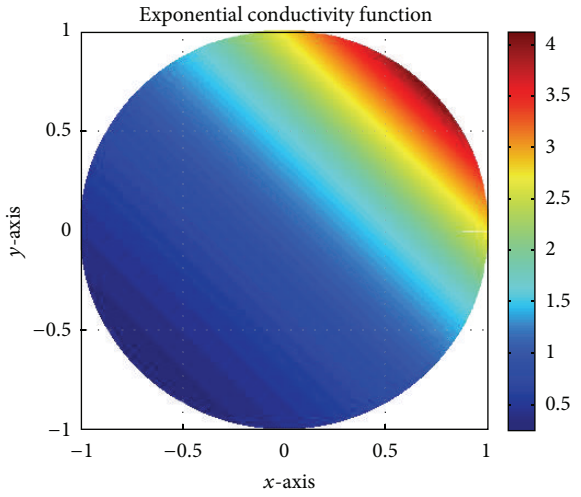

Figure 1: Example of a separable-variables exponential conductivity function $\sigma = e^{x+y}$.

Table 1: Relation between the error $\mathscr{E}$ and the number of formal powers, for the case when σ possesses an exponential form.

Number of radii R	Points per radius P	Number of formal powers N	$\mathscr{E}$
500	500	45	1.4370×10^{-15}
100	100	45	1.9996×10^{-15}
100	100	35	2.0001×10^{-15}
100	100	25	2.0094×10^{-15}
100	100	15	2.0524×10^{-15}
100	100	5	3.1333×10^{-14}

for the iterative expressions (36) that can be performed at each angle $\theta[r]$. When the full procedure is complete, we will possess a set of $N+1$ formal powers $Z^{(n)}(1,0;z)$, approached for R radii, and with P points per radius. Thus, by collecting the real parts of $Z^{(n)}(1,0;z)$ valued at the points $z[P-1]$, which are precisely those located at the boundary Γ, we will obtain a numerical approximation of the set

$$\left\{\operatorname{Re} Z^{(n)}(1,0;z)|_{\Gamma}\right\}_{n=0}^{N}. \tag{39}$$

An identical procedure can be performed for obtaining the elements of

$$\left\{\operatorname{Re} Z^{(n)}(i,0;z)|_{\Gamma}\right\}_{n=0}^{N}. \tag{40}$$

Since the numerical approaching of the set (34) is complete, a standard Gram-Schmidt method will reach the orthonormal system (31) for approaching the boundary condition $u|_{\Gamma}$.

The effectiveness of this numerical approach has been analyzed in several works (see [8, 10]). Here we will only analyze two particular examples of separable-variables conductivity functions σ, before studying those that are not separable variables.

Table 2: Relation between the error $\mathscr{E}$ and the number of formal powers, for the case when σ has a Lorentzian form.

Number of radii R	Points per radius P	Number of formal powers N	$\mathscr{E}$
500	500	45	2.2968×10^{-8}
100	100	45	2.3753×10^{-8}
100	100	35	5.8069×10^{-7}
100	100	25	1.9710×10^{-5}
100	100	15	7.2801×10^{-4}
100	100	5	4.8875×10^{-2}

3. The Cases When the Conductivity σ Possesses a Separable-Variables Form

3.1. Example When σ Is an Exponential Function

Proposition 12. *Let $\sigma = e^{x+y}$. Then the function $u = e^{-x-y}$ will be a particular solution of* (1).

Figure 1 plots an illustration of the exponential conductivity.

The numerical procedure described in Section 2.4 will be employed for approaching the forward Dirichlet boundary value problem when σ possesses the form of the proposition above, imposing as the boundary condition the exact solution

$$u|_{\Gamma} = e^{-x-y}. \tag{41}$$

The error $\mathscr{E}$ will be defined according to the Lebesgue measure

$$\mathscr{E} = \left(\int_{\Gamma} \left(u|_{\Gamma} - \sum_{n=0}^{2N+1} \alpha_n u_n \right)^2 dl \right)^{1/2}, \tag{42}$$

where the addition within the integral expression corresponds to the approached solution (32).

Table 1 contains the relation between the error $\mathscr{E}$ and the number of formal powers N. The parameters R and P have been fixed at the value 100, since for this particular case, as displayed in the table, they do not significantly influence the diminution of the error when increasing.

3.2. The Case When σ Has a Lorentzian Form

Proposition 13. *Let*

$$\sigma = \left(\frac{1}{x^2 + 0.1} \right) \left(\frac{1}{y^2 + 0.1} \right). \tag{43}$$

Then the function

$$u = \frac{x^3 + y^3}{3} + 0.1\,(x + y) \tag{44}$$

will be a particular solution of (1).

An illustration of the conductivity function (43) is displayed in Figure 2.

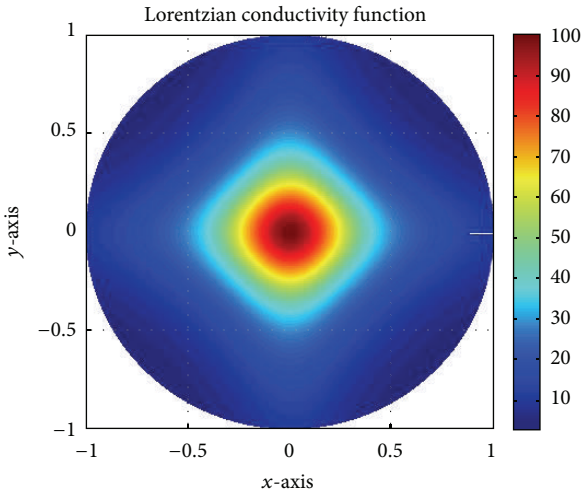

Figure 2: Example of a separable-variables Lorentzian conductivity function $\sigma = (x^2 + 0.1)^{-1} \cdot (y^2 + 0.1)^{-1}$.

Once more, the exact solution (44) will be imposed as the boundary condition. The numerical results are shown in Table 2. This, indeed, is a more interesting case, since the number N of formal powers strongly influences the accuracy of the approach. The increment of the number of points per radius P and the number of radii R, as in the previous case, do not significantly increase the accuracy.

3.3. Construction of a Piecewise Separable-Variables Conductivity Function. Consider a bounded domain $\Omega(\mathbb{R}^2)$ (in this case the unit circle) and divide it into a finite number of subsections S, taking care that the point to be considered the center of the formal powers z_0 (see Definition 7) does not reside onto the boundary of two subsections. For simplicity, let us make the division by employing a finite set of parallel lines to the x-axis, equidistant to one another, and let us locate $z_0 = 0$.

Supposing that the values of the electrical conductivity are defined for every point within the domain $\Omega(\mathbb{R}^2)$, let us locate a straight line crossing every subsection, that does not intersect the bounding parallel lines of its corresponding subsection. Indeed, such lines can be simply parallel to the bounding ones.

The following step is to collect finite sets of conductivity values, corresponding to a number C of points located at the crossing lines. For every line, the quantity of collected values C must be big enough to warrant that an interpolating process, in this case performed with straight lines, will adequately approach all the remaining conductivity values defined over the line points.

Since we have already assumed that every crossing line will be parallel to the subsection-bounding lines, and in consequence to the x-axis, all collected points corresponding to the same crossing line will possess the same y-coordinate. Let us propose that the conductivity within every subsection can be represented according to the expression

$$\sigma = \frac{y + K}{\Upsilon + K} \cdot f(x), \tag{45}$$

where Υ denotes the y-coordinate that is common to all points along the crossing line, $f(x)$ is an interpolating function that approaches the collected conductivity values, and K is a real positive constant such that $y + K \neq 0$, for all $y \in \Omega$.

Applying this idea in every subsection, the conductivity σ within the bounded domain Ω can be approached by means of the piecewise-defined function:

$$\sigma(x, y) = \begin{cases} \dfrac{y + K}{\Upsilon_1 + K} \cdot f_1(x) : y \in [y_{(1)}, y_{(2)}); \\ \dfrac{y + K}{\Upsilon_2 + K} \cdot f_2(x) : y \in [y_{(2)}, y_{(3)}); \\ \vdots \\ \dfrac{y + K}{\Upsilon_S + K} \cdot f_S(x) : y \in [y_{(S)}, y_{(S+1)}]. \end{cases} \tag{46}$$

Here $y_{(1)}$ represents the first y-coordinate found within the domain Ω when broaching the y-axis from ∞ up to $-\infty$, whereas $y_{(S)}$ represents the last one. The pairs of y-axis parallel lines $(y_{(j)}, y_{(j+1)})$, where $j = 1, \ldots, S + 1$, are given by the common y-coordinates belonging to every pair of lines delimiting the subsections. Notice the piecewise function (46) is separable variables.

Thus, according to Section 2.2, it immediately follows that

$$F_0 = \begin{cases} \left(\dfrac{y + K}{\Upsilon_1 + K} \cdot f_1^{-1}(x) \right)^{1/2} : y \in [y_{(1)}, y_{(2)}), \\ \left(\dfrac{y + K}{\Upsilon_2 + K} \cdot f_2^{-1}(x) \right)^{1/2} : y \in [y_{(2)}, y_{(3)}), \\ \vdots \\ \left(\dfrac{y + K}{\Upsilon_S + K} \cdot f_S^{-1}(x) \right)^{1/2} : y \in [y_{(S)}, y_{(S+1)}], \end{cases} \tag{47}$$

whereas

$$G_0 = \begin{cases} i\left(\dfrac{\Upsilon_1 + K}{y + K} \cdot f_1(x) \right)^{1/2} : y \in [y_{(1)}, y_{(2)}), \\ i\left(\dfrac{\Upsilon_2 + K}{y + K} \cdot f_2(x) \right)^{1/2} : y \in [y_{(2)}, y_{(3)}), \\ \vdots \\ i\left(\dfrac{\Upsilon_S + K}{y + K} \cdot f_S(x) \right)^{1/2} : y \in [y_{(S)}, y_{(S+1)}]. \end{cases} \tag{48}$$

Table 3: Relation between the error $\mathscr{E}$ and the number of sections S and samples per section C, when $\sigma = e^{x+y}$.

Number of radii R	Points per radius P	Number of formal powers N	Number of sections S	Collected values per section C	$\mathscr{E}$
100	100	45	20001	20001	4.4935×10^{-5}
100	100	45	10001	10001	6.9358×10^{-5}
100	100	45	5001	5001	6.8149×10^{-4}
100	100	45	2501	2501	5.7113×10^{-4}
100	100	45	1001	1001	3.3381×10^{-3}
100	100	45	501	501	1.5105×10^{-3}
100	100	45	101	101	5.3048×10^{-3}

For the generating pair (F_1, G_1) we will have

$$F_1 = \begin{cases} \left(\dfrac{y+K}{\Upsilon_1+K}\cdot f_1(x)\right)^{1/2} : y \in [y_{(1)}, y_{(2)}), \\ \left(\dfrac{y+K}{\Upsilon_2+K}\cdot f_2(x)\right)^{1/2} : y \in [y_{(2)}, y_{(3)}), \\ \vdots \\ \left(\dfrac{y+K}{\Upsilon_S+K}\cdot f_S(x)\right)^{1/2} : y \in [y_{(S)}, y_{(S+1)}], \end{cases}$$

$$G_1 = \begin{cases} i\left(\dfrac{\Upsilon_1+K}{y+K}\cdot f_1^{-1}(x)\right)^{1/2} : y \in [y_{(1)}, y_{(2)}), \\ i\left(\dfrac{\Upsilon_2+K}{y+K}\cdot f_2^{-1}(x)\right)^{1/2} : y \in [y_{(2)}, y_{(3)}), \\ \vdots \\ i\left(\dfrac{\Upsilon_S+K}{y+K}\cdot f_S^{-1}(x)\right)^{1/2} : y \in [y_{(S)}, y_{(S+1)}]. \end{cases} \tag{49}$$

We will use these piecewise-defined functions to perform the numerical procedure described in Section 2.4. The first case to analyze will be the exponential conductivity $\sigma = e^{x+y}$ studied in Section 3.1, imposing as the boundary condition $u|_\Gamma = e^{-x-y}$ the exact solution presented in Proposition 12.

The second case will be the Lorentzian conductivity treated in Section 3.2, whose boundary condition will be the exact solution $u|_\Gamma$ shown in Proposition 13. The results of these cases are exposed in Tables 3 and 4. For both, we can observe that the accuracy is strongly related with the number of sections S and the number of collected values per section C, as well as with the number N of formal powers. Once more, the increment of the number of points per radius P and the number of radii R do not significantly improve the accuracy.

Beside, since the tables presented in the previous subsection have shown that the accuracy of the method is not considerably improved when neither the number of points per radius P nor the number of radii R increase, we will fix both values $P = R = 100$ hereafter.

Tables 3 and 4 show that the piecewise separable-variables conductivity function (46) can be positively employed for numerically approaching solutions of this boundary value problem, because even the magnitudes of the errors $\mathscr{E}$ are considerable bigger than those obtained when employing the original σ, their magnitudes are still acceptable when compared with other classical numerical methods.

More precisely, employing a standard finite element method technique for solving forward Dirichlet boundary value problems of elliptic partial differential equations in the plane, when considering the exponential conductivity $\sigma = e^{x+y}$ and imposing the boundary condition $u|_\Gamma = e^{-x-y}$, the error was $\mathscr{E} = 6.1638 \times 10^{-4}$, utilizing 8257 nodes in the mesh, corresponding to 16256 triangular elements. For the Lorentzian conductivity $\sigma = (x^2 + 0.1)^{-1}(y^2 + 0.1)^{-1}$, with the boundary condition $u|_\Gamma = (1/3)(x^3 + y^3) + 0.1(x + y)$, employing identical number of nodes in the mesh, the resulting error was $\mathscr{E} = 2.6424 \times 10^{-4}$.

A more detailed description of the behavior of the method is provided in Tables 5, 6, and 7.

Notice that the comparison with the finite element method is given as a basic reference. Indeed, the number of nodes in the mesh was taken at 8257, because it is the closest value to the number of points located in Ω obtained when we multiply $P \cdot R = 10000$.

4. Analysis of Conductivity Functions That Are Not Separable Variables

This section is fully dedicated to study conductivity functions that do not possess a separable-variables form, but for which we are able to obtain exact solutions of (1), in order to impose them as boundary conditions.

4.1. The Nonseparable-Variables Exponential Case

Proposition 14. *Let the conductivity function*

$$\sigma = e^{xy}. \tag{50}$$

Then, a particular solution of (1) *will be*

$$u = e^{-xy}. \tag{51}$$

Figure 3 illustrates the conductivity funcion of (50).

Tables 7 and 8 contain the information about the behavior of the error $\mathscr{E}$ when changing the values of S, C, and N. In this case the diminution of the number of sections S

Table 4: Relation between the error $\mathscr{E}$ and the number of formal powers N, when $\sigma = e^{x+y}$.

Number of radii R	Points per radius P	Number of formal powers N	Number of sections S	Collected values per section C	$\mathscr{E}$
100	100	45	10001	10001	6.9358×10^{-5}
100	100	35	10001	10001	4.0388×10^{-4}
100	100	25	10001	10001	5.3651×10^{-4}
100	100	15	10001	10001	3.4733×10^{-3}
100	100	5	10001	10001	4.5714×10^{-2}

Table 5: Relation between the error $\mathscr{E}$ and the number of sections S and samples per section C, when $\sigma = (x^2 + 0.1)^{-1}(y^2 + 0.1)^{-1}$.

Number of radii R	Points per radius P	Number of formal powers N	Number of sections S	Collected values per section C	$\mathscr{E}$
100	100	45	20001	20001	6.1214×10^{-6}
100	100	45	10001	10001	1.1241×10^{-5}
100	100	45	5001	5001	1.3062×10^{-5}
100	100	45	2501	2501	7.2332×10^{-5}
100	100	45	1001	1001	1.7079×10^{-4}
100	100	45	501	501	3.5471×10^{-4}
100	100	45	101	101	1.0553×10^{-3}

Table 6: Relation between the error $\mathscr{E}$ and the number of formal powers N, when $\sigma = (x^2 + 0.1)^{-1}(y^2 + 0.1)^{-1}$.

Number of radii R	Points per radius P	Number of formal powers N	Number of sections S	Collected values per section C	$\mathscr{E}$
100	100	45	10001	10001	1.1241×10^{-5}
100	100	35	10001	10001	9.1964×10^{-5}
100	100	25	10001	10001	5.0855×10^{-4}
100	100	15	10001	10001	4.2633×10^{-3}
100	100	5	10001	10001	2.9065×10^{-2}

Table 7: Relation between the error $\mathscr{E}$ and the number of sections S and samples per section C, when $\sigma = e^{xy}$.

Number of radii R	Points per radius P	Number of formal powers N	Number of sections S	Collected values per section C	$\mathscr{E}$
100	100	45	20001	20001	3.8759×10^{-6}
100	100	45	10001	10001	5.4177×10^{-6}
100	100	45	5001	5001	2.1470×10^{-5}
100	100	45	2501	2501	1.5406×10^{-5}
100	100	45	1001	1001	6.6917×10^{-5}
100	100	45	501	501	1.5059×10^{-4}
100	100	45	101	101	8.7576×10^{-4}

Table 8: Relation between the error $\mathscr{E}$ and the number of formal powers N, when $\sigma = e^{xy}$.

Number of radii R	Points per radius P	Number of formal powers N	Number of sections S	Collected values per section C	$\mathscr{E}$
100	100	45	10001	10001	5.4177×10^{-6}
100	100	35	10001	10001	2.6425×10^{-5}
100	100	25	10001	10001	3.2504×10^{-5}
100	100	15	10001	10001	3.4497×10^{-5}
100	100	5	10001	10001	1.0798×10^{-2}

Table 9: Relation between the error $\mathscr{E}$ and the number of sections S and samples per section C, when $\sigma = ((x+y)^2+1)^{-1}$.

Number of radii R	Points per radius P	Number of formal powers N	Number of sections S	Collected values per section C	$\mathscr{E}$
100	100	45	20001	20001	8.8364×10^{-3}
100	100	45	10001	10001	8.9246×10^{-3}
100	100	45	5001	5001	9.4573×10^{-3}
100	100	45	2501	2501	9.9164×10^{-3}
100	100	45	1001	1001	1.0330×10^{-2}
100	100	45	501	501	8.6507×10^{-3}
100	100	45	101	101	9.5800×10^{-3}

Table 10: Relation between the error $\mathscr{E}$ and the number of formal powers N, when $\sigma = ((x+y)^2+1)^{-1}$.

Number of radii R	Points per radius P	Number of formal powers N	Number of sections S	Collected values per section C	$\mathscr{E}$
100	100	45	10001	10001	8.9246×10^{-3}
100	100	35	10001	10001	4.3227×10^{-2}
100	100	25	10001	10001	5.9625×10^{-2}
100	100	15	10001	10001	8.2125×10^{-2}
100	100	5	10001	10001	1.4064×10^{-1}

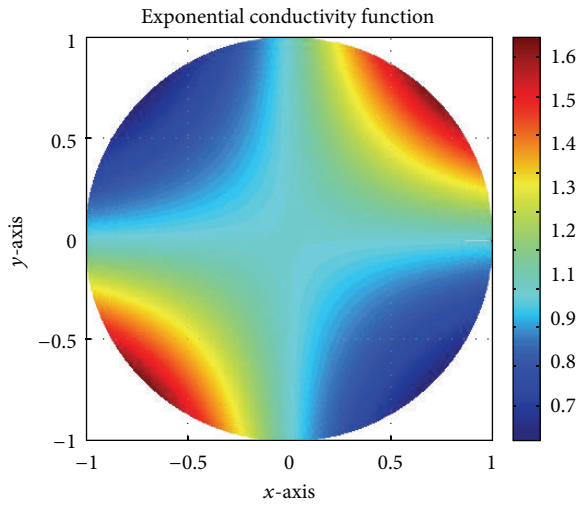

Figure 3: Example of nonseparable-variables conductivity function $\sigma = e^{xy}$.

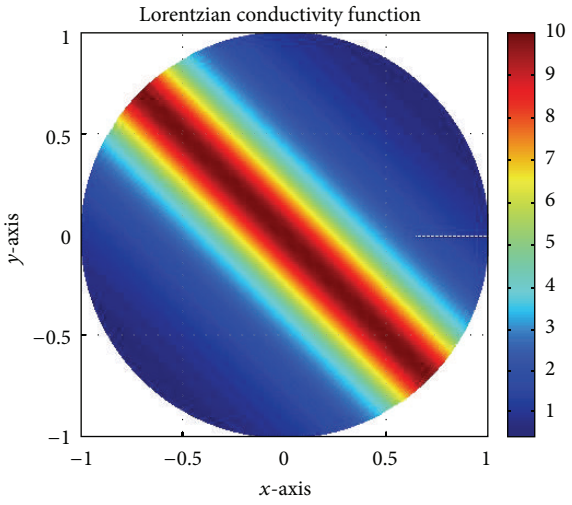

Figure 4: Example of nonseparable-variables Lorentzian conductivity function $\sigma = ((x+y)^2+1)^{-1}$.

and diminution of the samples per section C do influence the accuracy, but their influence is not so significant as the diminution of the formal powers N.

The error obtained when employing the finite element method approach was $\mathscr{E} = 2.3966 \times 10^{-4}$, employing 8257 points in the mesh.

4.2. The Nonseparable-Variables Lorentzian Case

Proposition 15. *Let the conductivity function have the form*

$$\sigma = \frac{1}{(x+y)^2+1}. \tag{52}$$

An exact solution for (1) *is*

$$u = \frac{(x+y)^3}{3} + x + y. \tag{53}$$

The conductivity function with the form (52) is illustrated in Figure 4.

Table 9 shows an abnormal behavior of the error $\mathscr{E}$ when decreasing the number of sections S and samples C. That is, it does not follow a clear pattern. But more important is to remark that the finite element method reported an error $\mathscr{E} = 5.4311 \times 10^{-4}$, which implies that is better situated for analyzing this class of conductivity functions. Table 10

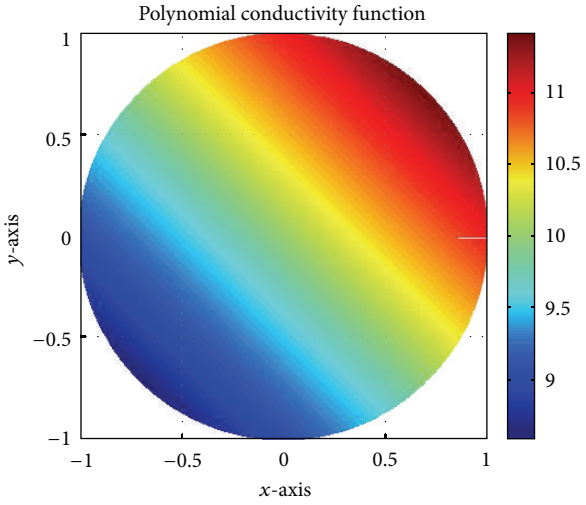

FIGURE 5: Examples of nonseparable-variables polynomial conductivity function $\sigma = x + y + 10$.

states that the diminution of the number of formal powers N decreases the accuracy.

4.3. The Nonseparable-Variables Polynomial Case

Proposition 16. *Let one assume that the conductivity function has the form*

$$\sigma = x + y + 10, \tag{54}$$

thus the function

$$u = \ln\left(x + y + 10\right) \tag{55}$$

will be a solution of (1).

In Figure 5 it is illustrated the polynomial conductivity function of (54).

Tables 11 and 12 show a regular behavior of the error $\mathscr{E}$, because it decreases when the values S and C do. This case possesses a singular characteristic when compared to the cases above: The diminution of the number of formal powers N does not provoke a considerable loss of the accuracy. This exception will be remarked since it has not been detected in other class of conductivity functions.

On the other hand, the finite element method proved to provide a very similar accuracy for analyzing this case, because the obtained error was $\mathscr{E} = 2.8958 \times 10^{-6}$.

4.4. The Nonseparable-Variables Sinusoidal Case

Proposition 17. *Let one consider the sinusoidal conductivity*

$$\sigma = 2 + \sin\left(x + y\right). \tag{56}$$

One can verify by direct substitution that the function

$$u = \frac{2}{\sqrt{3}} \arctan\left(\frac{2\tan\left(\left(x + y\right)/2\right) + 1}{\sqrt{3}}\right) \tag{57}$$

is a solution of (1).

The Figure 6(a) illustrates the conductivity (56), whereas the Figure 6(b) illustrates the case (58).

Tables 13 and 14 show that the behavior of $\mathscr{E}$ is not fully regular, because a diminution of the number S and C does not necessarily imply a reduction of the accuracy, whereas the diminution of the formal powers N provokes significant changes of the error $\mathscr{E}$. For this case, the finite element method reported an error $\mathscr{E} = 0.0192$.

Notice that the exact solution (57) that was imposed as the boundary condition $u|_\Gamma$ cannot be employed when a constant factor multiplies the argument of the trigonometric function, because the tangent would not be defined at certain points. Nevertheless, one last experiment is worth of research.

Let us suppose that the conductivity function possesses the form

$$\sigma = 2 + \sin 5\left(x + y\right), \tag{58}$$

and let us approach the solution to the forward problem keeping as the boundary condition the expression (57). Tables 15 and 16 display the biggest error $\mathscr{E}$ found in the present work, even the behavior of $\mathscr{E}$ could be considered regular, because it decreases while S, C, and N do. The reader will appreciate that the accuracy is, in general, unsatisfactory for applications. Indeed, the finite element method obtained an error $\mathscr{E} = 0.0043$, hence it is quite better situated for analyzing this kind of conductivity functions.

5. Conclusions

The comparison of the numerical method posed in this work and the finite element method is far to be complete. Thus the selected examples will be considered a basic reference from which many other trials must be adequately performed, since they could not be included in these pages because they constitute independent research topics. For instance, a detailed description of the computational complexity [12] of both methods would provide a point of view less dependent on the platform on which the methods are programmed; thus we could focus our attention into the basic properties.

Still, we will remark an important characteristic of the pseudoanalytic functions-based method. It provides information about the solutions of the forward Dirichlet boundary value problem for (1), that is not clear how to obtain when utilizing the finite element method.

More precisely, the numerical approach based upon the pseudoanalytic analysis reaches a full set of functions defined at the boundary, that might contain relevant data if we desire to examine the electrical impedance tomography problem.

For instance, let us consider the base functions $\{u_n\}_{n=0}^{2N+1}$ approached for the case when $\sigma = e^{xy}$, as examined in (50). The absolute values of the coefficients α_n, employed for approaching the boundary condition $u|_\Gamma = e^{-xy}$, are displayed in the semilogarithmic graphic of Figure 7. This calculation was performed considering $S = 20001$ sections, $C = 10001$ samples per section, $R = 100$ radii, $P = 101$ points per radii, and $N = 45$ formal powers; thus we will have $2N + 1 = 91$ base functions u_n, defined at the boundary Γ.

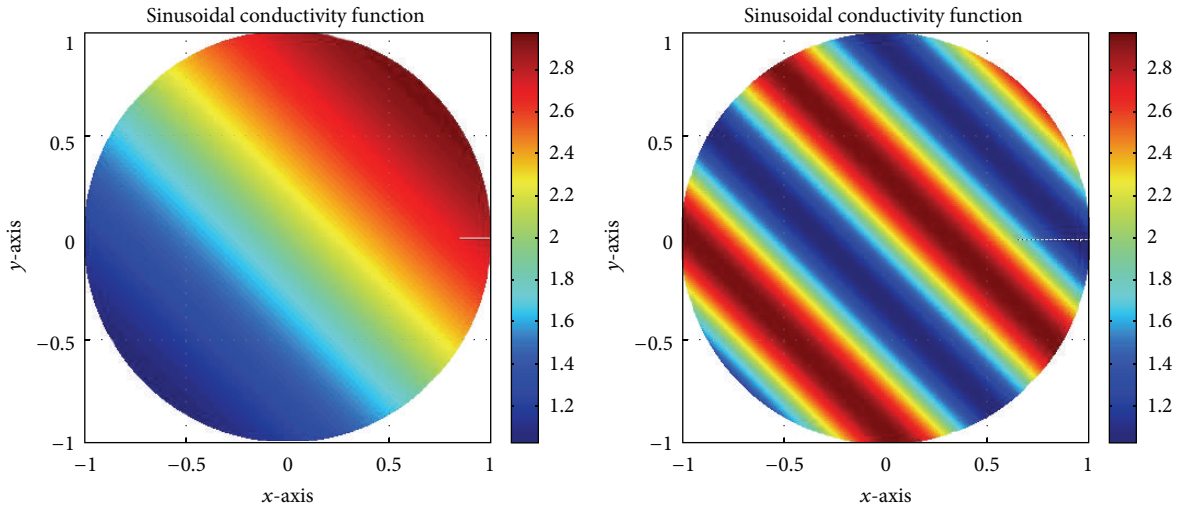

(a) $\sigma = 2 + \sin(x + y)$ (b) $\sigma = 2 + \sin 5(x + y)$

Figure 6: Examples of sinusoidal conductivity functions.

Table 11: Relation between the error $\mathscr{E}$ and the number of sections S and samples per section C, when $\sigma = x + y + 10$.

Number of radii R	Points per radius P	Number of formal powers N	Number of sections S	Collected values per section C	$\mathscr{E}$
100	100	45	20001	20001	3.0640×10^{-6}
100	100	45	10001	10001	2.3420×10^{-6}
100	100	45	5001	5001	8.1962×10^{-6}
100	100	45	2501	2501	1.9286×10^{-5}
100	100	45	1001	1001	6.4916×10^{-5}
100	100	45	501	501	1.5166×10^{-4}
100	100	45	101	101	4.5938×10^{-4}

Table 12: Relation between the error $\mathscr{E}$ and the number of formal powers N, when $\sigma = x + y + 10$.

Number of radii R	Points per radius P	Number of formal powers N	Number of sections S	Collected values per section C	$\mathscr{E}$
100	100	45	10001	10001	2.3420×10^{-6}
100	100	35	10001	10001	1.0616×10^{-5}
100	100	25	10001	10001	1.6275×10^{-5}
100	100	15	10001	10001	1.8396×10^{-5}
100	100	5	10001	10001	1.9909×10^{-5}

Table 13: Relation between the error $\mathscr{E}$ and the number of sections S and samples per section C, when $\sigma = 2 + \sin(x + y)$.

Number of radii R	Points per radius P	Number of formal powers N	Number of sections S	Collected values per section C	$\mathscr{E}$
100	100	45	20001	20001	7.5333×10^{-2}
100	100	45	10001	10001	7.6129×10^{-2}
100	100	45	5001	5001	7.4343×10^{-2}
100	100	45	2501	2501	6.9999×10^{-2}
100	100	45	1001	1001	8.4363×10^{-2}
100	100	45	501	501	6.4758×10^{-2}
100	100	45	101	101	9.0737×10^{-2}

Table 14: Relation between the error $\mathscr{E}$ and the number of formal powers N, when $\sigma = 2 + \sin(x + y)$.

Number of radii R	Points per radius P	Number of formal powers N	Number of sections S	Collected values per section C	$\mathscr{E}$
100	100	45	10001	10001	7.6129×10^{-2}
100	100	35	10001	10001	1.3551×10^{-1}
100	100	25	10001	10001	2.0886×10^{-1}
100	100	15	10001	10001	3.3854×10^{-1}
100	100	5	10001	10001	5.3026×10^{-1}

Table 15: Relation between the error $\mathscr{E}$ and the number of sections S and samples per section C, when $\sigma = 2 + \sin 5(x + y)$.

Number of radii R	Points per radius P	Number of formal powers N	Number of sections S	Collected values per section C	$\mathscr{E}$
100	100	45	20001	20001	7.5333×10^{-2}
100	100	45	10001	10001	7.6129×10^{-2}
100	100	45	5001	5001	7.4343×10^{-2}
100	100	45	2501	2501	6.9999×10^{-2}
100	100	45	1001	1001	8.4363×10^{-2}
100	100	45	501	501	6.4758×10^{-2}
100	100	45	101	101	9.0737×10^{-2}

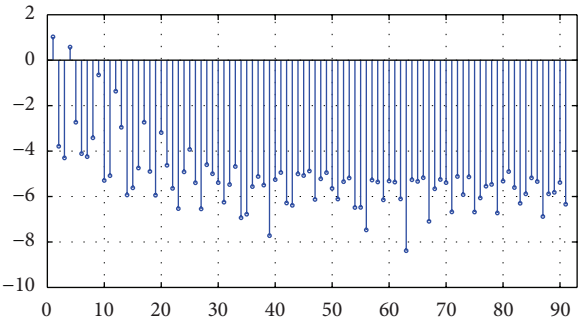

Figure 7: Absolute values of the coefficients α_n employed for approaching the boundary condition $u|_\Gamma = e^{-xy}$, utilizing the base elements $\{u_n\}$ corresponding to the conductivity function $\sigma = e^{xy}$.

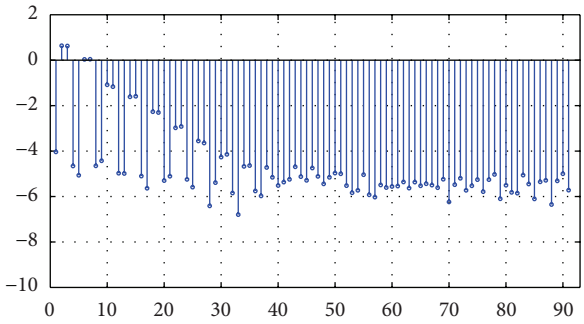

Figure 8: Absolute values of the coefficients α_n employed for approaching the boundary condition $u|_\Gamma = (1/3)(x + y)^3 + 0.1(x + y)$, utilizing the base elements $\{u_n\}$ corresponding to the conductivity function $\sigma = e^{xy}$.

Notice that in Figure 7 the values of the coefficients α_n possess a particular distribution, even we will not point an evident pattern. But since the set $\{u_n\}_{n=0}^{2N+1}$ is an orthonormal base, it can be used to approach any other boundary condition. In particular, if we use this base for approaching the condition

$$u|_\Gamma = \frac{1}{3}(x + y)^3 + 0.1\,(x + y)\,, \tag{59}$$

that indeed corresponds to the conductivity $\sigma = ((x + y)^2 + 0.1)^{-1}$, we will observe that the values of the coefficients α_n, plotted in Figure 8, behave in a very different way.

As a complementary example, let us consider the base functions $\{u_n\}$ corresponding to a Lorentzian conductivity $\sigma = ((x + y)^2 + 0.1)^{-1}$ studied in Section 4.2. Figure 9 displays the absolute values of the coefficients α_n when we impose the boundary condition $u|_\Gamma = (1/3)(x + y)^3 + 0.1(x + y)$, as posed in (53).

But if we impose a boundary condition of the form

$$u|_\Gamma = e^{-xy}, \tag{60}$$

upcoming from (51), we can appreciate, as plotted in Figure 10, that the absolute values of the obtained coefficients α_n are, once more, very different to those of Figure 9.

This implies that the behavior of the values of the coefficients α_n could well serve as a criterion for understanding if some conductivity function σ can effectively provoke a certain electric potential distribution at the boundary Γ of same domain $\Omega(\mathbb{R}^2)$, when physical measurements provide the boundary condition.

Taking into account that most of the algorithms dedicated to approach solutions of the electrical impedance tomography problem recursively solve the forward problem [2], this novel information will be used to introduce changes in σ; thus the boundary condition is fulfilled with a better convergence, and with less computational time.

Table 16: Relation between the error $\mathscr{E}$ and the number of formal powers N, when $\sigma = 2 + \sin 5(x + y)$.

Number of radii R	Points per radius P	Number of formal powers N	Number of sections S	Collected values per section C	$\mathscr{E}$
100	100	45	10001	10001	7.6129×10^{-2}
100	100	35	10001	10001	1.3551×10^{-1}
100	100	25	10001	10001	2.0886×10^{-1}
100	100	15	10001	10001	3.3854×10^{-1}
100	100	5	10001	10001	5.3026×10^{-1}

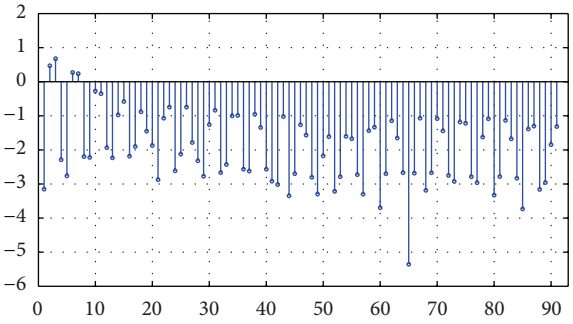

Figure 9: Absolute values of the coefficients α_n employed for approaching the boundary condition $u|_\Gamma = (1/3)(x + y)^3 + 0.1(x + y)$, utilizing the base elements $\{u_n\}$ corresponding to the conductivity function $\sigma = ((x + y)^2 + 0.1)^{-1}$.

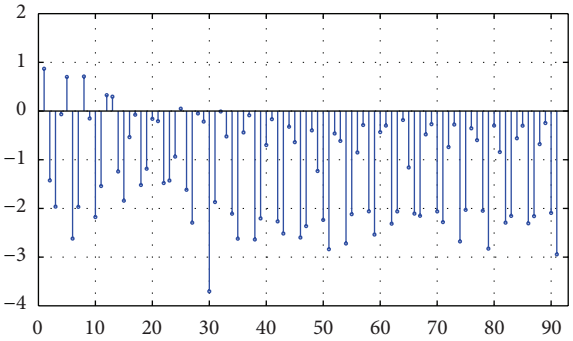

Figure 10: Absolute values of the coefficients α_n employed for approaching the boundary condition $u|_\Gamma = e^{-xy}$, utilizing the base elements $\{u_n\}$ corresponding to the conductivity function $\sigma = ((x + y)^2 + 0.1)^{-1}$.

Even it is not possible yet to estimate when this new method will be employed to approach solutions for the electrical impedance tomography problem, we will remark that the main contribution of this work is to provide a new technique for fully applying the elements of the modern Pseudoanalytic function theory into the analysis of conductivity functions that originated from physical experimental models, which will certainly provide additional information for better understanding the inverse Dirichlet boundary value problem of (1) in the plane.

In other words, before this proposal, the mathematical advances were exclusively improving the study of separable-variables conductivity functions, rarely useful for representing physical cases. These pages have shown that, under certain limits, any conductivity function is susceptible to be analyzed employing pseudoanalytic functions, whether they possess an exact mathematical form or not. As a matter of fact, it is enough that the conductivity values are fully defined over the points within a bounded domain Ω, with a smooth enough boundary Γ. The research will continue to better understand the limiting cases and the certain conditions of smoothness of the boundary; thus the posed ideas can be adequately employed in the applied sciences.

Disclosure

The numerical methods used along this work were fully developed in GNU C/C++ Compiler, employing a CPU64B@ 2.4 GHz, on SLACKWARE 13.37 LINUX operating system. The experimental procedures showed that the numerical results can vary when using different platforms based on 32 B and 64 B processor architecture, or compilers between other operating systems, including different LINUX distributions or Registered Trade Mark operating systems. If the reader wishes to perform his own numerical trials, please contact the authors to obtain the resource codes.

Acknowledgments

The authors would like to acknowledge the support of CONACyT Projects 106722 and 81599, Mexico. Marco Pedro Ramirez-Tachiquin is grateful for the support of HILMA S.A. de C.V., Mexico; Ariana Guadalupe Bucio Ramirez would like to acknowledge the support of CONACyT and UPIITA, IPN; Rogelio Adrian Hernandez-Becerril and Cesar Marco Antonio Robles Gonzalez would like to acknowledge the support of CONACyT and ESIME, IPN.

References

[1] A.-P. Calderon, "On an inverse boundary value problem," in *Seminar on Numerical Analysis and Its Applications to Continuum Physics*, pp. 65–73, Sociedade Brasileira de Matematica, Rio de Janeiro, Brazil, 1980.

[2] J. G. Webster, *Electrical Impedance Tomography*, Adam Hilger Series on Biomedical Engineering, Adam Hilger, Briston, UK, 1990.

[3] V. Kravchenko, "On a relation of pseudoanalytic function theory to the two-dimensional stationary Schrödinger equation and Taylor series in formal powers for its solutions," *Journal of Physics A*, vol. 38, no. 18, pp. 3947–3964, 2005.

[4] K. Astala and L. Päivärinta, "Calderón's inverse conductivity problem in the plane," *Annals of Mathematics*, vol. 163, no. 1, pp. 265–299, 2006.

[5] I. N. Vekua, *Generalized Analytic Functions*, International Series of Monographs on Pure and Applied Mathematics, Pergamon Press, London, UK, 1962.

[6] V. V. Kravchenko and H. Oviedo, "On explicitly solvable Vekua equations and explicit solution of the stationary Schrödinger equation and of the equation $(\sigma \nabla u) = 0$," *Complex Variables and Elliptic Equations*, vol. 52, no. 5, pp. 353–366, 2007.

[7] L. Bers, *Theory of Pseudoanalytic Functions*, IMM, New York University, New York, NY, USA, 1953.

[8] H. M. Campos, R. Castillo-Pérez, and V. V. Kravchenko, "Construction and application of Bergman-type reproducing kernels for boundary and eigenvalue problems in the plane," *Complex Variables and Elliptic Equations*, vol. 57, no. 7-8, pp. 787–824, 2012.

[9] V. V. Kravchenko, *Applied Pseudoanalytic Function Theory*, Frontiers in Mathematics, Birkhäuser, Basel, Switzerland, 2009.

[10] R. Castillo-Pérez, V. V. Kravchenko, and R. Reséndiz-Vázquez, "Solution of boundary and eigenvalue problems for second-order elliptic operators in the plane using pseudoanalytic formal powers," *Mathematical Methods in the Applied Sciences*, vol. 34, no. 4, pp. 455–468, 2011.

[11] A. Bucio R, R. Castillo-Perez, and M. P. Ramirez T., "On the numerical construction of formal powers and their application to the Electrical Impedance Equation," in *Proceedings of the 8th International Conference on Electrical Engineering, Computing Science and Automatic Control (CCE '11)*, IEEE Catalog Number: CFP11827-ART, pp. 769–774, mex, October 2011.

[12] A. Sanjeev and B. Boaz, *Computational Complexity: A Modern Approach*, Cambridge University Press, Cambridge, UK, 2009.

New Characterization of an Improved Numerical Method for Solving the Electrical Impedance Equation in the Plane: An Approach from the Modern Pseudoanalytic Function Theory

C. M. A. Robles G. *IAENG, Member*, A. Bucio R. *IAENG, Member* and M. P. Ramirez T. *IAENG, Member*.

***Abstract*—Employing an improved numerical method, we approach solutions for the Dirichlet boundary value forward problem of the Electrical Impedance Equation in the plane. Some of the considered conductivity functions posses an exact mathematical representation. The rest arise from geometrical figures. Both classes of conductivity functions are analyzed within bounded domains, emphasizing the results corresponding to non-smooth boundaries, for which not any additional regularization method was required.**

***Index Terms*—Bers, Impedance, Non-smooth, Pseudoanalytic, Vekua.**

I. Introduction

THE elements of the modern Pseudoanalytic Function Theory have allowed to establish the relation between the two-dimensional Electrical Impedance Equation (1), and a special class of Vekua equation [12].

More precisely, we are able to write the general solution of the equation:

$$\operatorname{div}(\sigma \operatorname{grad} u) = 0, \tag{1}$$

where σ is the conductivity function, and u denotes the electric potential, in terms of the so-called Taylor series in formal powers [2]. The relation was first noticed in [8] and [1], independently. After that, a variety of works dedicated to the exact and numerical mathematical analysis, appeared in the literature (see e.g. [7], [9] and [10]).

This new approach is very important because solving the forward problem is fundamental if we are to understand the inverse problem, commonly known as Electrical Impedance Tomography [13].

These pages are dedicated to analyze the numerical solutions for the Dirichlet boundary value forward problem of (1) in the plane, employing an improved numerical method presented in [10], and based upon a conjecture proposed in [9].

The work includes a wide variety of examples, both analytic and geometrical, for representing electrical conductivity functions. Indeed, every example is illustrated taking into account a long enough quantity of parameters, thus we can assert that we proposed a more detailed characterization of the improved numerical method, than those published previously in [10] and [11].

The experimental results reported in further pages, can be classified from two different points of view. The first perspective would separate the results in two classes: Those that correspond to exact mathematical representations of conductivity functions, and those whose conductivity functions arise from geometrical distributions. A second point of view is to classify the results according to the domain within their conductivity functions were defined. Hence, we would have those that correspond to smooth-bounded domains, and those upcoming from non-smooth-bounded domains.

The second point of view is the one to be considered, because the last example exposed in these pages, corresponds to one special case of non-smooth-bounded domain for which not any additional regularization is required for approaching the solution of the boundary value problem.

Indeed, this last example is based into a purely geometrical conductivity function, which also includes non-smooth points. Our objective is to show that even for this special class of conductivity functions, and domains, the improved numerical method is useful for approaching solutions of (1).

In this sense, the contribution of the present work is the procedure for emphasizing the property cited in the last paragraph, which was the headmost topic of [11] but where the number of base functions for approaching the boundary condition was limited, due to the technique employed for obtaining the coefficients applied in the approximation. Here we approach the boundary condition taking into account almost twice the quantity of base functions considered in [11]. Hence the current characterization shall be more representative, because the significant increment in the number of base functions enhances in the limiting cases where the method works efficiently.

The conclusions are omitted because of the large quantity of experimental results included in the work. As a matter of fact, a proper description of the behavior of the method along every posed example, is not available yet, and it would be out of the scope of this paper.

II. Preliminaries

In agreement with the Pseudoanalytic Function Theory posed by L. Bers [2], we will consider a pair of complex-valued functions (F, G), that satisfy the following condition:

$$\operatorname{Im}\left(\overline{F}G\right) > 0. \tag{2}$$

C. M. A. Robles G. is with the National Polytechnique Institute, ESIME C. Mexico, cesar.robles@lasallistas.org.mx

A. Bucio R. is with the National Polytechnique Institute, UPIITA, Mexico, ari.bucio@gmail.com

M. P. Ramirez T. is with the Communications and Digital Signal Processing Group, Engineering Faculty of La Salle University, Mexico, marco.ramirez@lasallistas.org.mx.

Each author equally contributed to the research work.

Here $\overline{F} = \mathrm{Re}F - i\mathrm{Im}F$ is the complex conjugation of F, and i is the standard imaginary unit: $i^2 = -1$.

Thus, any complex function W can be expressed by the linear combination of F and G:

$$W = \phi F + \psi G,$$

where ϕ and ψ are real-valued functions. Because of that, the pair (F, G) is called (F, G)-*generating pair*

Professor Bers also introduced the concept of the (F, G)-*derivative* of a complex function W, and the condition for its existence. The derivative is given in conformity with the expression

$$\partial_{(F,G)}W = (\partial_z \phi)\, F + (\partial_z \psi)\, G, \tag{3}$$

and only exist iff

$$(\partial_{\overline{z}} \phi)\, F + (\partial_{\overline{z}} \psi)\, G = 0, \tag{4}$$

where

$$\partial_z = \partial_x - i\partial_y, \;\; \partial_{\overline{z}} = \partial_x + i\partial_y.$$

The operators ∂_z and $\partial_{\overline{z}}$ are classically introduced with the factor $\frac{1}{2}$, but for this work it will be more convenient to work without it.

Set forth the functions

$$\begin{aligned} A_{(F,G)} &= \frac{\overline{F}\partial_z G - \overline{G}\partial_z F}{F\overline{G} - G\overline{F}}, \\ a_{(F,G)} &= -\frac{\overline{F}\partial_{\overline{z}} G - \overline{G}\partial_{\overline{z}} F}{F\overline{G} - G\overline{F}}, \\ B_{(F,G)} &= \frac{F\partial_z G - G\partial_z F}{F\overline{G} - G\overline{F}}, \\ b_{(F,G)} &= -\frac{G\partial_{\overline{z}} F - F\partial_{\overline{z}} G}{F\overline{G} - G\overline{F}}; \end{aligned} \tag{5}$$

the (F, G)-derivative expression in (3) will become

$$\partial_{(F,G)}W = \partial_z W - A_{(F,G)}W - B_{(F,G)}\overline{W}, \tag{6}$$

and the condition (4) will be written as

$$\partial_{\overline{z}} W - a_{(F,G)}W - b_{(F,G)}\overline{W} = 0. \tag{7}$$

The expressions (5) are called *characteristic coefficients* of the generating pair (F, G), whereas (7) is known as the Vekua equation [12]. Indeed, every function W solution of (7) is called an (F, G)-*pseudoanalytic* function.

The following statements were first proposed by [2], and we shall appoint that they have been adapted for the present work.

***Theorem** 1:* Every element of the (F, G)-generating pair is (F, G)-pseudoanalytic. Beside, the (F, G)-derivative of these functions, introduced in (6), vanishes:

$$\partial_{(F,G)}F = \partial_{(F,G)}G = 0.$$

***Remark** 1:* Let us consider a non-vanishing function p within a bounded domain $\Omega(\mathbb{R}^2)$. The functions

$$F_0 = p, \;\; G_0 = \frac{i}{p}, \tag{8}$$

constitute a generating pair, whose characteristic coefficients (5) are

$$\begin{aligned} A_{(F_0,G_0)} &= a_{(F_0,G_0)} = 0, \\ B_{(F_0,G_0)} &= \frac{\partial_z p}{p}, \\ b_{(F_0,G_0)} &= \frac{\partial_{\overline{z}} p}{p}. \end{aligned} \tag{9}$$

***Definition** 1:* Supposed (F_0, G_0) and (F_1, G_1) as two generating pairs in form of (9), their characteristic coefficients fulfil

$$B_{(F_1,G_1)} = -b_{(F_0,G_0)}. \tag{10}$$

Therefore, (F_1, G_1) will be referred as successor pair of (F_0, G_0), since (F_0, G_0) will be called a predecessor of (F_1, G_1).

***Definition** 2:* Considering

$$\{(F_m, G_m)\}, \;\; m = 0, \pm 1, \pm 2, ...$$

as a set of generating pairs, where (F_{m+1}, G_{m+1}) is always a successor of (F_m, G_m). The set $\{(F_m, G_m)\}$ will be known as a generating sequence. In addition, if there exist a number c such that $(F_m, G_m) = (F_{m+c}, G_{m+c})$ the generating sequence posses period c. Furthermore, if $(F, G) = (F_0, G_0)$, we will assert that (F, G) is embedded into $\{(F_m, G_m)\}$.

***Theorem** 2:* Let (F_0, G_0) be a generating pair of the form (8), and let p be a separable-variables function within a bounded domain $\Omega(\mathbb{R}^2)$:

$$p = p_1(x) \cdot p_2(y),$$

where $x, y \in \mathbb{R}$. Thereby, (F_0, G_0) will be embedded into a periodic generating sequence, with period $c = 2$. More precisely, for an even number m the generating pair will posses the form

$$F_m = \frac{p_2(y)}{p_1(x)}, \;\; G_m = i\frac{p_1(x)}{p_2(y)};$$

whereas for an odd m we have

$$F_m = p_1(x) \cdot p_2(y), \;\; G_m = \frac{i}{p_1(x) \cdot p_2(y)};$$

Moreover, if $p_1(x) \equiv 1, \;\; x \in \Omega\left(\mathbb{R}^2\right)$, it is easy to see that the generating sequence in which (F_0, G_0) is embedded, will be periodic with period $c = 1$.

L. Bers first stated the concept of the (F_0, G_0)-*integral* of a complex-valued function W. On behalf of conciseness, we refer the reader to the specialized literature [2] and [7], for a complete and detailed description of the conditions for the existence of such integral. In the following pages, every complex function contained into an (F_m, G_m)-integral will be, by definition, integrable.

***Definition** 3:* Let (F_m, G_m) be a generating pair of the form (8). According to the formulas

$$F_m^* = -iF_m, \;\; G_m^* = -iG_m;$$

are defined the elements of the *adjoin* generating pair (F_0^*, G_0^*).

***Definition** 4:* The (F_m, G_m)-integral of a complex-valued function W (if it exists [2]) is defined as:

$$\int_\tau W d_{(F_m,G_m)}z =$$

$$= F_m \mathrm{Re} \int_\tau G_m^* W dz + G_m \mathrm{Re} \int_\tau F_m^* W dz,$$

where τ is a rectifiable curve, connecting the fixed point z_0 with $z = x + iy$, within a bounded domain Ω, in the complex plane. More precisely, when considering the (F_m, G_m)-integral of the (F_m, G_m)-derivative of W, we will obtain:

$$\int_{z_0}^{z} \partial_{(F_m,G_m)} W(z) d_{(F_m,G_m)} z =$$
$$= -\phi(z_0) F_m(z) - \psi(z_0) G_m(z) + W(z). \quad (11)$$

In agreement with the Theorem 1, the (F_m, G_m)-derivatives of F_m and G_m vanish identically. Hence the expression (11) can be taken into as the (F_m, G_m)-*antiderivative* of $\partial_{(F_m,G_m)} W$.

A. Formal Powers

***Definition** 5:* The formal power $Z_m^{(0)}(a_0, z_0; z)$, associated to the generating pair (F_m, G_m), with formal degree 0, complex constant coefficient a_0, center at z_0, and depending upon $z = x+iy$, is defined in agreement with the expression:

$$Z_m^{(0)}(a_0, z_0; z) = \lambda F_m(z) + \mu G_m(z), \quad (12)$$

where λ and μ are complex constants that fulfill the following condition:

$$\lambda F_m(z_0) + \mu G_m(z_0) = a_0.$$

For approaching the formal powers with higher degrees (n), it is necessary to employ the following recursive formulas:

$$Z_m^{(n)}(a_n, z_0; z) =$$
$$= n \int_{z_0}^{z} Z_{(m-1)}^{(n-1)}(a_n, z_0; z)\, d_{(F_m,G_m)} z,$$

where $n = 1, 2, 3, ...$ Notice that the integral operators in the right-hand side of the last expression are (F_m, G_m)-antiderivatives.

***Theorem** 3:* The formal powers hold on the following properties:

1) Every $Z_m^{(n)}(a_n, z_0; z)$, being $n = 0, 1, 2, 3, ...$ is an (F_m, G_m)-pseudoanalytic function.
2) Let $a_n = a_n' + i a_n''$, where $a_n', a_n'' \in \mathbb{R}$. The following relation holds:

$$Z_m^{(n)}(a_n, z_0; z) =$$
$$= a_n' Z_m^{(n)}(1, z_0; z) + a_n'' Z_m^{(n)}(i, z_0; z). \quad (13)$$

3) For $n = 0, 1, 2, 3, ...$ it holds that

$$\lim_{z \to z_0} Z_m^{(n)}(a_n, z_0; z) = a_n (z - z_0)^n. \quad (14)$$

***Theorem** 4:* Let W be an (F_m, G_m)-pseudoanalytic function. Thus, we can express it in terms of the so-called *Taylor series in formal powers*:

$$W = \sum_{n=0}^{\infty} Z_m^{(n)}(a_n, z_0; z). \quad (15)$$

Since every (F_m, G_m)-pseudoanalytic function W accepts this expansion, (15) is an analytic representation of the general solution for the Vekua equation (9).

B. The two-dimensional Electrical Impedance Equation.

Let us consider the Electrical Impedance Equation (1) in the plane, and let the conductivity σ be a separable-variables function:

$$\sigma(x, y) = \sigma_1(x) \sigma_2(y), \quad (16)$$

As it has been shown in several previous works (e.g. [1], [8] and [9]), introducing the following notations,

$$W = \sqrt{\sigma} \left(\partial_x u - i \partial_y u \right), \quad p = \left(\sigma_1^{-1} \cdot \sigma_2 \right)^{\frac{1}{2}}; \quad (17)$$

the two-dimensional case of the equation (1), can be rewritten into a Vekua equation with form

$$\partial_{\bar{z}} W - \frac{\partial_{\bar{z}} p}{p} \overline{W} = 0. \quad (18)$$

As a matter of fact, a generating pair corresponding to this Vekua equation is

$$F_1 = p,\ G_1 = \frac{i}{p}. \quad (19)$$

Taking into account the theorem 2, the reader can notice that this generating pair is embedded into a periodic generating sequence, with period $c = 2$, for p is separable-variables function.

C. Numerical approach of the formal powers.

In [10], it was studied an improved numerical method for approaching the elements the finite subset of formal powers:

$$\left\{ Z_0^{(n)}(1, 0; z), Z_1^{(n)}(i, 0; z) \right\}_{n=0}^{N}, \quad (20)$$

whose linear combination will allows to approach any pseudoanalytc function W, solution of (18). Furthermore, in [5], it was proven that the real parts of the elements of (20), valued at the boundary Γ of the domain Ω, constitute a complete set to approach solutions for the Dirichlet boundary value forward problem of (1) in the plane.

Since the results of the integral expressions (11) are path-independent [2], the numerical calculations can be performed on a set of radial trajectories, whose origin coincides with the zero of the plane. Thus, the following procedure will be employed in each radius R within the domain Ω, going from the coordinates origin until the boundary Γ.

Let us consider τ as a radius R within, *e.g.*, the unitary circle with center at $z_0 = 0$. For the interpolation process, we will use $P + 1$ points equidistantly distributed on R, being the first $r[0] = 0$ and the last $r[P] = 1$:

$$\left\{ r[p] = \frac{p}{P} \right\}_{p=0}^{P}. \quad (21)$$

We can immediately construct a set of coordinates according to the formulas:

$$x[p] = r[p] \cos\theta_q, \quad y[p] = r[p] \sin\theta_q; \quad (22)$$

where θ_q is the angle that matches to R. In agreement with (8), the coordinates (22) will be employed to obtain the sets of values

$$\{F_0(z[p]), G_0(z[p])\},\ \{F_1(z[p]), G_1(z[p])\}; \quad (23)$$

where the complex numbers $z[p]$ have the form:

$$z[p] = x[p] + iy[p].$$

The set of values of the adjoin pairs

$$\{F_0^*(z[p]), G_0^*(z[p])\},\ \{F_1^*(z[p]), G_1^*(z[p])\} \tag{24}$$

will have the form shown in the Definition 3.

From the expression (5), it follows that

$$\begin{aligned} Z_0^{(0)}(1,0;z[p]) &= F_0(z[p]), \\ Z_1^{(0)}(1,0;z[p]) &= F_1(z[p]); \end{aligned}$$

Hereafter, each formal power with $n > 0$ will be always approached considering $P+1$ equidistant points within the closed interval $[0,1]$. Taking into account that not any methodological difference takes place when approaching the formal power with coefficients $a_n = i$, we will focus our explanation for the cases when $a_n = 1$.

At this point, a numerical property first noticed in [9], for approaching the formal powers, can significantly reduce the computational resources invested in the complete procedure, at the time it allows to employ the posed method for analyzing non-separable variables conductivity functions.

The following statements were presented and proved in [9], together with some representative examples.

Conjecture 1: Let σ be an arbitrary conductivity function defined within a bounded domain $\Omega\left(\mathbb{R}^2\right)$. It can be approached by means of a piece-wise separable-variables function of the form:

$$\sigma_{pw} = \begin{cases} \frac{x+g}{\chi_1-\chi_0+g} \cdot f_1(y) & : \quad x \in [\chi_0, \chi_1)\,; \\ \frac{x+g}{\chi_2-\chi_1+g} \cdot f_2(y) & : \quad x \in [\chi_1, \chi_2)\,; \\ \vdots & \\ \frac{x+g}{\chi_K-\chi_{K-1}+g} \cdot f_K(y) & : \quad x \in [\chi_{K-1}, \chi_K]\,; \end{cases}$$

where g is a real constant such that $x+g \neq 0 : x \in \Omega\left(\mathbb{R}^2\right)$; and $\{f_k\}_{k=1}^K$ are interpolating functions constructed with a finite number of samples $\mathcal{M}$ of the function σ, valued along an y-axis parallel line within the subdomains of Ω, created when tracing the set of y-axis parallel lines $\{\chi_k\}_{k=0}^K$. This piece-wise separable-variables conductivity function can be employed for numerically approaching the set of formal powers (24).

Proposition 1: [9] Let σ be an arbitrary conductivity function defined within a bounded domain $\Omega\left(\mathbb{R}^2\right)$. It can be considered as the limiting case of a piece-wise separable-variables function, with the form presented in the Conjecture 1, when the number of subdomains K and the number of samples $\mathcal{M}$ at every subdomain, tend to infinite:

$$\lim_{K,\mathcal{M}\to\infty} \sigma_{pw} = \sigma.$$

Furthermore, since:

$$\lim_{K,\mathcal{M}\to\infty} \frac{x+g}{\chi_k - \chi_{k-1} + g} = 1,\ k = 0, 1, ..., K;$$

according to the Theorem 2, the corresponding generating sequence will be periodic with period $c = 1$. This immediately implies that

$$F_0(z[p]) = F_1(z[p]) = F(z[p]),$$

that shall simplify the construction of the sets (23) and (24).

Employing this property, the numerical formal powers $Z_0^{(n)}(z[p])$ at the points $z[p] = x[p] + iy[p]$, located along the radius R, can be approached employing a variation of the trapezoidal integration method over the complex plane:

$$\begin{aligned} Z^{(n)}(z[p]) = \delta F(z[p])\cdot \\ \cdot \mathrm{Re} \sum_{s=0}^{p-1} \left(Z^{(n-1)}(z[s+1]) \cdot G^*\left(z[s+1]\right)\right) dz[s] + \\ + \delta F(z[p]) \mathrm{Re} \sum_{s=0}^{p} \left(Z_1^{(n-1)}(z[s]) \cdot G^*\left(z[s]\right)\right) dz[s] + \\ + \delta G(z[p])\cdot \\ \cdot \mathrm{Re} \sum_{s=0}^{p-1} \left(Z_1^{(n-1)}(z[s+1]) \cdot F^*\left(z[s+1]\right)\right) dz[s] + \\ + \delta G(z[p]) \mathrm{Re} \sum_{s=0}^{p} \left(Z_1^{(n-1)}(z[s]) \cdot F^*\left(z[s]\right)\right) dz[s]; \end{aligned} \tag{25}$$

where

$$dz[s] = \left(z[s+1] - z[s]\right),$$

and δ is a real constant factor, empirically selected, that contributes to the numerical stability of the method.

We shall remark that the use of the expression (25), for approaching the formal powers, as it was appointed in [9], implicitly performs a piecewise interpolating polynomial function of degree 1, to relate every value $Z^{(n)}(z[p])$, for $p = 0, 1, ..., P$; and $n = 0, 1, ..., N$; taking into consideration the third property of the Theorem 3, that implies $\forall n > 0$:

$$Z_0^{(n)}(1,0;z[0]) \equiv 0.$$

Performing the full procedure for a wide enough quantity Q of radii R, each one corresponding to some angle θ_q:

$$\left\{\theta_q = q \cdot \frac{2\pi}{Q}\right\}_{q=0}^{Q-1}, \tag{26}$$

we will be able to approach the finite set

$$\left\{\mathrm{Re}Z^{(n)}\left(1,0;z\right),\ \mathrm{Re}Z^{(n)}\left(i,0;z\right)\right\}_{n=0}^{N}, \tag{27}$$

that once is valued at the boundary Γ of the domain $\Omega\left(\mathbb{R}^2\right)$, will provide a set of $2N+1$ base functions for approaching solutions of the Dirichlet boundary value forward problem of (1), when a boundary condition $u_{\mathbf{c}}|_\Gamma$ is imposed.

Indeed, the set (27) can be orthonormalized, conforming a new base

$$\{\upsilon_0^{(n)}(l)\}_{n=0}^{2N},\ l \in \Gamma, \tag{28}$$

that can be interpolated by standard methods in order to obtain continuous functions at Γ.

Summarizing, if the number of radii R, points per radius P, and base functions $2N+1$, are adequate (as it will be explained further), a boundary condition $u_{\mathbf{c}}|_\Gamma$ can be approached by the linear combination:

$$u_{\mathbf{c}}|_\Gamma \sim \sum_{k=0}^{2N+1} \beta_k \upsilon_k,$$

where the real constant coefficients β_k are approached by the standard inner product

$$\beta_k = \langle \upsilon_k, u_{\mathbf{c}}|_\Gamma \rangle = \int_\Gamma \upsilon_k(l) \cdot u_{\mathbf{c}}|_\Gamma(l) dl. \tag{29}$$

III. Experimental Results.

We will perform a characterization of the method, using two classes of domains, and a variety of conductivity functions. This characterization employs the optimized method, first exposed in [10], using the Pseudoanalytic Function Theory, and taking into account that we can analyze any conductivity function, approaching the solution for the Dirichlet boundary value forward problem.

In this work, we will empathize the behavior of the method employing it into non-smooth domains, and comparing its effectiveness with the results obtained when analyzing the unitary disk. For both cases, we will use conductivity functions with exact representation. More precisely, we will examine exponential, Lorentzian, sinusoidal and polynomial functions. But we will also study conductivity functions upcoming from geometrical distributions, such like concentric circles, a circle out of center but within the domain, and a square.

A. The Unit Circle Domain.

The behavior of the method for this case, whenever the conductivity possesses a separable-variables form or not, is particularly stable. We refer the reader to the previous works [3] and [10] for more details.

Here we will propose a methodology that reaches the best approximation of the method, employing the Lebesgue measure for introducing an error parameter $\mathcal{E}$:

$$\mathcal{E} = \left(\int_{\Gamma} \left(u_{\mathbf{c}}|_{\Gamma} - u_{app} \right)^2 dl \right)^{\frac{1}{2}}. \tag{30}$$

where u_{app} represents the approached solution, according to (21).

Employing a variation of the algorithm posed in [10], we will only modify the number of formal powers N, since according to the work cited before, we know that employing a bigger number of formal powers riches, a better convergence. Also, we have detected that the number of radii R, and of points per radius P, do not introduce significant variations of $\mathcal{E}$. That is why we will fix $R = P = 200$.

1) An Exponential Conductivity Case: We will consider a non-separable variables exponential conductivity function with the form

$$\sigma = e^{\alpha xy}, \tag{31}$$

where α represents a coefficient that is used to change the behavior of the function. In this case we impose the boundary condition:

$$u|_{\Gamma} = e^{-\alpha xy}. \tag{32}$$

because it is an exact solution of (1), as appointed in [9]. Hereafter, we will employ the notation

$$M = 2N + 1.$$

We shall remember that Q represents the number of radii.

The Table I shows that when the maximum number of formal powers increases, the convergence improves.

TABLE I
Exponential conductivity function $\sigma = e^{-\alpha xy}$.

M	P	Q	α	$\mathcal{E}$
121	200	200	2	6.8875×10^{-15}
81	200	200	2	7.3145×10^{-15}
41	200	200	2	1.1101×10^{-6}
121	200	200	6	3.4109×10^{-14}
81	200	200	6	3.4243×10^{-14}
41	200	200	6	1.1768×10^{-7}
121	200	200	10	4.2244×10^{-14}
81	200	200	10	4.3088×10^{-14}
41	200	200	10	2.3561×10^{-6}

2) Lorentzian Conductivity Function: For this case we propose a conductivity function with the form:

$$\sigma = \left((x + d_x)^2 + L_c \right)^{-1} \cdot \left((y + d_y)^2 + L_c \right)^{-1}, \tag{33}$$

where d_x and d_y represent displacements over the x-axis and y-axis respectively, and L_c denotes a real constant.

We will imposed the boundary condition [9]:

$$u|_{\Gamma} = \frac{1}{3}(x+d_x)^3 + \frac{1}{3}(y+d_y)^3 + L_c(x+d_x+y+d_y); \tag{34}$$

since it is an exact solution of (1).

TABLE II
Lorentzian conductivity function.

M	P	Q	L_c	$\mathcal{E}$
121	200	200	0.2	2.4113×10^{-13}
81	200	200	0.2	2.1746×10^{-9}
41	200	200	0.2	2.5924×10^{-5}
121	200	200	0.4	1.5266×10^{-15}
81	200	200	0.4	3.8584×10^{-12}
41	200	200	0.4	1.2505×10^{-6}
121	200	200	0.6	2.1483×10^{-15}
81	200	200	0.6	4.3463×10^{-14}
41	200	200	0.6	1.4775×10^{-7}
121	200	200	0.8	2.1948×10^{-15}
81	200	200	0.8	2.5350×10^{-15}
41	200	200	0.8	2.7502×10^{-8}

We propose $L_c = \{0.2, 0.4, 0.6, 0.8\}$, whereas, for this case, $d_x = d_y = 0$. In the Table II the reader can notice that, every time the number of formal powers increases, the error decreases considerably. We also notice that if we use a small value of L_c, the error grows significantly.

3) Polynomial Conductivity Function: In this case, we use a polynomial conductivity function:

$$\sigma = \alpha + Cx + Cy, \tag{35}$$

imposing a boundary condition

$$u|_{\Gamma} = \ln\left(\alpha + Cx + Cy\right), \tag{36}$$

where α and C are constants such that $\alpha + Cx + Cy > 0,\ \forall x, y \in \Omega$ [9].

The Table III, shows that the increment of M provides better convergence.

4) Sinusoidal Conductivity Function: Let us consider a conductivity function with the form

$$\sigma = \left(\alpha + \cos \omega\pi x\right)\left(\alpha + \sin \omega\pi y\right), \tag{37}$$

We selected to impose a boundary condition:

$$u|_{\Gamma} = \left(\frac{\tan xy}{2} + 1 \right)^{-1}. \tag{38}$$

TABLE III
POLYNOMIAL CONDUCTIVITY FUNCTION $\sigma = \alpha + Cx + Cy$.

M	P	Q	α	C	$\mathcal{E}$
121	200	200	10	2	5.4318×10^{-15}
81	200	200	10	2	5.4318×10^{-15}
41	200	200	10	2	5.4398×10^{-15}
121	200	200	10	4	4.2384×10^{-15}
81	200	200	10	4	4.2384×10^{-15}
41	200	200	10	4	5.2431×10^{-12}
121	200	200	10	6	5.5207×10^{-15}
81	200	200	10	6	5.9757×10^{-12}
41	200	200	10	6	1.3718×10^{-6}

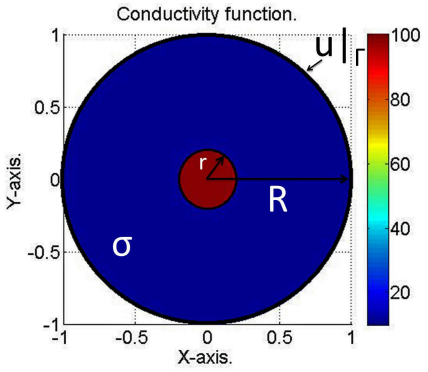

Fig. 1. First Geometrical Case: Two disks within the domain Ω, whose centers coincide.

It is necessary to remark that this function is not an exact solution of (1). Indeed, as posed in [9], it is an exact solution only for the case when $\sigma = 1 + \sin xy$. But the example becomes interesting when pointing out that, in general, the exact solutions of (1) when σ possesses the form (37), are unknown. Thus, this example is included to better illustrate the effectiveness of the method when arbitrary parameters are introduced in the analysis.

TABLE IV
SINUSOIDAL CONDUCTIVITY FUNCTION.

M	P	Q	α	ω	$\mathcal{E}$
121	200	200	5	2	7.8123×10^{-12}
41	200	200	5	2	8.5330×10^{-5}
121	200	200	5	6	4.5940×10^{-5}
41	200	200	5	6	2.7620×10^{-2}
121	200	200	5	10	3.5433×10^{-3}
41	200	200	5	10	1.9455×10^{-1}
121	200	200	10	2	1.2539×10^{-14}
41	200	200	10	2	9.2312×10^{-6}
121	200	200	10	6	4.0830×10^{-6}
41	200	200	10	6	1.1964×10^{-2}
121	200	200	10	10	8.5638×10^{-4}
41	200	200	10	10	9.7005×10^{-2}

The Table IV shows that when we increase M, we obtain a better convergence, but the results are the opposite if α or ω increase. In this sense, the Table IV offers the opportunity for establishing a limiting example for which the method is valid.

5) First Geometrical Case: We propose a geometrical conductivity distribution inside the domain Ω, displayed in the Figure 1. It consists of two disks, whose centers coincide at the origin. The red section represents $\sigma = 100$, whereas the blue section indicates $\sigma = 10$. The radius of the red section is denoted by r.

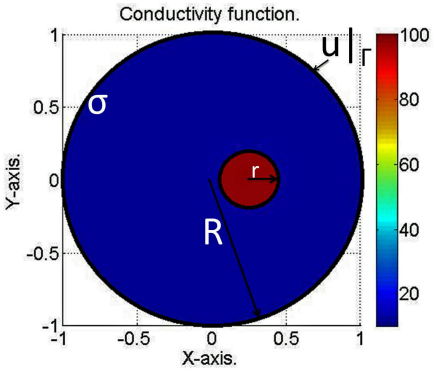

Fig. 2. Disk displaced from the center. Any other displacement can be considered a rotation of this example.

As it was previously indicated in [9], to establish a boundary condition without performing physical measurements, becomes a non-trivial task for conductivity functions arising from geometrical figures. That is why, hereafter, we will employ the boundary condition (34). The selection of this condition was arbitrary, being useful only for appreciating the behavior of the numerical method.

TABLE V
FIRST GEOMETRICAL CASE: RD INDICATES THE VALUE OF THE RED DISK, WHEREAS BD REPRESENTS THE BLUE DISK.

M	P	Q	r	RD	BD	$\mathcal{E}$
121	200	200	0.2	10	100	5.3266×10^{-15}
41	200	200	0.2	10	100	7.1940×10^{-15}
121	200	200	0.4	10	100	6.0657×10^{-15}
41	200	200	0.4	10	100	8.1351×10^{-15}
121	200	200	0.6	10	100	4.3213×10^{-15}
41	200	200	0.6	10	100	5.2102×10^{-15}
121	200	200	0.8	10	100	3.4712×10^{-15}
41	200	200	0.8	10	100	4.4355×10^{-15}

The Table V shows that the convergence increments when the number of formal powers M slightly increase. This behavior is also present when changing the magnitude of the radius r, exception done for the case when $r \sim \mathbf{R}$, the radius of the unit circle.

6) A variation of the First Geometrical Case: The alteration is the displacement of the disk with conductivity $\sigma = 100$, whose center is located at $x = 0.25,\ y = 0$.

Once more, the boundary condition is a variation of (34), noticing that, on behalf of simplicity, we have fixed $L_c = 0.5$, as displayed in Figure 2:

$$u|_\Gamma = \frac{1}{3}(x + 0.25)^3 + \frac{1}{3}y^3 + 0.5(x + 0.25 + y),$$

The table VI illustrates that if we use a bigger number of base functions M, the convergence increases, but what it becomes interesting with this example is the diameter of the red disk, which provokes significant variations in the convergence. Notice any other displacement of the interior disk, can be considered a geometrical rotation to the case we have studied in this section. Thus, the numerical results are fully equivalent to those reported here.

7) Second Geometrical Case: We propose a geometrical conductivity function consisting in one disk and four rings,

TABLE VI
VARIATION OF THE FIRST GEOMETRICAL CASE: RD INDICATES THE VALUE OF THE RED DISK, WHEREAS BD REPRESENTS THE BLUE DISK.

M	P	Q	r	RD	BD	$\mathcal{E}$
121	200	200	0.2	10	100	3.8194×10^{-2}
41	200	200	0.2	10	100	8.4548×10^{-2}
121	200	200	0.4	10	100	4.6197×10^{-3}
41	200	200	0.4	10	100	7.2787×10^{-3}
121	200	200	0.6	10	100	3.2798×10^{-3}
41	200	200	0.6	10	100	4.4617×10^{-3}
121	200	200	0.8	10	100	9.8760×10^{-2}
41	200	200	0.8	10	100	2.0676×10^{-1}

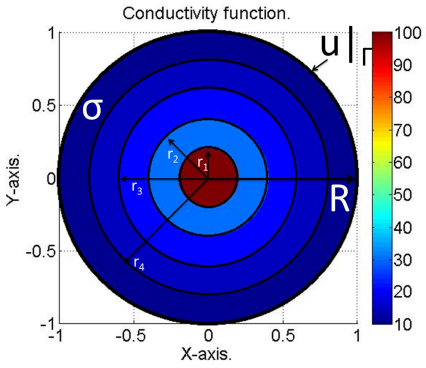

Fig. 3. Concentric disk and rings. The disk $r_1 = 0.2$ represents $\sigma = 100$; the ring delimited by the circles $r_2 = 0.4$ and r_1 represents $\sigma = 30$; for $r_3 = 0.6$ and r_2 we have $\sigma = 20$; for $r_4 = 0.8$ and r_3 it is $\sigma = 15$; finally for $\mathbf{R} = 1$ and r_4 we have $\sigma = 10$.

within the unit circle, whose centers concur, as displayed in Figure 3. The disk with radius $r_1 = 0.2$ represents $\sigma = 100$, the ring delimited by $r_2 = 0.4$ and r_1 possesses a conductivity $\sigma = 30$. For the ring between $r_3 = 0.6$ and r_2 we have $\sigma = 20$, whereas for the one within $r_4 = 0.8$ and r_3 exhibits $\sigma = 15$. Finally, the exterior ring delimited by $\mathbf{R} = 1$ and r_4 the conductivity is $\sigma = 10$.

The imposed boundary condition will be

$$u|_\Gamma = \frac{1}{3}(x^3 + y^3) + 0.5(x + y).$$

The table VII shows that when the number M increases, the convergence improves. It is interesting that the value of the error $\mathcal{E}$ does not increase by the diminution of the base functions M.

TABLE VII
A CONDUCTIVITY FUNCTION COMPOSED BY ONE DISK AND FOUR RINGS. HERE THE NUMBER OF RADII AND THE POINTS PER RADIUS ARE BOTH FIXED AT 200.

M	P	Q	$\mathcal{E}$
121	200	200	3.0440×10^{-15}
101	200	200	3.0216×10^{-15}
61	200	200	2.9303×10^{-15}
21	200	200	2.8133×10^{-15}

The Table VIII illustrates another interesting property of this example, for the error $\mathcal{E}$ does not experience significant changes when increasing the number of radii R and the number of points per radius Q. Nevertheless, the smaller error appears when less base functions are employed. This characteristic shall be studied with more detail in other works.

TABLE VIII
A CONDUCTIVITY FUNCTION COMPOSED BY ONE DISK AND FOUR RINGS. A COMPLEMENTARY EXAMPLE.

M	P	Q	$\mathcal{E}$
61	1000	200	5.0324×10^{-15}
61	600	200	5.4919×10^{-15}
61	200	200	2.9303×10^{-15}
41	1000	200	4.8146×10^{-15}
41	600	200	5.3062×10^{-15}
41	200	200	2.8885×10^{-15}
21	1000	200	4.3974×10^{-15}
21	600	200	4.9358×10^{-15}
21	200	200	2.8133×10^{-15}

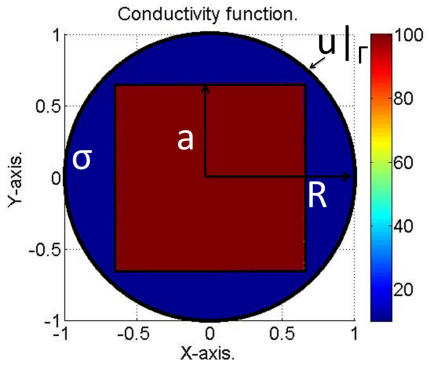

Fig. 4. A non-smooth figure is located within the unitary circle. One radius has been located at every non-smoothness of the square, being $a = 0.65$, so they are necessarily considered in the calculations.

8) Third Geometrical Case. A Non-Smooth Figure Within the Unit Circle: This case is representative because it could require additional regularization techniques, if it was solved with classical methods, as the variations of the Finite Element Method. The figure into the domain is a perfect square, whose apothem is $a = 0.65$. Beside, every corner of the square has the same distance to the center of the unit circle. We forced four radii to cross every corner, thus the non-smoothness of the figure is effectively considered into the calculations. The area of the square will represent $\sigma = 100$, whereas the rest of the domain will possess $\sigma = 10$.

The boundary condition, once more, will be:

$$u|_\Gamma = \frac{1}{3}(x^3 + y^3) + 0.5(x + y).$$

When compared to the other examples, the Table IX illustrates that the error $\mathcal{E}$ is considerably bigger. To explain this, we shall point out that the boundary condition was arbitrarily imposed, thus the error is expected to decrease when a physical measured is performed. Still, we could assert that the convergence of the method is stable from a certain point of view, since $\mathcal{E}$ decreases when the number of base functions M grows.

TABLE IX
A NON-SMOOTH FIGURE LOCATED WITHIN THE UNITARY CIRCLE.

M	P	Q	$\mathcal{E}$
121	200	200	1.3229×10^{-2}
101	200	200	1.6389×10^{-2}
81	200	200	2.2319×10^{-2}
61	200	200	3.0232×10^{-2}
41	200	200	5.4568×10^{-2}
21	200	200	1.1610×10^{-1}

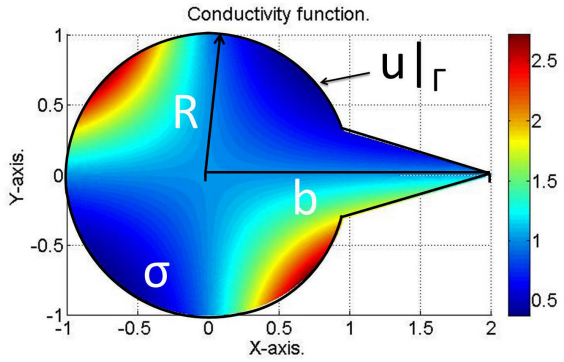

Fig. 5. Non-smooth conductivity exponential case.

We shall also enhance that, according to the information of the Table X, the convergence of the method does not improve when increasing the number of radii R and the number of points per radius Q.

TABLE X
A NON-SMOOTH FIGURE LOCATED WITHIN THE UNITARY CIRCLE: A COMPLEMENTARY EXAMPLE.

M	P	Q	$\mathcal{E}$
121	500	500	2.9031×10^{-2}
101	500	500	3.2493×10^{-2}
81	500	500	3.8417×10^{-2}
61	500	500	4.6756×10^{-2}
41	500	500	6.7906×10^{-2}
21	500	500	1.2200×10^{-1}

B. Brief Study of Conductivity Functions Within a Non-Smooth Domain.

The Figure 5 illustrate a domain Ω conformed by a unit circle with radius $\mathbf{R} = 1$, just as in the examples posed before, but only defined within the interval $x \in \left(-1, \cos\frac{\pi}{10}\right)$; and a triangular area quoted by the line segments $y_0(x) = \cos\frac{\pi}{10}$, $y_1 = \mathbf{k}_1 x + \mathbf{k}_2$ and $y_2 = -\mathbf{k}_1 x + \mathbf{k}_2$. Indeed, we will employ the same parameters posed in [9] and [11]. This is: $\mathbf{k}_1 = 0.5629$ and $\mathbf{k}_2 = 0.8443$. It will be also useful to introduce a parameter b, that will denote the distance between the coordinates origin and the intersection of the lines y_1 and y_2.

We remark that, for all cases shown further, the boundary conditions do not correspond to analytic solutions of (1), but they are all variations of a Lorentzian case. This will allow us to enhance the effectiveness of the method in what it could be considered exalted non-smoothness points at the boundary Γ.

Notice that the reference to the Figure 5 is exclusively for illustrating the shape of the non-smooth domain, since every example will consider a different class of conductivity.

1) An Exponential Conductivity Function: As before, let us suppose a conductivity function with the form

$$\sigma = e^{\alpha xy},$$

We will examine the cases $\alpha = 2, 4, 6, 8, 10$, imposing the boundary condition (34), noticing only that it will be valued, as all cases hereafter, at the boundary Γ of the domain presented in the paragraph above.

TABLE XI
EXPONENTIAL CONDUCTIVITY FUNCTION IN A NON-SMOOTH DOMAIN: $\sigma = e^{\alpha xy}$.

M	P	Q	b	α	$\mathcal{E}$
121	200	200	1.0	2	7.7189×10^{-5}
101	200	200	1.0	2	1.1321×10^{-4}
41	200	200	1.0	2	5.4926×10^{-4}
21	200	200	1.0	2	2.3060×10^{-3}
121	200	200	1.0	4	1.8890×10^{-4}
101	200	200	1.0	4	2.4912×10^{-4}
41	200	200	1.0	4	9.7697×10^{-4}
21	200	200	1.0	4	4.1727×10^{-3}
121	200	200	1.0	6	3.8650×10^{-6}
101	200	200	1.0	6	5.3340×10^{-4}
41	200	200	1.0	6	1.1522×10^{-3}
21	200	200	1.0	6	8.2815×10^{-3}
121	200	200	1.0	8	5.8860×10^{-5}
101	200	200	1.0	8	8.2280×10^{-4}
41	200	200	1.0	8	3.4367×10^{-3}
21	200	200	1.0	8	1.5269×10^{-2}
121	200	200	1.0	10	7.5198×10^{-4}
101	200	200	1.0	10	1.0642×10^{-3}
41	200	200	1.0	10	4.6709×10^{-3}
21	200	200	1.0	10	3.2356×10^{-2}

For the Table XI, we do observe a diminution of the error when increasing the number of base functions M. Notice we have fixed the parameter $b = 1$.

As a complementary experiment, the table XII shows the results of the case when we fix $b = 1.5$.

TABLE XII
EXPONENTIAL CONDUCTIVITY FUNCTION IN NON-SMOOTH DOMAIN: SECOND EXAMPLE.

M	P	Q	b	α	$\mathcal{E}$
121	200	200	1.5	2	1.9190×10^{-3}
101	200	200	1.5	2	1.4889×10^{-3}
41	200	200	1.5	2	3.8482×10^{-4}
21	200	200	1.5	2	6.1853×10^{-4}
121	200	200	1.5	4	7.8734×10^{-3}
101	200	200	1.5	4	4.6606×10^{-3}
41	200	200	1.5	4	1.5679×10^{-3}
21	200	200	1.5	4	5.5688×10^{-3}
121	200	200	1.5	6	5.5224×10^{-3}
101	200	200	1.5	6	5.0001×10^{-3}
41	200	200	1.5	6	3.0569×10^{-3}
21	200	200	1.5	6	1.2475×10^{-2}
121	200	200	1.5	8	1.1044×10^{-2}
101	200	200	1.5	8	8.9217×10^{-3}
41	200	200	1.5	8	4.5972×10^{-3}
21	200	200	1.5	8	2.2350×10^{-2}
121	200	200	1.5	10	2.0529×10^{-2}
101	200	200	1.5	10	1.2371×10^{-2}
41	200	200	1.5	10	6.1075×10^{-3}
21	200	200	1.5	10	4.1741×10^{-2}

The Table XII displays an abnormal behavior, since the error $\mathcal{E}$ does not decrease as the number of base functions M grows. The behavior becomes even more interesting when performing the experiment for $b = 2$. The table XIII shows that, for the cases when α is big enough, the error increases when M does. For this, it is convenient to remark that the non-smoothness is notorious.

We do not show the behavior when a variation is introduced in the number of radii R, since it affects only when a geometrical figure is placed within the domain. This analysis will be exposed in further paragraphs.

2) Lorentzian Conductivity Function: Let us propose σ in the form (33), imposing the condition (34).

TABLE XIII
EXPONENTIAL CONDUCTIVITY FUNCTION IN NON-SMOOTH DOMAIN: A THIRD EXAMPLE.

M	P	Q	b	α	$\mathcal{E}$
121	200	200	2.0	2	2.9221×10^{-2}
101	200	200	2.0	2	2.2211×10^{-2}
41	200	200	2.0	2	4.7667×10^{-3}
21	200	200	2.0	2	1.0047×10^{-2}
121	200	200	2.0	4	2.9221×10^{-2}
101	200	200	2.0	4	2.2211×10^{-2}
41	200	200	2.0	4	4.7667×10^{-3}
21	200	200	2.0	4	1.0047×10^{-2}
121	200	200	2.0	6	2.9221×10^{-2}
101	200	200	2.0	6	2.2211×10^{-2}
41	200	200	2.0	6	4.7607×10^{-3}
21	200	200	2.0	6	1.0047×10^{-2}
121	200	200	2.0	8	2.5025×10^{-1}
101	200	200	2.0	8	1.8884×10^{-1}
41	200	200	2.0	8	1.5368×10^{-2}
21	200	200	2.0	8	3.6063×10^{-2}
121	200	200	2.0	10	6.8271×10^{-1}
101	200	200	2.0	10	4.9283×10^{-1}
41	200	200	2.0	10	2.1281×10^{-2}
21	200	200	2.0	10	6.4350×10^{-2}

Employing the methodology posed above, we begin the experiments fixing $P = Q = 200$, considering $b = 1$. The results are shown in the table XIV. Similarly to the exponential case with $b = 1$ in the non-smooth domain, the increment of the number of base functions M gives to us a better convergence in the numerical method. And once more, this is not valid when $b = 1.5$, as showed in the Table XV. Moreover, the Table XVI indicates that for such non-smoothness, when $b = 2$, the method presents an unexpected behavior, since when M increases, the error $\mathcal{E}$ changes without a clear pattern.

TABLE XIV
LORENTZIAN CONDUCTIVITY FUNCTION IN NON-SMOOTH DOMAIN.

M	P	Q	b	L_c	$\mathcal{E}$
121	200	200	1.0	0.2	3.7046×10^{-4}
101	200	200	1.0	0.2	5.4768×10^{-4}
41	200	200	1.0	0.2	2.5055×10^{-3}
21	200	200	1.0	0.2	7.8163×10^{-3}
121	200	200	1.0	0.4	3.7511×10^{-4}
101	200	200	1.0	0.4	5.5286×10^{-4}
41	200	200	1.0	0.4	2.5378×10^{-3}
21	200	200	1.0	0.4	8.9281×10^{-3}
121	200	200	1.0	0.6	3.8343×10^{-4}
101	200	200	1.0	0.6	5.6391×10^{-4}
41	200	200	1.0	0.6	2.6002×10^{-3}
21	200	200	1.0	0.6	9.3482×10^{-3}
121	200	200	1.0	0.8	3.9114×10^{-4}
101	200	200	1.0	0.8	5.7438×10^{-4}
41	200	200	1.0	0.8	2.6563×10^{-3}
21	200	200	1.0	0.8	9.6121×10^{-3}

3) Polynomial Conductivity Function: Let us propose a conductivity function with the form (35), with a boundary condition (34). The behavior is regular when $b = 1$, as displayed in the values of the Table XVII. But once again, when $b = 1.5$, we can not notice the presence of a pattern, as the reader can verify in the Table XVIII. The method behaves abnormally when $b = 2$, according to the values of the Table XIX.

TABLE XV
LORENTZIAN CONDUCTIVITY FUNCTION IN NON-SMOOTH DOMAIN: A SECOND EXAMPLE.

M	P	Q	b	L_c	$\mathcal{E}$
121	200	200	1.5	0.2	2.1045×10^{-2}
101	200	200	1.5	0.2	1.3569×10^{-2}
41	200	200	1.5	0.2	3.9952×10^{-3}
21	200	200	1.5	0.2	1.5850×10^{-2}
121	200	200	1.5	0.4	1.4743×10^{-2}
101	200	200	1.5	0.4	9.4131×10^{-3}
41	200	200	1.5	0.4	3.6909×10^{-3}
21	200	200	1.5	0.4	1.3262×10^{-2}
121	200	200	1.5	0.6	1.9460×10^{-2}
101	200	200	1.5	0.6	1.2236×10^{-2}
41	200	200	1.5	0.6	3.5889×10^{-3}
21	200	200	1.5	0.6	1.2248×10^{-2}
121	200	200	1.5	0.8	2.5640×10^{-2}
101	200	200	1.5	0.8	1.6610×10^{-2}
41	200	200	1.5	0.8	3.5508×10^{-3}
21	200	200	1.5	0.8	1.1735×10^{-2}

TABLE XVI
LORENTZIAN CONDUCTIVITY FUNCTION IN NON-SMOOTH DOMAIN: A THIRD EXAMPLE.

M	P	Q	b	L_c	$\mathcal{E}$
121	200	200	2.0	0.2	2.7463×10^{-1}
101	200	200	2.0	0.2	2.0323×10^{-1}
41	200	200	2.0	0.2	1.9108×10^{-2}
21	200	200	2.0	0.2	4.3151×10^{-2}
121	200	200	2.0	0.4	1.9367×10^{-2}
101	200	200	2.0	0.4	1.8948×10^{-2}
41	200	200	2.0	0.4	1.5901×10^{-2}
21	200	200	2.0	0.4	3.5373×10^{-2}
121	200	200	2.0	0.6	2.8857×10^{-2}
101	200	200	2.0	0.6	2.4264×10^{-2}
41	200	200	2.0	0.6	1.4621×10^{-2}
21	200	200	2.0	0.6	3.2738×10^{-2}
121	200	200	2.0	0.8	2.1095×10^{-1}
101	200	200	2.0	0.8	1.5468×10^{-1}
41	200	200	2.0	0.8	1.3982×10^{-2}
21	200	200	2.0	0.8	3.1410×10^{-1}

4) Sinusoidal Conductivity Function: Suppose that the conductivity function is expressed as

$$\sigma = (\alpha + \cos \omega\pi x)\,(\alpha + \sin \omega\pi y)\,, \tag{39}$$

where α is a coefficient such that $\sigma > 1$. For this case, the condition to be imposed is

$$u|_\Gamma = \frac{1}{3}(x^3 + y^3) + 0.5(x + y). \tag{40}$$

The Table XX reports that the behavior for $b = 1$ becomes unstable when $\omega > 4$. According to the Table XXI, when $b = 1.5$, the method becomes unstable when $\omega > 6$, which was indeed not expected when analyzing the previous examples of conductivity functions. Already in the Table XXII we observe that the error $\mathcal{E}$ behaves without a pattern for $\omega > 4$.

5) First Example of Geometrical Conductivity: Let us consider a geometrical conductivity function σ, such as the one posed in the Figure 6, a circle whose center coincides with the origin and with radius $r = 0.2$, also possessing a conductivity $\sigma = 100$, whereas the rest of the non-smooth domain has $\sigma = 10$.

For this example, the imposed condition is (40). The table XXIII indicates the existence of a pattern between the number of base functions M and the error $\mathcal{E}$, for the case $b = 1$.

TABLE XVII
POLYNOMIAL CONDUCTIVITY IN A NON-SMOOTH DOMAIN.

M	P	Q	b	α	C	$\mathcal{E}$
121	200	200	1.0	10	2	1.4507×10^{-4}
101	200	200	1.0	10	2	2.0777×10^{-4}
41	200	200	1.0	10	2	9.4643×10^{-4}
21	200	200	1.0	10	2	3.5689×10^{-3}
121	200	200	1.0	10	4	1.2662×10^{-4}
101	200	200	1.0	10	4	1.7973×10^{-4}
41	200	200	1.0	10	4	8.1138×10^{-4}
21	200	200	1.0	10	4	3.1555×10^{-3}
121	200	200	1.0	10	6	1.0788×10^{-4}
101	200	200	1.0	10	6	1.5092×10^{-4}
41	200	200	1.0	10	6	6.6334×10^{-4}
21	200	200	1.0	10	6	2.7058×10^{-3}

TABLE XVIII
POLYNOMIAL CONDUCTIVITY IN NON-SMOOTH DOMAIN: SECOND EXAMPLE.

M	P	Q	b	α	C	$\mathcal{E}$
121	200	200	1.5	10	2	5.1091×10^{-3}
101	200	200	1.5	10	2	3.3772×10^{-3}
41	200	200	1.5	10	2	1.1974×10^{-3}
21	200	200	1.5	10	2	3.2404×10^{-3}
121	200	200	1.5	10	4	3.4689×10^{-3}
101	200	200	1.5	10	4	2.3707×10^{-3}
41	200	200	1.5	10	4	1.0601×10^{-3}
21	200	200	1.5	10	4	2.8097×10^{-3}
121	200	200	1.5	10	6	5.6592×10^{-3}
101	200	200	1.5	10	6	3.5610×10^{-3}
41	200	200	1.5	10	6	9.3362×10^{-4}
21	200	200	1.5	10	6	2.3665×10^{-3}

The pattern is kept for the case when $b = 1.5$, according to the results presented in the Table XXIV. Nevertheless, for $b = 2$ we do not detect the pattern anymore, as shown in the Table XXV.

6) Second Example of Geometrical Conductivity: This example is a variation of the previous one, since the red disk with radius $r = 0.2$ locates its center at $x = 0.25$ and $y = 0$. Once more, the red disk represents $\sigma = 100$, and the rest of the domain possesses $\sigma = 10$. The boundary condition is again the expression (40).

This example is interesting, because it possesses a pattern between the number of base functions M and the values of the errors $\mathcal{E}$ when $b = 1$ and $b = 1.5$, according to the values shown in the Tables XXVI and XXVII. The exception appears when $b = 2$, as reported in the Table XXVIII.

7) Third Example of Geometrical Conductivity: For this case, the conductivity function is composed as follows: one

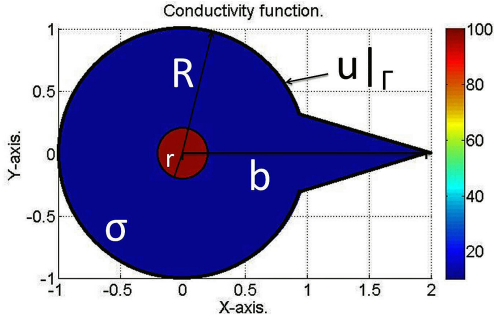

Fig. 6. First example of geometrical conductivity within a non-smooth domain. The red disk represents $\sigma = 100$ and the blue section $\sigma = 10$.

TABLE XIX
POLYNOMIAL CONDUCTIVITY IN NON-SMOOTH DOMAIN: THIRD EXAMPLE.

M	P	Q	b	α	C	$\mathcal{E}$
121	200	200	2.0	10	2	5.9419×10^{-2}
101	200	200	2.0	10	2	4.4223×10^{-2}
41	200	200	2.0	10	2	3.9702×10^{-3}
21	200	200	2.0	10	2	9.2331×10^{-3}
121	200	200	2.0	10	4	7.5193×10^{-2}
101	200	200	2.0	10	4	5.5540×10^{-2}
41	200	200	2.0	10	4	3.4802×10^{-3}
21	200	200	2.0	10	4	8.2482×10^{-3}
121	200	200	2.0	10	6	1.2689×10^{-2}
101	200	200	2.0	10	6	1.2223×10^{-2}
41	200	200	2.0	10	6	3.0911×10^{-3}
21	200	200	2.0	10	6	7.5234×10^{-3}

TABLE XX
SINUSOIDAL CONDUCTIVITY FUNCTION.

M	P	Q	b	α	ω	$\mathcal{E}$
121	200	200	1.0	10	2	1.5628×10^{-4}
101	200	200	1.0	10	2	2.2878×10^{-4}
41	200	200	1.0	10	2	1.1579×10^{-3}
21	200	200	1.0	10	2	4.9768×10^{-3}
121	200	200	1.0	10	4	1.5644×10^{-4}
101	200	200	1.0	10	4	2.3374×10^{-4}
41	200	200	1.0	10	4	2.6001×10^{-3}
21	200	200	1.0	10	4	4.3351×10^{-3}
121	200	200	1.0	10	6	1.7351×10^{-4}
101	200	200	1.0	10	6	2.6993×10^{-4}
41	200	200	1.0	10	6	1.2813×10^{-2}
21	200	200	1.0	10	6	7.1034×10^{-2}
121	200	200	1.0	10	8	7.1695×10^{-4}
101	200	200	1.0	10	8	1.0520×10^{-3}
41	200	200	1.0	10	8	5.2719×10^{-2}
21	200	200	1.0	10	8	7.7114×10^{-2}
121	200	200	1.0	10	10	7.9694×10^{-4}
101	200	200	1.0	10	10	1.1403×10^{-3}
41	200	200	1.0	10	10	6.7853×10^{-2}
21	200	200	1.0	10	10	8.2767×10^{-2}

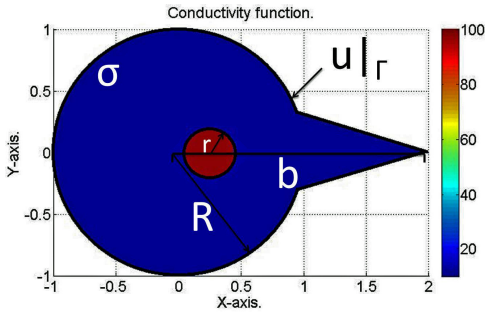

Fig. 7. Second example of geometrical conductivity within a non-smooth domain. The red disk represents $\sigma = 100$ and the blue section $\sigma = 10$.

disk with radius $r_1 = 0.2$ representing $\sigma = 100$, the ring delimited by $r_2 = 0.4$ and r_1 possessing a conductivity $\sigma = 30$, another ring between $r_3 = 0.6$ and r_2 having $\sigma = 20$, whereas the one within $r_4 = 0.8$ and r_3 exhibits $\sigma = 15$. Finally, the remaining value within the boundary is $\sigma = 10$. One more time, the boundary condition is the expression (40). The behavior of the method is only stable for the case when $b = 1$. The cases $b = 1.5$ and $b = 2$ do not show any patterns to be discussed. The results are summarized in the Table XXIX.

TABLE XXI
SINUSOIDAL CONDUCTIVITY FUNCTION: A SECOND EXAMPLE.

M	P	Q	b	α	ω	$\mathcal{E}$
121	200	200	1.5	10	2	2.3734×10^{-3}
101	200	200	1.5	10	2	1.7035×10^{-3}
41	200	200	1.5	10	2	1.2907×10^{-3}
21	200	200	1.5	10	2	5.3456×10^{-3}
121	200	200	1.5	10	4	3.5305×10^{-3}
101	200	200	1.5	10	4	2.2305×10^{-3}
41	200	200	1.5	10	4	1.4848×10^{-3}
21	200	200	1.5	10	4	4.6142×10^{-2}
121	200	200	1.5	10	6	1.9220×10^{-2}
101	200	200	1.5	10	6	1.1637×10^{-2}
41	200	200	1.5	10	6	1.8806×10^{-2}
21	200	200	1.5	10	6	9.3615×10^{-2}
121	200	200	1.5	10	8	1.2419×10^{-1}
101	200	200	1.5	10	8	8.3360×10^{-2}
41	200	200	1.5	10	8	6.3304×10^{-2}
21	200	200	1.5	10	8	9.2504×10^{-2}
121	200	200	1.5	10	10	1.0707×10^{-1}
101	200	200	1.5	10	10	6.8588×10^{-1}
41	200	200	1.5	10	10	8.5009×10^{-2}
21	200	200	1.5	10	10	1.0212×10^{-1}

TABLE XXII
SINUSOIDAL CONDUCTIVITY FUNCTION: A THIRD EXAMPLE.

M	P	Q	b	α	ω	$\mathcal{E}$
121	200	200	2.0	10	2	7.8761×10^{-2}
101	200	200	2.0	10	2	5.9083×10^{-2}
41	200	200	2.0	10	2	4.7198×10^{-3}
21	200	200	2.0	10	2	3.4681×10^{-2}
121	200	200	2.0	10	4	3.3441×10^{-1}
101	200	200	2.0	10	4	2.4975×10^{-1}
41	200	200	2.0	10	4	1.4579×10^{-2}
21	200	200	2.0	10	4	8.3672×10^{-2}
121	200	200	2.0	10	6	5.7939×10^{-1}
101	200	200	2.0	10	6	4.1222×10^{-1}
41	200	200	2.0	10	6	6.3855×10^{-2}
21	200	200	2.0	10	6	1.0279×10^{-1}
121	200	200	2.0	10	8	5.7939×10^{-1}
101	200	200	2.0	10	8	4.1222×10^{-1}
41	200	200	2.0	10	8	6.3835×10^{-2}
21	200	200	2.0	10	8	1.0279×10^{-1}
121	200	200	2.0	10	10	6.5661×10^{-1}
101	200	200	2.0	10	10	4.9436×10^{-1}
41	200	200	2.0	10	10	9.5676×10^{-2}
21	200	200	2.0	10	10	1.1995×10^{-1}

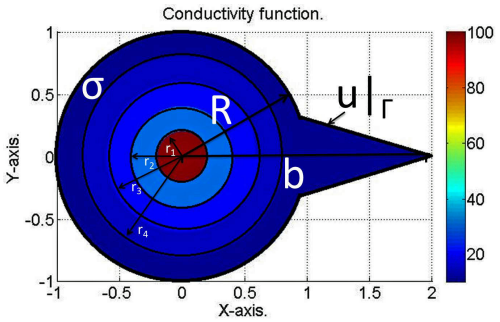

Fig. 8. Third example of geometrical conductivity within a non-smooth domain. Combination of a disk and concentric rings, within a non-smooth domain.

8) Fourth Example of Geometrical Conductivity: To describe the conductivity posed in Figure 9 is better to resemble the square within the unit circle posed before. For this case, the unit circle shall be substituted for the non-smooth domain described at the beginning of the Section. We shall only

TABLE XXIII
FIRST CASE OF GEOMETRICAL CONDUCTIVITY: $b = 1$.

M	P	Q	b	r	$\mathcal{E}$
121	200	200	1.0	0.2	5.2372×10^{-4}
101	200	200	1.0	0.2	6.6056×10^{-4}
41	200	200	1.0	0.2	1.2839×10^{-3}
21	200	200	1.0	0.2	4.5100×10^{-3}
121	200	200	1.0	0.4	5.0633×10^{-4}
101	200	200	1.0	0.4	5.9736×10^{-4}
41	200	200	1.0	0.4	1.1950×10^{-3}
21	200	200	1.0	0.4	4.5522×10^{-3}
121	200	200	1.0	0.6	2.7401×10^{-4}
101	200	200	1.0	0.6	3.2291×10^{-4}
41	200	200	1.0	0.6	1.1389×10^{-3}
21	200	200	1.0	0.6	4.8769×10^{-3}
121	200	200	1.0	0.8	4.3356×10^{-4}
101	200	200	1.0	0.8	4.6767×10^{-4}
41	200	200	1.0	0.8	1.4232×10^{-3}
21	200	200	1.0	0.8	5.3167×10^{-3}

TABLE XXIV
FIRST CASE OF GEOMETRICAL CONDUCTIVITY: $b = 1.5$.

M	P	Q	b	r	$\mathcal{E}$
121	200	200	1.5	0.2	9.5416×10^{-3}
101	200	200	1.5	0.2	6.2105×10^{-3}
41	200	200	1.5	0.2	1.9162×10^{-3}
21	200	200	1.5	0.2	4.4915×10^{-3}
121	200	200	1.5	0.4	1.0555×10^{-2}
101	200	200	1.5	0.4	6.5522×10^{-3}
41	200	200	1.5	0.4	1.7201×10^{-3}
21	200	200	1.5	0.4	4.3942×10^{-3}
121	200	200	1.5	0.6	1.0426×10^{-2}
101	200	200	1.5	0.6	6.5709×10^{-3}
41	200	200	1.5	0.6	1.7658×10^{-3}
21	200	200	1.5	0.6	4.2230×10^{-3}
121	200	200	1.5	0.8	5.8011×10^{-3}
101	200	200	1.5	0.8	3.8069×10^{-3}
41	200	200	1.5	0.8	1.7020×10^{-3}
21	200	200	1.5	0.8	3.9797×10^{-3}

remembered that the apothem $a = 0.65$, and all corners of the square are equidistant to the center of the semicircle section. The square possesses a conductivity $\sigma = 100$, whereas the remaining domain possesses $\sigma = 10$. The boundary condition is again the expression (40).

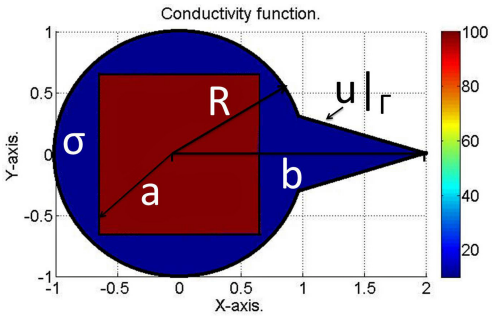

Fig. 9. Fourth example of geometrical conductivity within a non-smooth domain.

The relevance of this case is given by the multiple non-smoothness included in the geometrical conductivity. This is three non-smooth points are located at the boundary Γ, and four non-smooth points are presented in the figure within the domain Ω. For every point of non-smoothness, one radius was forced to pass on, hence all points were taken into consideration. We shall remark, as it was done in [11], that

TABLE XXV
FIRST CASE OF GEOMETRICAL CONDUCTIVITY: $b = 2$.

M	P	Q	b	r	$\mathcal{E}$
121	200	200	2.0	0.2	1.1542×10^{-1}
101	200	200	2.0	0.2	8.6105×10^{-2}
41	200	200	2.0	0.2	5.5541×10^{-3}
21	200	200	2.0	0.2	1.2137×10^{-2}
121	200	200	2.0	0.4	8.8265×10^{-2}
101	200	200	2.0	0.4	6.6393×10^{-2}
41	200	200	2.0	0.4	5.5459×10^{-3}
21	200	200	2.0	0.4	1.2121×10^{-2}
121	200	200	2.0	0.6	6.6141×10^{-2}
101	200	200	2.0	0.6	4.8414×10^{-2}
41	200	200	2.0	0.6	5.0902×10^{-3}
21	200	200	2.0	0.6	1.1946×10^{-2}
121	200	200	2.0	0.8	7.9164×10^{-2}
101	200	200	2.0	0.8	5.8350×10^{-2}
41	200	200	2.0	0.8	4.8985×10^{-3}
21	200	200	2.0	0.8	1.1917×10^{-2}

TABLE XXVI
FIRST CASE OF GEOMETRICAL CONDUCTIVITY: $b = 1$.

M	P	Q	b	r	$\mathcal{E}$
121	200	200	1.0	0.2	2.4385×10^{-2}
101	200	200	1.0	0.2	2.8740×10^{-2}
41	200	200	1.0	0.2	5.4220×10^{-2}
21	200	200	1.0	0.2	9.2323×10^{-2}
121	200	200	1.0	0.4	2.8627×10^{-3}
101	200	200	1.0	0.4	3.2700×10^{-3}
41	200	200	1.0	0.4	4.7071×10^{-3}
21	200	200	1.0	0.4	5.9983×10^{-3}
121	200	200	1.0	0.6	1.9667×10^{-3}
101	200	200	1.0	0.6	2.1911×10^{-3}
41	200	200	1.0	0.6	2.8597×10^{-3}
21	200	200	1.0	0.6	5.0975×10^{-3}

TABLE XXVII
FIRST CASE OF GEOMETRICAL CONDUCTIVITY: $b = 1.5$.

M	P	Q	b	r	$\mathcal{E}$
121	200	200	1.5	0.2	8.2351×10^{-2}
101	200	200	1.5	0.2	5.4311×10^{-2}
41	200	200	1.5	0.2	5.4607×10^{-2}
21	200	200	1.5	0.2	9.2429×10^{-2}
121	200	200	1.5	0.4	1.4896×10^{-3}
101	200	200	1.5	0.4	9.5441×10^{-3}
41	200	200	1.5	0.4	4.9048×10^{-3}
21	200	200	1.5	0.4	6.1276×10^{-3}
121	200	200	1.5	0.6	1.0957×10^{-2}
101	200	200	1.5	0.6	1.0532×10^{-2}
41	200	200	1.5	0.6	3.3790×10^{-3}
21	200	200	1.5	0.6	4.7420×10^{-3}

TABLE XXVIII
FIRST CASE OF GEOMETRICAL CONDUCTIVITY: $b = 2$.

M	P	Q	b	r	$\mathcal{E}$
121	200	200	2.0	0.2	1.9481×10^{-1}
101	200	200	2.0	0.2	1.4364×10^{-1}
41	200	200	2.0	0.2	5.7088×10^{-2}
21	200	200	2.0	0.2	9.3510×10^{-2}
121	200	200	2.0	0.4	9.5951×10^{-2}
101	200	200	2.0	0.4	7.2123×10^{-2}
41	200	200	2.0	0.4	6.6501×10^{-3}
21	200	200	2.0	0.4	1.1058×10^{-2}
121	200	200	2.0	0.6	9.0504×10^{-3}
101	200	200	2.0	0.6	7.6307×10^{-3}
41	200	200	2.0	0.6	5.5504×10^{-3}
21	200	200	2.0	0.6	1.0790×10^{-2}

not any additional regularization method was employed to warrant the convergence at the non-smooth points. This is a particular characteristic of the method, first noticed in [9], and shall be studied with more detail in further works.

TABLE XXIX
THIRD EXAMPLE OF GEOMETRICAL CONDUCTIVITY WITHIN A NON-SMOOTH DOMAIN: $b = 1,\ 1.5,\ 2$.

M	P	Q	b	$\mathcal{E}$
121	200	200	1.0	2.3863×10^{-4}
101	200	200	1.0	3.4388×10^{-4}
41	200	200	1.0	1.4742×10^{-3}
21	200	200	1.0	5.0487×10^{-3}
121	200	200	1.5	5.7241×10^{-3}
101	200	200	1.5	3.2691×10^{-3}
41	200	200	1.5	2.2058×10^{-3}
21	200	200	1.5	7.8255×10^{-3}
121	200	200	2.0	1.1136×10^{-1}
101	200	200	2.0	8.2529×10^{-2}
41	200	200	2.0	8.4147×10^{-3}
21	200	200	2.0	1.4548×10^{-2}

The Table XXX presents a summary of the calculations performed for this last example. Only for the case when $b = 1$ a pattern between the number of base elements M and the error $\mathcal{E}$ is observed. The other two cases do not report any visible pattern.

TABLE XXX
FOURTH EXAMPLE OF GEOMETRICAL CONDUCTIVITY IN NON-SMOOTH DOMAIN.

M	P	Q	b	$\mathcal{E}$
121	200	200	1.0	8.1631×10^{-3}
101	200	200	1.0	1.0347×10^{-2}
41	200	200	1.0	3.3239×10^{-2}
21	200	200	1.0	7.3480×10^{-2}
121	200	200	1.5	1.1063×10^{-1}
101	200	200	1.5	7.5019×10^{-2}
41	200	200	1.5	4.3609×10^{-2}
21	200	200	1.5	9.1848×10^{-2}
121	200	200	2.0	4.3692×10^{-1}
101	200	200	2.0	3.2518×10^{-1}
41	200	200	2.0	6.1231×10^{-2}
21	200	200	2.0	1.2170×10^{-1}

ACKNOWLEDGEMENT

The authors would like to acknowledge the support of CONACyT projects 106722 and 81599; A. G. Bucio R. thanks to UPIITA-IPN and CONACyT; M.P. Ramirez T. acknowledges the support of HILMA S.A. de C.V.; C. M. A. Robles G. would like to thank La Salle University for the research stay and to CONACyT.

REFERENCES

[1] K. Astala, L. Päivärinta (2006), *Calderon's inverse conductivity problem in the plane*, Annals of Mathematics, Vol. 163, pp. 265-299.
[2] L. Bers (1953), *Theory of Pseudoanalytic Functions*, IMM, New York University.
[3] A. Bucio R., R. Castillo-Perez, M.P. Ramirez T.,C.M.A. Robles G. (2012), *A Simplified Method for Numerically Solving the Impedance Equation in the Plane*, 9th International Conference on Electrical Engineering, Computing Science and Automatic Control 2012, IEEE Catalog Number: CFP12827-CDR, ISBN: 978-1-4673-2168-6.
[4] A. P. Calderon (1980), *On an inverse boundary value problem*, Seminar on Numerical Analysis and its application to Continuum Physics.
[5] H. M. Campos, R. Castillo-Perez, V. V. Kravchenko (2011), *Construction and application of Bergman-type reproducing kernels for boundary and eigenvalue problems in the plane*, Complex Variables and Elliptic Equations, 1-38.

[6] R. Castillo-Perez., V. Kravchenko, R. Resendiz V. (2011), *Solution of boundary value and eigenvalue problems for second order elliptic operators in the plane using pseudoanalytic formal powers*, Mathematical Methods in the Applied Sciences, Vol. 34, Issue 4.

[7] V. V. Kravchenko (2009), *Applied Pseudoanalytic Function Theory*, Series: Frontiers in Mathematics, ISBN: 978-3-0346-0003-3.

[8] V. V. Kravchenko (2005), *On the relation of pseudoanalytic function theory to the two-dimensional stationary Schrödinger equation and Taylor series in formal powers for its solutions*, Journal of Physics A: Mathematical and General, Vol. 38, No. 18, pp. 3947-3964.

[9] M. P. Ramirez T., R. A. Hernandez-Becerril, M. C. Robles G. (2012), *Study of the Numerical Solutions for the Electrical Impedance Equation in the Plane: A Pseudoanalytic approach of the Forward Dirichlet Boundary Value Problem*, Mathematical Methods in the Applied Sciences (submited for publication). Available in electronic format at http://ArXiv.com

[10] C. M. A. Robles G., A. Bucio R., M. P. Ramirez T. (2012), *An Optimized Numerical Method for Solving the Two-Dimensional Impedance Equation*, Lecture Notes in Engineering and Computer Science: Proceedings of The World Congress on Engineering and Computer Science 2012, WCECS 2012, 24-26 October, 2012, San Francisco, USA, pp. 116-121.

[11] C. M. A. Robles G., A. Bucio R., M. P. Ramirez T., V. D. Sanchez N. (to be published), *On the Numerical Solutions of Boundary Value Problems in the plane for the Electrical Impedance Equation: A Pseudoanalytic Approach for Non-Smooth Domains*, Lecture Notes in Electrical Engineering, IAENG Transactions on Engineering Technologies-Special Issue of the World Congress On Engineering and Computer Science 2012, Springer.

[12] I. N. Vekua (1962), *Generalized Analytic Functions,* International Series of Monographs on Pure and Applied Mathematics, Pergamon Press.

[13] J. G. Webster (1990), *Electrical Impedance Tomography*, Adam Hilger Series on Biomedical Engineering.

Book chapters

On the Numerical Solutions of Boundary Value Problems in the plane for the Electrical Impedance Equation: A Pseudoanalytic Approach for Non-Smooth Domains

Ariana Guadalupe Bucio Ramirez, Marco Pedro Ramirez Tachiquin, Cesar Marco Antonio Robles Gonzalez and Victor Daniel Sanchez Nava.*

Abstract We study the Electrical Impedance Equation within a special class of domains, whose boundaries posses non-smooth points. The forward Dirichlet boundary value problem is solved bias a novel numerical method, based upon the Pseudoanalytic Function Theory, that does not require additional regularization techniques to fulfill the boundary condition at the non-smooth points.

Key words: Electrical Impedance Equation, Non-smooth boundary, Pseudoanalytic Functions.

1 Introduction

The study of the solutions of the forward Dirichlet boundary value problem in the plane, corresponding to the Electrical Impedance equation

$$\operatorname{div}(\sigma \operatorname{grad} u) = 0, \tag{1}$$

where $\sigma = \sigma_1(x)\sigma_2(y)$ is the conductivity function, and u is the electric potential, constitutes the base for analyzing the inverse problem, commonly known as Electrical Impedance Tomography.

The discovery of the relation between (1) in the plane, and the Vekua equation [9], by V. Kravchenko [6], and shortly after by K. Astala and L. Päivärinta [1], opened a complete new path for constructing numerical solutions of the forward problem corresponding to (1), based upon the modern Pseudoanalytic Function The-

*The authors appear in alphabetical order. A. G. Bucio R. is with UPIITA-IPN, Mexico, e-mail: ari.bucio@gmail.com; C. M. A. Robles G. is with ESIME-IPN, Mexico, e-mail: cesar.robles@lasallistas.org.mx; M. P. Ramirez T. e-mail: marco.ramirez@lasallistas.org.mx and V. D. Sanchez N. e-mail: ddansanchez@gmail.com, are with The Communications and Digital Signal Processing Group, Engineering Faculty of La Salle University, Mexico.

Conference proceedings

On the Artificial Neural Networks used for the Forward Problem for the Electrical Impedance Equation

C. M. A. Robles G.,*Member,IAENG,*, V. Ponomaryov and M. P. Ramirez T.,*Member, IAENG,*

***Abstract*—To achieve a recognition of a solution for the forward value problem of the electrical impedance equation, two different artificial neural networks are used and compared: the multilayer perceptron and the backpropagation neural networks.**

***Index Terms*—Artificial Neural Network, Backpropagation, Electrical Impedance Equation, Multilayer Perceptron.**

I. Introduction

THE artificial neural networks (ANN) [14] are commonly used to recognise or classify the information contained in a data base. The information depends upon the problem that is trying to be solved, but in general, to obtain an approximation is very difficult or the computational resources that needs is very high. For this reason ANNs help to obtain a faster recognition or classification for this complicated problem.

In this case, the main problem is the forward problem for the electrical impedance equation posed by A. P. Calderon in 1980 [4], that is an easy task in comparison with the inverse problem for the same equation. The equation that is trying to be solved is the follows:

$$\text{div}\left(\sigma \text{grad} u\right) = 0, \tag{1}$$

where the σ is the conductivity and the u denotes the electric potential for a domain Ω with boundary Γ. This equation is also known as the electrical impedance equation and it can be solved through the Pseudoanalytic function theory [1] and [6], using the Taylor series in formal powers method, exposed in [8] and [9].

Several works utilize ANNs to recognize or classify the data they possess [2], [14] and [7]. In [10], the usage of the ANNs, in combination of genetic algorithms and multilayer perceptron [5] is employ to recognise an earthquake by its wave. Acoording to [12], in which a Bayesian multilayer perception neural network (BMLP-ANN)[11] is used to analyse the information, in order to relate it with the boundary measurements, and employed before with the finite-element method (FEM). In [13] and [3], a radial basis function that is a variation of ANN employed together with the FFM, this method works with the information of the forward problem of electrical impedance equation for training and testing. Its information successfully recognise the solution related with resistivity in the electrodes and inside the domain.

In current pages, ANNs intend to recognize the information contained in a data set, which is obtained by the Taylor series in formal powers. This information represents the forward problem solution of the electrical impedance equation. The analysis is performed to prove that ANN could be used to find a faster solution, once the ANNs are correctly trained.

This work is distributed as follows: section II is dedicated to study the multilayer perceptron and backpropagation. In section III we presented the procedure to use both ANNs for recognizing the solution. The section IV performs the analysis of the information constructed for the forward problem. Finally, section V closed this work.

II. Preliminaries

An artificial neural network (ANN) is a computational model inspired in biological neural networks (BNN). It consists of an interconnection group of pseudo neurons [2]. Akin to the BNN, ANN has the same structure where the axon is represented by the weights; dendrite is expressed by input of the system; the body that is defined by the activation function and the synapses that is described by the connection between neurons.

The ANN simulates the functionality and structure of BNN, such as the human brain does. Then, ANN can have multiple inputs and outputs, and it can have several amounts of neurons per hidden layer that exist in the system, and its purpose is to interconnect the inputs with the outputs.

The ANN mathematically represents the dynamics of the information flow; this function is called network function.

$$f\left(x\right) = K\left(\sum_{i} w_i \cdot g_i(x)\right), \tag{2}$$

where w_1 denotes the weights, K refers to an activation function and $g_i(x)$ is the collection of functions $g_i(x) = (g_1, g_2, ..., g_3)$ that represents the function of neurons in ANN. The activation function is represented by any desire function, the most commonly used is the step function represented by:

$$g(x) = \begin{cases} 1 & \text{if } x \geq 0; \\ 0 & \text{if } x < 0. \end{cases} \tag{3}$$

In the figure 1, a simple neuron is shown.

It is important to study the ANN learning paradigms, such as the supervised learning in which the solution is looked after by an expert. Another learning paradigm is the

Manuscript received July 10, 2015; revised July 10, 2015. This work was supported by Escuela Superior de Ingeniería Mecánica y Eléctrica campus Culhuacan (ESIME-Cu) at Instituto Politécnico Nacional (IPN).

C. M. A. Robles G.[1] **and V. Ponomaryov**[2] are with Postgraduate Section of Mechanical Engineering School at Instituto Politécnico Nacional, Mexico City, Mexico. [1]croblesg1101@alumno.ipn.mx and [2]vponomar@ipn.mx.

M. P. Ramirez T. is with Asaji Audio International S.A. de C.V., Guadalupe I.R. 687, C.P. 16030, Mexico. marco.ramirez@asajiaudio.com

ISBN: 978-988-19253-6-7
ISSN: 2078-0958 (Print); ISSN: 2078-0966 (Online)

Parallel Hybrid Algorithm for Solution in Electrical Impedance Equation

Volodymyr Ponomaryov*[a], Marco Robles-Gonzalez[a], Ariana Bucio-Ramirez[b], Marco Ramirez-Tachiquin[a], Eduardo Ramos-Diaz[c]

[a] Instituto Politecnico Nacional ESIMECu, Mexico City, Mexico;
[b] Instituto Politecnico Nacional UPIITA, Mexico City, Mexico;
[c] Universidad Autonoma de la Ciudad de Mexico (UACM), Mexico City, Mexico;

ABSTRACT

This work is dedicated to the analysis of the forward and the inverse problem to obtain a better approximation to the Electrical Impedance Tomography equation. In this case, we employ for the forward problem the numerical method based on the Taylor series in formal power and for the inverse problem the Finite Element Method.

For the analysis of the forward problem, we proposed a novel algorithm, which employs a regularization technique for the stability, additionally the parallel computing is used to obtain the solution faster; this modification permits to obtain an efficient solution of the forward problem. Then, the found solution is used in the inverse problem for the approximation employing the Finite Element Method.

The algorithms employed in this work are developed in structural programming paradigm in C++, including parallel processing; the time run analysis is performed only in the forward problem because the Finite Element Method due to their high recursive does not accept parallelism.

Some examples are performed for this analysis, in which several conductivity functions are employed for two different cases: for the analytical cases: the exponential and sinusoidal functions are used, and for the geometrical cases the circle at center and five disk structure are revised as conductivity functions. The Lebesgue measure is used as metric for error estimation in the forward problem, meanwhile, in the inverse problem PSNR, SSIM, MSE criteria are applied, to determine the convergence of both methods.

Keywords: Electrical Impedance Equation, Forward Problem, Finite Element Method, Inverse Problem, Parallel Computing.

1. INTRODUCTION

The Electrical Impedance Tomography is a medical imaging procedure, which investigates the conductivity inside a body to reconstruct it.[1] This problem posses a high complex equation also known as electrical impedance equation, that is represented as follows:

$$\operatorname{div}(\sigma \operatorname{grad} u) = 0, \tag{1}$$

where σ is the conductivity inside a domain Ω, and u denotes the electric potential in the boundary Γ.

This equation was proposed in mathematically correct form by A. P. Calderon in 1980,[2] and the general solution can not be obtained by now. But an interesting alternative for solving eq. (1) appeared when K. Astala and L. Päivärinta[3] first noticed that the two dimensional case of eq. (1) was directly related with a special class of Vekua equation; then, V. Kravchenko et al.[4] posed the structure of its general solution in analytic form by means of Taylor series in formal powers, employing elements of the Pseudoanalytic Function Theory.[5]

Since this analysis was studied, different works were fully dedicated to study the forward problem,[6–8] employing the Pseudoanalitic Function Theory by means of the Taylor series in formal powers. This method proved to be an good mathematical tool to approach the solution for this equation.

The Taylor series in formal powers actually can not be employed to approach the solution in the inverse problem, but there exist many different techniques that approach a solution for this problem, where the most

*vponomar@ipn.mx, phone: +52-55-56562058; fax: +52-55-56562058

Real-Time Image and Video Processing 2015, edited by Nasser Kehtarnavaz, Matthias F. Carlsohn,
Proc. of SPIE-IS&T Electronic Imaging, SPIE Vol. 9400, 94000I · © 2015 SPIE-IS&T
CCC code: 0277-786X/15/$18 · doi: 10.1117/12.2075315

On the Performance of Sequential and Parallel Algorithm for Solving the Forward Problem of the Two-Dimensional Impedance Equation

A. Bucio R. *IAENG, Member*, A. Hernandez-Becerril *IAENG, Member*,
C. M. A. Robles G. *IAENG, Member* and M. P. Ramirez T. *IAENG, Member*.

***Abstract*—We study the performance of the numerical method for solving the forward problem of the two-dimensional Impedance Equation [15]. This numerical method is based upon the elements of the modern Pseudoanalytic Function Theory. Considering divide and conquer technique for constructing the parallel algorithm, some sub process can be taking advantage by processing them independently, we parallelize some processes of the numerical method through CUDA technology, obtaining considerable reduction of the temporal complexity. The processing time of the posed method is evaluated comparing with its sequential version and the speed-up rate of the parallel algorithm respect to the sequential one posed in [15]. The collection of experiments are displayed for illustrating its effectiveness.**

***Index Terms*—Algorithm, CUDA, Electrical Impedance Tomography, Pseudoanalytic Functions Theory, Parrallel Processing, Vekua Equation.**

I. Introduction

THE Pseudoanalytic Function Theory [3] has been just found to be an important tool for modern Mathematical Physics, and in sequel, for different branches of Engineering. Perhaps, beyond the original expectations that its main creators, professors L. Bers [3] and I. Vekua [20], could have foreseen at the time they first published the foundations of the theory.

The elements of the modern Pseudoanalytic Function Theory [12], have been considered as an important tool in Applied Mathematics and Theoretical Physics (see *e.g.* [4], [12] and [18]). This tool has been successfully applied for solving the forward problem of the two-dimensional Impedance Equation [15]

$$\operatorname{div}(\sigma \operatorname{grad} u) = 0, \tag{1}$$

where σ is the conductivity and u is the electric potential. It is possible to approach the general solution of (1) in asymptotic form, through the Taylor series in formal powers [3].

The detection of the relation between (1) in the plane, and the Vekua equation [20], by V. Kravchenko [13], and shortly after by K. Astala and L. Päivärinta [1], opened a complete new path for constructing numerical solutions of the forward problem corresponding to (1), based upon the modern Pseudoanalytic Function Theory [3].

The most important fact of caring about efficiently solving the forward problem for (1), is to use this problem as an approach to the solution of the Electrical Impedance Tomography Problem (also called inverse problem). This problem was widely exposed in plenty works, among which [21] is one of the most important. In this sense, the results posed in [13], and subsequently rediscovered in [1], are indeed very significant, because they allowed to find out the rink for approaching the general solution of the two-dimensional Impedance Equation.

The main contribution of this work is to analyse the performance of the numerical method and its sequential algorithm posed in [15] versus the parallel algorithm to be presented in this work. Employing this numerical method we propose the design of a parallel algorithm using *divide and conquer* technique [14] with CUDA technology, this will help us to obtain an adequate balance between the computational cost and accuracy. Then we examine some specific examples, in order to illustrate a comparison of the performance and effectiveness between the sequential and parallel method. The conclusions contain the arguments that justify the viability of employing this numerical method as an approach for employing it in medical image [21] this is for solving the Electrical Impedance Tomography Problem [6]. This work is organized as follows: In the second Section , we will explain the mathematical tools necessaries for the construction of the numerical method and algorithm for the forward problem of the two-dimensional Impedance Equation. In Section 3, we describe both algorithms. Then we will show some experimental results of the implementation of both algorithms employing different conductivity functions and finally the conclusions of this work.

II. Elements of Pseudoanalytic Function Theory and its relation with the Electrical Impedance Equation.

Let us consider the two-dimensional case of the Electrical Impedance Equation:

$$\operatorname{div}(\sigma \operatorname{grad} u) = 0,$$

where u is the electric potential and σ is a separable-variables non-vanishing function within a bounded domain Ω, with boundary Γ, such that:

$$\sigma = \sigma_1(x) \cdot \sigma_2(y). \tag{2}$$

Introducing the following notations:

$$W = \sqrt{\sigma}\partial_x u - i\sqrt{\sigma}\partial_y u, \quad p = \sqrt{\frac{\sigma_2(y)}{\sigma_1(x)}}, \tag{3}$$

A. Bucio R. is with the National Polytechnique Institute, UPIITA, Mexico, ari.bucio@gmail.com

A. Hernandez-Becerril, C. M. A. Robles G. and M. P. Ramirez T. are with Postgraduate Section of Mechanical Engineering School, Instituto Politecnico Nacional Mexico City, Mexico., croblesg1101@alumno.ipn.mx

ISBN: 978-988-19252-0-6
ISSN: 2078-0958 (Print); ISSN: 2078-0966 (Online)

Construction of a New Cryptographic Method, Employing Pseudoanalytic Function Theory

A. Bucio R. *IAENG, Member*, A. Hernandez-Becerril *IAENG, Member*,
C. M. A. Robles G. *IAENG, Member*, M. P. Ramirez T. *IAENG, Member*, A. Arista-Jalife.*

***Abstract*—Employing the Pseudoanalytic Function Theory, and based upon the inverse Dirichlet boundary value problem for the two-dimensional Electrical Impedance Equation, an open problem also known as Electrical Impedance Tomography, we propose a new cryptographic method whose main characteristics are the Confidentiality and the Data Integrity.**

***Index Terms*—Cryptography, Electrical Impedance Tomography, Pseudoanalytic Functions, Vekua Equation.**

I. Introduction

THE study of techniques for secure communication is the main goal of Cryptography [6]. That is why this discipline is strongly related with other branches of Science, as Applied Mathematics and Computation. There are many other disciplines on which the Cryptography can be based on. Yet, the paragraphs shown further will show that, in this particular proposal, both Mathematics and Computes Sciences will provide enough material to ensure the successful performance of the novel method. Therefor, the Figure 1 shall be adequate to appoint the basic execution of a ciphering method.

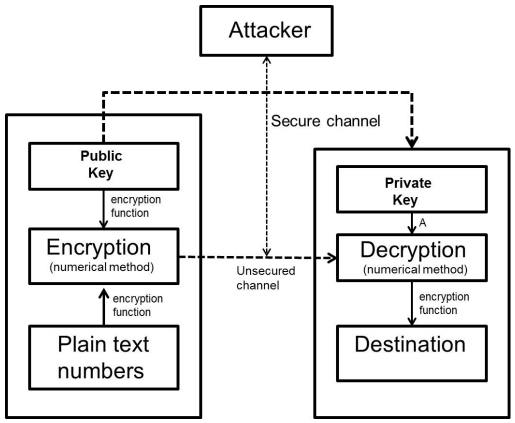

Fig. 1: A general description of a cryptographic method.

This work pays particular attention to the Pseudoanalytic Function Theory [3], that has recently proved to be an important tool in Theoretical Physics, and Applied Mathematics (see *e.g.* [4], [11], and [15]). More precisely, since the pseudoanalytic functions have been employed for analyzing the Electrical Impedance Tomography [18] (a mathematical problem that remains open), it is possible to propose a new cryptographic method that will positively posses characteristics as Confidentiality and Data Integrity.

From the scope of these pages, a cryptographic algorithm will be considered a mathematical method whose main purpose is to convert information into encrypted data, such that the decryption is available only for those that posses the key. For that, the cryptographic algorithm will arise employing numerical techniques that allowed the approaching of the so-called Taylor Series in Formal Powers.

Starting with a brief study of the Pseudoanalytic Function Theory, and its relation with the two-dimensional Electrical Impedance Equation, we expose the details of the methodology for constructing a cryptographic method.

Based upon the material previously posed in a variety of works, fully dedicated to the forward Dirichlet boundary value problem for the Electrical Impedance Equation, we explain that this method is effective for ciphering numerical data whose values are significantly bigger than 10^{-12}. Thus, the variety of data classes on which this method could be useful, can be considered wide enough for engineering applications.

II. The Cryptographic Proposal.

The idea of proposing a new cryptographic algorithm arises from the study of the Electrical Impedance Tomography problem, employing modern elements of the Pseudoanalytic Functions [11]. Nevertheless, we shall appoint that these numerical techniques do not provide yet an adequate solution for the problem.

As a matter of fact, most works (see *e.g.* [4] and [13]) mainly analyze the forward Dirichlet boundary value problem for the Electrical Impedance Equation (the Electrical Impedance Tomography constitutes the inverse problem, correctly posed in mathematical form by A.P. Calderon in [5]). Thus, even the new techniques do provide additional information for better understanding the field, it is impossible to assert that the Electrical Impedance Tomography problem could be solved for arbitrary cases.

Taking into account the last statement, we shall propose the employment of the Pseudoanalytic Function Theory for constructing a cryptographic method, because any attempt to unlock the encrypted information would be equivalent to fully solve an arbitrary case of the Electrical Impedance Tomography problem.

A. Bucio R. is with the National Polytechnique Institute, UPIITA, Mexico, ari.bucio@gmail.com
C. M. A. Robles G. and A. Hernandez-Becerril are with the National Polytechnique Institute, ESIME C. Mexico, cesar.robles@lasallistas.org.mx
M. P. Ramirez T. and A. Arista-Jalife are with the Communications and Digital Signal Processing Group, Engineering Faculty of La Salle University, Mexico, marco.ramirez@lasallistas.org.mx.
*Each author equally contributed to the research work.

ISBN: 978-988-19252-3-7
ISSN: 2078-0958 (Print); ISSN: 2078-0966 (Online)

NUMERICAL ALGORITHM FOR ELECTRICAL IMPEDANCE TOMOGRAPHY PROBLEM USING PSEUDOANALYTIC APPROACH

M. Robles-Gonzalez[1], V. Ponomaryov[1], M. Ramirez-Tachiquin[2], A. Bucio-Ramirez[3]
[1] Instituto Politécnico Nacional, ESIME-Culhuacan,
Av. Santa Ana 1000, San Fco Culhuacan, 044230, Mexico-city, Mexico.
Tel/fax +525556562058; croblesg1101@alumno.ipn.mx
[2] La Salle University, Mexico, [3] IPN-UPIITA, Mexico

1. We perform a comparison between the accuracy of two numerical techniques those permit solving the direct *Dirichlet* boundary value problem in the 2D electrical impedance equation. The first technique is a variation of the Finite Element Method (*FEM*) for elliptic partial differential equations, whereas the second is a new technique based on the modern pseudoanalytic function theory [1].
Initial 2D electrical impedance equation

$$\nabla(\sigma \nabla u) = 0, \tag{1}$$

so-called *electrical impedance tomography* problem, is presented in the work [2].
The above equation possesses special relevance in several areas, for example in *medical imaging*, since the electrical impedance tomography allows the monitoring of different tissues inside of a body applying very small quantities of electrical current, thus it is considered a non-invasive technique.
Using the eq. (1), the inverse *Dirichlet* boundary value problem is formulated as follows: for a given (measured) electrical potential u at the boundary Γ of the domain $\Omega(\Re^2)$, it should be reconstructed the conductivity σ within the domain $\Omega(\Re^2)$.
Considering the inverse problem, there exist a variety of works [3] that are dedicated to approach its solution recursively solving the direct problem under the *FEM*. Since the numerical pseudoanalytic method (*NPSM*) has been mainly dedicated to solve the direct problem, obtaining sufficiently high accuracy for certain cases, it seems important to perform a comparison between two methods (*FEM* and *NPSM*), presenting limitations, drawbacks and advantages of each ones. Thus, this should better appreciate how a novel technique could be employed when dealing with the inverse problem in future. Below, we present such study for both techniques.
To perform the comparing analysis let study some examples of the conductivity functions σ, for which there exist the exact solutions of eq. (1) within the unit circle, employing both *FEM* and *NPSM* in numerical estimations for boundary conditions in the direct problem.
2. As it was shown in several works [1, 4], the eq. (1) is completely equivalent to the *Vekua* equation [5] in such form:

$$\partial_{\bar{z}} W - p^{-1}\partial_{\bar{z}} p\overline{W} = 0, \qquad W = \sqrt{\sigma}\left(\partial_x u - i\partial_y u\right), \qquad \partial_{\bar{z}} = \partial_x + i\partial_y, \tag{2}$$

where: $p = \sqrt{\sigma_1(x)^{-1}\sigma_2(y)}$, $\overline{W} = \mathrm{Re}\, W - i\,\mathrm{Im}\, W$, and $i^2 = -1$.
The general solution for the eq. (2) can be expressed by the Taylor series in formal powers [5]:

$$W = \sum_{n=0}^{\infty} Z^{(n)}(a_n, z_0; z), \qquad z = x + iy \tag{3}$$

More details about the mathematical technique using the Taylor series in formal powers $Z^{(n)}(a_n, z_0; z)$ can be found in [1, 7]. A detailed explanation of the numerical approach of the formal powers in eq. (3) is given in [6, 7].
3. To compare the precision obtained by *FEM* or *NPSM* techniques, we employ the *Lebesgue* measure:

$$\varepsilon = \left(\int_{\Gamma} \left(u|_{\Gamma} - u_{app}\right)^2 dl\right)^{1/2}, \tag{4}$$

where $u|_{\Gamma}$ is the electric potential imposed in the domain boundary Γ, and u_{app} is the electric potential obtained by *FEM* or *NPSM*. This measure exposes the error between the analytical solution and numerical result obtained by a method analyzed.
Let consider an exponential conductivity function [6] that gives the exact solution $u|_{\Gamma} = e^{-\alpha \cdot x \cdot y}$ for eq. (1):

2012 9th International Conference on Electrical Engineering, Computing Science and Automatic Control
Mexico City, Mexico. September 26-28, 2012

A Simplified Method for Numerically Solving the Impedance Equation in the Plane

A. Bucio R.[1], R. Castillo-Perez[2], M.P. Ramirez T.[3], C.M.A. Robles G.[4]*
[1]UPIITA IPN, Mexico, ari.bucio@gmail.com
[2]ESIME Z. IPN, Mexico, raulcastillop@hotmail.com
[3]Communications and Digital Signal Processing Group, FI ULSA, Mexico, marco.ramirez@lasallistas.org.mx
[4]ESIME C. IPN, Mexico, cesar.robles@lasallistas.org.mx, *IEEE student member, 90680212.*

***Abstract*—**Employing elements of the modern pseudoanalytic function theory, we propose one of the most simplified numerical methods for solving the forward boundary value problem of the two-dimensional Impedance Equation, remarking the possible contribution of the obtained results, into the modern theory of the Electrical Impedance Tomography.

***Keywords*—** Impedance Equation, Pseudoanalytic Functions, Tomography.

I. Introduction

The use of modern pseudoanalytic function theory [6] for solving the forward problem of the two-dimensional Impedance Equation

$$\operatorname{div}(\sigma \operatorname{grad} u) = 0, \tag{1}$$

where σ is the conductivity and u is the electric potential, has proven to be one of the most interesting possibilities, since e.g. by mean of it, is possible to approach the general solution of (1) in asymptotic form, employing Taylor series in formal powers [2].

An alternative to avoid what could be a restriction for adequately using this technique, when dealing with engineering problems, was posed in [8], since for fully applying the numerical tools based upon the elements of the pseudoanalytic functions, it is a requisite that the electrical conductivity σ can be represented as a separable-variables function.

Indeed, [8] showed that any physical conductivity distribution within a bounded domain, can be considered a limit case of a separable variables function. Thus the Dirichlet boundary value problem of (1) can be approached, as properly shown in [4] and [5], when an electric potential u is imposed as the boundary condition.

As it was clearly posed in [11], the capability of solving the forward problem of (1) is crucial if we are to study the solution of its inverse problem, commonly known as Electrical Impedance Tomography.

The possibility of approaching the general solution of the Impedance Equation in the plane, was first noticed in [1] and [7]. After that, many researches were published, dedicated to solve the Dirichlet boundary value problem of (1).

This work is also dedicated to the numerical solution of such problem, yet its main contribution shall be the low computational resources needed for this end. Basically, the existing algorithms are very accurate, but the required computing capacity is still high. This could limit their use into biomedical engineering applications, when dealing, for instance, with Electrical Impedance Tomography problems in clinical situations.

Therefore, the suggestion of a simplified numerical method is in order, and the following paragraphs contain the description of what could be one of the most simplified algorithms, capable of solving the Dirichlet boundary value problem for (1), causing less requirement of computational resources.

After reviewing the general concepts that stablish the connexion between the two-dimensional Impedance Equation and the Vekua equation [10], and that allows us to express its general solution in terms of Taylor series in formal powers, we study the algorithm on which the simplified numerical method is based. Then we provide an example of its performance considering the classical unitary circular domain.

We also present a basic description of the performance of the method, when certain variations of the main parameters take place, closing the work with some commentaries that point out the immediate advantages obtained when employing the simplified method is used.

II. Preliminaries

Following [2], let us consider two complex-valued functions (F, G) fulfilling the condition

$$\operatorname{Im}\left(\overline{F}G\right) > 0, \tag{2}$$

where $\overline{F}$ represents the complex conjugate of F. Thence any complex function W can be expressed by the linear combination of F and G:

$$W = \phi F + \psi G.$$

Here ϕ and ψ are real-valued functions. A pair (F, G) catering (2) is named *Bers generating pair*. Indeed, L. Bers [2] introduced a derivative based upon such pair. It is expressed in the form

$$\partial_{(F,G)} W = (\partial_z \phi)\, F + (\partial_z \psi)\, G, \tag{3}$$

where $\partial_z = \frac{\partial}{\partial x} - i\frac{\partial}{\partial y}$, and $i^2 = -1$. This derivative will exist if and only if

$$(\partial_{\overline{z}} \phi)\, F + (\partial_{\overline{z}} \psi)\, G = 0, \tag{4}$$

where $\partial_{\overline{z}} = \frac{\partial}{\partial x} + i\frac{\partial}{\partial y}$. By acquainting the notations

$$A_{(F,G)} = \frac{\overline{F}\partial_z G - \overline{G}\partial_z F}{F\overline{G} - \overline{F}G}, \quad B_{(F,G)} = \frac{F\partial_z G - G\partial_z F}{F\overline{G} - \overline{F}G},$$
$$a_{(F,G)} = \frac{\overline{G}\partial_{\overline{z}} F - \overline{F}\partial_{\overline{z}} G}{F\overline{G} - \overline{F}G}, \quad b_{(F,G)} = \frac{F\partial_{\overline{z}} G - G\partial_{\overline{z}} F}{F\overline{G} - \overline{F}G}; \tag{5}$$

*The authors appear in alphabetical order.

IEEE Catalog Number: CFP12827-CDR
ISBN: 978-1-4673-2168-6
978-1-4673-2169-3/12/$31.00 ©2012 IEEE

Proceedings of the World Congress on Engineering 2011 Vol III
WCE 2011, July 6 - 8, 2011, London, U.K.

On the Construction of Separable-Variables Conductivity Functions, and Their Application for Approaching Numerical Solutions of the Two-Dimensional Electrical Impedance Equation

M.P. Ramirez T., IAENG Member, M. C. Robles G., R. A. Hernandez-Becerril

Abstract—**We analyze a technique for obtaining piecewise separable-variables conductivity functions, employing standard cubic polynomial interpolation. Our goal is to start making possible the practical use of the Pseudoanalytic Function Theory in medical imaging, by allowing the construction of numerical solutions, in terms of Taylor series in formal powers, of the two-dimensional Electrical Impedance Equation.**

Keywords: Electrical Impedance Equation, pseudoanalytic functions

I. Introduction

The analysis of the two-dimensional Electrical Impedance Equation

$$\nabla \cdot (\sigma \nabla u) = 0, \tag{1}$$

is the departure point for any proper study of the Electrical Impedance Tomography problem.

As a matter of fact, we will find that the complexity of this governing equation, appears just at the very beginning, when the selection of the mathematical representation for the conductivity σ takes place.

There exists a wide collection of interesting methods for approaching the electric potential u once σ has been chosen. Many of them are based upon variations of the well known Finite Element Method (see e.g. [9]), which effectiveness has been well proved in many classes of boundary value problems belonging to the Electromagnetic Theory.

Still, most of the known variations of the Finite Element Method present instability when approaching solutions for the inverse problem of (1), and it is not clear yet how to overpass this situation.

An interesting alternative for solving (1) appeared when K. Astala and L. Païvarïnta [1] first noticed that the two-dimensional case of (1) was directly related with a special class of Vekua equation [11], and V. Kravchenko et al. [6] posed the structure of its general solution in analytic form by means of Taylor series in formal powers, employing elements of the Pseudoanalytic Function Theory developed by L. Bers [2].

We may also remark that the use of this new mathematical tools allowed to approach the solution of the direct boundary value problem for (1), with high accuracy, once σ was posed as a separable-variables function [4].

These new results are, with no doubt, relevant for better understanding the dynamics of the Electrical Impedance Equation. Thus, a natural path to follow, is to search for the interpolating methods that will allow us to apply these novel techniques, when studying cases situated nearer to the medical imaging engineering.

This work is dedicated to analyze one interpolating method posed in [7], that allows to obtain separable-variables functions σ when a finite set of conductivity values is properly defined within a bounded domain.

Specifically, after reviewing a collection of statments corresponding to the Pseudoanalytic Function Theory, we will discuss how to construct a piecewise polynomial separable-variables function by using standard interpolation methods.

Starting with the case used in [4], for approaching solutions of the boundary value problem for (1), we present the results of performing a basic numerical analysis, in order to test the convergence of the interpolation method. We illustrate the behavior of a certain class of maxima errors, taking into account the number of subregions in which we divided a unitary circle, and the number of points considered within every subregion.

We close with a brief discussion about the validity and use of these preliminary results, emphasizing the necessary work before we can use effectively this interpolation method in medical imaging.

II. Preliminaries

Following [2], let the pair of complex-valued functions (F, G) fulfil the condition

$$\mathbf{Im}\left(\overline{F}G\right) > 0, \tag{2}$$

where $\overline{F}$ denotes the complex conjugation of F. Thus any complex function W can be expressed by means of the linear combination of F and G:

$$W = \phi F + \psi G.$$

Here ϕ and ψ are real functions. A pair of functions satisfying (2) is named a *Bers generating pair*. Indeed, L. Bers introduced a derivative based upon the generating pair (F, G). It has the form

$$\partial_{(F,G)} W = (\partial_z \phi)\, F + (\partial_z \psi)\, G, \tag{3}$$

Facultad de Ingenieria de la Universidad La Salle, A.C., B. Franklin 47, C.P. 06140, Mexico D.F., Mexico. email: marco.ramirez@lasallistas.org.mx

The authors would like to acknowledge the support of CONACyT project 106722, Mexico.

ISBN: 978-988-19251-5-2
ISSN: 2078-0958 (Print); ISSN: 2078-0966 (Online)

2010 7th International Conference on Electrical Engineering, Computing Science and Automatic Control (CCE 2010)
Tuxtla Gutiérrez, Chiapas, México. September 8-10, 2010.

On the Computational Methods Employed in Two-Dimensional Electrical Impedance Tomography

M.P. Ramirez T., M. C. Robles G., R. A. Hernandez-Becerril
Escuela de Ingenieria de la Universidad La Salle
Benjamin Franklin 47, Del. Cuauhtemoc, C.P. 06140,
Mexico D.F., Mexico.
email: marco.ramirez@lasallistas.org.mx

***Abstract*— We analyze the State of Art in computational methods, employed for analyzing the two-dimensional Electrical Impedance Tomography problem (EIT). We broach an assortment of techniques that may be considered among the most important innovations on this area, emphasizing that the Finite Element Method has played a central role for solving the forward problem of the Electrical Impedance Equation, backbone of EIT. We finally study a novel numerical method, based onto the modern theory of Pseudoanalytic Functions, that could well improve the quality of the reconstructed images, when applied in lieu of the Finite Element Method.**

Keywords- Electrical Impedance Tomography, Pseudoanalytic Functions.

I. Introduction

The Argentine mathematician A. P. Calderon posed in 1980 [1] a boundary valued problem for the Electrical Impedance Equation

$$\operatorname{div}(\sigma \operatorname{grad} u) = 0, \tag{1}$$

where σ represents the conductivity and u denotes the electric potential. The goal is to approach σ inside some domain Ω when the values of the potential u are given at the boundary Γ. This problem immediately became of great interest for medical imaging, because it could be used as an auxiliary tool for the diagnosis of a wide class of diseases. Beside, when compared to another imaging techniques, the *Electrical Impedance Tomography* (EIT) -as the Calderon problem is actually referred in the medical terminology- possesses the quality of being a noninvasive procedure, due to the low ranges of electrical currents used on it.

Nonetheless, the maximum resolution that the computational methods can achieve is not satisfactory yet for establishing EIT as a standard method for medical image reconstruction. And, in many senses, this is because the inverse problem for equation (1) can not be solved bias a *mathematical extension* of the boundary function $u|_{\Gamma}$, as it is possible to do for other boundary value problems of partial differential equations (e.g. the Laplace equation [2]).

The inverse problem for the Electrical Impedance Equation (1) might be approached by solving the forward problem through an iterative procedure, that could be briefly described as follows: Once a conductivity function σ is proposed, we must solve (1) in order to obtain the corresponding electric potential u with the highest possible accuracy. Then, a comparison between the approached u and the collected data will take place, reaching an error function that may be used for modifying σ in order to minimize such error. The procedure will continue until the error function fulfills some minimum criteria.

The first interesting problem lies at the very beginning of the algorithm, because the mathematical complexity of equation (1) is considerable. Moreover, many experts suggested that to achieve the general solution for (1) was impossible (see [3], Chap. 10, Sec. 10.2.3), even for the simplest cases of σ (excluding the constant case, of course). Due to this fact, the numerical methods have played a central role on these matters during the last three decades, being the variations of the *Finite Element Method* some of the most often used, since it had already shown its effectiveness when approaching solutions for a wide variety of partial differential equations of Electromagnetic Theory.

The second interesting question is located around the adjustment of the conductivity function σ when an error is estimated. This is a mayor challenge since the EIT problem is considered to be very unstable, as well as ill-posed. It is about this second topic that we will start our discussion, because the variety of techniques suggested for better modifying the function σ is extensive, and none of them should be considered less important than the rest. The selection of the presented methods was based onto their clinical applications, and their achieved image resolution, leaving the computational complexity for further discussions.

We will close our study with a brief review of a recently posed method for solving (1), that (despite the fact its application is not as general as the Finite Element Method) opens a new path for solving the Electrical Impedance Equation with considerable grown profits of accuracy.

II. Methods for approaching the conductivity function σ

A. Variations of Sparse Matrix Method

Let us establish a finite set of points $\{z_k\}_{k=1}^{N}$ belonging to the boundary Γ of the domain Ω, and let $\{u_k\}_{k=1}^{N}$ be the values of the electric potential u at such points. Let the unitary vector $\overrightarrow{n}_k$ be tangent to some point $z_k \in \{z_k\}_{k=1}^{N}$. The Neumann

IEEE Catalog Number: CFP10827-ART
ISBN: 978-1-4244-7314-4
978-1-4244-7314-4/10/$26.00 ©2010 IEEE

Appendix C: Awards granted